Synthesis and Structural Studies of Polynuclear Copper Complexes

A thesis submitted for the degree of Doctor of Philosophy

by

Christopher W. Baxter

School of Chemistry
Faculty of Science and Engineering
University of Edinburgh
December 2004

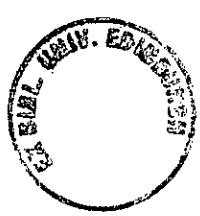

Declaration

I hereby declare that this thesis has been entirely composed by myself and that the work described herein is my own except where clearly mentioned either in acknowledgement, reference or text. It has not been submitted in whole or in part, for any other degree, diploma or other qualification.

Christopher W. Baxter

December 2004

This thesis is dedicated
to my family and Elaine.

Acknowledgements

I would like to thank a number of people for their assistance and encouragement throughout my Phd.

Prof Peter Tasker, for excellent supervision, assistance and encouragement during this project.

Dr Timothy C. Higgs, for supervision and guidance, for sharing his wealth of experience and making the lab an enjoyable place to work.

Dr Phil Bailey, for useful discussions and supervision.

Prof Mary McPartlin, for solving crystal structures and providing excellent suggestions during discussions.

Dr Simon Parsons for solving crystal structures and being very helpful in all matters crystallographic.

The crystallography group at the University of Edinburgh, in particular Dr Iain Oswald, for carrying out single crystal X-ray diffraction measurements.

Dr Anita Jones, for her guidance and advice during the spectroscopy work.

Dr Eric McInnes, Dr Euan Brechin and David Low for allowing me the use of their equipment at the University of Manchester and looking after me during my visit.

All the technical staff at the Chemistry Department for their skill and helpfulness. In particular, John Millar for help with NMR and Alan Taylor and Robert Smith for help with Mass Spectrometry.

All the members of the Tasker, Bailey, Robertson and Mareque groups for making the top corridor a great place to work. Particular thanks must go to Dr Paul Plieger,

Dr Lee West and Dr Dave Henderson for always being willing to give advice and share their experience.

My family, for support and encouragement throughout my university career, without which this thesis would not have been possible. Elaine, for her support and friendship and all my friends in Edinburgh for such an enjoyable time here.

Abstract

This thesis investigates the effect of varying the ligand component in a cluster forming reaction recently developed for the synthesis of molecules with general formula, $[Cu_{x+y}(C{\equiv}CR)_x(hfac)_y]$ where hfac is 1,1,1,5,5,5-hexafluoropentanedione and C≡CR is a straight chain terminal alkynyl ligand (R = $-C_3H_7$, $-C_4H_9$, $-C_5H_{11}$, $-C_6H_{13}$). Using the 'bulky' alkynyl ligands, 3,3-dimethyl-1-butyne ($^tBuC{\equiv}CH$) and trimethylsilylacetylene ($Me_3SiC{\equiv}CH$) has led to the successful isolation of five clusters containing ten or twelve copper atoms. These molecules are structurally related to a family with formula, $[Cu_4(aryl)_4]$ and display an alkynyl bridged Cu_4 central core 'capped' by peripheral Cu-hfac chelate rings.

Six additional clusters are reported that have nuclearities ranging between sixteen and twenty-six copper atoms. These were obtained by replacing hfacH with the trifluorinated 1,3,-diketonyl ligands, 4,4,4-trifluoro-1-phenyl-1,3-butanedione, (Ph-tfacH), 4,4,4-trifluoro-1-phenyl-1,3-butanedione (^{t}Bu-tfacH) and 1,1,1-trifluoro-2,4-pentanedione (tfacH) or using 3,3-dimethyl-1-butyne ($^tBuC{\equiv}CH$) or 3-phenyl-1-propyne ($PhCH_2C{\equiv}CH$) in the cluster forming reaction. The new additions to the $[Cu_{x+y}(C{\equiv}CR)_x(hfac)_y]$ family of molecules are diverse in nuclearity and display interesting structural features. Using alkynyl or 1,3-diketone ligands with bulky substituents affects the ability of the clusters to adopt a 'conventional' structure and as a result interesting structural variations are observed. Using ligands with substituents that are able to form weak but significant π-stacking type intramolecular interactions also causes a distortion from a 'conventional' structure.

Despite the apparent differences in structure depending on nuclearity and ligand properties, there is an interesting common structural motif that appears throughout the $[Cu_{x+y}(C{\equiv}CR)_x(hfac)_y]$ family. This motif has the formula, $[Cu_4(C{\equiv}CR)_4(Cu\text{-}hfac)_x]$ and all the clusters in the series are found to contain one, two or three such fragments. A cluster-forming mechanism has been tentatively proposed based on the assembly of these 'building blocks' followed by their aggregation to form either low

(ten or twelve copper atoms), medium (sixteen to twenty copper atoms) or high (twenty four or twenty six copper atoms) nuclearity clusters.

The photophysical properties of $[Cu_{x+y}(hfac)_x(C{\equiv}CR)_y]$ type clusters have been explored and a fluorescence study of a range of clusters is reported. The room temperature luminescence spectra of all the molecules analysed are remarkably similar. Comparison with related monomeric complexes has shown that the room temperature luminescent emissions, irrespective of cluster nuclearity, are derived from transitions from within the electron delocalised Cu-hfac chelate ring. Low temperature studies of a Cu_{26} cluster tentatively suggest emissive features derived from transitions within the complex Cu-alkynyl core.

An additional study is reported into the use of bifunctional benzotriazole ligands to interlink pentametallic clusters with general formula, $[Cu_5(bta)_6(acac)_4]$ (bta = benzotriazole, acac = acetylacetonate). Bta and acac ligands in these clusters have been shown to undergo substitution by competitive ligands in solution. In light of this discovery, a series of bifunctional benzotriazole ligands were designed and synthesised. Using these ligands and a bifunctional acac ligand, cluster-linking experiments have been attempted. Although initial attempts have been unsuccessful, some important observations about requirements for suitable 'linker' ligands have been made.

Table of Contents

Abbreviations

δ	chemical shift
λ	wavelength
λ_{em}	Emission wavelength
λ_{ex}	Excitation wavelength
ε	extinction coefficient
°	degree
°C	degree centigrade
Å	Angstrom
abtaH	5-aminobenzotriazole
acacH	2,4-pentanedione
ca	*circa*
btaH	Benzotriazole
^{n}Bu	Normal butyl
^{t}Bu	Tertiary butyl
cbtaH	Benzotriazole-5-carboxylic acid
$CDCl_3$	deuterated chloroform
cm^{-1}	wavenumber
CLD	Chemical Liquid Deposition
Cod	cyclooctadiene
CVD	Chemical Vapour Deposition
d (NMR)	doublet
DMF	Dimethyl formamide
d_6-DMSO	deuterated dimethyl sulfoxide
DMSO	Dimethyl sulfoxide
dnbtaH	5,6-dinitro-1H-benzotriazole
Ed.	Editor
Edn.	Edition

et al	*et alli* (and others)
eV	electron Volts
Et_2O	Diethyl ether
EtOH	ethanol
FABMS	fast atom bombardment mass spectroscopy
g	gram
$H_{2(g)}$	Hydrogen gas
hfacH	1,1,1,5,5,5-hexafluoropentanedione
HOMO	Highest Occupied Molecular Orbital
hr	hour
IR	infra-red
K	Kelvin
K	equilibrium constant
Kcal	kilocalories
K_f	formation constant
LMCT	Ligand to Metal Charge Transfer
m	*meta*
m (IR)	medium
m (NMR)	multiplet
m.p.	melting point
m/z	mass per unit charge
MeCN	acetonitrile
MeOH	methanol
MHz	mega hertz
min	minute
ml	millilitre
MLCT	Metal to Ligand Charge Transfer
mmol	milli moles
mol	moles
NMR	nuclear magnetic resonance
o	*ortho*

OH	hydroxide anion
p	*para*
pH	negative logarithm (base ten) of the hydrogen ion concentration
Ph	phenyl
Ph-tfacH	4,4,4-trifluoro-1-phenyl-1,3-butanedione
pK_a	negative logarithm (base ten) of the acid dissociation constant
pr	propyl
q (NMR)	quartet
s (IR)	strong
s (NMR)	singlet
SMe_2	dimethylsulphide
T	temperature
t (NMR)	triplet
tfacH	1,1,1-trifluoropentanedione
THF	tetrahydrofuran
TMS	trimethylsilyl
trans	*transoid*
traH	1H-1,2,3-triazole
^tBu-tfacH	6,6,6-Trifluoro-2,2-dimethyl-3,5-hexanedione
UV/vis	ultra violet/visible
V	Volts
w (IR)	weak

Chapter One

Introduction

1.1 Introduction

The work described in this thesis is concerned with the synthesis and characterisation of polynuclear copper complexes or aggregates using a combination of 'bridging' and 'capping' ligands. In an earlier programme of research aimed at using Cu(I)diketonate complexes for ink-jet printing conducting circuitry, an interesting family of molecules was discovered in Edinburgh with general formula, $[Cu_{x+y}(hfac)_x(C{\equiv}CR)_y]$ (hfac-1,1,1,5,5,5-hexafluoropentanedionyl).[1] The aim of the current work is to extend this family by systematically varying the properties of the 'bridging' alkynyl and 'capping' hfac ligands, and thus gain an understanding of the limitations of the cluster-forming reaction and the mechanism by which the molecules assemble. A series of molecules have been isolated and these structures analysed.

Metal-alkynyl clusters have received an increasing amount of interest in recent years due to their potential applications as advanced materials and in particular, their luminescence properties have been widely studied.[2] A second aim of the current work is to investigate the photo-physical properties of the $[Cu_{x+y}(hfac)_x(C{\equiv}CR)_y]$ molecules. The luminescence of this family has been studied and the results are discussed.

A second area of work focuses on a series of complexes with the general formula, $[Cu_5(bta)_6(acac)_4]$ where benzotriazolate (bta^-) acts as a polynucleating ligand and acetyl acetonate ($acac^-$), acts as a 'capping' ligand addressing single copper atoms. The aim was to interlink discrete clusters by the substitution of one or more of the 'polynucleating' bta^- with a bifunctional ligand and create potentially useful new materials. The strategy employed to achieve this aim is discussed.

Information on ink-jet printing conducting circuitry and how studies in this area resulted in the isolation of $[Cu_{x+y}(hfac)_x(C{\equiv}CR)_y]$ clusters is discussed in chapter 1. In addition, the fundamental properties of the 'bridging' and 'capping' ligands used and their coordination chemistry with copper is considered.

1.2 Copper

Copper has been important since the early days of the human race, in southern Turkey examples of its uses date back nine millennia.[3] In modern times the electrical and thermal conductivity of copper made it an essential material in electroconductive devices and heating or cooling systems. As alloys with metals such as zinc and tin, its strength and resistance to corrosion has lead to widespread use in construction and engineering. Compounds of copper account for only a fraction of its worldwide usage but have a multitude of applications throughout industry and agriculture. They are employed in fungicides, nutritional additives, catalysis and pigments as well as many other important technologies. It is 26th in order of abundance of elements in the accessible sphere of the earth and is present in the first sixteen km of the earth's crust at an average level of 50 ppm.[3] Chalcopyrite ($CuFeS_2$), chalcocite (Cu_2S) and cuprite (Cu_2O) are the major ores although there are more than 200 minerals known that contain copper in definable amounts. The predominant sources of the metal are the iron containing sulfide ores on which pyrometallurgical and hydrometallurgical techniques are employed to obtain 'blister' copper which is then purified electrolytically.[3]

1.2.1 Chemical Properties

Copper has atomic number 29 and an atomic mass of 63.546 (± 0.003) (IUPAC, 1983). The two stable isotopes with slight differences in abundance prevent a more accurate atomic weight. It lies in group eleven in the periodic table and although traditionally considered as a subdivision of the alkali metals group (due to the similarities in electronic configurations, i.e. $3d^{10}4s^1$ and p^6s^1) it is largely transitional because it can form ions with incomplete d shells. In the ionic form copper exists primarily in the +1 and +2 oxidation states. The stabilities of the various valence states are illustrated by the following standard reduction potentials:

$$Cu^+ + e^- \rightarrow Cu^0 \qquad E^0 = +0.52\ V$$
$$Cu^{2+} + 2e^- \rightarrow Cu^0 \qquad E^0 = +0.34\ V$$
$$Cu^{2+} + e^- \rightarrow Cu^+ \qquad E^0 = +0.15\ V$$

$$Cu^{3+} + e^- \rightarrow Cu^{2+} \qquad E^0 = +1.80\ V$$
$$2Cu^{+} + e^- \rightarrow Cu^{0} + Cu^{2+} \qquad E^0 = -0.37\ V$$

In aqueous solution the free copper (I) is an unstable entity however the +1 oxidation state can be stabilized with respect to disproportionation using ligands such as ammonia, cyanide and chloride.[3]

1.2.2 +1 Oxidation State

The Cu (I) ion has electronic configuration $[Ar]3d^{10}$ and forms diamagnetic compounds. As a consequence of the filled 3d orbitals only minimal electronic distortions occur so the stereochemistry around the metal ion is dictated by anion size, electrostatic and covalent bonding forces. The most common geometry for Cu (I) is tetrahedral although numerous linear and trigonal planar compounds are known. It is a soft metal using the classification established by Pearson[4] which reflects the polarisable and richly covalent nature of the metal in the +1 state and its relatively small frontier orbital separations. It therefore has a strong affinity for soft ligands such as CN^-, CO, R_3P and R_2S.

1.2.3 +2 Oxidation State

The Cu (II) ion has electronic configuration $[Ar]3d^9$ and forms paramagnetic compounds. Cu(II) complexes tend to have either square-planar or tetragonally distorted octahedral configuration. This is due to the Jahn-Teller effect, where a molecule distorts by an elongation of metal-ligand bonds in the z-direction and compression in the x and y direction so as to remove degeneracy and achieve a lower energy. This explains why Cu(II) complexes have the largest formation constants of all the divalent cations in the first row of the transition metals as shown in the Irving-Williams series.[5] The stabilizing influence of the Jahn-Teller distortion lowers the ligand field stabilization energy compared to the pure octahedral ligand field and enhances the value of K_f. According to the classification established by Pearson[4] in the +2 oxidation state Cu is a borderline hard acid.

1.3 Deposition of copper

The low resistivity of copper has led to its use as an interconnect metal[6] in microelectronic devices and methods of depositing pure copper on circuit boards have been widely studied. Current methods include electroless plating technology[7] and chemical vapour deposition (CVD)[8-11]. Electroless plating involves the submersion of a pre-treated circuit board in a solution containing a Pd/Sn colloidal suspension. Pre-treatment promotes the adhesion of colloidal particles to the substrate surface. After adsorption of the metal colloid, the surface is coated with a photoresist and developed to reveal the circuit pattern. Copper is grown on this pattern by placing the board in a copper sulphate bath containing formaldehyde. Copper reduction is catalysed by the exposed metal colloid and the metal is deposited as a circuit board.

Chemical vapour deposition involves evaporation of a volatile copper-containing compound followed by the transfer of this vapour to a reaction compartment. Here, the volatile material decomposes under low vacuum and in the presence of $H_2(g)$ and the metal is deposited on a substrate as a film. Thermal decomposition is the most commonly used process and is induced by irradiation or exposure to plasma.

The programme of research from which the study of $[Cu_{x+y}(hfac)_x(C{\equiv}CR)_y]$ type molecules evolved focused on adapting metal deposition techniques for use in conjunction with ink-jet printing technology. The project was a joint venture between the University of Edinburgh, Avecia and Seiko-Epsom and the work was driven by demand for miniaturization and ease of fabrication in the micro-electronics industry. Strategies were developed for the deposition of metal based on electroless plating and CVD technologies however for the purposes of this discussion, only the work relating to CVD will be considered.

1.3.1 Adaptation of chemical vapour deposition (CVD) to a chemical liquid deposition (CLD) process

To be a suitable precursor for use in chemical vapour deposition the volatile copper containing compound must undergo sublimation and re-sublimation in a high vacuum at

relatively low temperature without decomposition, must undergo thermal decomposition at a relatively low temperature and must result in a low level of contamination of the resultant metal film due to ligand by-products.

The CVD of copper films has traditionally been carried out using copper β-diketonate compounds.[12-18] [Cu(II)(β-diketonate)$_2$] type complexes decompose *via* the cleavage of Cu-O bonds in the presence of H_2(g) to form metallic copper and acacH. This technique has disadvantages as there is only a small, relatively high temperature range where deposition occurs and H_2(g) is required in the reactor.

As a result of these difficulties, a family of [Cu(I)(β-diketonate)(L)$_x$] (L = neutral ligand) type clusters were developed.[15, 18-20] These decompose *via* a thermally induced disproportionation pathway (Scheme 1-1).

$$2[Cu(I)(\beta\text{-diketonate})(L)_x] \longrightarrow Cu(0) + [Cu(II)(\beta\text{-diketonate})_2] + L_x$$

Scheme 1-1. Disproportionation of [Cu(I)(β-diketonate)(L)$_x$] complexes.

The aim of the work carried out in Edinburgh was to adapt the CVD process to be used in a chemical liquid deposition application. The CLP approach to metal deposition uses an ink-jet printer to lay down a 'liquid metal' solution of a copper-containing compound in a circuit board pattern. The circuit board is heated and decomposition takes place, resulting in a copper circuit board and volatile by-products that can be easily removed either by washing or evaporation. This method allows the majority of the process to take place in the liquid phase and reduces the temperatures required to achieve deposition.

Due to their low decomposition temperature *via* a disproportionation pathway and the formation of volatile by-products that can easily be removed, a programme of research was instigated using [Cu(I)(hfac)(L)$_x$] type complexes (hfac = 1,1,1,5,5,5-hexafluoro-pentanedionyl, L = neutral ligands such as: MeCN, CH_2=CHCN and $CH_3OC(=O)CHC=CH_2$), x = 1 or 2)[21] as potential CLP precursors. A crude method was

developed for preliminary testing of these reagents for suitability as 'liquid metals'. This involved the addition of hfacH to a suspension of Cu_2O and anhydrous $MgSO_4$ in a solution of L (Figure 1-1). Where possible the neutral ligand was used as the solvent but in some cases non-polar solvents such as *n*-hexane were required to dilute the reaction mixture for ease of handling. An acid/base reaction took place between Cu_2O and hfacH, generating a Cu-hfac complex stabilised by the neutral ligand, L, and water, which was removed from the system by the $MgSO_4$. Following this reaction, the mixture was filtered leaving a solution of $[Cu(hfac)(L)_x]$ in an excess of L. This 'liquid metal' solution was heated under vacuum to induce the disproportionation decomposition reaction (Scheme 1-1). A suitable reagent deposits a film of copper metal on the surface of the reaction vessel and allows the volatile byproducts, $[Cu(hfac)_2]$ and L to be removed under vacuum.

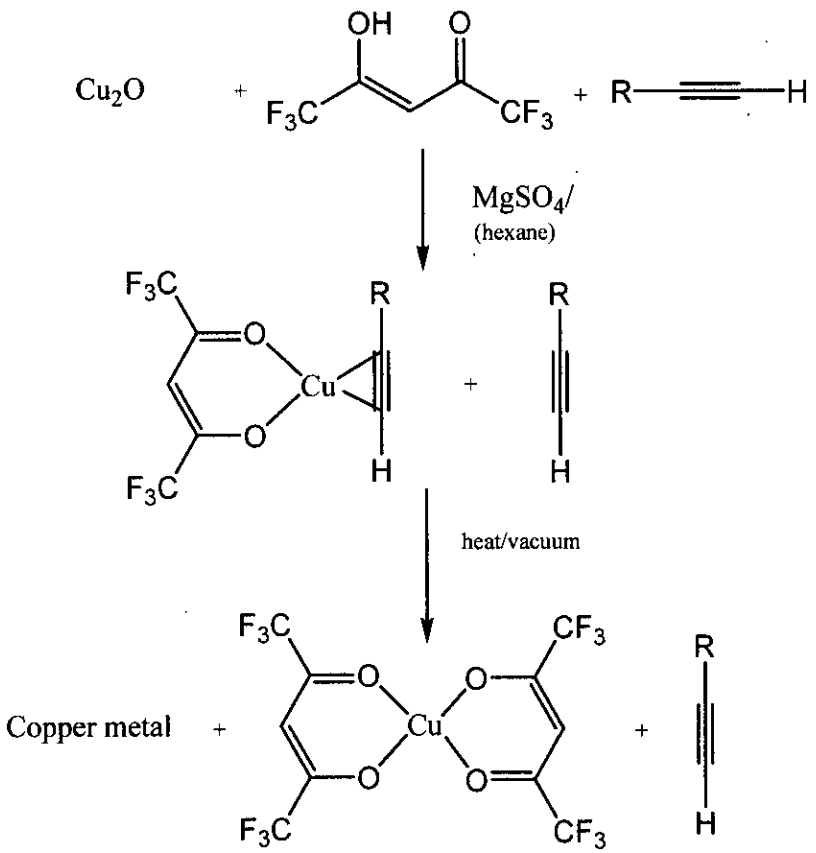

Figure 1-1. Reaction scheme for testing of $[Cu(hfac)(L)_x]$ complexes for suitability as CLP reagents.

1.3.2 Isolation of $[Cu_{x+y}(hfac)_x(C{\equiv}CR)_y]$ clusters from metal deposition experiments

A number of 'liquid metal' complexes were tested for potential use in CLP systems using the reaction described in Section 1.3.1 (Figure 1-1) and some useful observations were made that will not be discussed further. The most relevant discovery to this thesis was made when the metal deposition experiment was performed using $[Cu(hfac)_x(HC{\equiv}CC_3H_7)]$ as the 'liquid metal' precursor. During the heat/vac process, instead of disproportionation and copper deposition taking place, an orange/red solid

was obtained. This material was recrystallised and X-ray structure determination revealed a structure with formula, $[Cu_{26}(hfac)_{11}(C{\equiv}C\ C_3H_7)_{15}]$ (Figure 2-2).[1]

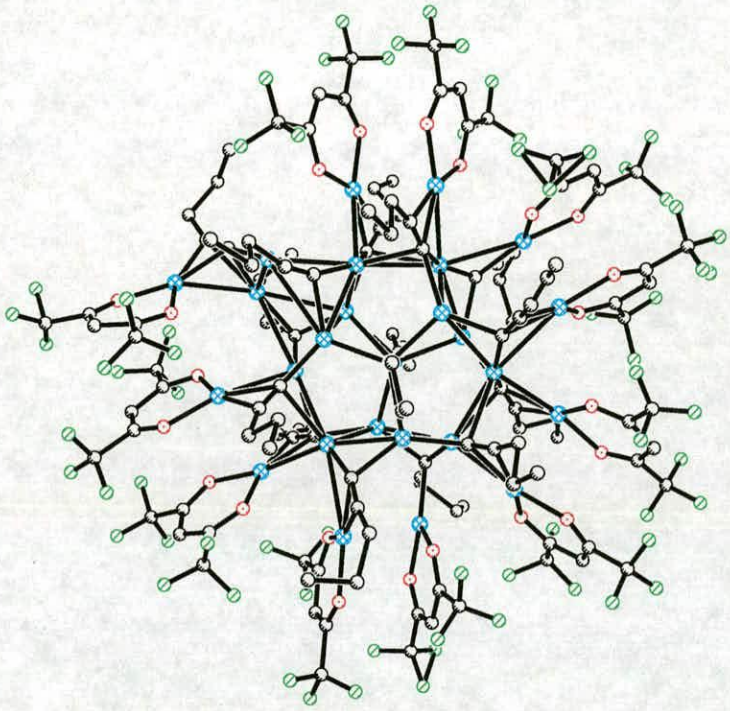

Figure 2-2. Structure of $[Cu_{26}(hfac)_{11}(C{\equiv}C\ C_3H_7)_{15}]$

This result was significant as alkynyl–bridged clusters of this size are unusual. In addition, the cluster was obtained *via* a facile procedure from readily available starting materials and contained a complex network of alkynyl-bridged close Cu-Cu contacts, making the molecule an attractive system for further study.

Following the initial discovery a series of clusters were obtained, using similar reaction conditions, by varying the length of the alkyne ligand used in cluster synthesis.[22, 23] The series ranged in nuclearity between twelve and twenty-six copper atoms (Table 1-1) and some interesting structural features were observed which will be discussed in detail later in this thesis.

In order to understand how the nature of the ligand components effect the outcome of the reaction in Figure 1-1, some background information on the chemistry of β-diketonate and alkynyl ligands will be given in the following sections. In addition, a

brief review of recent developments in metal-alkynyl chemistry, focusing particularly on interesting physical properties will be presented.

General Formula: $[Cu_{x+y}(hfac)_x(alkynyl)_y]$			
Alkyne	x+y	x	y
1-pentyne	12	8	4
	18	10	8
	26	11	15
1-hexyne	18	10	8
	26	12	14
1-heptyne	26	12	14
1-octyne	26	12	14

Table 1-1. Nuclearity and ligand ratios[1, 21-23] observed in $[Cu_{x+y}(hfac)_x(alkynyl)_y]$ clusters prior to the work undertaken in this thesis

1.4 The chemistry of β-diketonate ligands

The ability of β-diktonates to form stable metal complexes has long been recognized. The earliest example, $[Cu(acac)_2]$ (Figure 1-2), was reported in 1887[24] and by the early 1960's, over sixty copper(II) β-diketonates were known.[25, 26]

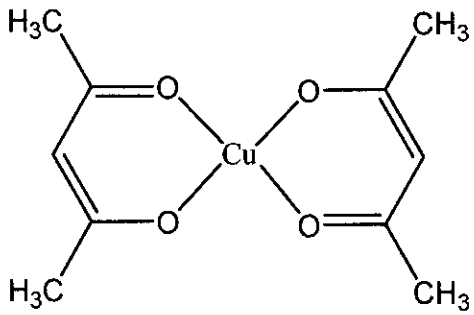

Figure 1-2. Structure of $[Cu(acac)_2]$

Since these early investigations a vast amount of research has been published on β-diketonate coordination chemistry and it is outside the scope of this report to give a

comprehensive review. The following section focuses on the fundamental properties of fluorinated β-diketone ligands and how the presence of $-CF_3$ groups effect their coordination behaviour.

1.4.1 Keto-enol tautomerisation in hfacH and its derivatives

The solution and solid-state properties of β-diketones has been the subject of extensive investigations. Of particular interest is the study of keto–enol tautomerism in solution as this is directly linked to the behaviour of the β-diketonate as a chelating ligand.

NMR, photoelectron and infrared spectroscopy along with theoretical calculations have shown that the most stable tautomer of acetylacetone (acacH), in solution and the gas phase, is the enol (Figure 1-3).[27-39] The asymmetric structure is strongly stabilized by intramolecular C=O --- H-O-C hydrogen bonding, forming a conjugated π-electron system.

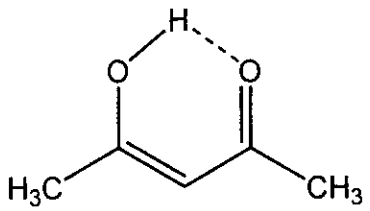

Figure 1-3. Enol configuration of acacH

Similar studies have been performed on the fluorinated acacH derivative, hfacH, and related asymmetric β-diketones.[30, 40-47] These studies have shown that hfacH also adopts an enol tautomer with a H–bonding bridge. Where asymmetric β-diketone ligands have an electron withdrawing substituent, the formation of the enol is favoured where the O-H group lies on the adjacent carbon to the substituent. As the $-CF_3$ group is highly electron withdrawing, trifluorinated acacH derivatives adopt the enolic configuration in solution where the O-H group lies on the adjacent carbon to the CF_3- (Figure 1-4).

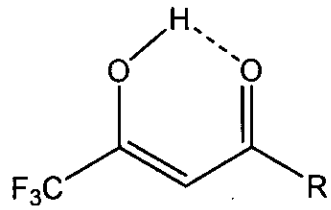

Figure 1-4. Enol configuration adopted by trifluorinated acacH derivatives

In fluorinated β-diketone ligands, the propensity to form the enolic tautomer is intrinsically linked to the basicity of the ligand and therefore the stability of the metal-diketonate complexes they form. Groups that are capable of decreasing electron density near the oxygen atoms decrease the basicity of the ligand. In trifluorinated β-diketone ligands, the enol group resides on the carbon adjacent to the CF_3- group and so the enolic proton is acidic relative to corresponding non-fluorinated molecules. As a result the nature of the non-fluorinated substituent have relatively little effect on ligand pK_a (Table 1-2).

R_1	R_2	pK_a
CF_3	CF_3	6.0
CF_3	CH_3	8.7
CF_3	C_6H_5	9.2
CH_3	CH_3	12.70
C_6H_5	C_6H_5	12.85

Table 1-2. Acid dissociation constants of selected β-diketone ligands, R_1-C(OH)CHCO-R_2[40]

1.4.2 The coordination chemistry of fluorinated β-diketone ligands

The majority of fluorinated Cu-β-diketonate complexes have been reported as part of studies into suitable CVD precursors and have the formula, [Cu(β-diketonate)L] (L = neutral ligand). Table 1-3 shows some examples of combinations observed.

[Cu(β-diketonate)L]		
β-diketonate	**L**	**Reference**
hfac	7-t-BuO-NBD	14
tfac	7-t-BuO-NBD	14
acac	7-t-BuO-NBD	14
tfac	7-t-BuO-NBD	14
Ph-tfac	7-t-BuO-NBD	14
hfac	$(PMe_3)_{1 \text{ or } 2}$	10
tfac	$(PMe_3)_{1 \text{ or } 2}$	10
acac	$(PMe_3)_{1 \text{ or } 2}$	10
hfac	1,5-COD	12
hfac	BTMSA	12
hfac	2-butyne	12
hfac	PEt_3	12
hfac	$(MeCN)_2$	15
hfac	$(Me_3CCN)_2$	15
hfac	$(MeOC(O)CHCN)_2$	15

Table 1-3. Examples of [Cu(β-diketonate)L_x] type complexes where7-t-BuO-NBD = 7-*tert*-butoxynorbornadiene, 1,5-COD = 1,5-cyclooctadiene, BTMSA = bis(trimethylsilyl)acetylene, tfac = trifluoroacetylacetonate and Ph-tfac = 4,4,4-trifluoro-1-phenyl-1,3-butanedione.

The series of [Cu(β-diketonate)L_x] complexes is synthesized from a range of ligands that have similar coordinating properties. The β-diketonate ligands coordinate copper through the oxygen atoms, forming six-membered Cu-chelate rings. These are stabilised by additional neutral ligands that accept electron density from the d^{10} copper(I), preventing spontaneous disproportionation.

As part of the analysis into suitability for use in CVD processes, a number of thermal stability experiments were performed on molecules with formula, [Cu(hfac)L_x]. [16] The stability of [Cu(β-diketonate)L_x] complexes was shown to increase as the degree of fluorination of the β-diketonate ligand increases, hfac>tfac>acac and as a result, copper complexes coordinated to hfac were found to be better CVD precursor than corresponding tfac and acac complexes. These were sufficiently stable to reach a temperature were the disproportionation decomposition pathway is induced whereas tfac

and acac derivatives had the tendency to thermally decompose prior to disproportionation.

1.5 The chemistry of alkynyl ligands

The alkyne group, RC≡CH, is a versatile functional group and has proved useful in a variety of applications. The presence of loosely held π electrons within the C≡C triple bond makes the alkyne group highly reactive towards electrophilic reagents. The relatively acidic terminal alkyne allows the formation of organometallic species, M^{+-} C≡CR, which can be used in the formation of carbon-carbon bonds through reaction with an electrophilic carbon.[48] It is the use of terminal alkynes and alkynyl groups as ligands in coordination chemistry, however, that is of interest in this thesis.

1.5.1 The alkynyl group

The alkyne group has a C≡C triple bond consisting of two perpendicular overlapping *P*-orbitals and one overlapping *sp* hybridised orbital (Figure 1-5). It coordinates metals through the donation of π-electron density from the overlapping *p* orbitals into metal σ-acceptor orbitals. It acts as a two-electron donor when coordinated to a single metal centre and as a four-electron donor when in a bridging coordination mode where it donates electrons from both its orthogonal π-orbitals. The two sets of π bonding orbitals give rise to two π* anti-bonding orbitals. These can accept electron density from filled metal d orbitals which leads to significant C-C bond lengthening.

Terminal alkyne protons are acidic relative to those bonded to sp^3- and sp^2- hybridised carbon atoms. This can be attributed to the electronic configuration of the conjugate anions. The lone pair of electrons on an acetylide anion ($HC{\equiv}C^-$) occupies a *sp* orbital so has a high degree of s-orbital character. Consequently the lone pair of the acetylide anion is held closely to the carbon atom nucleus making the anion weakly basic relative to the corresponding ethyl ($CH_3CH_2^-$) or vinyl ($CH_2{=}CH^-$) anions. Conversely, the alkyne hydrogen atom is more acidic than ethane or ethene hydrogens. The weak acidity

of the terminal alkyne proton allows the formation of organometallic metal-alkynyl species.

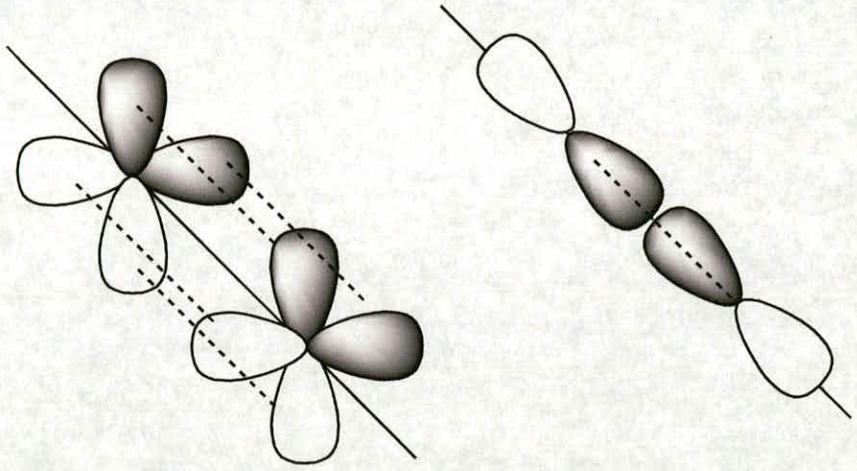

Perpendicular *p* orbital overlap *sp* hybridised orbital overlap

Figure 1-5. Bonding orbital overlap in the alkyne functional group

When a terminal alkyne is deprotonated to form an alkynyl, the electron pair of the *sp* hybridised orbital that formed the terminal carbon-hydrogen bond becomes available for donation into metal orbitals. The alkynyl ligand has three populated orbitals capable of donor interactions with metal centres (one *sp* and two $p\pi$ overlaps) acting as two-, four- or six-electron donors[49] and can accept 'back bonding' metal d electrons into vacant π^* orbitals. As a result, terminal alkynyls are versatile bridging ligands and can form numerous bridging modes (Figure 1-6). Two comprehensive reviews of metal alkynyl chemistry have been published by Nast[50] and Manna *et al*[51] and these deal with the full range of metal-alkynyl complexes reported to date. However for the purposes of this report the remainder of this section will focus on Cu-alkynyl complexes.

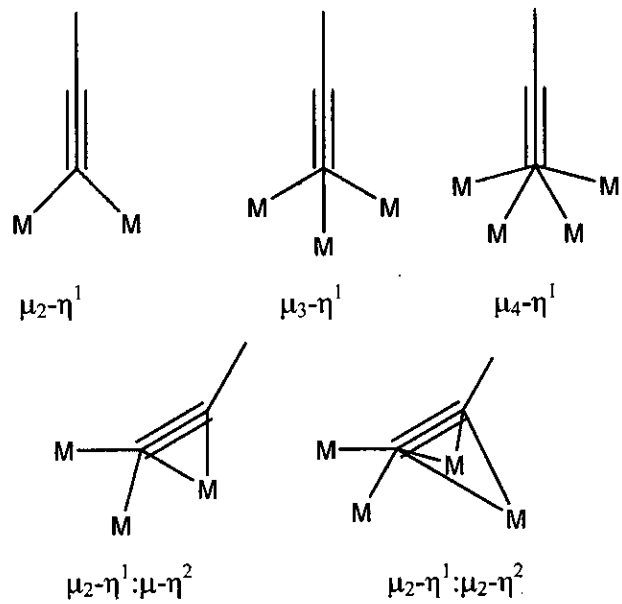

Figure 1-6. Potential alkynyl-metal bridging modes

1.5.2 Cu(I) – alkynyl coordination chemistry

A variety of polynuclear Cu-alkynyl complexes and clusters have been reported and synthetic strategies for the preparation of a wide variety of compounds are available.[52] The vast majority contain between two and six copper atoms and, as well as bridging alkynyl ligands, these molecules generally contain soft donor ligands such as phosphines and nitriles. The range of structures reflects the versatility of the alkynyl group as a bridging ligand with examples of all the bonding modes in Figure 1-6 present.

The first structurally characterised discrete Cu(I)-alkynyl system, $[PhC{\equiv}CCuP(CH_3)_3]_4$ (Figure 1-7) was reported in 1966 by Corfield and Shearer.[53] It was prepared by partial disruption of the polymeric structure of $[(PhC{\equiv}C)Cu]_n$ with the soft donor ligand, $P(CH_3)_3$. The molecule crystallized as a tetramer, bridged by μ_2-η^1:μ-η^2 alkynyl ligands (Figure 1-6). Similar techniques have been used to synthesise complexes containing two and four copper atoms.[54, 55]

A more controllable synthetic route to trimetallic Cu-alkynyl systems was reported by Gimeno *et al.*[56] By reacting $[Cu_2(\mu\text{-dppm})_2(MeCN)_2][BF_4]$ (dppm = bis-

(diphenylphosphino)methane) with LiC≡CR (R = Ph, ^{t}Bu and CH_2OCH_3) in a molar ratio of 3:2, a triangular alkynyl capped complex with formula $[Cu_3(\mu_3\text{-}\eta^1\text{-}C{\equiv}CR)(\mu\text{-}dppm)_3][BF_4]_2$ was prepared similar to that shown in Figure 1-8. This strategy has been used by Yam *et al.* to tune the physical properties of Cu_3 complexes by varying the bridging bis-phosphine ligand and the alkynyl substituent.[57-60]

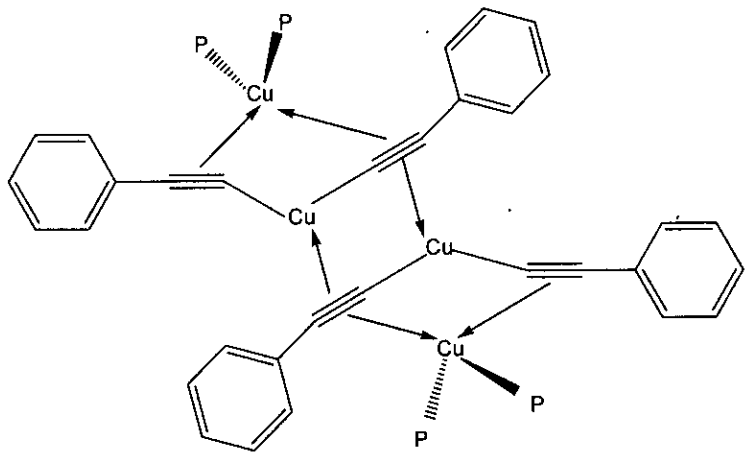

Figure 1-7. Bonding scheme for $[Me_3PCuC{\equiv}CPH)]_4$

Copper-alkynyl complexes have also been prepared by ligand exchange of monoanionic bridging ligands with alkynyl ligands on pre-formed molecules.[61-66] Several examples of this approach have been reported and involve the reaction of halide bridged Cu complexes with LiC≡CR. The highest nuclearity systems obtained in this way have six copper atoms.

Numerous other Cu-alkynyl complexes have been reported using a variety of different synthetic procedures as well as many mixed metal systems. [67-79]

1.6 Physical properties of metal-alkynyl complexes

The field of metal-alkynyl chemistry is expanding rapidly due to the increasing interest in their physicochemical properties for use in advanced materials applications. Metal containing organic acetylene polymers were first reported by Hagihara *et al.*[80, 81] have been shown to have numerous potentially interesting properties. They consist of chains of metals separated by a highly conjugated π- backbone. This extended, delocalised

electronic system allows the mobility of charge carriers to create conducting materials and[82, 83] is thought to be responsible for third order non-linear optical polarization properties.[84, 85]

One of the most widely studied properties of non-polymeric metal alkynyl systems in recent years is their photoluminescence and a large percentage of the reported metal-alkynyl complexes were synthesised as part of these investigations.[2, 60, 86, 87] In the following section a brief review of this work is provided, focusing on Cu-alkynyl complexes.

1.6.1 Luminescence of Cu-alkynyl complexes

Yam *et al.* have made a significant contribution to the field of luminescent d^{10} metal-alkynyl complexes[2] and a summary of their findings is given below.

A series of trinuclear systems with formulae, $[Cu_3(\mu\text{-dppm})_3(\mu_3\text{-}\eta^1\text{-}C{\equiv}CR)_2]^+$ and $[Cu_3(\mu\text{-dppm})_3(\mu_3\text{-}\eta^1\text{-}C{\equiv}CR)]^{2+}$ (Figure 1-8) were obtained where the substituents on the phenyl group, R, and the bridging phosphine ligand were systematically varied.[58, 88, 89] All complexes in this series displayed intense and long-lived luminescence upon photoexcitation. It was shown that increasing the electron-donating ability of the alkynyl group by variation of the phenyl, R, group resulted in a shift of emission to lower energy. The origin of the emission in this series was assigned to substantial LMCT [$RC{\equiv}C \rightarrow Cu_3$] character with the possibility of mixing of a metal-centred $3d^9 4s^1$ state into the lowest lying emissive state.[2]

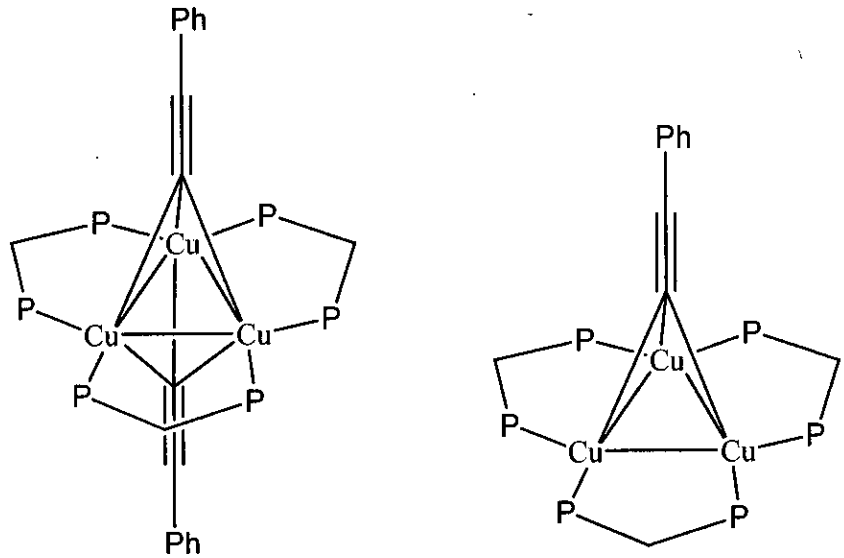

Figure 1-8. Diagram of $[Cu_3(\mu\text{-dppm})_3(\mu_3\text{-}\eta^1\text{-}C{\equiv}CR)_2]^+$ and $[Cu_3(\mu\text{-dppm})_3(\mu_3\text{-}\eta^1\text{-}C{\equiv}CR)]^{2+}$

A series of tetranuclear copper-alkynyl complexes, $[Cu_4(PR_3)_4(\mu_3\text{-}\eta^1\text{-}C{\equiv}C\text{-}R')_4]$ (Figure 1-9) and $[Cu_4(\mu\text{-dppm})_4(\mu_4\text{-}\eta^1, \eta^2\text{-}C{\equiv}C)]^{2+}$, were also shown to exhibit rich luminescent properties.[68] The excited state of the $[Cu_4(PR_3)_4(\mu_3\text{-}\eta^1\text{-}C{\equiv}C\text{-}R')_4]$ systems was tentatively assigned to cluster centred (*d-s*) character mixed with some LMCT [$RC{\equiv}C \rightarrow Cu_4$] character whereas the excited state of $[Cu_4(\mu\text{-dppm})_4(\mu_4\text{-}\eta^1, \eta^2\text{-}C{\equiv}C)]^{2+}$ was thought to contain only [$C{\equiv}C^{2-} \rightarrow Cu_4$] character.

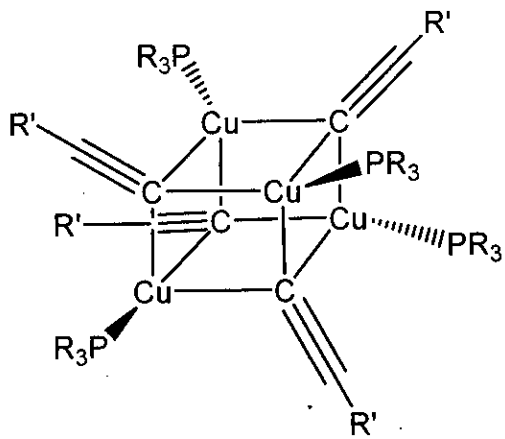

Figure 1-9. Diagram of $[Cu_4(\mu\text{-dppm})_4(\mu_4\text{-}\eta^1, \eta^2\text{-}C{\equiv}C)]^{2+}$

Trinuclear complexes of the type shown in Figure 1-8 were used as 'building blocks' and linked *via* a 1,4-diethynylbenzene linker to obtain a hexanuclear system.[57] As with the tri- and tetra- nuclear clusters, the emission of this molecule was shown to derive from a highly mixed combination of metal (*d-s*) and LMCT [RC≡C → Cu_3] excited states.[57]

Recently, derivatives of the trimeric and tetrameric systems have been synthesised using diynyl (RC≡CC≡C$^-$) in place of alkynyl ligands.[90, 91] The diynyl ligands bridge the copper atoms *via* the same bonding mode as the alkynyl ligands and are thought to make a similar contribution to the luminescent properties of the molecules.

As a result of the initial work into the luminescence of copper(I)-alkynyl complexes by Yam *et al*, the area has attracted wider interest and a number of other groups have also reported interesting examples. Mak *et al* reported a structure with formula, $[Cu_4(\mu\text{-}Ph_2Ppypz)_4(\mu_4\text{-}\eta^1, \eta^2\text{-}C{\equiv}C)]^{2+}$ [Ppypz = 2-(diphenylphosphino-6-pyrazol-1-yl)pyridine][67] that was closely related, structurally and spectroscopically, to the $[Cu_4(\mu\text{-}dppm)_4(\mu_4\text{-}\eta^1, \eta^2\text{-}C{\equiv}C)]^{2+}$ system reported by Yam. Mao *et al* described a series of heteronuclear Ag^I-Cu^I complexes with formula, $[Ag_4Cu_2(\mu\text{-}Ph_2PNHPPh_2)_4(C{\equiv}CC_6H_4R\text{-}4)_4](ClO_4)_2]$, $[Ag_6Cu_2(\mu\text{-}Ph_2PCH_2PPh_2)_3(C{\equiv}CC_6H_4R\text{-}4)_6(MeCN)](ClO_4)_2]$ (R = H, CH_3) and $[Ag_6Cu_2(\mu\text{-}Ph_2PCH_2PPh_2)_3(C{\equiv}CC_6H_4COCH_3\text{-}4)_6]_2(ClO_4)_4]$, which as well as displaying interesting new structures, had intense luminescent properties derived from a LMCT [RC≡C → Ag_4Cu_2 or Ag_4Cu_2] transition mixed with a metal cluster centred ($d \rightarrow s$) excited state.[92]

1.7 Project aims and layout of the thesis

As copper-alkynyl complexes are of great current interest due to their potential use in NLO, conducting and luminescent materials it is important to define the synthetic scope of reactions to form $[Cu_{x+y}(hfac)_x(RC{\equiv}C)_y]$ clusters and then establish to what extent the structures and properties can be tuned by varying the nature of the ligands.

The work in this thesis had three aims,

i) to vary the ligand components of the cluster-forming reaction to extend the family of $[Cu_{x+y}(hfac)_x(RC{\equiv}C)_y]$ clusters,

ii) to understand how these complex molecules assemble and

iii) to identify and study potentially interesting physical properties.

The results described in chapter 2-4 do not represent the chronological order of the work. The clusters are described in order of increasing nuclearity allowing us to define structural similarities and analyse the factors which lead to high or low nuclearity. Chapter 5 outlines a study of the photoluminescent properties of a selection of $[Cu_{x+y}(hfac)_x(C{\equiv}CR)_y]$ clusters and related complexes. Chapter six describes some preliminary studies aimed at linking polynuclear complexes with formula, $[C_5(bta)_6(acac)_4]$ using bifunctional ligands.

References

1 T. C. Higgs, P. J. Bailey, S. Parsons, and P. A. Tasker, *Angew. Chem. Int. Ed.* , 2002, **41**, 3038.

2 V. W. W. Yam and K. K. W. Lo, *Chem. Soc. Rev.*, 1999, **28**, 323.

3 F. Habashi, in 'Handbook of extractive metallurgy / edited by Faith Habashi.' Weinheim ; Chichester :, 1997.

4 R. G. Pearson, *Inorganic Chemistry*, 1988, **27**, 734.

5 D. F. Shriver and P. W. Atkins, 'Inorganic Chemistry', Oxford University Press, 1999.

6 S. P. Murarka and M. C. Peckerar, 'Electronic Materials Science and Technology', Academic Press, 1989.

7 J. Kim, S.-H. Wen, D. Y. Jung, and R. W. Johnson, *IBM J. Res. Dev.*, 1984, **28**, 697.

8 S. P. Murarka and S. W. Hymes, *Crit. Rev. Solid State Mater. Sci.* , 1995, **20**, 87.

9 I. P. Herman, *Chem. Rev.*, 1989, **89**, 1323.

10 V. N. Vertoprakhov and S. A. Krupoder, *Russ. Chem. Rev.*, 2000, **69**, 1057.

11 A. Sherman, 'Chemical Vapour Deposition for Microelectronics', Noyes Publications, 1987.

12 F. A. Houle, C. R. Jones, T. Baum, C. Pico, and C. A. Kovac, *Appl. Phys. Lett.* , 1985, **46**, 204.

13 C. Oehr and H. Suhr, *Appl. Phys. A* 1988, **A45**, 151.

14 Y. Hazuki, H. Yano, and K. Horioka, *Mater. Res. Soc., Symp. Proc.* 1990, **115**, 351.

15 H. K. Shin, K. M. Chi, J. Farkas, M. J. Hampden-Smith, T. T. Kodas, and E. N. Duesler, *Inorg. Chem.*, 1992, **31**, 424.

16 H. K. Shin, K. M. Chi, M. J. Hampden-Smith, T. T. Kodas, J. D. Farr, and M. Paffett, *Chem. Mater.* , 1992, **4**, 788.

17 H. K. Shin, M. J. Hampden-Smith, T. T. Kodas, and A. L. Rheingold, *Chem. Commun.* , 1992, 217.

18 A. Jain, K. M. Chi, T. T. Kodas, M. J. Hampden-Smith, J. D. Farr, and M. F. Paffett, *Chem. Mater.* , 1991, **3**, 995.

19 K. M. Chi, H. K. Shin, M. J. Hampden-Smith, T. T. Kodas, and E. N. Duesler, *Inorg. Chem.*, 1991, **30**, 4293.

20 K.-M. Chi, H.-C. Hou, P.-T. u. Hung, S.-M. Peng, and G.-H. Lee, *Organometallics.*, 1995, **14**, 2641.

21 T. C. Higgs and P. A. Tasker, *Unpublished work, University of Edinburgh*, 2003.

22 T. C. Higgs, S. Parsons, P. J. Bailey, A. C. Jones, F. McLachlan, A. Parkin, A. Dawson, and P. A. Tasker, *Organometallics.*, 2002, **21**, 5692.

23 T. C. Higgs, S. Parsons, A. C. Jones, P. J. Bailey, and P. A. Tasker, *Dalton Trans.* , 2002, 3427.

24 A. Combes, *C.R. Hebd. Seacnces Acad. Sci.*, 1887, **105**, 868.

25 J. P. Fackler, Jr. and F. A. Cotton, *Inorg. Chem.*, 1963, **2**, 102.

[26] J. P. Fackler, Jr., *Prog. Inorg. Chem.* , 1966, 7, 361.

[27] A. Schweig, H. Vermeer, and U. Weidner, *Chem. Phys. Lett.* , 1974, **26**, 229.

[28] M. M. Folkendt, B. E. Weiss-Lopez, J. P. Chauvel, Jr., and N. S. True, *J. Phys. Chem.* , 1985, **89**, 3347.

[29] M. T. Rogers and J. L. Burdett, *Can. J. Chem.* , 1965, **43**, 1516.

[30] M. Bassetti, G. Cerichelli, and B. Floris, *Tetrahedron*, 1988, **44**, 2997.

[31] R. Mecke and E. Funck, *Z. Elektrochem.*, 1956, **60**, 1124.

[32] H. Ogoshi and K. Nakamoto, *J. Chem. Phys.* , 1966, **45**, 3113.

[33] T. Chiavassa, P. Verlaque, L. Pizzala, A. Allouche, and P. Roubin, *J. Phys. Chem.* , 1993, **97**, 5917.

[34] S. F. Tayyari, F. Milani-Nejad, and H. Rahemi, *Spectrochim. Acta, Part A* 2002, **58A**, 1669.

[35] H. Nakanishi, H. Morita, and S. Nagakura, *Bull. Chem. Soc. Jpn.* , 1977, **50**, 2255.

[36] K. N. Walzl, I. M. Xavier, Jr., and A. Kuppermann, *J. Chem. Phys.* , 1987, **86**, 6701.

[37] D. Veierov, T. Bercovici, E. Fischer, Y. Mazur, and A. Yogev, *J. Am. Chem. Soc.* , 1977, **99**, 2723.

[38] P. Roubin, T. Chiavassa, P. Verlaque, L. Pizzala, and H. Bodot, *Chem. Phys. Lett.* , 1990, **175**, 655.

[39] T. Chiavassa, P. Verlaque, L. Pizzala, and P. Roubin, *Spectrochim. Acta, Part A* 1994, **50A**, 343.

[40] R. L. Lintvedt and H. F. Holtzclaw, Jr., *Inorg. Chem.*, 1966, **5**, 239.

[41] T. J. Pinnavaia and R. C. Fay, *Inorg. Chem.*, 1966, **5**, 233.

[42] G. Buemi, *THEOCHEM* 2000, **499**, 21.

[43] N. Nagashima, S. Kudoh, and M. Nakata, *Chem. Phys. Lett.* , 2003, **374**, 59.

[44] Y. Kwon, *Magn. Reson. Chem.* , 2001, **39**, 89.

[45] Y. Minoura, N. Nagashima, S. Kudoh, and M. Nakata, *J. Phys. Chem. A* 2004, **108**, 2353.

[46] C. F. G. C. Geraldes, M. T. Barros, C. D. Maycock, and M. I. Silva, *J. Mol. Struct.* , 1990, **238**, 335.

[47] M. Gorodetsky, Z. Luz, and Y. Mazur, *J. Am. Chem. Soc.* , 1967, **89**, 1183.

[48] K. Osakada and T. Yamamoto, *Coord. Chem. Rev.*, 2000, **198**, 379.

[49] E. W. Abel, F. G. A. Stone, G. Wilkinson, and Editors, 'Comprehensive Organometallic Chemistry II: A Review of the Literature 1982-1994, 14 Volume Set', 1995.

[50] R. Nast, *Coord. Chem. Rev.*, 1982, **47**, 89.

[51] J. Manna, K. D. John, and M. D. Hopkins, *Adv. Organomet. Chem.* , 1995, **38**, 79.

[52] W. Beck, B. Niemer, and M. Wieser, *Angew.-Chem.-Int. Ed.*, 1993, **32**, 923.

[53] P. W. R. C. H. M. M. Shearer, *Acta Crystallographica*, 1966, **21**, 957.

[54] V. W. W. Yam, W. K. Lee, and K. K. Cheung, *Dalton Trans.*, 1996, 2335.

[55] V. W. W. Yam, W. K. Lee, K. K. Cheung, H. J. Lee, and W. P. Leung, *Dalton Trans.*, 1996, 2889.

[56] J. Diez, M. P. Gamasa, J. Gimeno, E. Lastra, A. Aguirre, and S. Garcia Granda, *Organometallics*, 1993, **12**, 2213.

[57] V. W. W. Yam, W. K. M. Fung, and K. K. Cheung, *Chem. Commun.*, 1997, 963.

[58] V. W. W. Yam, W. K. M. Fung, and M. T. Wong, *Organometallics*, 1997, **16**, 1772.

[59] V. W. W. Yam, W. K. M. Fung, and K. K. Cheung, *Angewandte Chemie-International Edition in English*, 1996, **35**, 1100.

[60] V. W. W. Yam, W. K. M. Fung, and K. K. Cheung, *Organometallics*, 1998, **17**, 3293.

[61] J. G. Noltes, G. van Koten, *Chem. Commun.*, 1974, 575.

[62] A. J. Edwards, M. A. Paver, P. R. Raithby, M. A. Rennie, C. A. Russell, and D. S. Wright, *Organometallics.*, 1994, **13**, 4967.

[63] M. D. Janssen, J. G. Donkervoort, S. B. van Berlekom, A. L. Spek, D. M. Grove, and G. van Koten, *Inorg. Chem.*, 1996, **35**, 4752.

[64] J. Diez, M. P. Gamasa, J. Gimeno, A. Aguirre, and S. Garcia Granda, *Organometallics.*, 1997, **16**, 3684.

[65] J. Diez, M. P. Gamasa, J. Gimeno, A. Aguirre, S. Garcia-Granda, J. Holubova, and L. R. Falvello, *Organometallics.*, 1999, **18**, 662.

[66] V. W. W. Yam, C. H. Lam, and K. K. Cheung, *Inorg. Chim. Acta* 2001, **316**, 19.

[67] H.-B. Song, Q.-M. Wang, T. C. W. Mak, and Z.-Z. Zhang, *Chem. Commun.*, 2001, 1658.

[68] V. W.-W. Yam, W. K.-M. Fumg, and K.-K. Cheung, *Angew. Chem. Int. Ed.* , 1996, **35**, 1100.

[69] G. van Koten, J. G. Noltes. R.W. M. ten Hoedt, *J. Organomet. Chem.* , 1977, **133**, 113.

[70] J. G. Noltes, R. W. M. ten Hoedt, G. van Koten, A. L. Spek, *Dalton Trans.* , 1978, 1800.

[71] M. P. Gamasa, J. Gimeno, E. Lastra, and X. Solans, *J. Organomet. Chem.* , 1988, **346**, 277.

[72] L. Naldini, F. Demartin, M. Manassero, M. Sansoni, G. Rassu, and M. A. Zoroddu, *J. Organomet. Chem.* , 1985, **279**, C42.

[73] D. M. Knotter, A. L. Spek, D. M. Grove, and G. Vankoten, *Organometallics.*, 1992, **11**, 4083.

[74] K. Osakada, T. Takizawa, and T. Yamamoto, *Organometallics.*, 1995, **14**, 3531.

[75] V. W. W. Yam, S. W. K. Choi, C. L. Chan, and K. K. Cheung, *Chem. Commun.*, 1996, 2067.

[76] M. G. B. Drew, F. S. Esho, and S. M. Nelson, *Chem. Commun.*, 1982, 1347.

[77] D. M. Knotter, A. L. Spek, and G. van Koten, *Chem. Commun.*, 1989, 1738.

[78] Y. G. Ma, W. H. Chan, X. M. Zhou, and C. M. Che, *New J. Chem.*, 1999, **23**, 263.

[79] F. Olbrich, J. Kopf, and E. Weiss, *Angew. Chem.-Int. Edit. Engl.*, 1993, **32**, 1077.

[80] S. Takahashi, M. Kariya, T. Yatake, K. Sonogashira, and N. Hagihara, *Macromolecules*, 1978, **11**, 1063.

[81] K. Sonogashira, K. Ohga, S. Takahashi, and N. Hagihara, *J. Organomet. Chem.* , 1980, **188**, 237.

82 H. S. Nalwa, *Appl. Organomet. Chem.* , 1990, **4**, 91.

83 P. F. H. Schwab, M. D. Levin, and J. Michl, *Chem. Rev. (Washington, D. C.)*, 1999, **99**, 1863.

84 N. J. Long, *Angew. Chem.-Int. Edit. Engl.*, 1995, **34**, 21.

85 ACS Symp. Ser., 1983, p. 233.

86 V. W. W. Yam, K. K. W. Lo, W. K. M. Fung, and C. R. Wang, *Coord. Chem. Rev.*, 1998, **171**, 17.

87 V. W.-W. Yam, *J. Organomet. Chem.* , 2004, **689**, 1393.

88 V. W. W. Yam, W. K. Lee, and T. F. Lai, *Organometallics.*, 1993, **12**, 2383.

89 V. W. W. Yam, W. K. M. Fung, and K. K. Cheung, *J. Clust. Sci.*, 1999, **10**, 37.

90 V. W.-W. Yam, C.-H. Lam, and N. Zhu, *Inorg. Chim. Acta* 2002, **331**, 239.

91 W.-Y. Lo, C.-H. Lam, V. W.-W. Yam, N. Zhu, K.-K. Cheung, S. Fathallah, S. Messaoudi, B. Le Guennic, S. Kahlal, and J.-F. Halet, *J. Am. Chem. Soc.* , 2004, **126**, 7300.

92 Q.-H. Wei, G.-Q. Yin, L.-Y. Zhang, L.-X. Shi, Z.-W. Mao, and Z.-N. Chen, *Inorg. Chem.*, 2004, **43**, 3484.

Chapter two

Cu_{10} and Cu_{12} Clusters

2.1 Introduction

The new Cu_{10}-alkynyl and Cu_{12}-alkynyl clusters described in this chapter have structures based on *pseudo* four-fold symmetric cores which are related to smaller Cu_4-organometallic complexes containing other bridging ligands which have been previously reported. A survey of the structure and bonding in these is described below.

2.1.1 Cu_4 based molecules

The widespread use of organocopper reagents in organic synthesis[1] has led to numerous studies of their solution and solid-state behavior. As a result several complexes that contain a carbon bridged Cu_4C_4 structural motif (Figure 2-1) are known. Jarvis *et al.*[2] reported the first crystal structure of a Cu – alkyl complex, $(Me_3SiCH_2Cu)_4$, with a planar square arrangement of Cu atoms (Cu – Cu 2.42 Å) bridged by μ_2-CH_2SiMe_3 ligands. Each alkyl ligand forms 3C-2e$^-$ bonds with two copper centres resulting in C – Cu – C angles of 164° and a 'pinching in' of the Cu atoms on the sides of the C_4 square.

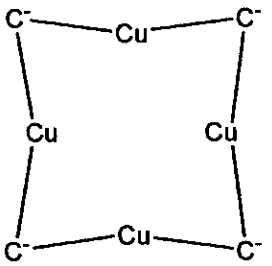

Figure 2-1. Cu_4C_4 Core.

Since the first report of a tetranuclear organocopper structure a number of clusters with the general formula $[Cu_4(aryl)_4]$ have been characterised using the aryl ligands, 2,4,6-triisopropylphenyl (2,4,6-iPr$_3$C$_6$H$_2^-$),[3] pentamethylphenyl ($C_6Me_5^-$),[4] thienyl ($C_4H_3S^-$),[5] pentafluorophenyl ($C_6F_5^-$),[6] mesityl (2,4,6-$Me_3C_6H_2^-$)[7] and *o*-vinylphenyl.[8] These clusters also have a planar square arrangement of four Cu atoms bridged by aryl ligands aligned perpendicular to the Cu plane and adjacent Cu – Cu distances in the range 2.413(2) – 2.507(3) Å.

Where the aryl ligands are pentamethylphenyl,[4] mesityl[7] and thienyl[5] the coordinating C_{ipso} atoms lie in the same plane as the Cu_4 core forming a planar Cu_4C_4 ring (Figure 2-1). The bridging modes are symmetrical and the C_{ipso} – Cu – C_{ipso} bond angles all fall in the range 162.8° – 164.8° which is close to the value estimated for a C – Cu – C fragment in which linear sp copper hybrid orbitals participate (Figure 2-2).[9]

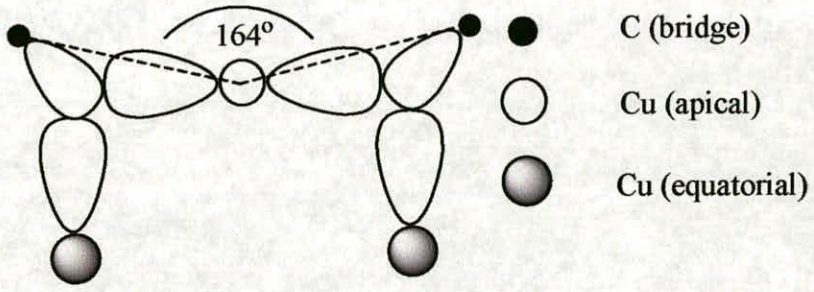

Figure 2-2. Preferred central angle in the 3C-2e⁻ bridged C_2Cu_3 unit

Bridging C_{ipso} atoms in tetrameric triisopropylphenylcopper,[3] pentafluorophenylcopper[6] and o-vinylphenylcopper[8] lie alternately above and below the Cu plane forming a 'puckered' ring (Figure 2-3). [Triisopropylphenylcopper]$_4$ and [pentafluorophenyl-copper]$_4$ show unusual unsymmetrical Cu – C_{ipso} – Cu bridging modes. These are attributed to a slightly different bonding mode from the example in Figure 2-2. In the asymmetric bridging modes one C_{ipso} forms a 2c–2e⁻ σ-bond with one Cu and another slightly longer bond between an electron-rich π-orbital perpendicular to the plane of the ring with an empty *ds* orbital of the neighbouring Cu atom. Consistent with this is the fact that the C – Cu – C angles are almost linear. It has been suggested that this asymmetric bridging mode and deviation from Cu_4C_4 planarity is a result of steric interactions.[10]

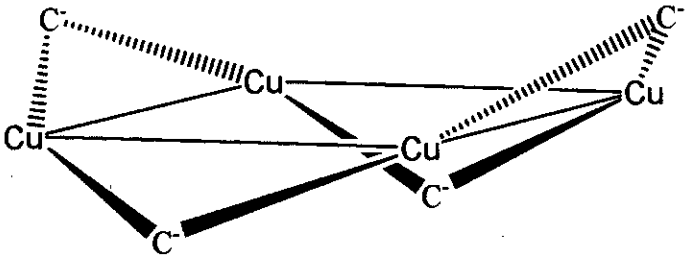

Figure 2-3 . Puckered Cu_4C_4 ring

Using Me_2S or tetrathiophene as reaction or crystallization solvents led to solvated examples of the $[Cu_4(aryl)_4]$ systems, $[Cu_4Ph_4(SMe_2)_2]$,[11] $[Cu_4Mes_4(C_4H_8S)_2]$,[12-14] and $[Cu_4(C_6H_4Me\text{-}2)_4(SMe_2)_2]$[14] were isolated in this way. These complexes have rhombus-shaped coplanar Cu_4 cores with one short [2.600(3) - 2.717(2) Å] and one long [4.0105(7) – 4.101(3) Å] diagonal Cu – Cu contact. The sulphur ligands coordinate to two opposed copper atoms which define the longer diagonal of the rhombus (Figure 2-4).

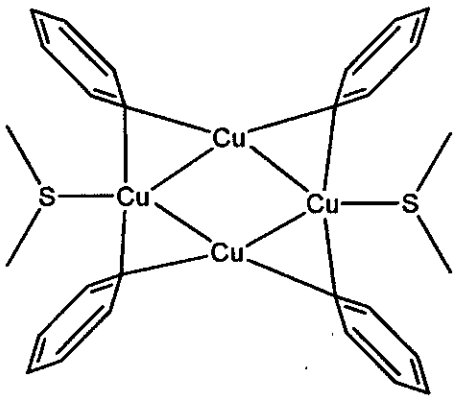

Figure 2-4. Rhombus shaped Cu_4 core in solvated $[Cu_4(aryl)_4]$ type clusters

$[Cu_4Mes_4(SC_4H_8)_2]$ and $[Cu_4(C_6H_4Me\text{-}2)_4(SMe_2)_2]$ have similar ligand disposition to the puckered $[Cu_4(aryl)_4]$ complexes with the C_{ipso} atoms lying alternately above and below the Cu_4 plane as shown in Figure 2-3.

A higher thermal stability of these complexes relative to their unsubstituted analogues was observed which was attributed to the stabilising effect of additional metal coordination by Lewis bases.[14]

Another strategy employed to achieve greater stability of arylcopper clusters was to use aryl ligands that incorporate coordinating *ortho*-substituents. Several clusters with the formula $[Cu_4(L)_4]$ were structurally characterised [L = $C_6H_4CH_2NMe_2$-2,[15] 5-Me-$C_6H_3CH_2NMe_2$-2[16] and 8-(dimethylamino)naphthyl][17] where the *ortho*-substituents act as intramolecular ligands, stabilising the Cu_4C_4 ring. In the case of $[Cu_4(C_6H_4CH_2NMe_2\text{-}2)_4]$ and $[Cu_4(5\text{-}Me\text{-}C_6H_3CH_2NMe_2\text{-}2)_4]$ each Cu is bonded to an amino group and the planarity of the Cu_4 core is lost. Instead the metals adopt a distorted square arrangement.

One opposite pair of Cu atoms in the Cu_4 core of $[Cu_4(8\text{-(dimethylamino)naphthyl})_4]$ is coordinated by two napthylamino groups while the other pair of Cu atoms is bonded only to bridging carbons. The planarity of the Cu_4 core is retained and a rhombic distribution of Cu atoms is observed, similar to the distribution of Cu atoms seen in the $[Cu_4(aryl)_4(Me_2S)]$ series.

2.1.2 Theoretical studies of bonding arrangements

Group 11 metals in the +1 oxidation state have the propensity to form clusters with short metal – metal bond lengths[18] that show unusual chemical and physical properties. In order to explain these phenomena there has been extensive spectroscopic and theoretical research into the nature of the closed-shell interactions between d^{10} metals, in particular Au^+. A series of papers by Pykko *et al.* described the advances made in this field to date. It was shown that closed shell interactions in Au(I) compounds can be as large as 7 – 12 Kcal mol^{-1} and can be attributed to a correlation effect strengthened by relativistic contributions.[19-23]

Understanding of attractive Cu(I) - Cu(I) interactions is less well developed and some researchers dispute their existence, preferring to class them as nonbonding close contacts.[24, 25] Despite this, an increasing amount of evidence has appeared in the form of

crystal structures showing short Cu - Cu separations,[26, 27] convergent beam electron diffraction studies of Cu_2O,[28] spectroscopic studies[29] and theoretical studies.[19, 30-33]

Compounds of the type $[Cu_nR_n]$ (n = 3 – 5) have attracted the attention of theoretical chemists with an interest in cuprophilicity[34, 35] due to Cu – Cu contacts shorter than the corresponding distances found in the pure metal (256 pm).[36] These studies have provided useful evidence in support of proposed bridging modes.

The proposed MOs describing[10] aryl-copper bonding in $[Cu_4(aryl)_4]$ type systems are shown in Figure 2-5.

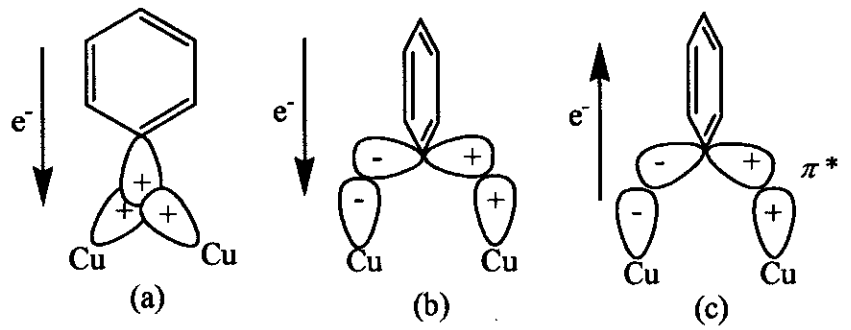

Figure 2-5. Proposed bonding schemes in $C_{ipso} – Cu_2$ bonding schemes

The lowest energy MO [Figure 2-5(a)] is a bonding combination of the $sp^2 – C_{ipso}$ orbital with mutually bonding orbitals on the two copper atoms (due to mixing of Cu 4s and 4p orbitals). The second MO [Figure 2-5(b)] is a combination of a $\pi – C_{ipso}$ orbital with anti-bonding combination of Cu orbitals and requires perpendicular orientation of the aryl ligand with respect to the Cu_4 plane. The third MO [Figure 2-5(c)] involves back donation from the Cu atoms to the aryl bridging ligand *via* overlap of filled mutually antibonding copper orbitals to a $\pi^* - C_{ipso}$ orbital.

Belanzoni *et al.*[34] used density functional methods to provide evidence for the proposed bonding interactions shown in Figure 2-5. It was calculated that two Cu(I) centers with occupation $3s^23p^63d^94s^1$ have an attractive interaction (-3.07 eV) and that this Cu_2^{2+} fragment can form a strong bond with one $(C_6H_5)^-$ group as indicated by the binding energy of –18.5 eV. The calculations showed that the bond consists of sp^2 orbitals of the bridging C^- atom overlapping the HOMO orbital of the Cu_2^{2+} fragment, a combination of

the 4s orbitals with some contribution from $4p_y$ and $3d_{x^2-y^2}$ orbitals [Figure 2-5(a)]. A small contribution to the bonding by the second MO [Figure 2-5(b)] was inferred and no back donation form Cu_2^{2+} to $(C_6H_5)^-$ [Figure 2-5(c)] was observed.

Schwerdtfeger *et al.*[35] used *ab-initio* quantum chemical methods to investigate whether the inward bending in $[Cu_4(aryl)_4]$ compounds is due to ring constraints or cuprophilic interactions and to what extent metal–metal bonding influences the cluster structure. It was shown that the C – Cu – C bond angles and short Cu–Cu contacts observed in these systems are partly due to Cu–Cu bonding with bond energies of up to 4 Kcal mol^{-1}. The calculations also indicated that Cu–Cu attractions become greater with increasing σ-donor and π-acceptor capability of the ligand.

2.1.3 Summary

In all known examples, C^- bridged Cu_4 cores adopt a square arrangement in the absence of additional coordinating groups. This is consistent with the explanation of bonding in the Cu_4C_4 core, i.e. bonding orbitals of the Cu_2^{2+} fragment overlap with aryl sp^2 orbitals creating C – Cu – C bonds that deviate slightly from linearity. When two opposed copper atoms are also bonded to S and N donors a planar rhombic conformation is adopted. When all four Cu atoms have additional coordinating groups, planarity is lost and a distorted tetrahedral 'butterfly' conformation is observed. The Cu_4C_4 ring can either adopt a completely planar arrangement or a 'puckered' configuration depending on the steric properties of the bridging ligand.

2.1.4 Novel Cu_4C_4 based clusters

This chapter reports the synthesis of five novel clusters: $[Cu_{12}(hfac)_8(C{\equiv}CBu^t)_4]$ **(2)**; $[Cu_{12}(hfac)_8(C{\equiv}CSiMe_3)_4]$ **(3)**; $[Cu_{10}(hfac)_6(C{\equiv}CBu^t)_4(Et_2O)]$ **(4a)**; $[Cu_{10}(hfac)_6(C{\equiv}CBu^t)_3(C{\equiv}CPr^n)(Et_2O)]$ **(4b)** and $[Cu_{10}(hfac)_6(C{\equiv}CBu^t)_4(Et_2O)]$ **(5)**, isolated as part of the investigation into the chemistry of the $[Cu_{x+y}(hfac)_x(alkynyl)_y]$ family. The specific aim of this piece of work was to investigate the effect of using bulky alkyne ligands such as $SiMe_3C{\equiv}CH$ and $Bu^tC{\equiv}CH$ in cluster synthesis.

These molecules can be considered to be additional members to the series of carbon bridged Cu_4 clusters described in the sections above. The central copper atoms are bridged by the terminal carbon atoms of four alkynyl ligands (Figure 2-6) that coordinate to either one or two additional copper atoms through *d* - π interactions. As a result more complex clusters than the $[Cu_4(aryl)_4]$ systems are observed although the basic Cu_4C_4 structural feature has been retained.

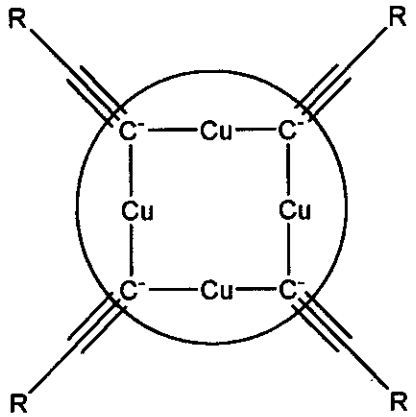

Figure 2-6. The Cu_4C_4 structural motif observed in Cu_{10} and Cu_{12} family

Another structurally similar molecule, $[Cu_{12}(hfac)_8(C{\equiv}CPr^n)_4(THF)_6].THF$ **(1)** previously isolated[37] by Dr. Timothy Higgs *via* an alternative route will be included in the discussion.

2.2 Cluster Synthesis

The only previous example of a $[Cu_{x+y}(hfac)_x(alkynyl)_y]$ type cluster, $[Cu_{12}(hfac)_8(C{\equiv}CPr^n)_4(THF)_6].THF$ **(1)**, with a nuclearity of twelve was isolated by a solvent-mediated rearrangement of a larger Cu_{18} cluster. In this chapter a series of molecules that are structurally related to **1** are reported that have been synthesised as direct products of the standard cluster forming reaction using bulky alkynes.

2.2.1 General synthetic procedure

The protocol recently established[38] for the synthesis of clusters with general formula $[Cu_{x+y}(hfac)_x(alkynyl)_y]$ was used to synthesize the new compounds discussed in this

chapter. This involves the addition of hfacH to a suspension of Cu_2O and $MgSO_4$ in an excess of a terminal alkyne. Filtration of the reaction mixture gives a solution of [Cu(hfac)(η^2-alkyne)] monomer in an excess of alkyne. Assembly of alkynyl-bridged complexes takes place on heating *in vacuo* as both hfacH and 1-alkyne are removed from the system. Their recovery has been confirmed by condensation in traps during a test reaction. This is outlined in Scheme 2-1.

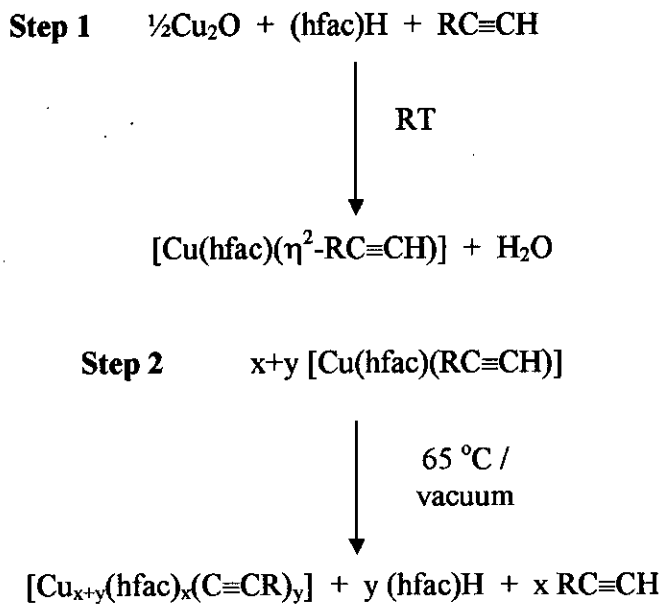

Scheme 2-1. Proposed cluster-formation mechanism

With the exception of **1** the compounds reported in this chapter were all prepared using variations of this method.

2.2.2 $[Cu_{12}(hfac)_8(C{\equiv}CPr^n)_4(THF)_6]$.THF (1)

$[Cu_{12}(hfac)_8(C{\equiv}CPr^n)_4(THF)_6]$.THF (**1**) was isolated by Dr Timothy Higgs following two recrystallisations of the cluster $[Cu_{18}(hfac)_{10}(C{\equiv}CPr^n)_8]$ (**6**) from THF. The molecule crystallized in the orthorhombic $Cmc2_1$ space group and the structure is shown in Figure 2-7. The symmetric unit contains one half molecule with the overall molecular

structure having crystallographic C_s symmetry. The molecule has an approximately planar disposition of twelve copper atoms that are solvated by two THF molecules located slightly above and two molecules below the Cu_{12} equatorial plane forming weak interactions with the copper atoms of the peripheral Cu-hfac units. Two THF molecules are positioned axially, above and below the Cu_{12} plane coordinating copper atoms in the central Cu core. The solvent molecules appear to fill vacant space around the molecule 'protecting' any exposed copper atoms. The solvents molecules were found to be disordered. A detailed description of the structure is given in section 2.3.1.

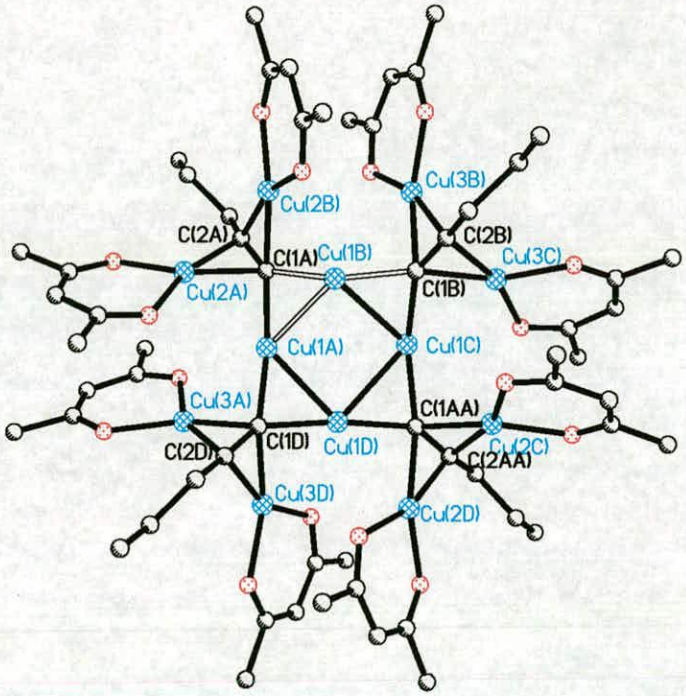

Figure 2-7. Plot of **1** (solvent molecules, H and F atoms are removed for clarity)

2.2.3 $[Cu_{12}(hfac)_8(C{\equiv}CBu^t)_4]$ (2), $[Cu_{10}(hfac)_6(C{\equiv}C^tBu)_4(OEt_2)]$ (4a) and $[Cu_{10}(hfac)_6(C{\equiv}CBu^t)_3(C{\equiv}CPr^n)(OEt_2)]$ (4b)

$[Cu_{12}(hfac)_8(C{\equiv}CBu^t)_4$ (**2**), $[Cu_{10}(hfac)_6(C{\equiv}CBu^t)_4(OEt_2)]$ (**4a**) and $[Cu_{10}(hfac)_6(C{\equiv}CBu^t)_3(C{\equiv}CPr^n)(OEt_2)]$ (**4b**) were obtained from an attempt to synthesise mixed alkynyl clusters by the standard preparative procedure using a $^tBuC{\equiv}CH$: $^nPrC{\equiv}CH$ (1:1) solvent system diluted with hexane. A mixture of products

was isolated. X-ray quality crystals of **2** were grown from a saturated hexane solution and crystallised in the monoclinic $P2_1/n$ space group. The structure has no crystallographically imposed symmetry and is shown in Figure 2-8. A second crop of crystals separated from hexane/diethyl ether on standing at -30 °C in the triclinic $P\bar{1}$ space group with molecules **4a** and **4b** in the asymmetric unit. The molecules of **4a** and **4b** differ in the replacement of one t-hexylalkyne ligand (**4a**) by a n-pentylalkyne group (**4b**) (Figure 2-9) and this results in small but significant differences in the metal framework. As a consequence, although parts of the two molecules are approximately related by inversion, the crystals provide a rare example of the chiral space group P1. This is the first example of a molecule with general formula, $[Cu_{x+y}(hfac)_x(alkynyl)_y]$ containing a mixture of alkynyl ligands.

2.2.4 $[Cu_{12}(hfac)_8(C{\equiv}CSiMe_3)_4]$ (3)

$[Cu_{12}(hfac)_8(C{\equiv}CSiMe_3)_4]$ (**3**) was a major product of the standard cluster-forming reaction[38] using $Me_3SiC{\equiv}CH$ as the solvent. X-ray quality crystals separated from a saturated hexane solution in the orthorhombic $C222_1$ space group. The symmetric unit contains a half molecule with the remainder of the structure generated by C_2 axis of symmetry. The structure is shown in Figure 2-8.

2.2.5 $[Cu_{10}(hfac)_6(C{\equiv}CBu^t)_4]$ (5)

Crystals of $[Cu_{10}(hfac)_6(C{\equiv}CBu^t)_4]$ (**5**) were obtained in very low yield from a reaction where the major product was a higher nuclearity compound. The yellow crystals that separated were extremely susceptible to decomposition preventing elemental analysis. The molecule crystallized in the monoclinic $C2/c$ space group with a half molecule in the symmetric unit. The overall molecular structure has crystallographic C_2 symmetry and the structure is shown in Figure 2-9.

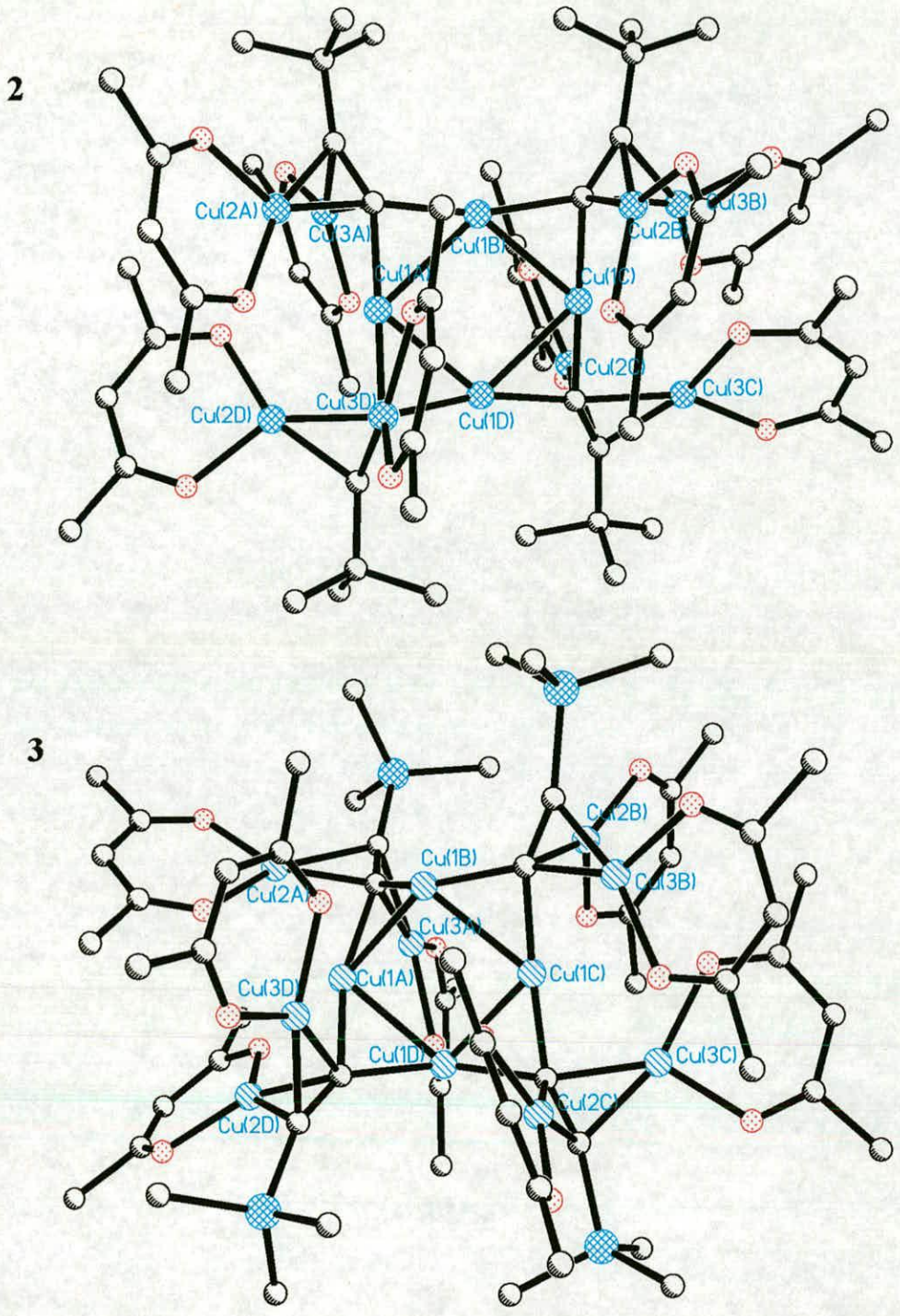

Figure 2-8. Molecular structure of the Cu_{12} clusters **2** and **3**. For clarity H and F atoms have been omitted and only the most predominant form of any disordered component has been shown.

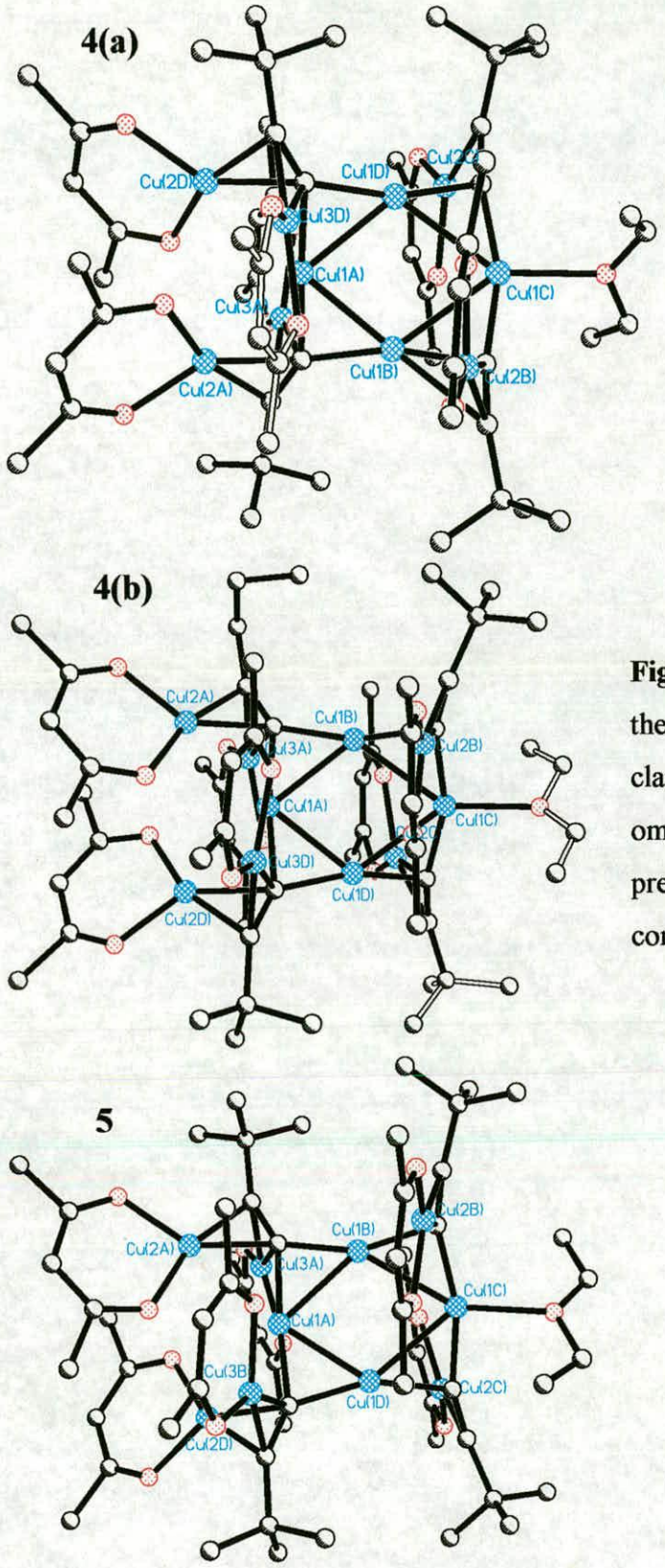

Figure 2-9. Molecular structure of the Cu_{10} clusters **4a**, **4b** and **5**. For clarity H and F atoms have been omitted and only the most predominant form of any disordered component has been shown.

2.3 Structural Features

Although prepared by a very different method there are remarkable similarities between the structure of **1** and the structures of **2**, **3**, **4a**, **4b**, and **5** isolated by direct synthesis. The molecules have essentially the same connectivity even though the 'shapes' of the molecules are different.

2.3.1 Structure of 1

The structure of **1** (Figure 2-7) consists of four central Cu atoms (Cu1A, Cu1B, Cu1C and Cu1D), linked by the terminal carbons of four η^1-bridging alkynyl ligands (C1A≡C2A, C1B≡C2B, C1C≡C2C and C1D≡C2D). Each alkynyl ligand is further coordinated to two Cu-hfac chelate rings containing the copper atoms Cu2A and Cu2B, Cu3B and Cu3C, Cu2C and Cu2D, Cu3A and Cu3D respectively. Each of these units forms a (μ_2-η^1:μ_2-η^2)-alkynyl bridge that resembles a 'butterfly' where Cu-hfac chelate rings form the 'wings' and the C≡C unit forms the backbone (Figure 2-10).

The four central Cu atoms form a slightly distorted square arrangement with Cu-Cu bond distances [2.427(2) – 2.538(2) Å] and diagonal Cu – Cu contacts that are approximately equal in length [Cu1A-Cu1C = 3.419(2) Å, Cu1B-Cu1D = 3.448(2) Å]. Diagonally disposed Cu atoms are displaced to the same side of the Cu1A, Cu1B, Cu1C and Cu1D least squares plane with a maximum distortion of +0.28(1) Å.

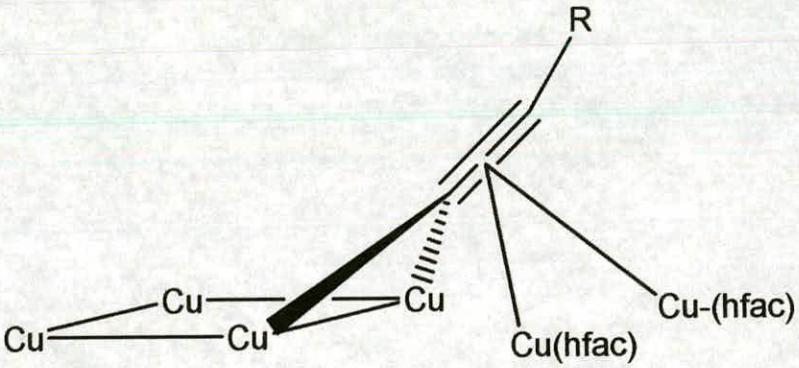

Figure 2-10. (μ_2-η^1:μ_2-η^2)-alkynyl bridge

The plane of the Cu_4 core of **1** extends to contain the remaining eight Cu atoms with the maximum displacements from the least square plane of all 12 Cu atoms being -0.52(1) Å and +0.55(1) Å for Cu1B and Cu1C respectively. This is possible because the alkynyl backbones point, alternately, above and below the Cu_{12} least squares plane at angles of approximately 40° and the butterfly 'wings' associated with each alkynyl point back towards the Cu_{12} plane. For the alkynyl ligands that point 'up', the associated Cu atoms lie slightly below the Cu_{12} least squares plane and *vice versa*.

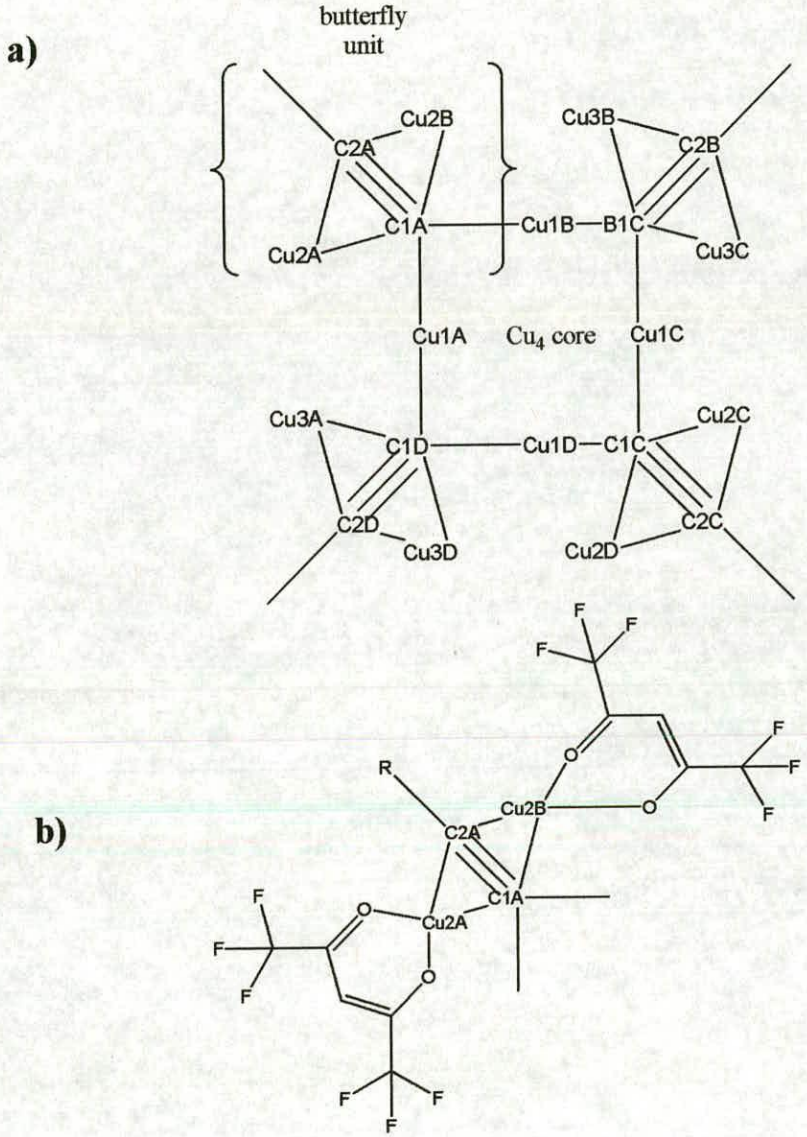

Figure 2-11. Numbering scheme for the central alkynyl bridged core (a) and the 'butterfly' units (b) in the Cu_{12} cluster **1**

The butterfly units appear to be aligned so as to optimise the facial interaction between Cu-hfac chelate rings of neighbouring units (Figure 2-12). Pairs of approximately parallel Cu-hfac rings form these interactions in which the rings appear to overlay each other to maximize attractive Cu...O dipolar interactions with interchelate Cu...O contacts in the range 3.203(5) – 3.363(5) Å (Table 2-1). Interacting Cu-hfac chelate rings adopt a staggered configuration as shown in Figure 2-13. This minimizes steric hindrance between CF_3 groups and allows the Cu atoms (CuX and CuY) to form a close contact with one oxygen atom on the opposite ring (OX and OY respectively).

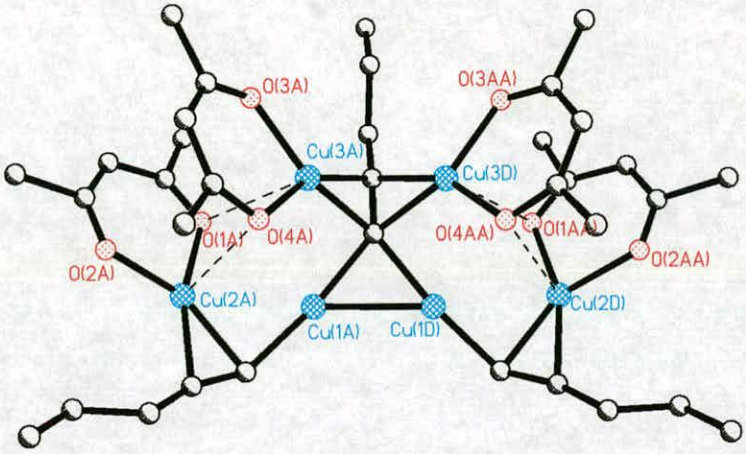

Figure 2-12. Fragment of **1** showing examples of Cu...O contacts between Cu-hfac chelate rings

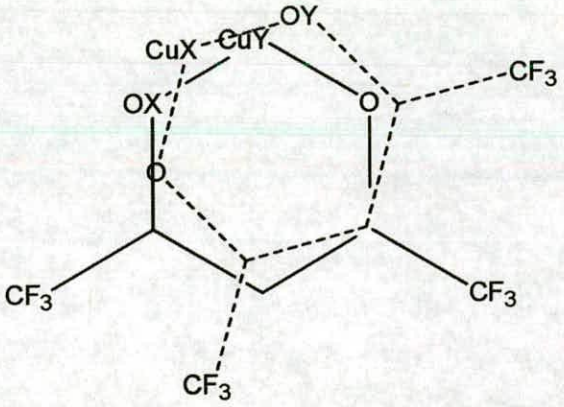

Figure 2-13. Staggered arrangement of interacting Cu-hfac chelate rings in **1**. CuX and CuY form close contacts with OX and OY respectively.

CuX...OX (Å)		CuY...OY (Å)	
Cu2A...O4A	3.259(5)	Cu3A...O1A	3.203(5)
Cu3D...O1AA	3.203(5)	Cu2D...O4AA	3.259(5)
Cu2C...O4BA	3.242(5)	Cu3C...O1BA	3.363(5)
Cu3B...O1B	3.363(5)	Cu2B...O4B	3.242(5)

Table 2-1. Short inter-ring Cu...O contacts in **1**

2.3.2 Structures of the Cu_{12} and Cu_{10} clusters 2, 3, 4a, 4b and 5

Although the three-dimensional disposition of copper atoms makes it difficult to view the connectivities in their central copper core, the structures of **2**, **3**, **4a**, **4b** and **5** are in fact remarkably similar to that of **1**. They have the same connectivities in the central cores, although the distribution of the peripheral structural units is more complex and differs significantly between the Cu_{12} and Cu_{10} compounds. To facilitate comparison between the structures in the series a generic numbering scheme has been assigned (Figure 2-14a). For **3** and **5**, where the full molecules are generated by an axis of symmetry, there are some discrepancies in the numbering scheme. To explain these discrepancies a key has been included in Appendix 1.

All five clusters have a core of four Cu atoms bridged by the terminal carbon atoms of four alkynyl ligands. The Cu_{10} structures (**4a**, **4b** and **5**) differ from the generic Cu_{12} model because a diethyl ether molecule coordinates to Cu1C (Figure 2-14b). In order to accommodate the ether the two alkynyls (C1B≡C2B and C1C≡C2C) adopt a 'half-butterfly' configuration bonding to only one Cu-hfac chelate ring.

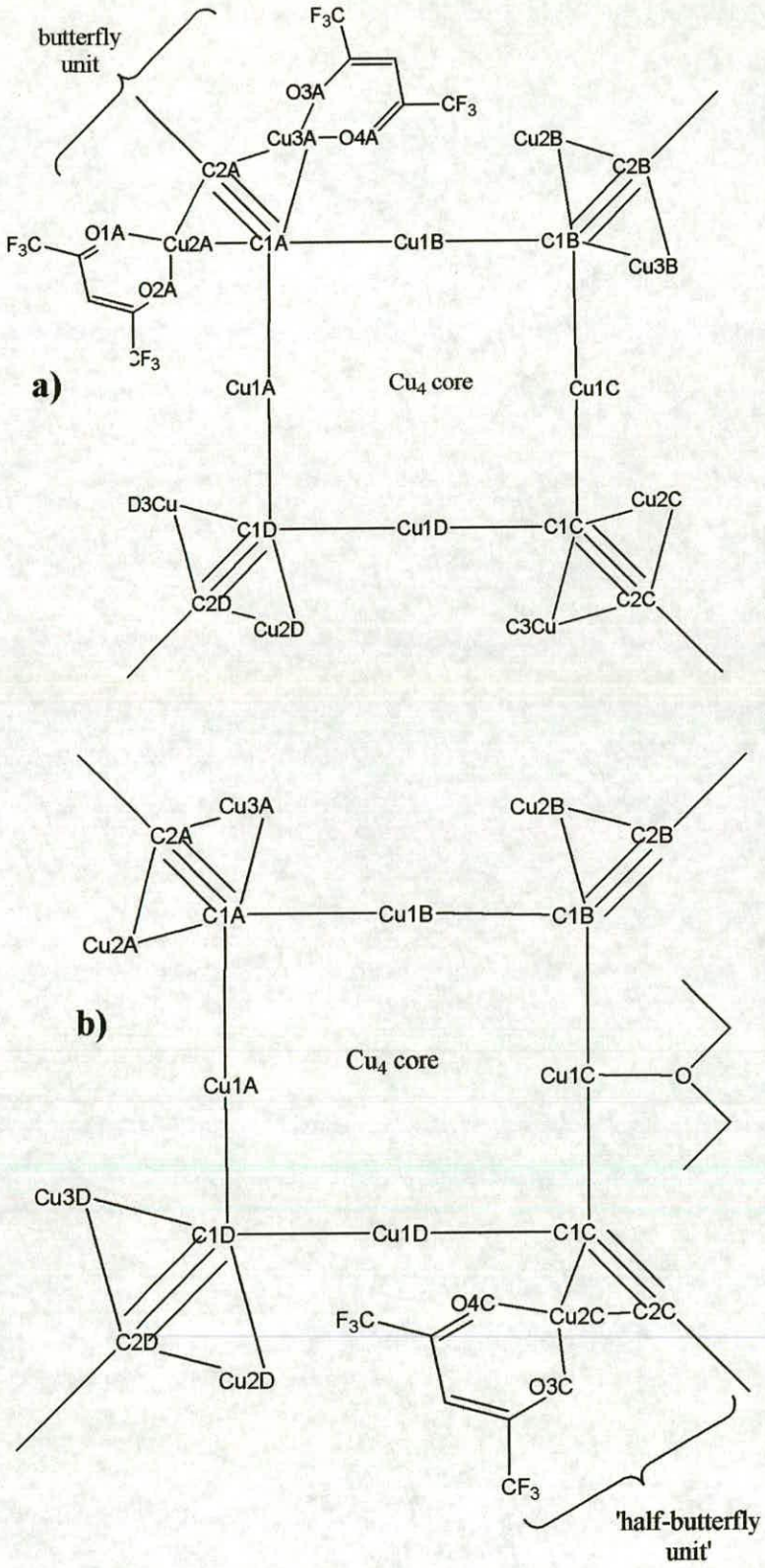

Figure 2-14. Connectivities and atom labelling schemes for, a) Cu_{12} clusters (only one of the four full butterfly units is shown) and b) Cu_{10} clusters (one of the two 'half butterfly' units is shown in full).

2.3.3 Cu_4 Core in 2, 3, 4a, 4b and 5

The central Cu_4 cores of the directly synthesised clusters, **2**, **3**, **4a**, **4b** and **5** are much more nearly planar than that in the rearranged cluster **1**. The maximum deviation of Cu1A, Cu1B, Cu1C and Cu1D from their least square plane is observed in **4b** (- 0.0124 Å for Cu1A) which is an order of magnitude smaller than for the equivalent Cu_4 plane in **1** (Table 2-2).

Atom	1	2	3	4a	4b	5
Cu1A	0.285(4)	0.011(1)	0.000(0)	-0.0026(4)	0.0124(4)	0.000(0)
Cu1B	-0.278(4)	-0.011(1)	0.000(0)	0.0024(4)	-0.012(4)	0.000(0)
Cu1C	0.264(4)	0.011(1)	0.000(0)	-0.0023(4)	0.0114(4)	0.000(0)
Cu1D	-0.270(4)	-0.011(1)	0.000(0)	0.0025(4)	-0.0118(4)	0.000(0)

Table 2-2. Deviations of Cu1A, Cu1B, Cu1C and Cu1D (Å) from their least squares planes in **1**, **2**, **3**, **4a**, **4b** and **5**. Atom labelling is defined in Figures 14a and 14b. Equations for the Cu_4 planes are given in Appendix 2

In the structures where there is no ether solvation/coordination i.e. **2** and **3**, the Cu_4 core adopts a rhombic arrangement (Figure 2-15). The four shortest Cu...Cu contacts fall in the range 2.424(1) – 2.630(1) Å (Table 2-3) with diagonal atoms, Cu1A and Cu1C further separated (3.737(2) Å and 3.700(3) Å in **2** and **3** respectively) than Cu1B and Cu1C (3.273(3) and 3.283(3) Å in **2** and **3** respectively). In both cases the C1A – Cu1A – C1D and C1B – Cu1C – C1C angles are approximately equal and greater than the C1A – Cu1B – C1B and C1C – Cu1D – C1A angles making the Cu_4C_4 ring appear 'pinched in' at the Cu1B and Cu1D atoms (Table 2-3).

In the Cu_{10} systems (**4a**, **4b** and **5**), which have an ether molecule coordinated to Cu1C, the Cu_4 diamond is distorted (Figure 2-15). As in **2** and **3**, Cu1A to Cu1C separations are greater than Cu1B to Cu1D, however, the interaction of Cu1C with the oxygen of the diethyl ether molecule displaces this copper atom towards the ether oxygen atom giving a kite-shaped arrangement of the central Cu_4 core. As a result the Cu1C...Cu1B and Cu1C...Cu1D distances are greater than those of Cu1A-Cu1B and Cu1A-Cu1C and the

C1B-Cu1C-C1C bond angles are greater [195.9(3)°-199.6(3)°] than those observed in the unsolvated Cu_4C_4 rings (Table 2-3).

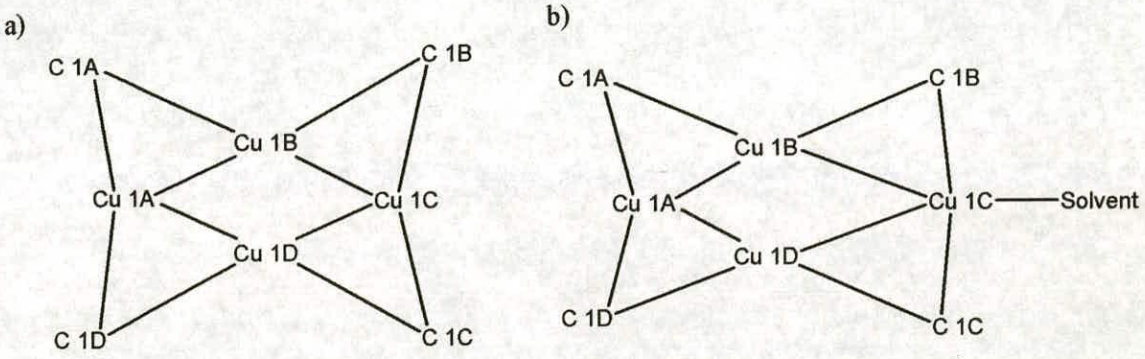

Figure 2-15. (a) The rhombic array of the planar Cu_4 core in **2** and **3** and (b) the kite-shaped Cu distribution seen in **4a**, **4b** and **5**

	1	**2**	**3**	**4a**	**4b**	**5**
Cu1A...Cu1B	2.427(2)	2.506(1)	2.444(2)	2.424(1)	2.431(1)	2.433(1)
Cu1B...Cu1C	2.520(2)	2.469(1)	2.503(2)	2.630(1)	2.532(1)	2.564(1)
Cu1C...Cu1D	2.538(2)	2.482(1)	2.503(2) ***(a)***	2.604(1)	2.565(1)	2.564(1) ***(b)***
Cu1A...Cu1D	2.422(2)	2.478(1)	2.444(2) ***(a)***	2.431(1)	2.432(1)	2.433(1) ***(b)***
Cu1A...Cu1C	3.419(3)	3.737(2)	3.700(3)	4.005(2)	3.975(2)	4.042(1)
Cu1B...Cu1D	3.448(3)	3.273(1)	3.283(3)	3.063(1)	2.990(1)	2.936(1)
Angles /°						
C1A-Cu1A-C1D	172.6(3)	177.3(3)	161.7(7)	178.1(2)	173.4(3)	175.1(3)
C1A-Cu1B-C1B	145.3(4)	164.7(3)	139.1(6)	165.3(2)	163.9(2)	157.5(2)
C1B-Cu1C-C1C	145.9(4)	173.3(3)	176.0(7)	198.7(3)	199.6(3)	195.9(3)
C1C-Cu1D-C1D	172.6(3)	165.1(3)	139.1(6)	164.5(2)	165.4(3)	157.5(2)
Cu1A-Cu1B-Cu1C	87.4(1)	97.4(1)	96.8(1)	104.8(1)	106.4(1)	108.0(1)
Cu1B-Cu1C-Cu1D	85.9(1)	82.8(1)	82.0(1)	71.6(1)	71.8(3)	69.9(1)
Cu1C-Cu1D-Cu1A	86.1(1)	97.8(1)	96.8(1)	105.4(1)	105.7(1)	108.0(1)
Cu1D-Cu1A-Cu1B	89.4(1)	82.1(1)	84.4(1)	78.2(1)	76.1(1)	74.2(1)

Table 2-3. Selected Cu...Cu distances (Å) in **1**, **2**, **3**, **4a**, **4b** and **5**. Atom labelling is defined in Figures 14a and 14b. **a** and **b** - these contact distances are related to Cu1A...Cu1B and Cu1B...Cu1C by a crystallographic mirror plane passing through C1A and C1C

2.3.4 Cu_4C_4 Core in 2, 3, 4a, 4b and 5

The Cu_4C_4 rings in **2**, **4a**, **4b** and **5** are 'puckered' with the η^2-alkynyl ligand bridging carbon atoms lying above and below the plane of the four metals (Figure 2-16) positioned alternately above and below the plane in an arrangement similar to that shown in Figure 2-3.

In **3**, an adjacent pair of bridging C atoms (C1B and C1C) lie approximately coplanar with the Cu_4 core whereas the opposite pair (C1A and C1D) are alternately displaced above and below the plane by considerable distances [C1A = 1.27(2), C1D = -1.27(2) Å displaced from Cu_4].

The Cu – $C_{terminal}$ – Cu bridging motifs are relatively symmetrical throughout the series with the most unsymmetrical example appearing in **1** where the difference in C1A-Cu1A [1.91(1) Å] and C1A–Cu1B [2.06(1) Å] is 0.15(1) Å.

2.3.5 'Butterfly' Units

The $C_{terminal}$ - C_β alkynyl bond lengths in ' butterfly' units (Table 2-4) fall in the range 1.22(2) Å- 1.32(2) Å and in 'half butterflies' in the range 1.22(1)-1.25(1) Å. These are slightly longer than the C-C distances found in non π-coordinating alkynyls.[39] The increase in bond length on formation of a 'full' and 'half butterfly suggests that the degree of π-coordination determines the strength of the C≡C bond.

	1	2	3	4a	4b	5
C1A-C2A	1.26(1)	1.29(1)	1.32(2)	1.28(1)	1.29(1)	1.28(1)
C1B-C2B	1.25(1)	1.29(1)	1.28(2)	1.23(1)	1.24(1)	1.22(1)
C1C-C2C	1.26(1)	1.26(1)	1.22(2)	1.25(1)	1.23(1)	1.22(1)
C1D-C2D	1.25(1)	1.29(1)	1.28(2)	1.27(1)	1.27(1)	1.28(1)

Table 2-4. Alkynyl bond lengths in **1**, **2**, **3**, **4a**, **4b** and **5**.

The Cu – $C_{terminal}$ and Cu - C_β bond distances fall in the range, 1.99(1)-2.06(1) and 1.98(1)-2.06(1) Å respectively which are typical for approximately symmetrical alkynyl – Cu π bonds. The π–bonded Cu atoms are part of planar six membered rings with hfac.

The CuC_2 unit of each butterfly 'wing' is approximately co-planar with the related Cu-hfac chelate ring. Butterfly units from **2** are shown in Figure 2-16. In **2** the C_2-Cu-hfac planar 'wings' on each butterfly are separated by angles that fall in the range 105.3(1)°-115.8(1)° which is typical for the whole series. The Cu-hfac rings have bond lengths and angles consistent with those observed in related systems.[40, 41]

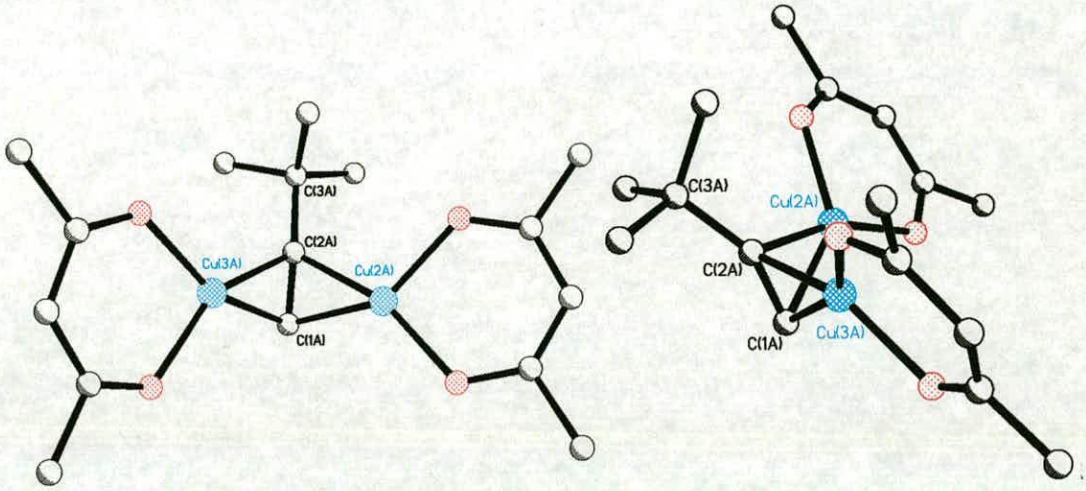

Figure 2-16. Two views of the C1A-C2A unit in **2**

2.3.6 Crystal structure of a discrete butterfly molecule, $[Cu_2(hfac)_2(HC{\equiv}CBu^t)]$ (7)

$[Cu_2(hfac)_2(HC{\equiv}CBu^t)]$ (7) was isolated in very small yield from a reaction where the major products were higher nuclearity clusters. The material crystallised in the monoclinic $P2_1/n$ space group with two molecules in the symmetric unit (Figure 2-17). The crystals obtained were pale yellow as opposed to the dark red colour of the major reaction product.

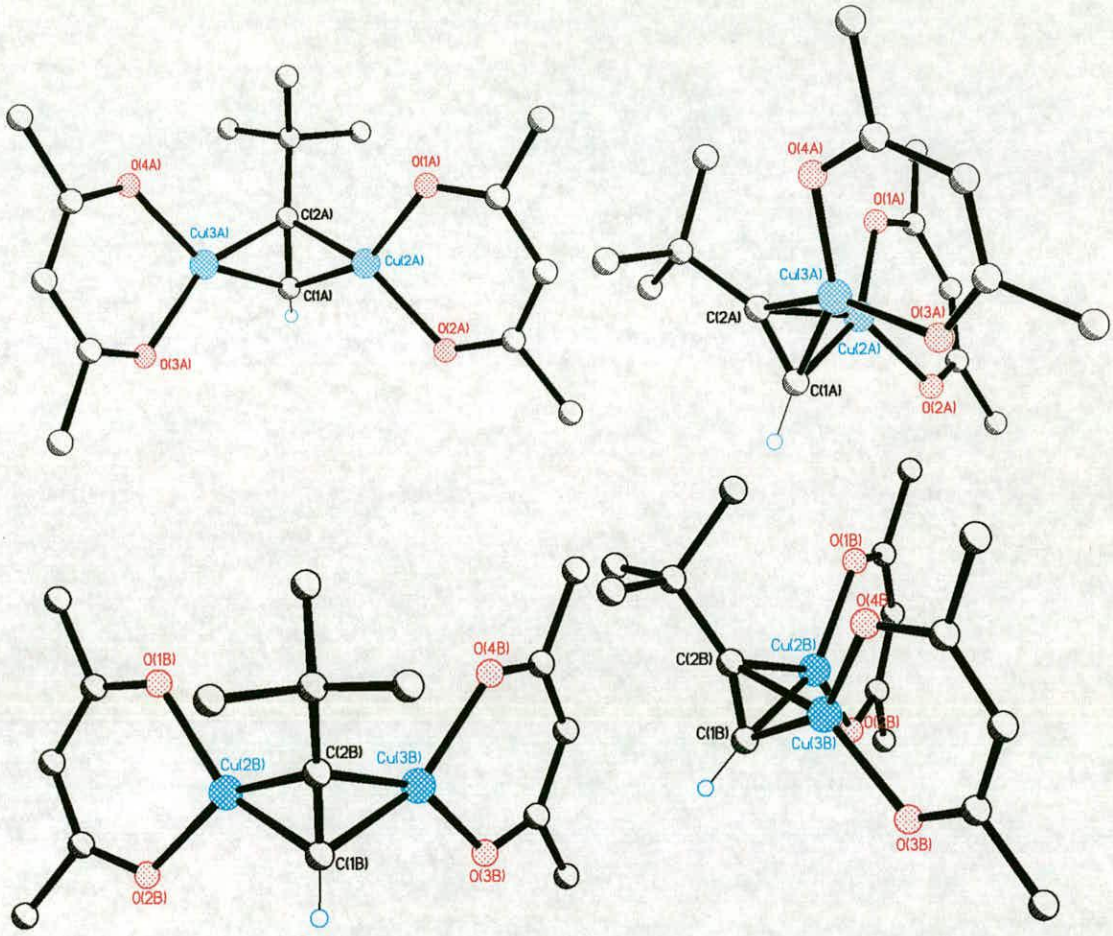

Figure 2-17. The two crystallographically independent molecules, $[Cu_2(hfac)_2(HC{\equiv}CBu^t)]$ 7, displayed to show the atom-labelling scheme and the similarity of their structures

The two molecules in the asymmetric unit have identical connectivity and consist of a neutral alkyne coordinating two copper atoms through π-interactions with each Cu atom forming a chelate ring with a hfac ligand. The chelate rings are approximately planar with the two carbon atoms of their associated alkynyl group. The least squares planes of the alkynyl-Cu-hfac units on each molecule are separated by angles of 100.5(2)° and 103.2(2)° and the alkynyl bond lengths are 1.28(2) and 1.22(2) Å for the C1A...C2A and C1B...C2B molecules respectively. The structure closely resembles the 'butterfly' fragments identified in the clusters and shown in Figure 2-16.

The way in which the two molecules in the asymmetric unit pack in the crystal structure is of considerable interest as *inter*molecular interactions between the Cu-hfac chelate rings (Figure 2-18) can be related to the *intra*molecular interactions in the clusters.

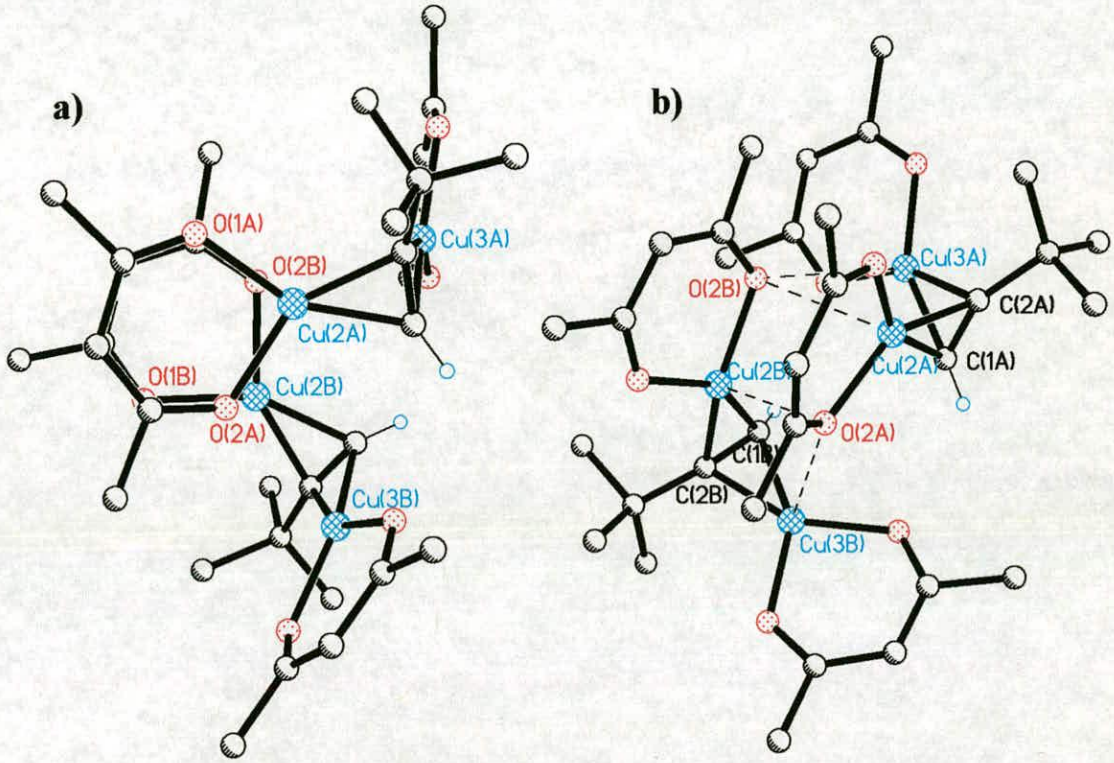

Figure 2-18. Two views of the interactions between two molecules of 7 in the asymmetric unit showing, a) the approximately cofacial overlap of Cu-hfac chelate rings and b) short Cu...O contacts between these rings and to neighbouring copper atoms Cu3A and Cu3B

The Cu-hfac ring containing Cu2B is orientated so that it faces the ring containing Cu2A with the planes of the six membered rings lying at an angle of 17.7(3)° relative to each other. There are short intermolecular Cu...O contacts between the Cu2B and O2A [2.85(1) Å] and Cu2A and O2B [2.79(1) Å] indicative of attractive dipolar interactions. The rings adopt a 'staggered' conformation so as to minimize steric interactions between CF_3 groups. This arrangement sets up another pair of slightly longer intermolecular contacts between Cu3B...O2A (3.22(1) Å) and Cu3A...O2B (3.14(1) Å) (Figure 2-18). From the crystal structure of 7 it appears that in order to adopt the lowest energy

configuration, an unconstrained butterfly unit 'interlocks' with another molecule forming intermolecular Cu...O dipolar interactions reminiscent of π-stacking. By 'interlocking' with another unit, a butterfly unit is prevented from rotating about the axis of the alkynyl C≡C bond by the 'wings' of the interlocking partner.

The π-stacking type orientation of Cu-hfac chelate rings found in **7** is similar to the arrangement of Cu-hfac rings in structure of **1** (Figure 2-12) in that both configurations maximize inter-ring Cu...O dipole interactions. In **7** the butterfly monomers interlock allowing cofacial overlap of chelate rings and additional Cu...O contacts. In **1** inter-ring Cu...O interactions are observed between Cu-hfac chelate rings on neighbouring butterflies (Figure 2-11) with a similar cofacial overlap of rings as in **7** although there is no interlocking of butterfly units.

2.3.7 Disposition of butterfly units in 2, 3, 4a, 4b and 5

It appears from the analysis of the structures of **1** and **7** that secondary bonding between the Cu-hfac units influences the conformation of the clusters. The extent to which this applies to the clusters **2**, **3**, **4a**, **4b** and **5** is considered below.

The unconstrained butterfly monomer (**7**) maximizes inter-ring Cu...O dipolar interactions by adopting an interlocking arrangement (Figure 2-18) of two molecules whereas the butterflies in **1** are arranged to allow Cu-hfac rings on neighbouring butterflies to interact without interlocking (Figure 2-12).

Butterfly units in **2**, **3**, **4a**, **4b** and **5** behave differently from those in **1** because each unit interlocks with one neighbouring unit generating clusters with pairs of interlocking butterflies on the opposite sides of the Cu_4 core (Figure 2-19). 'a' butterflies (i.e. alkynyl backbone coordinated to Cu2A and Cu3A) interlock with 'd' butterflies and 'b' butterflies interlock with 'c's. In **4a**, **4b** and **5**, **'b'** and **'c'** units are only 'half butterflies' and therefore cannot interlock.

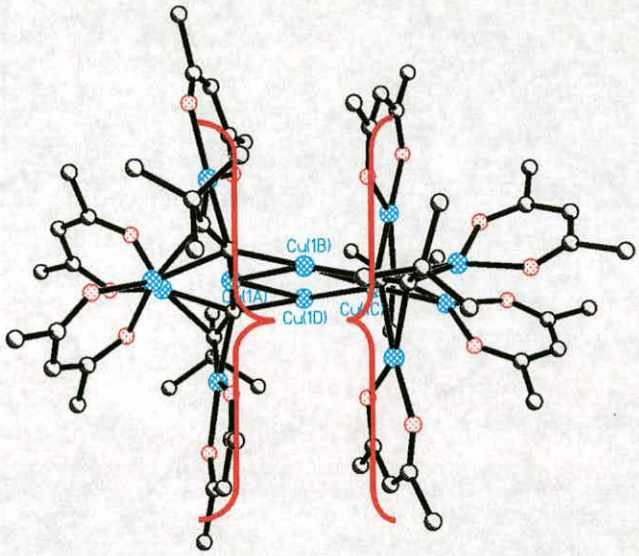

Figure 2-19. Structure of **2** showing pairs of interlocking butterfly units

Two types of interlocking interactions, **A** and **B**, have been identified and these can be illustrated using the structure of **2** which displays both interlocking modes (Figure 2-20).

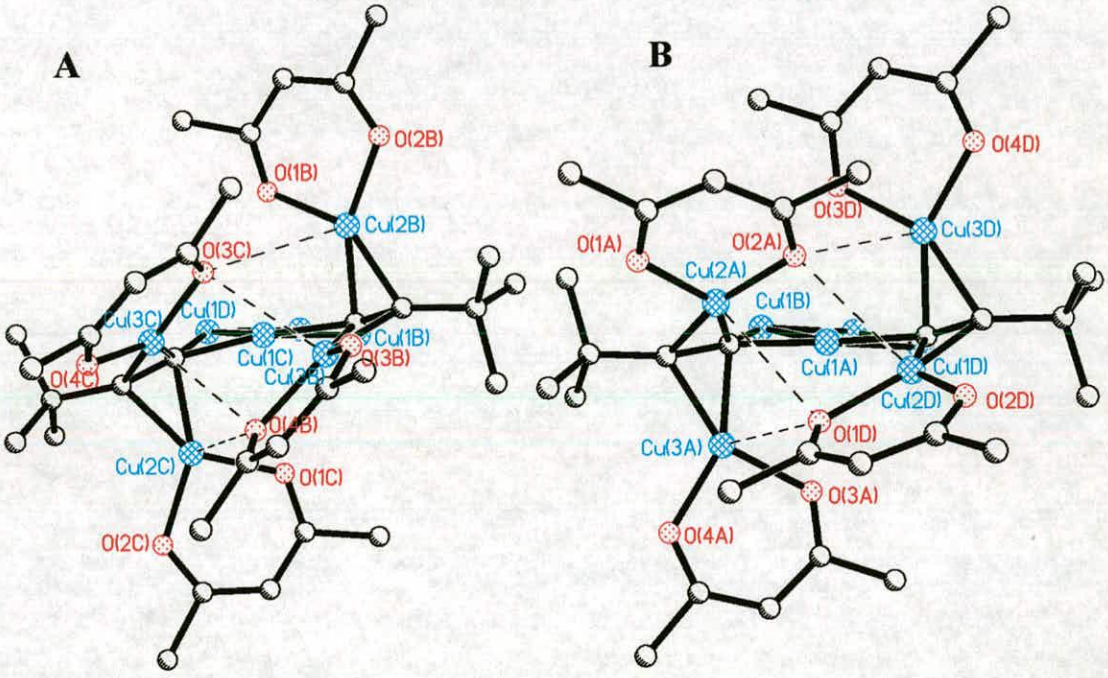

Figure 2-20. Cu_4 plane in **2** showing a) the **A** type interlocking of butterflies Cu2B/Cu3B (left) and b) the **B** type interlocking of butterflies Cu2A/Cu3A and Cu2D/Cu3D (right).

Mode **A** closely resembles the interlocking arrangement of butterfly units observed in the discrete butterfly monomer, **7**, and takes place between the 'b' (i.e. alkynyl backbone coordinated to Cu2B and Cu3B) and 'c' butterflies. One chelate ring from each butterfly overlaps to form a π-stacking type interaction with short inter-ring Cu...O contacts [Cu3B...O3C = 2.83(1), Cu3C...O4B = 2.87(1) Å] (Figure 2-21). There is an angle of 25.7(2)° between the two overlapping chelate rings whose planes are defined by the atoms of each six membered ring. As in **7** there are two slightly longer Cu...O contacts Cu2B...O3C (3.37(1) Å) and Cu2C...O4B (3.05(1) Å). These interactions occur between an oxygen atom from one of the 'overlapping' chelate rings and the copper atom on the opposite butterfly unit not involved in the cofacial interaction.

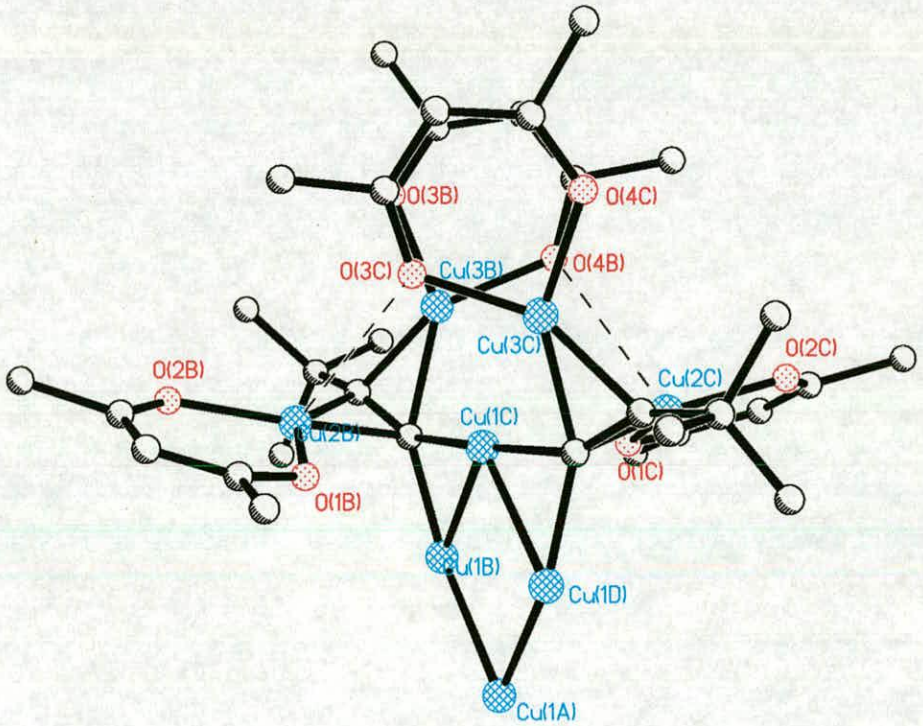

Figure 2-21. The overlap of 'b' and 'c' Cu-hfac chelate rings in mode **A** found in **2** showing O4B...Cu2C and O3C...Cu2B contacts.

Interlocking mode **B** in **2** occurs between the 'a' and 'd' butterflies (Figure 2-22). As in mode **A**, the butterfly units in the **B** mode are arranged so as to allow favourable Cu...O dipolar interactions between the two butterflies, but in mode **B**, cofacial overlap is not observed, instead one oxygen atom from each butterfly bridges the two copper atoms of the other butterfly in a symmetrical bridging mode. The bridging interactions are observed between O2A, Cu2D, Cu3D and O1D, Cu2A, Cu3A (Figure 2-22) and have contact distances, O2A...Cu2D = 2.98(1), O2A...Cu3D = 3.12(1), O1D...Cu2A = 3.09(1) and O1D...C3A = 3.14(1) Å.

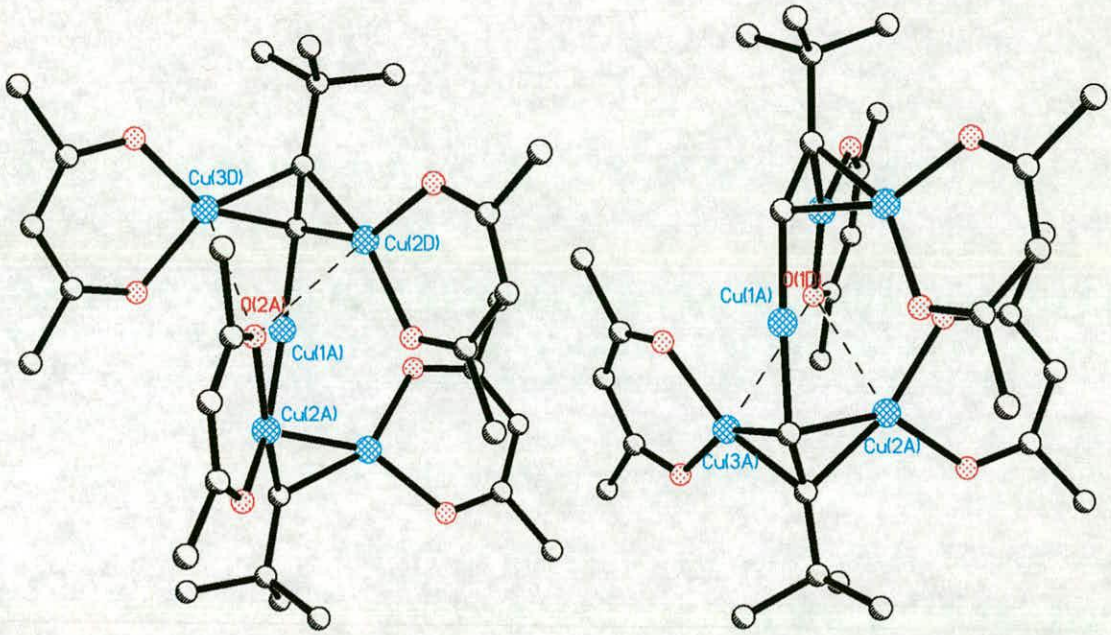

Figure 2-22. Approximately symmetrical bridging modes observed in the **B** type bridging mode in **2**.

In **4a, 4b** and **5** interlocking only takes place between 'a' and 'd' butterflies on account of ether coordination to Cu1C. In all three clusters mode **B** interactions are observed with the inter-ring Cu...O contacts falling in the range 2.767(4)-3.169(5) Å. A third non-interlocking cofacial interaction is found in **4a** and **4b** and these have been denoted **C** type interlocking modes. The **C** type molecules resemble the non-interlocking Cu-hfac inter-ring interactions observed in **1**. In these clusters 'a' and 'd' butterflies form a **B** type interlocking mode (Table 2-5) in the usual manner, however, additional non-interlocking

cofacial interactions occur between the Cu-hfac chelate rings of an 'a' butterfly with a 'c' butterfly and a 'b' butterfly with a 'd' butterfly (Figure 2-23). The Cu-hfac chelate rings are approximately planar to each other with dihedral angles between the planes of the two rings varying between 4.7(2)° and 8.8(2)° and inter-ring Cu…O contacts falling in the range 3.322(4) – 3.550(5) Å.

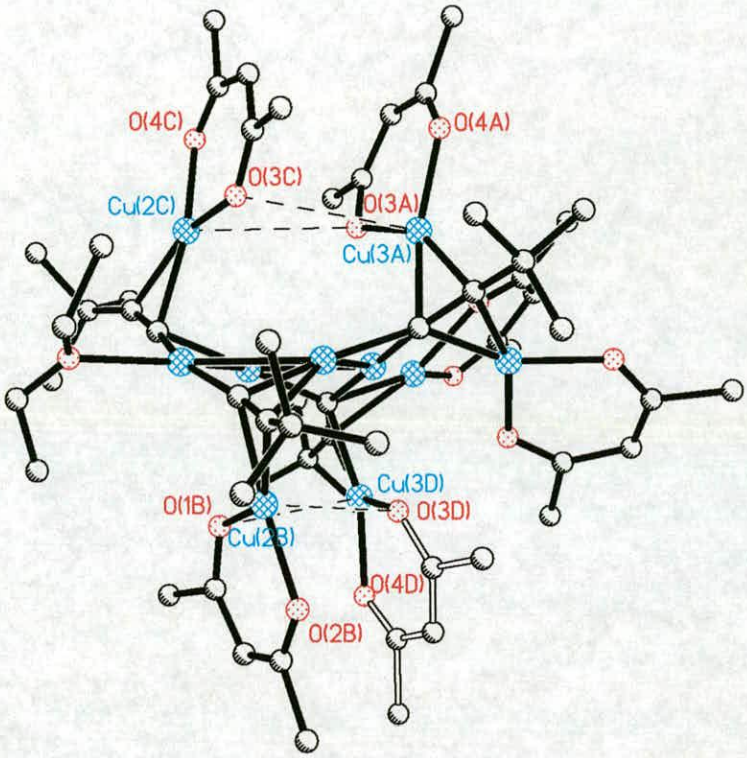

Figure 2-23. The chelate rings in **4a** involved in **C** type interactions.

Mode A	2	3	4a	4b	5
Interaction between 'b' (i.e. butterfly containing Cu2B and Cu3B) and 'c' butterflies					
Cu3B...O3C	2.83(1)				
Cu3C...O4B	2.87(1)				
Cu3B...Cu3C	3.501(1)				
Dihedral Angle	25.7(2)°				
Mode B					
Interaction between 'a' and 'd' butterflies					
O1D...Cu2A	3.09(1)	3.46(1)	2.767(4)	2.970(5)	3.068(3)
O1D...Cu3A	3.14(1)	3.55(1)	3.118(4)	3.144(5)	3.154(3)
O2A...Cu2D	2.98(1)	3.47(1)	2.790(5)	2.981(5)	3.068(3)
O2A...Cu3D	3.12(1)	3.55(1)	3.128(4)	3.169(5)	3.154(3)
Interaction between 'b' and 'c' butterflies					
O4BA...Cu2B		3.19(1)			
O4BA...Cu3B		3.15(1)			
O4B...Cu2C		3.19(1)			
O4B...Cu3C		3.15(1)			
Mode C					
Interaction between 'a' and 'c' butterflies					
Cu3A...O3C			3.550(5)	3.35(1)	
Cu3A...O4C			4.954(5)	4.76(1)	
Cu2C...O3A			3.358(5)	3.231(5)	
Cu2C...O4A			5.233(5)	5.09(1)	
Dihedral Angle			4.7(2)°	7.9(2)°	
Interaction between 'b' and 'd' butterflies					
Cu3D...O1B			3.526(5)	4.94(1)	
Cu3D...O2B			4.873(4)	3.44(1)	
Cu2B...O3D			3.322(4)	3.227(5)	
Cu2B...O4D			5.169(5)	5.083(5)	
Dihedral Angle			5.4(2)°	8.8(2)°	

Table 2-5. Interlocking modes (**A**, **B**, **C**)[a] of butterfly units observed in structures **1**-**5**.

a) Defined in pages 26, 27 and 28 respectively.

2.3.8 Disposition of the alkynyl units in 2, 3, 4a, 4b and 5

In the previous sections the presence of weak *intra*molecular interactions between Cu-hfac chelate rings were shown to significantly effect the disposition of the butterfly units on the periphery of the clusters. In the following section the disposition of the alkynyl ligands in **2**, **3**, **4a**, **4b** and **5** is discussed.

In **2** and **5** the alkynyl ligands of the butterfly units are displaced above and below the Cu_4 core (Table 2-6) by relatively small distances in comparison to **3**, **4a** and **4b** (Figure 2-25). **4a** and **4b** show large displacement of the alkynyl groups from the plane of the Cu_4 core. These are the only two clusters to display **C** type non-interlocking cofacial

interactions where 'a' and 'c' Cu-hfac rings and 'b' and 'd' Cu-hfac rings form short *inter*-ring Cu...O contacts. As a result of these contacts the alkynyl ligand are 'pulled' away from the central plane and are further displaced than in **2** and **5**.

	1	**2**	**3**	**4a**	**4b**	**5**
C1A	1.00(1)	-0.26(1)	1.27(2)	-0.613(6)	-0.694(6)	0.439(3)
C2A	1.88(1)	-0.58(1)	2.41(1)	-1.219(6)	-1.360(7)	0.892(3)
C1B	-0.43(1)	0.29(1)	0.03(1)	0.690(6)	0.799(6)	-0.482(5)
C2B	-1.10(1)	0.62(1)	0.23(1)	1.153(6)	1.401(6)	-0.919(5)
C1C	-0.17(1)	-0.49(1)	-0.03(1)	-0.679(6)	-0.803(6)	0.482(5)
C2C	0.22(1)	-1.04(1)	-0.23(1)	-1.154(6)	-1.404(6)	0.919(5)
C1D	-0.52(1)	0.36(1)	-1.27(2)	0.617(5)	0.718(6)	-0.439(3)
C2D	-1.30(1)	0.83(1)	-2.41(1)	1.213(6)	1.370(6)	-0.892(3)

Table 2-6. Deviations of alkynyl carbons (Å) from their least squares planes of Cu1A, Cu1B, Cu1C and Cu1D[a] in **1**, **2**, **3**, **4a**, **4b** and **5**. Atom labelling is defined in Figures 2-11, 2-14a and 2-14b and equations for the planes are given in Appendix 2

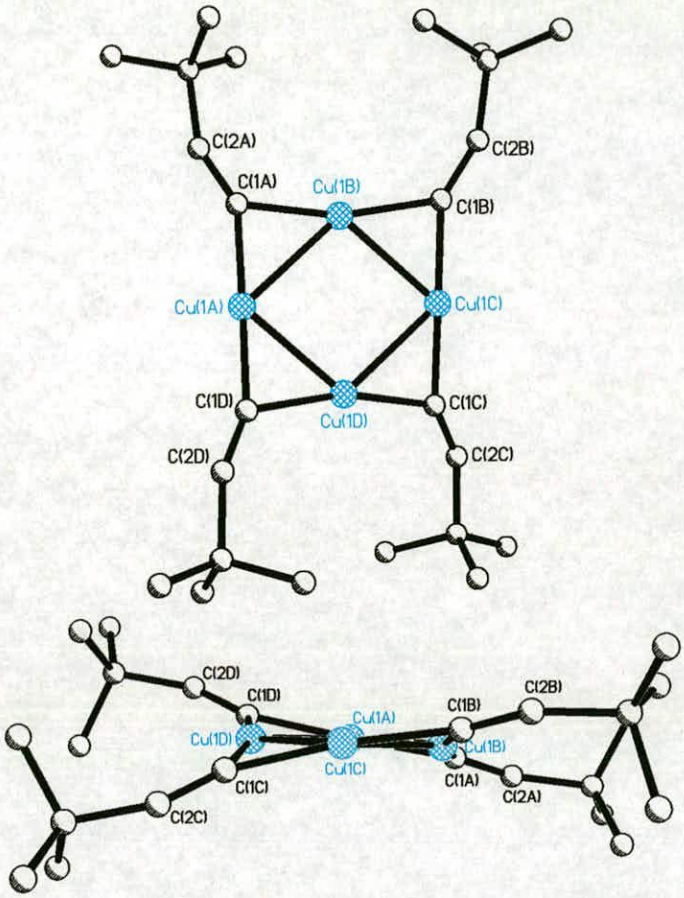

Figure 2-25. Two views showing the distribution of alkynyl ligands relative to the Cu_4 core in **2**.

The very bulky trimethylsilyl substituted alkynyl ligands in **3** significantly effects the arrangement of alkynyl ligands. In **2** and **5**, alkynyl groups are slightly displaced, pointing alternately above and below the Cu_4 core (Figure 2-25). In **3**, 'b' and 'c' alkynyls (i.e. C1B≡C2B and C1B≡C2B respectively) behave in a similar manner to 'b' and 'c' alkynyls in **2** and **5** and are relatively planar with the Cu_4 core. The 'a' and 'd' alkynyl groups, however, are significantly displaced above and below the Cu_4 core (Figure 2-26). This arrangement appears to be adopted in order to minimize steric interactions between the bulky $-SiMe_3$ groups.

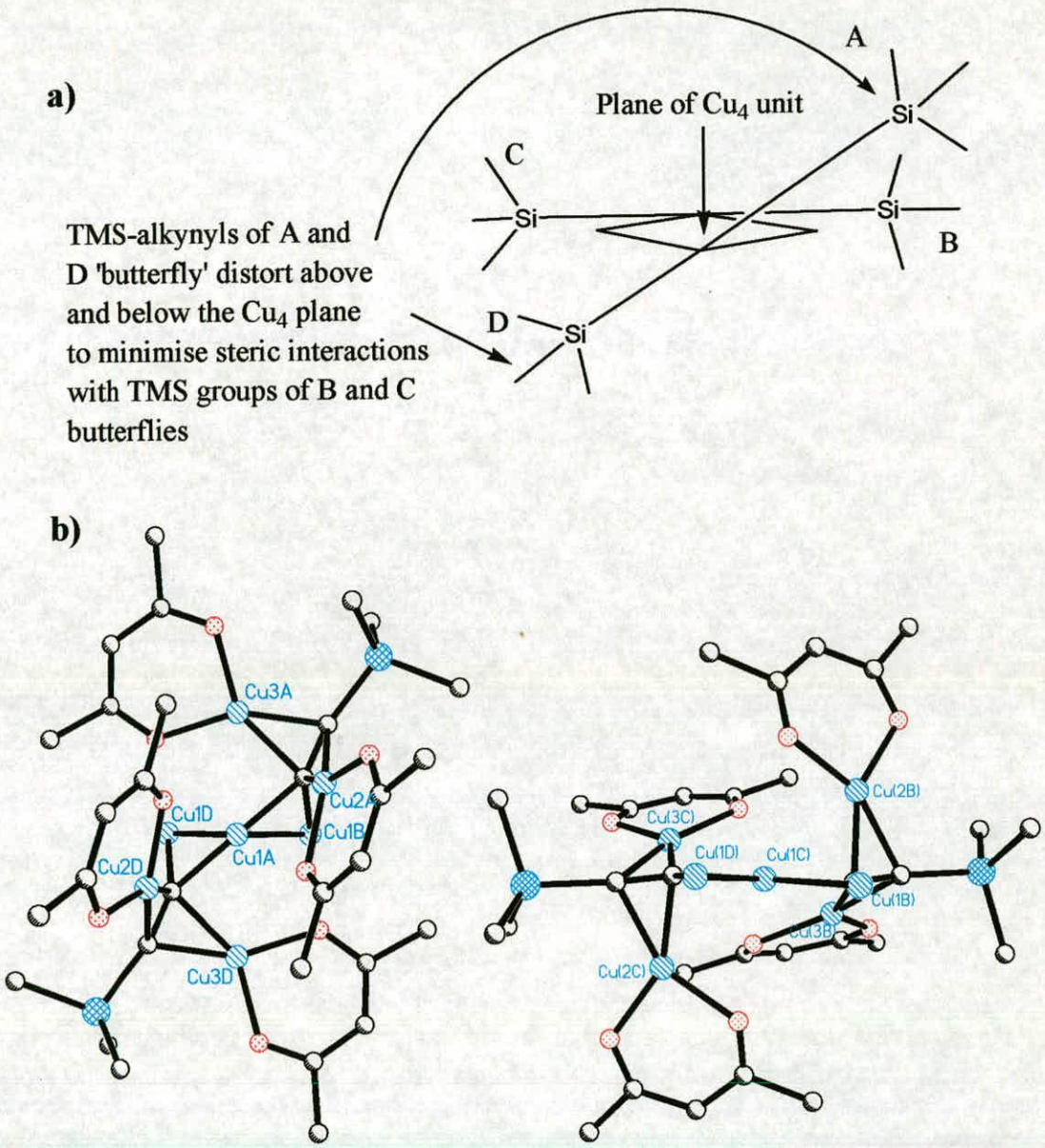

Figure 2-26. a) Distortion of A and D alkynyl ligands from the least square plane of Cu_4. b) Fragments of structure of **2** illustrating the distortion of interlocking butterfly units

2.4 Alkynyl ligand steric bulk

Detailed analysis of **1**, **2**, **3**, **4a**, **4b**, and **5** in the previous sections suggests that a number of subtle influences such as the formation of weak inter- and intra-molecular interactions

and the coordination of solvent molecules are important in determining the structures of the molecules. The degree to which the steric bulk of the alkynyl components in the system affects the outcome of the cluster forming reaction will be considered in the following section.

2.4.1 Ligand distribution in high and low nuclearity clusters

The clusters containing $Cu_{18} \rightarrow Cu_{26}$ that have been reported previously[37, 38, 42-44] have a characteristic distribution of ligand components.

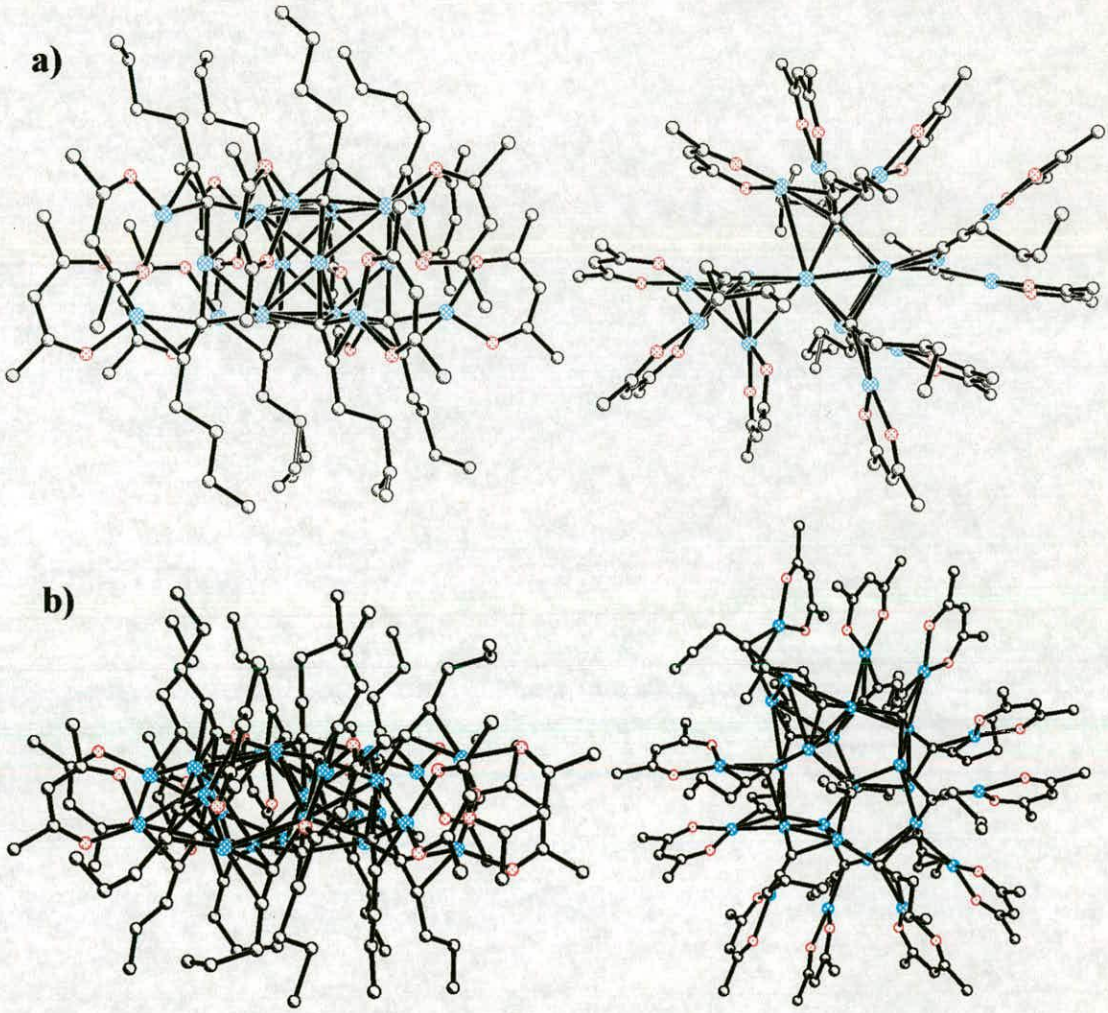

Figure 2-27. Perpendicular views of the structure of a) $[Cu_{18}(hfac)_{10}(1\text{-hexynyl})_8]$[43] and b) $[Cu_{26}(hfac)_{11}(1\text{-pentynyl})_{15}]$[38]

The examples shown in Figure 2-27 illustrate the asymmetric distribution of ligands. The alkyl chains of the alkynyl ligands are orientated above and below a 'disc' of copper atoms, approximately parallel to each other and in relatively close proximity. The hfac ligands form chelate rings with copper atoms on the rim of the disc, and thus radiate from the centre of the cluster.

It would appear that a requirement for aggregation to form high nuclearity Cu_{18} and Cu_{26} clusters is the ability of the alkyl chain alkynyl substituents to be able to pack closely without significant steric hindrance. It could then be inferred that using bulkier alkynyl ligands, which pack less efficiently would reduce the ability to form such large disc-shape structures and that smaller clusters might be formed. This hypothesis has been proved correct by the observation that the ligands, $C{\equiv}CSiMe_3$ and $C{\equiv}CBu^t$, form clusters containing ten and twelve copper atoms.

2.4.2 Effect of ligand bulk on the cluster forming reaction

It is likely that cluster assembly takes place when the volatile components of a solution of [Cu(hfac)(alkyne)] monomer in an excess of alkyne are removed *in vacuo*. At some stage during this process proton exchange must take place between the terminal alkyne and $hfac^-$. Free hfacH can then be removed from the system along with volatile free alkyne leaving coordinatively unsaturated Cu-hfac and Cu – alkynyl fragments (Scheme 2-2). These fragments would rapidly aggregate to form $[Cu_{x+y}(hfac)_x(alkynyl)_y]$ clusters. The mechanism of the aggregation processes is not known. The steric bulk of the alkynyl ligand appears to influence the assembly processes outlined in Scheme 2-2, and some important observations can be made as a result of the work described in this chapter.

Cu_{10} and Cu_{12} type clusters are only obtained directly from the cluster forming reaction when bulky alkyne ligands are used. These ligands are unable to form the close packed arrangement observed in the Cu_{18} and Cu_{26} clusters (Figure 2-27) so during the cluster forming step the degree of aggregation is limited, and Cu_{12} and Cu_{10} clusters are obtained.

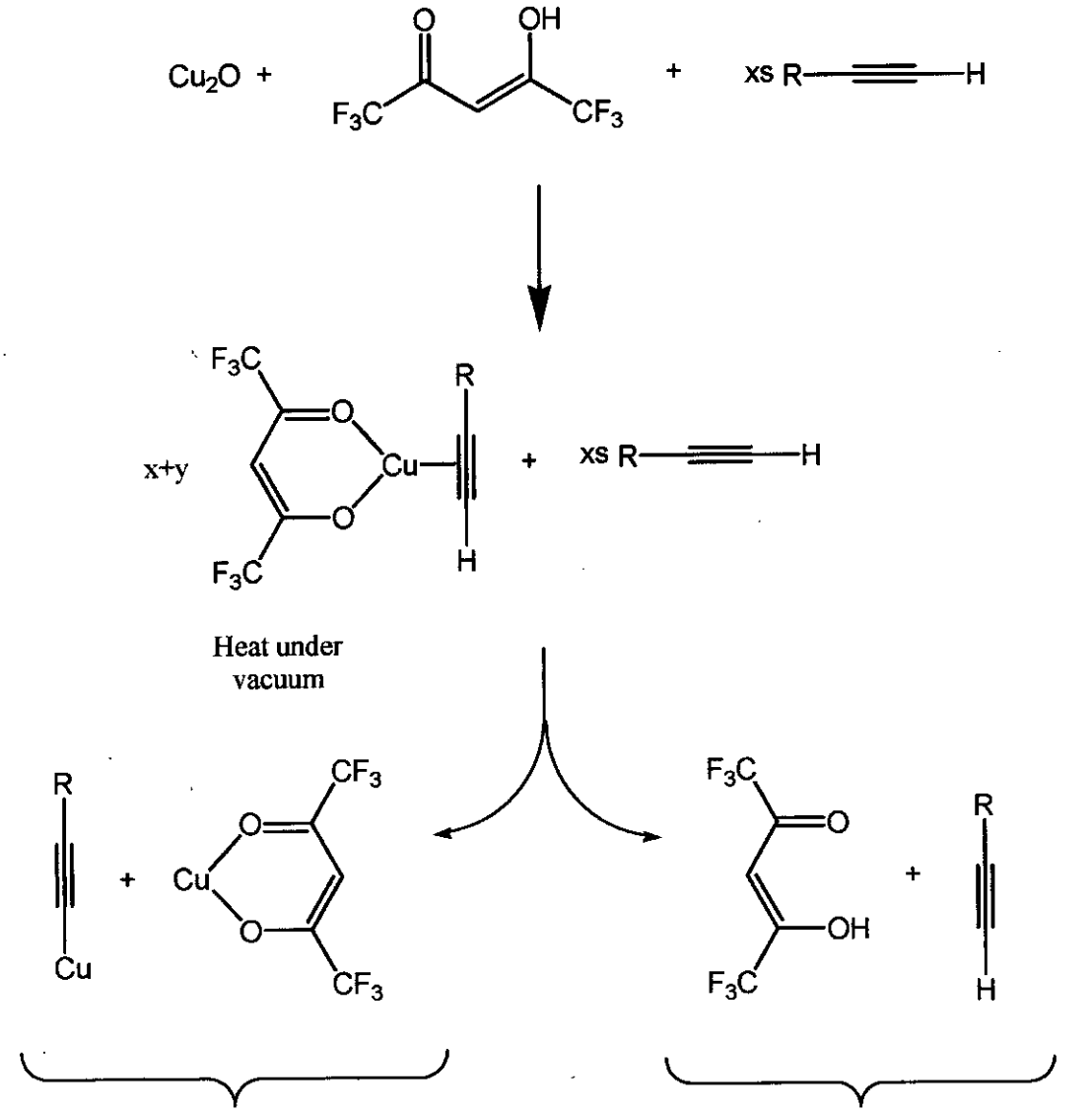

Scheme 2-2. Formation of polynuclear $[Cu_{x+y}(hfac)_x(RC{\equiv}C)_y]$ clusters *via* mononuclear $[Cu(hfac)(RC{\equiv}CH)]$ or $[Cu(hfac)(RC{\equiv}CH)_2]$

Low nuclearity clusters i.e. containing 10 or 12 copper atoms, comprising straight chain alkynyl ligands have only been observed when there are ether...Cu interactions present in the clusters. They have never been isolated directly from a cluster-forming reaction or from recrystallisation of materials from non-coordinating solvents. The incorporation of relatively bulky ether molecules as weakly coordinating ligands appears to increase the

separation of alkynyl ligands. The consequent reduction in the density of these bridging units limits the size of the copper core to a Cu_4C_4 unit which then can associate with Cu(hfac) units to give Cu_{10} or Cu_{12} clusters.

2.5 Nature of the Cu_4C_4 type cluster

The following section considers why Cu_4C_4 type clusters are obtained under aggregation limiting conditions.

2.5.1 Similarities between $[Cu_4(aryl)_4]$ and $[Cu_4(alkynyl)_4]$ clusters

Although additional peripheral (Cu-hfac)-alkynyl coordination adds an extra degree of complexity to the structures of the Cu_{10} and Cu_{12} clusters, they share a key structural feature with $[Cu_4(aryl)_4]$ type molecules described in Section 2.1. Both systems are comprised of a central Cu_4 core bridged by anionic carbon donor ligands with an approximately planar distribution of Cu atoms. The Cu...Cu distances in the core fall well below the sum of the van der Waal's radii (2.8 Å)[45] for two copper atoms. The structural and theoretical studies undertaken on the $[Cu_4(aryl)_4]$ series can help to explain the propensity of alkynyl ligands to form clusters based around a stable $[Cu_4(alkynyl)_4]$ unit.

Each copper atom in the $[Cu_4(aryl)_4]$ systems is bridged by two aryl ligands donating one electron from a carbon sp^2 hybrid orbital (Figure 2-2). In addition the ligands are aligned perpendicular to the Cu_4 plane to maximize π-interactions (Figure 2-5). The close Cu...Cu contacts observed in these clusters have been shown to be important in stabilising the ring *via* the formation of ligand-assisted metal–metal bonds by overlap of adjacent copper 3*d*, 4*s* and 4*p* orbitals and the aryl sp^2 hybrid orbital.[34] Calculations on $[Cu_4(aryl)_4]$ and related systems also suggested that Cu...Cu attractions in a Cu_4 core become greater with increasing σ-donor and π-acceptor capability of the bridging ligand.[35]

The alkynyl ligand is known[39] to be a good $1e^-$ σ-donor providing an electron from the terminal carbon *sp* hybrid orbital. It also has the ability to accept electron density into

vacant π^* orbitals. It seems likely, therefore, that the Cu_4C_4 rings, where the bridging carbon is an alkynyl group, should show comparable bonding and stability to $Cu_4(aryl)_4$ analogues. The four 3c–2e$^-$ bonds are formed by overlap of the $C_{terminal}$ 1 e$^-$-donating *sp* hybrid orbital with a bonding combination of Cu orbitals creating an alkynyl-assisted Cu – Cu bond.

It is difficult to infer any π contribution to the bonding in the $[Cu_4(alkynyl)_4]$ rings from crystal structures as variations in alkynyl bond lengths are dominated by the π interactions with Cu – hfac 'butterfly' wings. It seems likely, however, that there is some π-bonding as suggested by theoretical and structural studies on the $Cu_4(aryl)_4$ systems. [34]

When there is additional coordination by SMe_2 and related solvent molecules to the Cu_4 core of the $[Cu_4(aryl)_4]$ molecules, the square arrangement of Cu atoms is lost and a rhombic configuration is observed (Figure 2-4). The solvent molecules coordinate opposite Cu atoms in the Cu_4 core, elongating the Cu...Cu distances between solvated and non-solvated coppers. The Cu_4 cores in the $[Cu_{x+y}(hfac)_x(alkynyl)_y]$ series show similar Cu...Cu distances and consequently have the same planar rhombic Cu_4 arrangement as the $[Cu_4(aryl)_4(SMe_2)_2]$ series. In the $[Cu_4(aryl)_4(SMe_2)_2]$ series, the rhombic array is due to solvent coordination, whereas the Cu_4 core in the $[Cu_{x+y}(hfac)_x(alkynyl)_y]$ appears to be a result of the interactions between butterfly units. Interlocking occurs between 'a' and 'd' butterflies and 'b' and 'c' butterflies. These interactions appear to cause a distortion of the Cu_4 core from a square arrangement to a rhombic arrangement similar to that shown in Figure 2-4.

2.5.2 Cu_4C_4 as a cluster 'building block'

It has been observed that by employing a bulky alkynyl ligand system in the cluster - forming reactions it is possible to limit the degree of aggregation of the Cu-C≡CR and Cu-hfac fragments and isolate discrete molecules with formulae, $[Cu_{12}(hfac)_8(alkynyl)_4]$ and $[Cu_{10}(hfac)_6(alkynyl)_4]$. During this process the coordinatively unsaturated Cu-C≡CR fragment aggregates to form a $[Cu_4(C{\equiv}CR)_4]$ structure, similar to $[Cu_4(aryl)_4]$ compounds. At the same time Cu-hfac fragments that are also present in the medium

(Scheme 2-2) 'cap' the alkynyl groups through Cu-alkynyl π-interactions forming 'butterfly' and 'half-butterfly' units. It is therefore plausible that a key intermediate in the 'building up' of higher nuclearity clusters (i.e. Cu_{16} to Cu_{20}) is a structure with formula $[Cu_4(C{\equiv}CR)_4(Cu\text{-}hfac)_x]$ (Figure 2-28) that closely resembles clusters **1**, **2**, **3**, **4a**, **4b** and **5**.

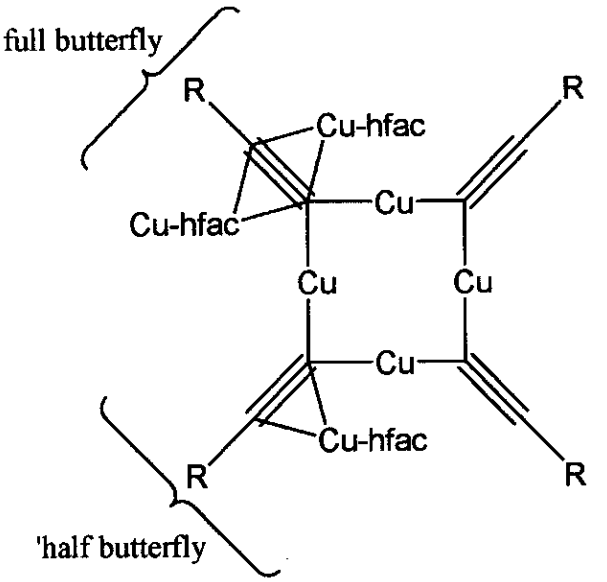

Figure 2-28. Proposed 'building block' with general formula $[Cu_4(C{\equiv}CR)_4(Cu\text{-}hfac)_x]$

2.6 Conclusions

The aim of defining how the synthetic scope of the reactions leading to $[Cu_{x+y}(hfac)_x(RC{\equiv}C)_y]$ clusters depends on the nature of the alkyne component has been clarified in this chapter with respect to the bulk of the alkyne substituents.

Increasing the steric bulk of an alkyne favours the formation of low nuclearity clusters (with 10 and 12 copper atoms) compared to the less bulkily substituted alkynes which form higher nuclearity systems i.e. Cu_{18} and Cu_{26}. **1**, **2**, **4a**, **4b** and **5** are the first examples of $[Cu_{x+y}(hfac)_x(alkynyl)_y]$ type clusters with low nuclearity (i.e. 10 and 12 copper atoms).

4b is the first example of a cluster containing more than one type of alkynyl ligand suggesting there is scope for the formation of other mixed alkynyl clusters.

All the Cu_{10}- and Cu_{12}- clusters which have been structurally characterised contain a similar $Cu_4(alkynyl)_4$ core. In the following two chapters the role of $[Cu_4(C{\equiv}CR)_4(Cu\text{-}hfac)_x]$ entities as 'building blocks' in cluster-aggregation will be considered. This will be done by first carrying out a detailed structural analysis of higher nuclearity systems, i.e. Cu_{16} to Cu_{26}, in order to identify fragments of the clusters that have $Cu_4(alkynyl)_4$ cores.

2.7 Experimental

Materials and reagents

All reagents were obtained from Aldrich Chemicals and used without further purification. *n*-Hexane was distilled from sodium/benzophenone/tetraglyme (trace) under N_2. N_2 gas was dried with 4Å molecular sieves and deoxygenated with BTS catalyst.[46] All preparations of copper(I) complexes were carried out under anaerobic and anhydrous conditions using standard Schlenk techniques. 3,3-Dimethyl-1-butyne, 3-phenyl-1-propyne and 1,1,1,5,5,5-hexafluoropentan-2,4-dione (hfacH) were degassed by freeze/vac/thaw cycles.

$[Cu_{12}(hfac)_8(C{\equiv}CPr^n)_4(THF)_6]$ (1)

$[Cu_{18}(hfac)_{10}(C{\equiv}CC_3H_7^n)_8]$ (2.50 g, 0.67 mmol) was dissolved in a minimum volume of hot THF (5 mL). The mixture was stored at 4 °C and after 4 days large pale orange blocks and deeper orange hexagonal plate crystals separated. The supernatant liquid was decanted using a cannula-needle. The crystals were washed with *n*-hexane (2 mL), re-dissolved in hot THF (7 mL) and set aside at -25°C for 4 days during which only the pale orange block crystals separated. The mother liquor was removed using a cannula-needle and the crystals were washed with cold THF (2 × 1 mL) and dried in vacuo to give $[Cu_{12}(hfac)_8(C{\equiv}CC_3H_7^n)_4(THF)_6]$, yield: 0.65 g (27 %). Found: C, 32.24; H, 2.64. Calc. for $C_{84}H_{84}Cu_{12}F_{48}O_{22}$: C, 32.34; H, 2.71%. IR Spectra (KBr disk): 3433w, 2972w, 2881w, 1642s, 1557m, 1532m, 1462s, 1345m, 1259s, 1217s, 1147s, 1099m, 1051w, 888w, 802m, 744w, 672m, 588m, 528w cm^{-1}.

$[Cu_{12}(hfac)_8(C{\equiv}CBu^t)_4]$ (2), $[Cu_{10}(hfac)_6(C{\equiv}CBu^t)_4$(diethyl ether)] (4a) and $[Cu_{10}(hfac)_6(C{\equiv}CBu^t)_3(C{\equiv}CPr^n)$(diethyl ether)] (4b). Cu_2O (1.64 g, 11.5 mmol) and anhydrous $MgSO_4$ (*ca.* 2 g) were added to a solution of 3,3-dimethyl-1-butyne (2.9 g, 35 mmol) and 1-pentyne (2.38 g, 35 mmol) in hexane (10 ml). Dropwise addition of hfacH (2.5 ml, 18 mmol) was accompanied by an exothermic reaction. After stirring for 18 h at room temperature the mixture was cannula-filtered and the solid residue washed with hexane (3 × 10ml). The combined lime green filtrate and washings were combined and the solvent removed *in vacuo*. The resulting brown/red solid was heated at 65 °C for 2 h under vacuum. To the solid was added hexane (5 ml) and the mixture heated to reflux. Approximately half the solid dissolved giving a dark red solution which was separated from insoluble yellow material by cannula filtration. This was set aside at 4 °C and after 48 hours yellow crystals had separated. Two further recrystallisations from hexane yielded yellow crystals suitable for X-ray diffraction. The supernatent liquid was removed and the crystals of **$[Cu_{12}(hfac)_8(C{\equiv}CBu^t)_4]$ (2)** were washed with hexane and dried *in vacuo*. Yield: 0.65 g (12.5 %). Found: C, 31.38; H, 2.03. Calc. for $C_{64}H_{44}O_{16}Cu_{12}F_{48}.C_{12}H_{28}$: C, 31.31; H 2.48 %.

The yellow solid that was insoluble in hexane and collected by filtration from the red solution was dissolved in a hexane : diethyl ether (1 : 1) solvent system (20 ml) and stored at -30 °C. After twelve weeks yellow crystalline blocks separated that were suitable for X-Ray diffraction. Two individual molecules were observed in the crystal structure, **$[Cu_{10}(hfac)_6(C{\equiv}CBu^t)_4$(diethyl ether)] (4a)** and **$[Cu_{10}(hfac)_6(C{\equiv}CBu^t)_3(C{\equiv}CPr^n)$(diethyl ether)] (4b).** The crystals were collected by filtration and dried *in vacuo*. Yield: 0.58 g (11.2 %). Found: C, 30.13; H, 2.16. Calc. for $C_{115}H_{102}O_{26}Cu_{20}F_{72}$: C, 30.13; H 2.16 %.

$[Cu_{12}(hfac)_8(C{\equiv}CSiMe_3)_4]$ (3). HfacH (2.5 ml, 18 mmol) was added dropwise to a suspension of Cu_2O (1.64 g, 11.5 mmol) and $MgSO_4$ (*ca.* 2g) in (trimethylsilyl)acetylene (7.2 ml, 51 mmol). The mixture was stirred for two hours then cannula-filtered. The solid residue was washed with hexane (3 × 10 ml) and the washings combined with the lime green filtrate. The volatile components were removed *in vacuo* leaving an oily red

material containing some yellow solid which was dried at 65 °C for two hours. The red oil was extracted in hexane (15 ml) and separated from the insoluble yellow solid by cannula-filtration. The solution was stored at 4 °C overnight during which time orange crystals separated suitable for X-ray diffraction. The supernatant liquid was removed and the crystals washed with hexane and dried *in vacuo*. Yield: 0.80 g (15 %). Found: C, 25.62; H 1.54. Calc. for $C_{60}H_{44}O_{16}F_{48}Si_4$: C, 25.67; H, 1.58 %.

$[Cu_{10}(hfac)_6(C{\equiv}CBu^t)_4$(diethyl ether)] (5)

5 was isolated using the same synthetic procedure described for **2**. During the recrystallisation step, a very small quantity of yellow crystalline material separated along with the red coloured Cu_{16} material. The yellow crystals were analysed by X-ray diffraction but due to the small quantities isolated and the instability of the material, further analysis was not possible.

$[Cu_{18}(hfac)_{10}(C{\equiv}CC_3H_7{}^n)_8]$ (6)

Into 1-pentyne (7.0 mL) was placed Cu_2O (2.53 g, 18 mmol) and anhydrous $MgSO_4$ (2.0 g, 17 mmol) forming a red suspension. Addition of hfacH (2.50 mL, 18 mmol) to the reaction mixture followed by stirring at RT for 66 hr resulted in a viscous orange suspension. *n*-Hexane (10 mL) was added to dilute the suspension to allow cannula-filtration. The residue was washed with *n*-hexane (3×10 ml) and the filtrate and washings combined to give a pale green solution. The volatile components of the solution were evaporated to dryness in vacuo yielding an orange-brown oil. This was dried at 65°C for 30 min *in vacuo* during which time the oil solidified. This solid was washed with hexane (20 ml, 2×5 mL), to remove a small quantity of disproportionation product, leaving a bright orange microcrystalline solid which was dried in vacuo to give $[Cu_{18}(hfac)_{10}(C{\equiv}CC_3H_7{}^n)_8]$. Yield: 2.87 g (44 %). Found: C, 28.93; H, 1.83. Calc. for $C_{90}H_{66}Cu_{18}F_{60}O_{20}$: C, 28.82; H, 1.77%. IR Spectra (KBr disk): 3499w, 2964w, 1672m, 1642s, 1554m, 1528s, 1513s, 1463m, 1255s, 1209s, 1146s, 1100m, 795m, 743w, 662m, 580m, 526w cm^{-1}.

References

1 G. H. Posner, 'An Introduction to Synthesis using Organocopper Reagents', Wiley Interscience, 1980.

2 J. A. J. Jarvis, B. T. Kilbourn, R. Pearce, and M. F. Lappert, *Chem. Commun.* , 1973, 475.

3 D. Nobel, G. Van Koten, and A. L. Spek, *Angew. Chem.* , 1989, **101**, 211.

4 H. Eriksson, M. Hakansson, and S. Jagner, *Inorg. Chim. Acta* 1998, **277**, 233.

5 M. Hakansson, H. Eriksson, A. Berglund Ahman, and S. Jagner, *J. Organomet. Chem.* , 2000, **595**, 102.

6 A. Sundararaman, R. A. Lalancette, L. N. Zakharov, A. L. Rheingold, and F. Jaekle, *Organometallics*, 2003, **22**, 3526.

7 H. Eriksson and M. Hakansson, *Organometallics*, 1997, **16**, 4243.

8 H. Eriksson, M. Oertendahl, and M. Haakansson, *Organometallics.*, 1996, **15**, 4823.

9 R. W. M. Ten Hoedt, J. G. Noltes, G. Van Koten, and A. L. Spek, *Dalton Trans.*, 1978, 1800.

10 E. W. Abel, F. G. A. Stone, G. Wilkinson, and Editors, 'Comprehensive Organometallic Chemistry II: A Review of the Literature 1982-1994, 14 Volume Set', 1995.

11 M. M. Olmstead and P. P. Power, *J. Am. Chem. Soc.*, 1990, **112**, 8008.

12 S. Gambarotta, C. Floriani, A. Chiesi-Villa, and C. Guastini, *Chem. Commun.*, 1983, 1156.

13 E. M. Meyer, S. Gambarotta, C. Floriani, A. Chiesi-Villa, and C. Guastini, *Organometallics*, 1989, **8**, 1067.

14 B. Lenders, D. M. Grove, G. van Koten, W. J. J. Smeets, P. Van der Sluis, and A. L. Spek, *Organometallics*, 1991, **10**, 786.

15 J. M. Guss, R. Mason, I. Soetofte, G. van Koten, and J. G. Noltes, *Chem. Commun.* , 1972, 446.

16 G. Van Koten and J. G. Noltes, *J. Organomet. Chem.* , 1975, **84**, 129.

17 E. Wehman, G. van Koten, M. Knotter, H. Spelten, D. Heijdenrijk, A. N. S. Mak, and C. H. Stam, *J. Organomet. Chem.* , 1987, **325**, 293.

18 M. Jansen, *Angew. Chem.* , 1987, **99**, 1136.

19 P. Pyykko, N. Runeberg, and F. Mendizabal, *Chem. Eur. J.* , 1997, **3**, 1451.

20 P. Pyykko and F. Mendizabal, *Chem. Eur. J.* , 1997, **3**, 1458.

21 P. Pyykko, *Chem. Rev.*, 1997, **97**, 597.

22 P. Pyykkoe and F. Mendizabal, *Inorg. Chem.*, 1998, **37**, 3018.

23 P. Pyykko, *Angew. Chem. Int. Ed.*, 2002, **41**, 3573.

24 F. A. Cotton, X. Feng, M. Matusz, and R. Poli, *J. Am. Chem. Soc.*, 1988, **110**, 7077.

25 F. A. Cotton, X. Feng, and D. J. Timmons, *Inorg. Chem.*, 1998, **37**, 4066.

26 G. Boche, F. Bosold, M. Marsch, and K. Harms, *Angew. Chem. Int. Ed.* , 1998, **37**, 1684.

27 M. John, C. Auel, C. Behrens, M. Marsch, K. Harms, F. Bosold, R. M. Gschwind, P. R. Rajamohanan, and G. Boche, *Chem. Eur. J.* , 2000, **6**, 3060.

28 J. M. Zuo, M. Kim, M. O'Keeffe, and J. C. H. Spence, *Nature*, 1999, **401**, 49.

29 C.-M. Che, Z. Mao, V. M. Miskowski, M.-C. Tse, C.-K. Chan, K.-K. Cheung, D. L. Phillips, and K.-H. Leung, *Angew. Chem. Int. Ed.* , 2000, **39**, 4084.

30 X.-Y. Liu, F. Mota, P. Alemany, J. J. Novoa, and S. Alvarez, *Chem. Commun.*, 1998, 1149.

31 C. Koelmel and R. Ahlrichs, *J. Phys. Chem.* , 1990, **94**, 5536.

32 C. He, J. L. DuBois, B. Hedman, K. O. Hodgson, and S. J. Lippard, *Angew. Chem. Int. Ed.* , 2001, **40**, 1484.

33 U. Siemeling, U. Vorfeld, B. Neumann, and H.-G. Stammler, *Chem. Commun.*, 1997, 1723.

34 P. Belanzoni, M. Rosi, A. Sgamellotti, E. J. Baerends, and C. Floriani, *Chem. Phys. Lett.* , 1996, **257**, 41.

35 H. L. Hermann, G. Boche, and P. Schwerdtfeger, *Chem. Eur. J.* , 2001, 7, 5333.

36 A. F. Wells, 'Structural Inorganic Chemistry. 5th Ed', 1983.

37 T. C. Higgs, *Unpublished work, University of Edinburgh*, 2004.

38 T. C. Higgs, P. J. Bailey, S. Parsons, and P. A. Tasker, *Angew. Chem. Int. Ed.* , 2002, **41**, 3038.

39 J. Manna, K. D. John, and M. D. Hopkins, *Adv. Organomet. Chem.* , 1995, **38**, 79.

40 C. Oehr and H. Suhr, *Appl. Phys. A* 1988, **A45**, 151.

41 H. K. Shin, K. M. Chi, M. J. Hampden-Smith, T. T. Kodas, J. D. Farr, and M. Paffett, *Chem. Mater.* , 1992, **4**, 788.

42 T. C. Higgs, S. Parsons, P. J. Bailey, A. C. Jones, F. McLachlan, A. Parkin, A. Dawson, and P. A. Tasker, *Organometallics.*, 2002, **21**, 5692.

43 T. C. Higgs, S. Parsons, A. C. Jones, P. J. Bailey, and P. A. Tasker, *Dalton Trans.* , 2002, 3427.

44 C. W. Baxter, T. C. Higgs, A. C. Jones, S. Parsons, P. J. Bailey, and P. A. Tasker, *Dalton Trans.* , 2002, 4395.

45 J. C. Slater, *J. Chem. Phys.* , 1964, **41**, 3199.

46 A. J. Gordon and R. A. Ford, *The Chemists Companion: A handbook of practical data, techniques and references, Wiley-Interscience.*

Chapter three

Cu_{16} to Cu_{20} Clusters

3.1 Introduction

One of the aims of this thesis was to define the scope of the synthetic procedure reported by Higgs *et al.*[1] used to obtain clusters with formulae, $[Cu_{x+y}(hfac)_x(alkynyl)_y]$. This has been done by systematically varying reaction parameters in order to understand how the structure of the resulting clusters can be influenced. This chapter describes the effect of using the alkyne ligands, 3,3-dimethyl-1-butyne ($Bu^tC{\equiv}CH$) and 3-phenyl-1-propyne ($PhCH_2C{\equiv}CH$) in cluster synthesis which have greater steric bulk than the straight chain alkynyl ligands used in the previously reported systems.[1-3] The outcome of the cluster-forming reaction using a phenyl-substituted hfacH derivative, phenyl-tfacH and how the ligand properties influence the characteristics of the cluster will also be described.

The synthesis and characterization of four novel clusters, $[Cu_{16}(hfac)_8(C{\equiv}CBu^t)_8]$ (**10**), $[Cu_{18}(phenyl\text{-}tfac)_{10}(C{\equiv}CBu^n)_8]$ (**11**), $[Cu_{18}(hfac)_{10}(C{\equiv}CPr^n)_6(C{\equiv}CBu^t)_2]$ (**12**) and $[Cu_{20}(hfac)_8(C{\equiv}CCH_2Ph)_{16}]$ (**13**) are described and structural comparisons made with previously obtained Cu_{18} systems, $[Cu_{18}(hfac)_{10}(C{\equiv}CPr^n)_8]$ (**8**) and $[Cu_{18}(hfac)_{10}(C{\equiv}CBu^n)_8]$ (**9**), as well as the lower nuclearity clusters described in chapter 2.

In chapter two, it was shown that the disposition of Cu-hfac chelate rings on the cluster periphery is influenced by weak inter-ring Cu...O interactions. In the first half of chapter three an analysis of Cu-diketonate...Cu-diketonate interactions in **10**, **11**, **12** and **13** will be undertaken and their influence on the cluster structures discussed. In the second half of chapter three the nature of the central copper core will be considered and the relationship between the cores of the $Cu_{16} \rightarrow Cu_{20}$ and the $Cu_{10} \rightarrow Cu_{12}$ series explored.

3.2 Cluster Synthesis

All four clusters were synthesized using variations of the standard cluster forming reaction first reported by Higgs *et al.*[1] Details are included in the experimental section 3.7.

3.2.1 $[Cu_{16}(hfac)_8(C{\equiv}CBu^t)_8]$ (10)

10 was the major product when 3,3-dimethyl-1-butyne ($HC{\equiv}CBu^t$), diluted in hexane, was used as the solvent system. Crystals were obtained from a saturated hexane solution and crystallized in the tetragonal *P*-4*n*2 space group. The cluster is composed of four crystallographically independent copper atoms, two hfac and two 3,3-dimethyl-1-butynyl ligands. The remainder of the cluster is generated by two mutually perpendicular C_2 axes and the structure is shown in Figure 3-7.

3.2.2 $[Cu_{18}(phenyl\text{-}tfac)_{10}(C{\equiv}CBu^n)_8]$ (11)

11 was the major product of the standard cluster reaction using the β-diketone ligand 4,4,4-trifluoro-1-phenyl-1,3-butanedione (Ph-tfac) (**14**) in place of hfacH. This is the first example of a $[Cu_{x+y}(hfac)_x(alkynyl)_y]$ type cluster where a trifluorinated hfacH derivative has been successfully used in cluster synthesis. The material crystallized in the monoclinic *P*-1 space group and the structure is shown in Figure 3-10. There are two crystallographically independent half molecules in the asymmetric unit. The full molecules, **11a** and **11b**, were generated by application of a two fold axis.

3.2.3 $[Cu_{18}(hfac)_{10}(C{\equiv}CPr^n)_6(C{\equiv}CBu^t)_2]$ (12)

The synthesis of **12** is of considerable interest as it is an example of a mixed alkynyl cluster containing six $C{\equiv}CPr^n$ and two $C{\equiv}CBu^t$ ligands. Incorporation of different alkynyl ligands was achieved by changing the conditions of the cluster-forming step in the standard preparative procedure. The initial reaction between Cu_2O, hfacH and the alkyne and subsequent filtration was carried out as normal. Instead of removing the volatile components rapidly *in vacuo*, however, the solution was allowed to evaporate over a two days. The brown solid residue was crystallized from a saturated hexane solution in the orthorhombic *Pbca* space group. The structure of **12** contains half a molecule in the asymmetric unit and the remainder of the molecule is generated by inversion. The structure is shown in Figure 3-14.

3.2.4 $[Cu_{20}(hfac)_8(C{\equiv}CCH_2Ph)_{12}]$ (13)

A variation of the standard cluster-forming reaction was used in the preparation of **13**. Due to the increased relative acidity of the terminal proton of 3-phenyl-1-propyne steps were taken to minimize spontaneous polymerization of the alkyne with copper. This involved cooling the reaction mixture to 0°C and adding Cu_2O as the last component to a solution of hfacH and $PhCH_2C{\equiv}CH$ in the presence of $MgSO_4$. Following this initial step the cluster was obtained according to the standard preparative procedure and crystals separated from a saturated hexane solution, crystallizing in the monoclinic $P2_1/c$ space group. The cluster has no crystallographically imposed symmetry and the structure can be seen in Figure 3-17.

3.2.5 Ligand synthesis

4,4,4-Trifluoro-1-phenyl-1,3-butanedione (**14**) was synthesized by Claisen condensation between acetophenone and ethyl trifluoroacetate using potassium *tert*-butoxide as the base. The reaction proceeded in high yield (91 %). ^1H NMR showed the ligand to exist in the enolic form in solution (Figure 3-1).

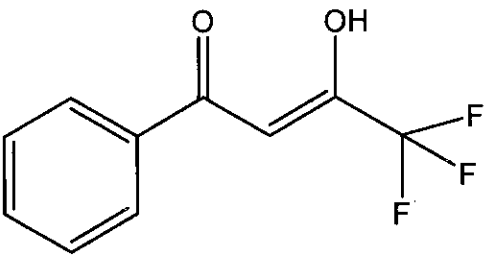

Figure 3-1. The enolic structure of 4,4,4-trifluoro-1-phenyl-1,3-butanedione (Ph-tfac) (**14**).

3.3 Structural Features

Clusters **10**, **11**, **12** and **13** show a number of structural features that are novel to the $[Cu_{x+y}(hfac)_x(alkynyl)_y]$ family as a result of varying the nature of the ligands. In order

to allow comparisons between the novel clusters and previously reported systems, a 'conventional' Cu_{18} structure will be defined in the following section based on the structures of **8** and **9**.

3.3.1 $[Cu_{18}(hfac)_{10}(C{\equiv}CPr^n)_8]$ (8) and $[Cu_{18}(hfac)_{10}(C{\equiv}CBu^n)_8]$ (9)

Using the synthetic method developed by Higgs *et al.*[1] two Cu_{18} clusters were isolated and characterised, $[Cu_{18}(hfac)_{10}(C{\equiv}CPr^n)_8]$ (**8**)[1] and $[Cu_{18}(hfac)_{10}(C{\equiv}CBu^n)_8]$ (**9**).[2, 3] The structures of these molecules are similar (Figure 3-2) and define the 'conventional' appearance of a Cu_{18} cluster.

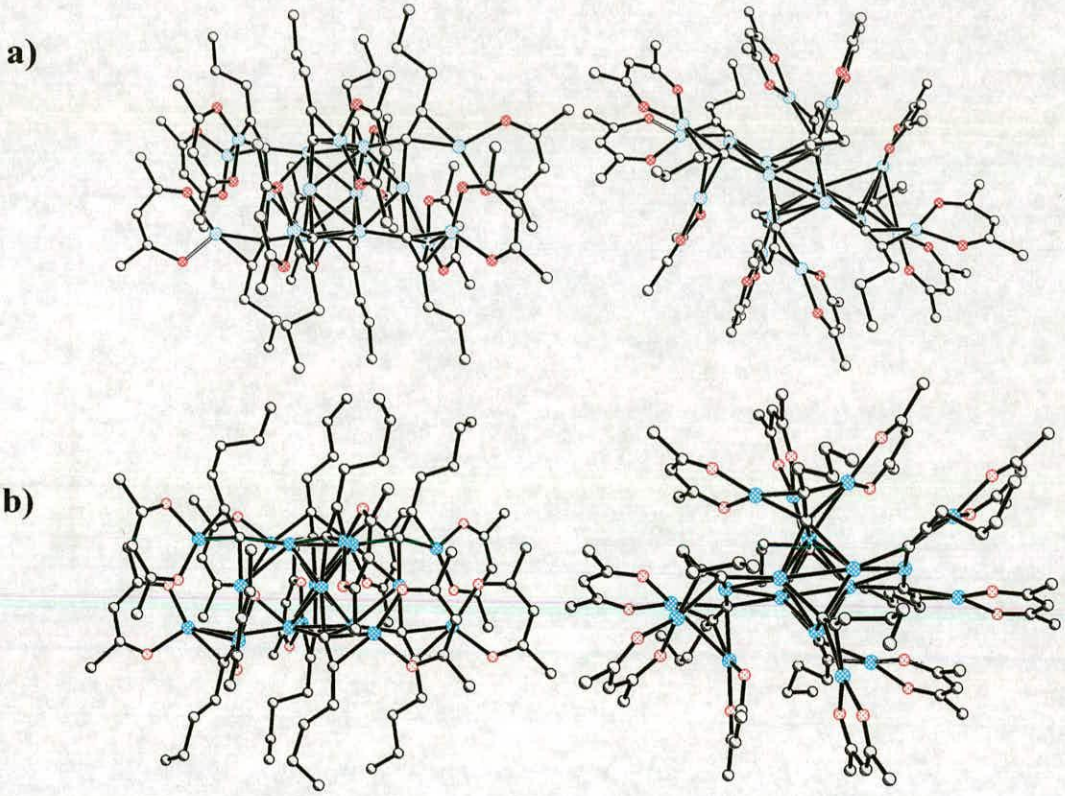

Figure 3-2. Perpendicular views of the structures of the Cu_{18} clusters, $[Cu_{18}(hfac)_{10}(C{\equiv}CPr^n)_8]$ (**8**) and $[Cu_{18}(hfac)_{10}(C{\equiv}CBu^n)_8]$ (**9**)

They both contain a central alkynyl bridged Cu core around which the alkynyl and hfac ligands are distributed unevenly. Alkyl chains align along the axial direction in a 'four up, four down' arrangement and Cu-hfac rings lie in the equatorial plane encircling the

cluster cores forming a 'girdle' around the widest part of the molecule. The alkynyl groups are located inside this 'girdle' with the alkyl chains lying approximately perpendicular to the plane (Figure 3-2).

The cores of **8** and **9** consist of eight copper atoms held together by a network of multiply bridging alkynyl ligands. The eight central metals have Cu...Cu contacts that fall in the range 2.479(3)–2.543(3) Å for **8** and 2.499(1)-2.7607(6) Å for **9** which are below the sum of the van der Waals radii for copper (2.8 Å).[4] The alkynyl ligands that support the central core adopt (μ_2-η^1:μ-η^2), (μ_3-η^1:μ-η^2), (μ_2-η^1:μ_2-η^2) and (μ_3-η^1:μ_2-η^2) bridging modes (Figure 3-3).

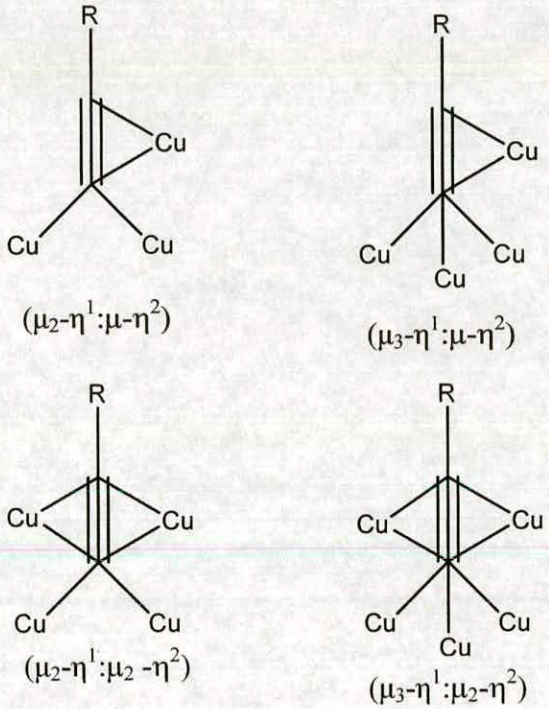

Figure 3-3. Alkynyl bridging modes in **8** and **9**

The remaining ten copper atoms in the Cu-hfac 'girdle' are associated with the central core *via* π-interactions to the alkynyl ligands. These chelate rings radiate from the centre of the core, and close inspection of both clusters shows the presence of a number of

short inter Cu-hfac ring contacts (< 3.4 Å, the sum of the van der Waals radii of copper and oxygen)[5] indicative of attractive dipole-dipole interactions. The distribution of Cu-hfac rings in **8** and **9** is shown in Figure 3-4.

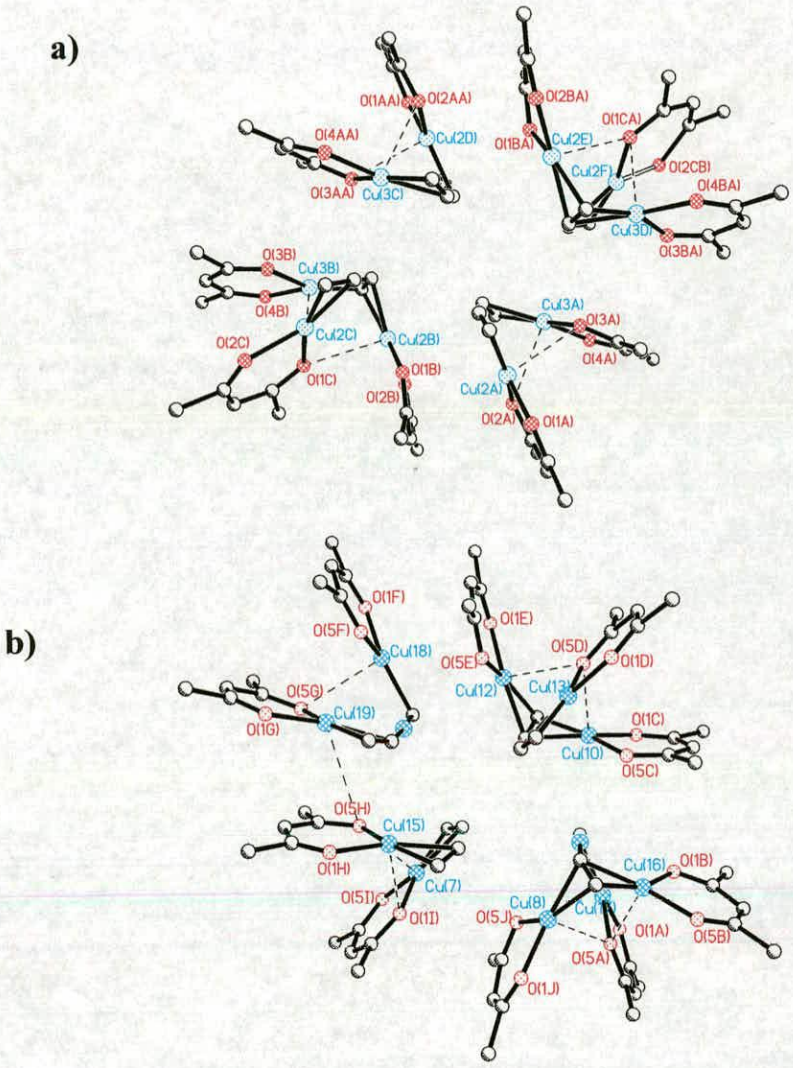

Figure 3-4. Distribution of Cu-hfac chelate rings in a) **8** and b) **9**

Both **8** and **9** contain fragments that resemble the 'butterfly' units described in chapter 2 where an alkynyl ligand coordinates two Cu-hfac rings through π-interactions. The remaining alkynyls coordinate only one Cu-hfac ring each resulting in fragments that resemble the 'half butterfly' units described in chapter 2 (Figure 2-14).

Each 'butterfly' unit in **8** and **9** encloses a 'half butterfly'. The 'half butterfly' resides in between the 'wings' of a full butterfly with an oxygen atom from the interlocked Cu-hfac ring bridging the two copper atoms of the 'butterfly' (Figure 3-5). This arrangement resembles the Mode B type interactions described in chapter 2 (Figure 2-20). In Mode B interactions, however, the Cu...O...Cu bridging modes are approximately symmetrical, whereas the Cu...O...Cu bridging modes in **8** and **9** these are relatively unsymmetrical (Table 3-1).

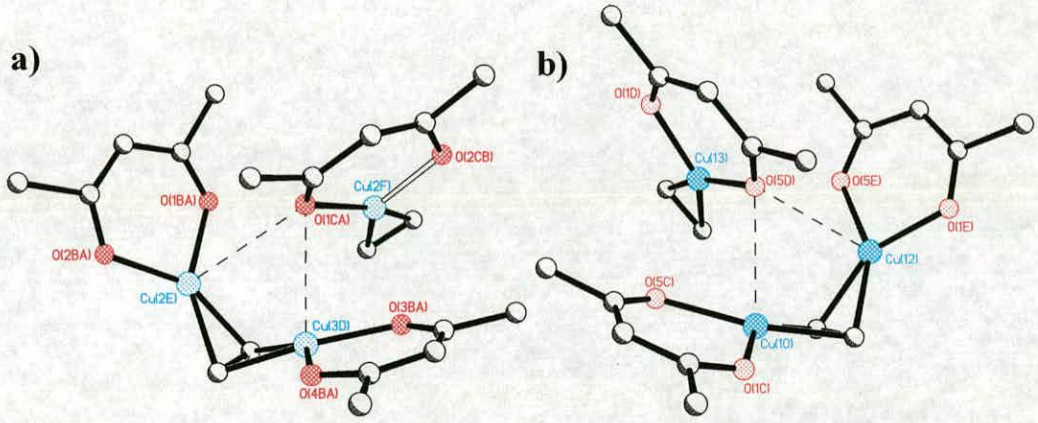

Figure 3-5. Butterfly units enclosing half butterfly units in **8** and **9**, (a) and (b) respectively

8			
O1C...Cu2B	3.171	O1CA...Cu2E	3.171
O1C...Cu3B	2.789	O1CA...Cu3D	2.789
9			
O5D...Cu12	3.035	O5A...Cu16	2.929
O5D...Cu10	2.807	O5A...Cu8	3.238

Table 3-1. Short inter-ring Cu...O contacts (Å) between interlocking units in **8** and **9**. Atom numbers correspond to the numbering schemes shown in Figures 3-4

In both clusters the four 'half butterflies' not involved in interlocking interactions form pairs of interacting rings (Figure 3-6). The rings are aligned to allow relatively close inter-ring Cu...O contacts although cofacial overlap often observed between interacting

Cu-hfac units does not occur. In **8** the two interacting pairs reside on opposite sides of the cluster whereas in **9** they are adjacent (Figure 3-4).

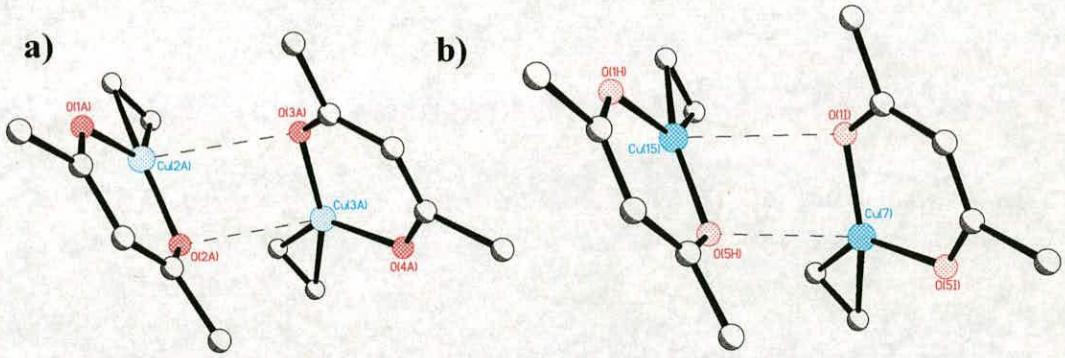

Figure 3-6. Pairs of interacting Cu-hfac rings in (a) **8** and (b) **9**.

8			
Cu2A...O3A	3.026	Cu2D...O3AA	3.026
Cu3A...O2A	3.080	Cu3C...O2AA	3.080
9			
Cu18...O5G	3.085	Cu7...O5H	2.958
Cu19...O5H	3.616	Cu15...O1I	3.009

Table 3-2. Short inter-ring Cu...O contacts (Å) between non-interlocking 'half butterflies' in **8** and **9**. Atom numbers correspond to the numbering schemes shown in Figure 3-4.

It appears that the uneven distribution of alkynyl and hfac ligands and therefore the overall appearance of **8** and **9** can be explained partly by the propensity for Cu-hfac rings to align to generate inter-ring Cu...O interactions. This results in a 'girdle' of interacting Cu-hfac rings that lies approximately parallel to the central copper core. The alkynyl ligands lie approximately perpendicular to the disc of copper atoms enclosed in the 'girdle' of chelate rings, and presumably they are disposed so as to optimize the packing of their pendant alkyl chains.

3.3.2 $[Cu_{16}(hfac)_8(C{\equiv}CBu^t)_8]$ (10)

The solid state structure of the Cu_{16}- cluster, **10**, is shown in Figure 3-7. There are four crystallographically independent copper atoms, two hfac and two 3,3-dimethyl-1-butynyl ligands and the molecule is generated by two mutually perpendicular C_2 axes. As in **8** and **9** the Cu(I) atoms are located in two environments. Eight copper atoms form a tightly packed inner cage bridged exclusively by alkynyl ligands. Cu...Cu distances in the interior of the cluster range between 2.5159(6)-3.0430(7) Å (Table 3-3) and several of these contacts are shorter than twice the van der Waals radius of copper (2.8 Å). The eight atoms in the outer shell are bonded to hfac ligands and each of these Cu(I)-hfac capping units is then linked to the inner shell by a π bond to a *t*-butylacetynyl ligand.

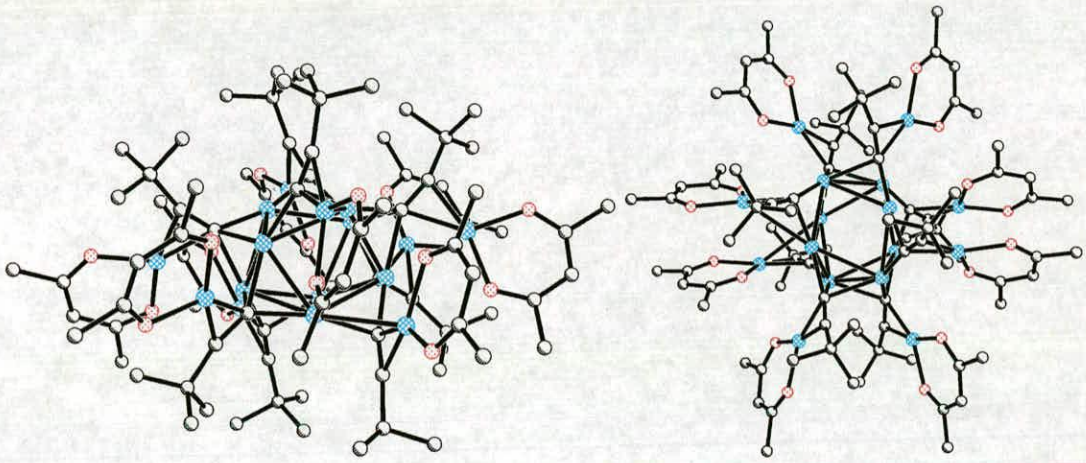

Figure 3-7. Two views of $[Cu_{16}(hfac)_8(C{\equiv}CBu^t)_8]$, (**10**)

The central copper core is bridged by alkynyl ligands acting as (μ_2-η^1:μ-η^2) and (μ_3-η^1:μ_2-η^2) bridging modes (Figure 3-3). There are two crystallographically independent alkynyl ligands. One of these bridges two copper atoms and the other bridges three copper atoms through σ interactions and both form one additional π interaction a Cu-hfac chelate ring. The terminal alkynyl-Cu bond lengths fall in the range 1.933(3) - 2.014(3) Å and the μ_3- bridging ligand has a third longer C...Cu interaction (2.270(4) Å) which must be less strongly bonding than the other two short interactions.

Cu...Cu distances in the inner shell			
Cu(1)...Cu(4)	2.5159(6)	Cu(1)...Cu(1A)	2.6116(8)
Cu(1)...Cu(4A)	2.8548(6)	Cu(1)...Cu(4B)	2.6428(6)
Cu(1A)...Cu(4)	2.8548(8)		
Cu...Cu distances between inner and outer shell atoms			
Cu(1)...Cu(2)	2.7595(7)	Cu(1)...Cu(2A)	3.954(1)
Cu(1)...Cu(3)	3.1698(7)	Cu(4)...Cu(3B)	3.0430(7)
Cu(4)...Cu(2)	3.667(1)		
Alkynyl bond lengths			
C(11)...C(12)	1.265(5)	C(17)-C(18)	1.253(5)
Alkynyl C...Cu distances			
Cu1...C11	2.014(3)	Cu1A...C11A	2.014(3)
Cu1...C17	1.933(3)	Cu1A...C17A	1.933(3)
Cu4...C11	1.949(4)	Cu4A...C11A	1.949(4)
Cu4...C17B	1.948(3)	Cu4A...C17C	1.948(3)
Cu1B...C17B	1.933(3)	Cu1C...C17C	1.933(3)
Cu1B...C11B	2.014(3)	Cu1C...C11C	2.014(3)
Cu4B...C11B	1.949(4)	Cu4C...C11C	1.949(4)
Cu4B...C17	1.948(3)	Cu4C...C17A	1.948(3)
Cu1...C11A	2.270(4)	Cu1A...C11	2.270(4)
Cu1B...C11C	2.270(4)	Cu1C...C11B	2.270(4)

Table 3-3. Selected bond distances (Å) from the crystal structure of **10**. The Cu...Cu contacts listed in this table and in all other tables in this thesis are generated using SHELX[6] crystallographic software and are defined as less than the covalent radii + 0.5 Å

The hfac and alkynyl ligands are disposed unevenly in a similar arrangement to that observed in **8** and **9**. The hfac units encircle the rim of the cluster and the alkynyl units located inside this ring lie approximately perpendicular to the plane it defines. As in **8** and **9** the Cu-hfac chelate rings appear to be aligned to allow the formation of relatively short Cu...O inter-ring interactions which are shown in Figure 3-8.

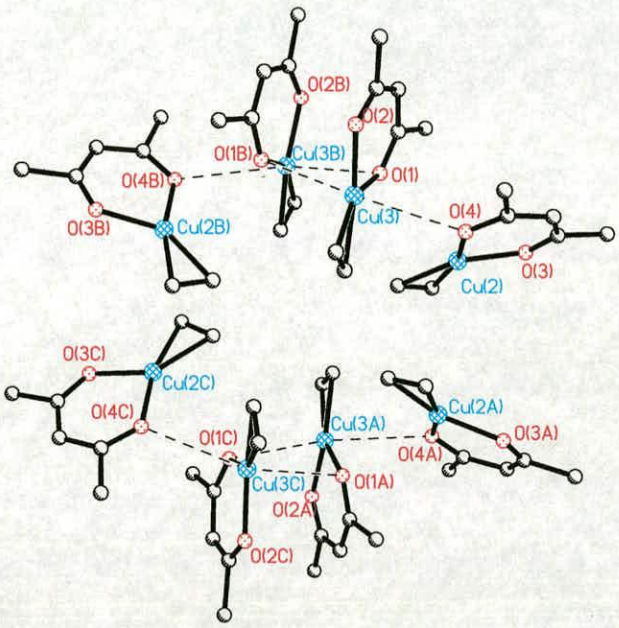

Figure 3-8. Disposition of Cu-hfac chelate rings in **10** showing close Cu…O contacts.

There are no full butterfly units in **10** and so no interlocking modes are present, however, each Cu-hfac chelate ring is involved in inter-ring interactions with one or two other rings. Rings containing Cu3 and Cu3B form a pair, as do rings containing Cu3A and Cu3C and these adopt a cofacial arrangement (Figure 3-9). The rings are staggered in order to reduce steric repulsion between $-CF_3$ groups and allow short Cu…O contacts to form (Table 3-4). The least squares plane of the overlapping rings defined by the six atoms of each ring are orientated at an angle of 7.7(1)° from each other. This overlapping arrangement of Cu-hfac rings is similar to the interaction observed in the Mode A interlocking described in chapter 2.

Cofacial interactions			
Cu3...O1A	3.161(3)	Cu3B...O1C	3.161(3)
Cu3A...O1	3.161(3)	Cu3C...O1B	3.161(3)
Angles between rings[a]	7.7(1)°	Angles between rings[b]	7.7(1)°
Non-cofacial interactions			
Cu3...O4	3.212(3)	Cu3C...O4C	3.212(3)
Cu3B...O4B	3.212(3)	Cu3A...O4A	3.212(3)

Table 3-4. Inter-ring Cu...O contacts (Å) and angles between interacting Cu-hfac chelate rings in **10**. Planes are defined by Cu3, O1, O2, C2, C3 and C4, Cu3B, O1B, O2B, C2B, C3B C4B for *a* and by Cu3A, O1A, O2A, C2A, C3A and C4A, Cu3C, O1C, O2C, C2C, C3C and C4C for *b*. Equations for the planes are given in appendix 2.

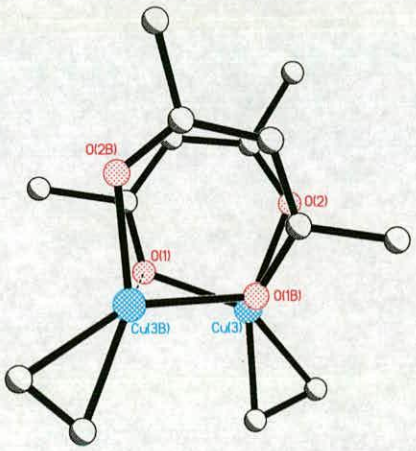

Figure 3-9. Cofacial overlap of Cu-hfac chelate rings containing Cu3 and Cu3B respectively in **10**

The copper atoms from the Cu-hfac units involved in π-stacking type interactions, and each form one additional short contact with an oxygen from an adjacent chelate ring (Table 3-4).

As in **8** and **9** the overall structure of **10** appears to be significantly influenced by secondary bonding between Cu-hfac units that encircle the copper core.

3.3.3 $[Cu_{18}(phenyl\text{-}tfac)_{10}(C{\equiv}CBu^n)_8]$ (11)

The structure of **11** is of interest because it is the first example of a cluster with general formula, $[Cu_{x+y}(hfac)_x\ (alkynyl)_y]$ that has been isolated using a trifluorinated 1,3-diketone ligand, 4,4,4-trifluoro-1-phenyl-1,3-butanedione (**14**) (phenyl-tfac) instead of hfac. There are two crystallographically independent half molecules, **11a** and **11b** in the asymmetric unit from which two full molecules are generated by two fold axes of symmetry. For the purpose of this discussion only the structure of **11a** (Figure 3-10) will be considered as **11a** and **11b** are structurally very similar.

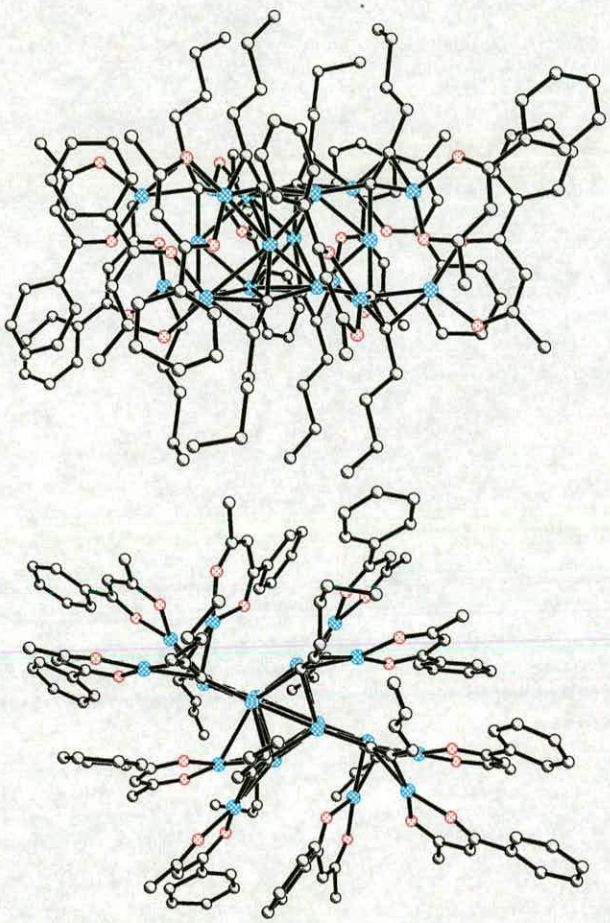

Figure 3-10. Two views of $[Cu_{18}(phenyl\text{-}tfac)_{10}(C{\equiv}CBu^n)_8]$ (**11a**)

Despite the fact that a phenyl ring has been incorporated into the 'capping' 1,3-diketonyl ligand, **11** adopts a similar structure to those discussed above. There is a central core of

eight copper atoms bridged exclusively by alkynyl ligands using all of the bridging modes, (μ_2-η^1:μ-η^2), (μ_3-η^1:μ-η^2), (μ_2-η^1:μ_2-η^2) and (μ_3-η^1:μ_2-η^2), shown in Figure 3-3. The Cu…Cu contacts in this core fall in the range, 2.493(2)-2.810(2) Å and the terminal alkynyl C-Cu distances are comparable to those observed in **10** (Table 3-5). The remaining ten copper atoms (Table 3-5) form chelate rings with the Ph-tfac ligands that encircle the central core. As with the other clusters described so far in this chapter each Cu-Ph-tfac chelate ring is associated with the core of the cluster through a π-interaction with one alkynyl ligand.

Cu…Cu distances in the central core (Å)			
Cu1A…Cu1B	2.811(2)	Cu1B…Cu1H	2.494(2)
Cu1B…Cu1C	2.490(2)	Cu1D…Cu1E	2.539(2)
Cu1C…Cu1D	2.493(2)	Cu1D…Cu1F	2.494(2)
Cu1A…Cu1D	2.786(2)	Cu1E…Cu1F	2.811(2)
Cu1A…Cu1F	2.575(2)	Cu1E…Cu1H	2.786(2)
Cu1B…Cu1E	2.575(2)	Cu1H…Cu1G	2.494(2)
Alkynyl bond lengths in the asymmetric unit (Å)			
C1A…C2A	1.19(2)	C1C…C2C	1.26(2)
C1B…C2B	1.24(2)	C1D…C2D	1.25(2)
Alkynyl terminal C-Cu bond lengths in the asymmetric unit (Å)			
C1A…Cu1A	1.91(2)	C1B…Cu1C	1.88(2)
C1D…Cu1A	1.93(2)	C1C…Cu1C	1.89(2)
C1B…Cu1B	2.00(2)	C1C…Cu1D	2.00(1)
C1D…Cu1B	2.08(1)	Cu1D…C1A	2.09(1)

Table 3-5. Selected bond lengths in **11a**

The effect of using a phenyl-substituted derivative of hfac is evident when considering how the Cu-(phenyl-tfac) chelate rings are disposed and the nature of inter-chelate interactions. In **8**, **9** and **10**, the peripheral Cu-hfac chelate rings are connected by a network of Cu…O contacts. These interactions are either cofacial interactions where overlap of approximately parallel rings is observed or non-cofacial where hfac oxygen atoms form contacts which are less than 3.4 Å with copper atoms from another Cu-hfac ring without overlapping. By substituting a phenyl ring into the chelating unit, there is

increased scope for intramolecular secondary bonding as the phenyl ring can form additional π stacking interactions. This can be seen in the disposition of Cu-(phenyl-tfac) chelate rings in **11** (Figure 3-11).

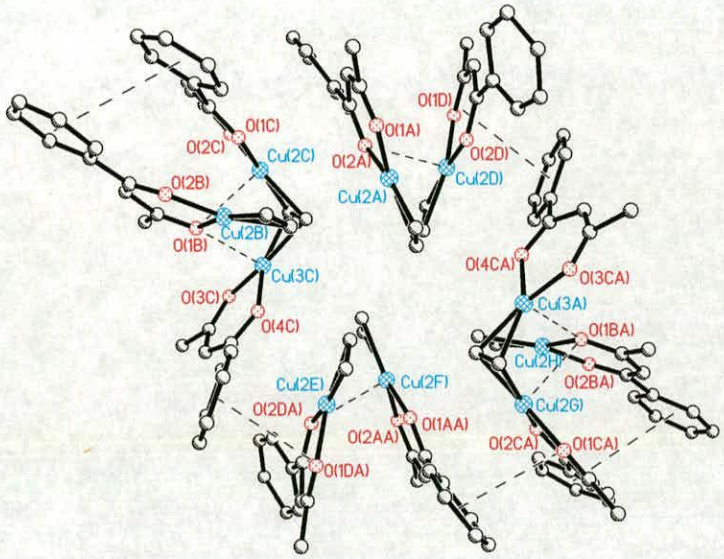

Figure 3-11. Disposition of Cu-Ph-tfac chelate rings in **11a** showing close Cu…O contacts

In order to consider the degree to which the overlap of chelate ring π-orbitals is responsible for the interaction shown in Figure 3-9 compared to Cu…O interactions and steric factors, the offset of centroids between interacting phenyl-phenyl and phenyl-chelate rings have been calculated. Hunter *et al.*[7] concluded that in many π-π interactions between delocalised rings such as porphyrin-porphyrin interactions, an offset or slipped geometry is observed in order to allow π-σ attractions to overcome π-π repulsions. Their model implied that it is the properties of the atoms in the regions of intermolecular contact that control the strength and geometry of interactions rather than the overall molecular oxidation or reduction potentials. To allow comparisons between the examples of 'π-stacking' rings described in this chapter, the degree of ring 'slipping' has been determined by calculating the offset between the centroids of interacting rings (Scheme 3-1). For each pair of interacting rings there are two 'centroid offset' values

and both are quoted in Table 3-6 and in all the following tables that contain information related to 'π-stacking' rings.

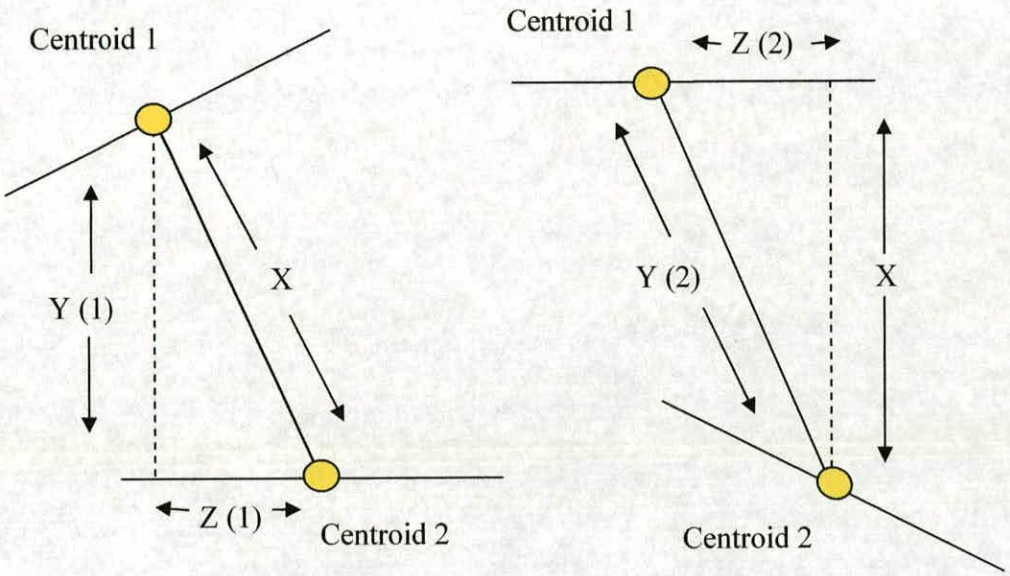

——— Plane of phenyl or Cu-diketonyl ring

X = distance between centroids of interacting rings
Y (1) = distance beween Centroid 1 and the plane of the opposite ring
Y (2) = distance between Centroid 2 and the plane of the opposite ring
Z (1) = centroid offset (1)
Z (2) = centroid offset (2)

$Z(1)^2 = X^2 - Y(1)^2$
$Z(2)^2 = X^2 - Y(2)^2$

Scheme 3-1. Method for calculating 'centroid offset' values between interacting rings

The periphery of **11** consists of two 'butterfly' units and six 'half butterfly' units. The 'butterfly' units interlock one 'half butterfly' in a Mode B interaction. This involves the oxygen of the 'half butterfly' forming an approximately symmetrical bridging motif with the two copper atoms of the 'butterfly' (Figure 3-12). This interlocking mode differs

from the conventional Mode B interaction described in chapter 2 as there is an additional π-interaction between the phenyl group of the 'half butterfly' unit and one phenyl ring from the 'butterfly' unit. The centroids of the two phenyl groups, C44, C45, C46, C47 C48, C49 and C54, C55, C56, C57, C58, C59 are offset by 1.99 or 2.03 Å respectively (Scheme 3-1), and the least squares plane of two rings are at an angle of 2.2° from each other. This approximately parallel arrangement of offset rings is indicative of π-stacking interactions as defined by Hunter *et al.*[7]

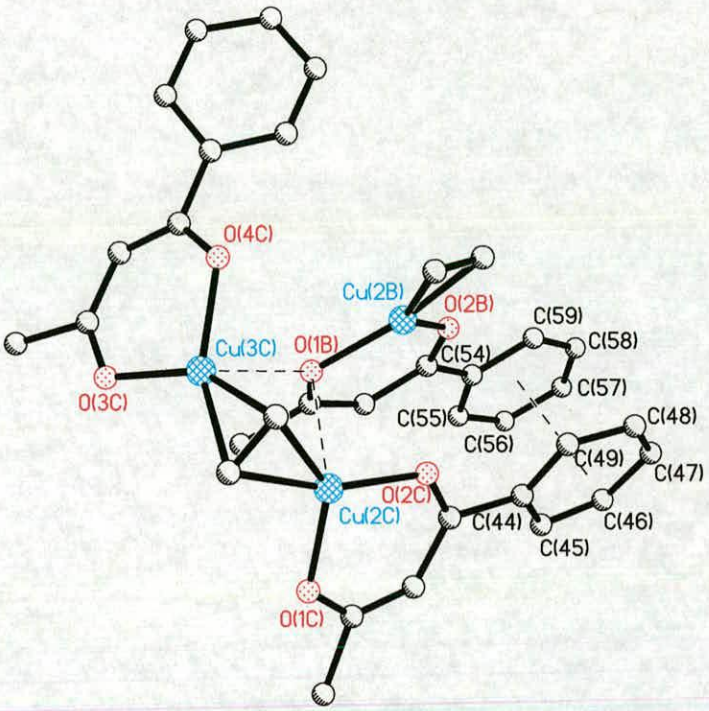

Figure 3-12. π-overlap between phenyl groups in the interlocking mode in **11**

In addition to the interlocking interactions, each butterfly 'wing' in **11** forms two phenyl-to-chelate 'π-stacking' type interactions with an adjacent 'half butterfly' unit (Figure 3-13). When the full molecule is generated the interacting butterfly units are located on opposite sides of the structure (Figure 3-11). One interaction involves the overlap of the chelate ring, Cu2D, O1D, O2D, C11, C12, C13, with the phenyl ring, C34A, C35A, C36A, C37A, C38A, C39A. The least squares plane of the two rings are

orientated at an angle of 8.8(6)°, the centroids of the rings are separated by 2.583 Å and are offset by 1.30 or 1.54 Å.

The second interaction involves the overlap of the chelate ring, Cu2G, O1CA, O2CA, C41A, C42A, C43A and the phenyl ring, C24A, C25A, C26A, C27A, C28A, C29A. The least squares plane of the two rings are orientated at an angle of 5.1(5)°, the centroids of the rings are separated by 3.456 Å and are offset by 0.86 or 0.834 Å (Table 3-6).

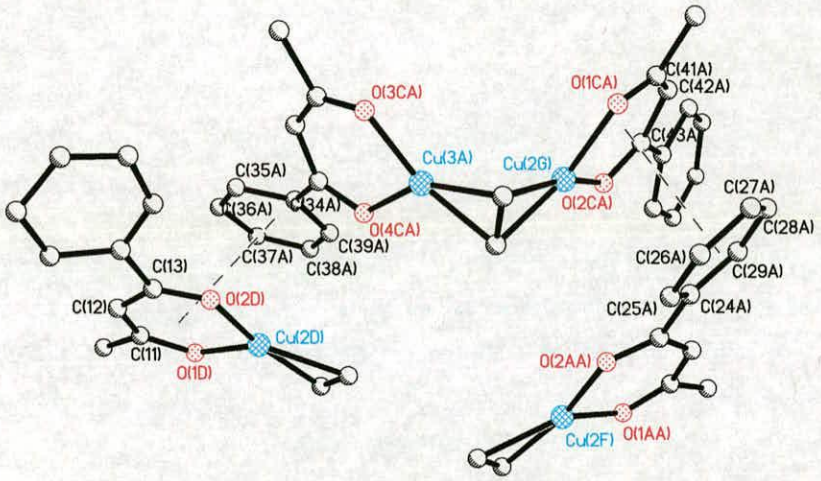

Figure 3-13. Butterfly 'wings' interacting with an adjacent Cu-(Ph-tfac) chelate ring.

Intramolecular Cu…O contacts (Å)			
O1B…Cu2C	2.929(8)	O1B…Cu2C	2.929(8)
O1B…Cu2C	2.921(8)	O1B…Cu2C	3.841(8)
Interacting rings	**Inclination /°**	**Centroid**	
		Separations/Å	Offsets /Å
Phenyl-phenyl π-stacking			
C44–C49, C54–C59[a]	2.2(6)	4.01	1.99 or 2.03
Phenyl – (Cu-phenyl-tfac) π-stacking			
Cu2D–C13, C34A–C39A[b]	8.8(6)	3.58	1.30 or 1.54
Cu2G–C43A, C24A–C29A[c]	5.1(5)	0.86	0.84

Table 3-6. Selected distances and angles in **11**. Planes are defined as (C44, C45, C46, C47 C48, C49) and (C54, C55, C56, C57, C58, C59) for *a*, (Cu2D, O1D, O2D, C11, C12, C13) and (C34A, C35A, C36A, C37A, C38A, C39A) for *b* and (Cu2G, O1CA,

O2CA, C41A, C42A, C43A) and (C24A, C25A, C26A, C27A, C28A, C29A) for *c* respectively. Equations for the planes are given in appendix 2.

3.3.4 $[Cu_{18}(hfac)_{10}(C{\equiv}CPr^{n})_6(C{\equiv}CBu^{t})_2]$ (12)

Two alkynyl ligands, 1-pentyne and 3,3-dimethyl-1-butyne are present in the core of **12**. The presence of two bulky ^{t}Bu-C≡C ligands does not appear to affect the configuration of the cluster significantly and there are similarities with the systems containing only 1-pentyne, **8**, and only 3,3-dimethyl-1-butyne, **10**, (Figure 3-14). Half the molecule is present in the asymmetric unit of **10** and the full molecule is generated by inversion.

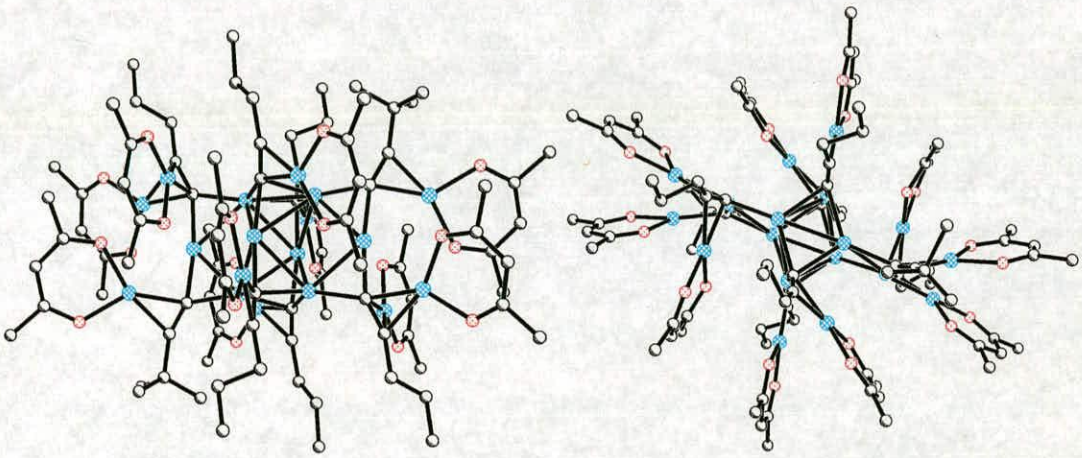

Figure 3-14. Two views of $[Cu_{18}(hfac)_{10}(C{\equiv}CPr^{n})_6(C{\equiv}CBu^{t})_2]$ (**12**)

As in the Cu_{16} and Cu_{18} clusters described earlier, eight copper atoms reside in a disc-shaped core. These are exclusively alkynyl bridged and the Cu…Cu contacts in this core fall in the range, 2.4920(14)-2.8130(16) Å (Table 3-7) and the remaining copper atoms are present in Cu-hfac chelate units around the rim.

The distribution of Cu-hfac chelate rings in **12** is shown in Figure 3-15 and the network of inter-ring Cu…O contacts are highlighted with dashed lines.

Cu...Cu distances in the central core (Å)			
Cu1...Cu3	2.8130(16)	Cu1...Cu4	2.5066(14)
Cu1...Cu5	2.4920(14)	Cu3...Cu4	2.5774(14)
Cu5...Cu4A	2.5199(15)	Cu3...Cu1A	2.5925(15)
Cu4A...Cu3	2.6643(15)		
Alkynyl bond lengths (Å)			
C26...C27	1.297(11)	C36...C37	1.227(11)
C31...C32	1.261(12)	C41...C42	1.226(13)
Alkynyl terminal C-Cu bond lengths (Å)			
C31...Cu3	1.910(8)	C26...Cu5	1.910(8)
C36...Cu3	1.927(8)	C26...Cu4A	2.010(8)
C36...Cu1	2.190(8)	C31...C4A	2.126(8)
C41...Cu1	2.008(8)	C31A...Cu1	2.106(9)
C41...Cu5	1.902(9)	C36...Cu4	2.124(8)

Table 7. Selected bond lengths in the asymmetric unit of **12**.

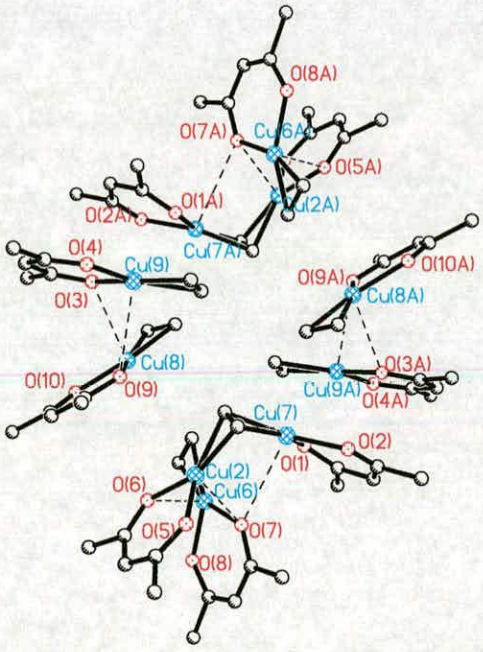

Figure 3-15. Disposition of Cu-hfac chelate rings in **12** showing close Cu...O contacts

The periphery of **12** consists of two 'full butterfly' units and six 'half butterfly units'. The 'full butterflys' each enclose one 'half butterfly' (Figures 3-15 and 3-16). This resembles

the 'Mode B' interaction described chapter 2 and the interactions in **11** shown in Figure 3-12. In addition to bridging the two butterfly copper atoms the half butterfly' chelate ring appears to be slightly aligned so as to allow a degree of cofacial overlap with one of the 'wings' of the butterfly. The overlapping rings are orientated at an angle of 38.9(3)° (Table 3-8) which is greater than previous examples of inter-chelate 'π-stacking' type interactions, however, relatively short inter-ring Cu…O contacts are established.

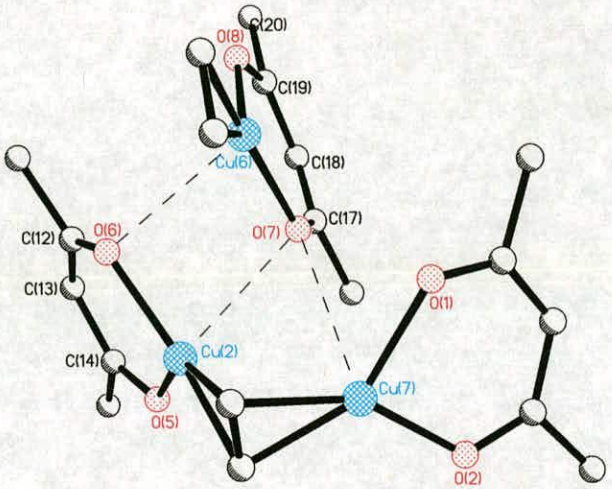

Figure 3-16. Interlocking Cu-hfac rings in **12** showing short inter-ring Cu…O contacts.

Intramolecular Cu…O contacts (Å)			
Cu2…O7	2.760(6)	Cu2A…O7A	2.760(6)
Cu6…O6	2.805(6)	Cu6A…O6A	2.805(6)
Cu7…O7	3.253(7)	Cu7A…O7A	3.253(7)
Cu8…O3	2.982(8)	Cu8A…O3A	2.982(8)
Cu9…O9	3.029(7)	Cu9A…O9A	3.029(7)
π-stacking rings			
		Centroids	
Interacting rings	Inclinations /°	Separations /Å	Offsets /Å
Cu6–C19, Cu2–C14[a]	38.9(3)	3.70	1.76 or 1.74
Cu6A-C19A, Cu2A-C14A[b]	38.9(3)	3.70	1.76 or 1.74

Table 3-8. Selected distances and angle from **11**. Planes are defined as (Cu6, O7, O8, C17, C18, C19) and (Cu2, O5, O6, C12, C13, C14) for *a* and (Cu6A, O7A, O8A, C17A, C18A, C19A) and (Cu2A, O5A, O6A, C12A, C13A, C14A) for *b*. Equations for the planes are given in appendix 2.

Despite having a mixture of two alkynyl ligands in the structure, including the bulky $^tBuC{\equiv}C$ ligand, **12** has a similar structure to the 'conventional' structures, **8** and **9**.

3.3.5 $[Cu_{20}(hfac)_8(C{\equiv}CCH_2Ph)_{12}]$ (13)

This is the first example of a cluster with general formula, $[Cu_{x+y}(hfac)_x(alkynyl)_y]$, to be isolated using an alkynyl ligand substituted with anything other than an alkyl group. The structure is shown in Figure 3-17 and has no crystallographically imposed symmetry. It differs from the other compounds discussed in this chapter and chapter 2 in having twelve alkynyl groups and copper atoms in the core. It is included in this chapter because its structure, like those with eight alkynyl groups and 'core' copper atoms can be related to the $[Cu_4(alkynyl)_4$ units described in chapter 2 (see section 2.3.2).

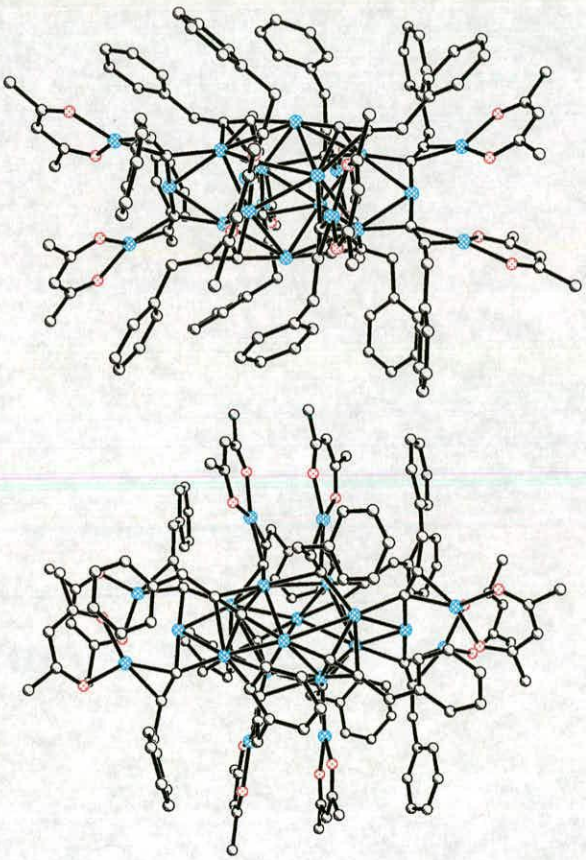

Figure 3-17. Two views of the structure of $[Cu_{20}(hfac)_8(C{\equiv}CCH_2Ph)_{12}]$ (**13**)

The alkynyl groups bridge the central core of twelve copper atoms to *via* σ-bonding in (μ_2-η^1:μ-η^2) and (μ_3-η^1:μ-η^2) bridging modes. Cu…Cu distances in the central core of **13** (Table 9) range between 2.4806(10)-3.0597(10) Å with many Cu…Cu contacts less than the sum of the van der Waals radii of Cu (2.8Å).

Cu…Cu distances in the central core (Å)			
Cu(1)…Cu(8)	2.6223(10)	Cu(2)…Cu(20)	2.7574(10)
Cu(8)…Cu(12)	2.6030(10)	Cu(5)…Cu(20)	2.9618(11)
Cu(12)…Cu(18)	2.8565(10)	Cu(5)…Cu(11)	2.5900(10)
Cu(1)…Cu(18)	2.7888(11)	Cu(2)…Cu(11)	2.7555(11)
Cu(1)…Cu(13)	2.5195(10)	Cu(5)…Cu(8)	2.8773(10)
Cu(1)…Cu(11)	2.8443(10)	Cu(2)…Cu(10)	2.6235(10)
Cu(8)…Cu(20)	2.7543(10)	Cu(2)…Cu(15)	3.0597(10)
Cu(10)…Cu(18)	2.9096(11)	Cu(5)…Cu(13)	2.5018(10)
Cu(10)…Cu(12)	2.9917(10)	Cu(15)…Cu(20)	2.7352(11)
Cu(12)…Cu(15)	2.5948(10)	Cu(11)…Cu(18)	2.7051(10)
Cu(4)…Cu(15)	2.4806(10)	Cu(4)…Cu(10)	2.4853(10)
Cu…Cu distances between inner and outer shell atoms (Å)			
Cu(13)…Cu(16)	2.7226(10)	Cu(6)…Cu(13)	2.9289(11)
Cu(2)…Cu(9)	2.8999(10)	Cu(7)…Cu(8)	3.0193(10)
Cu(4)…Cu(17)	2.7265(10)	Cu(12)…Cu(14)	2.8839(10)
Cu(4)…Cu(19)	2.7561(10)	Cu(3)…Cu(11)	2.8816(9)
Alkynyl bond lengths (Å)			
C(41)-C(42)	1.231(7)	C(95)-C(96)	1.241(7)
C(50)-C(51)	1.236(7)	C(104)-C(105)	1.230(7)
C(59)-C(60)	1.234(7)	C(113)-C(114)	1.222(8)
C(68)-C(69)	1.246(7)	C(122)-C(123)	1.224(8)
C(77)-C(78)	1.228(7)	C(131)-C(132)	1.201(8)
C(86)-C(87)	1.247(7)	C(140)-C(141)	1.219(8)
Alkynyl Terminal C-Cu Bond Lengths (Å)			
Cu(10)-C(113)	2.078(5)	Cu(15)-C(131)	2.095(5)
Cu(10)-C(114)	2.264(5)	Cu(15)-C(132)	2.519(5)
Cu(12)-C(113)	2.034(5)	Cu(5)-C(140)	2.085(5)
Cu(12)-C(114)	2.290(5)	Cu(5)-C(141)	2.346(6)
Cu(2)-C(131)	2.058(5)	Cu(8)-C(140)	2.041(5)
Cu(2)-C(132)	2.381(6)	Cu(8)-C(141)	2.241(6)

Table 9. Cu…Cu contact distances and Cu-C bond lengths in **13**

Five benzyl-alkynyl ligands are involved in π-stacking type interactions with Cu-hfac chelate rings (Figure 3-18). These alkynyl ligands are distorted from their 'conventional' positions, i.e. pointing above and below the copper core in the axial direction, and lie in approximately the same plane as the Cu-hfac rings to allow maximimum cofacial overlap. These interactions also cause the Cu-hfac rings to distort from their conventional positions and the anisotropic distribution of hfac and alkynyl ligands observed in **8** and **9** is lost. This deviation from the conventional appearance is a result of the benzyl groups on the alkynyl ligands forming π-stacking type interactions with Cu-hfac chelate rings.

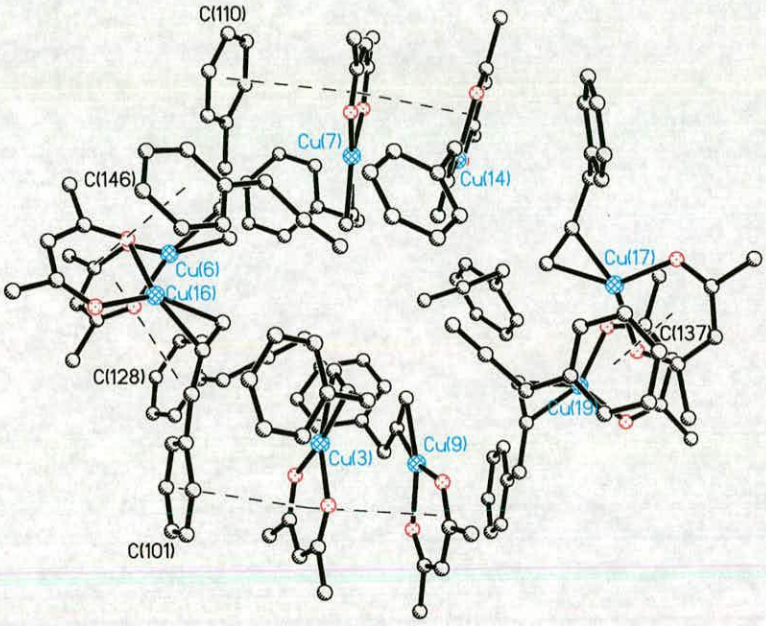

Figure 3-18. Peripheral interactions in **13**.

The π-stacking of phenyl groups with Cu-hfac units is a feature of this structure. In two cases π-stacking networks involve three overlapping rings and these are shown in Figure 3-19. One triple stack involves Cu-hfac units containing Cu3 and Cu9 and the phenyl group containing C101 (Figure 3-19) and the other involves Cu7 and Cu14 and the phenyl group containing C146. The least squares mean planes of the Cu3 and Cu9 rings are orientated at an angle of 9.2(2)° and the centroids of the respective rings are

separated by 3.46 Å. The least squares mean planes of the Cu3 ring and the phenyl rings are orientated at an angle of 6.3(2)° with centroids separated by 3.68 Å. The central ring in the other triple stack adopts a similar configuration and the details are given in Table 3-10.

In addition there are three pairs of interacting rings, each involving cofacial overlap of a phenyl group with a Cu-hfac chelate ring (Figure 3-18). The ring containing Cu17 interacts with the phenyl ring containing C137, the ring containing Cu16 interacts with the ring containing C146, and the rings containing Cu6 and C128 also interact with one other. The angles between the least square mean plane of overlapping rings fall in the range 6.6-21.8° and the distances between centroids varies between 3.566-3.795 Å (Table 3-10). The centroids of all the interacting rings on the rim of **13** are slightly offset (Table 3-10) suggesting that the overlap of ring π orbitals is to some degree responsible for these interactions.

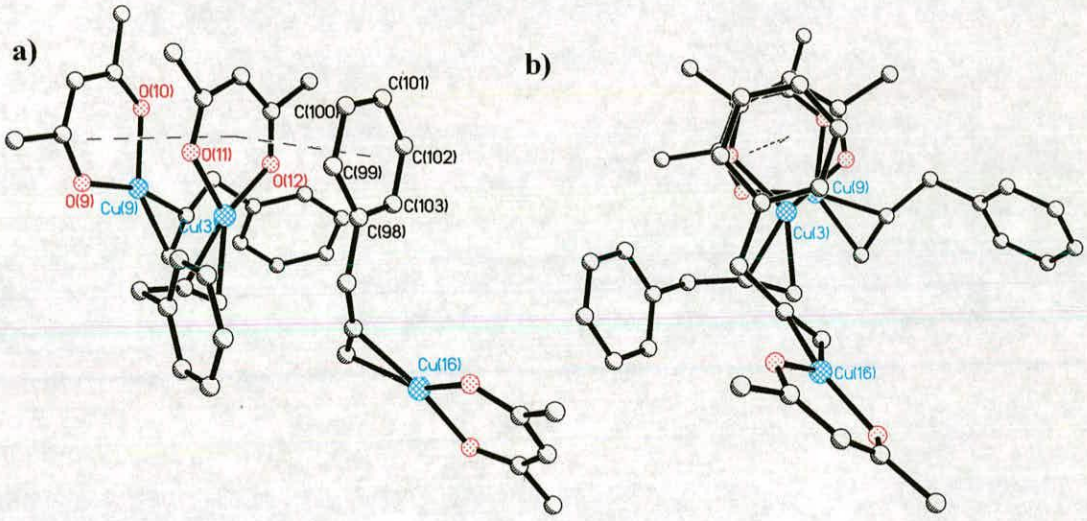

Figure 3-19. π-Stacking type interactions in **13**, showing a) three interacting rings and b) two interacting rings

π-Stacking Interactions			
Pairs of rings containing	Angles between planes /°	Distances between centroids (Å)	Offset between centroids (Å)
C101 and Cu3	6.3(2)	3.682	0.63, 0.35
Cu3 and Cu9	9.2(2)	3.462	0.93, 0.96
C110 and Cu7	6.6(2)	3.833	0.73, 1.63
Cu7 and Cu14	9.7(2)	3.399	0.68, 0.71
C137 and Cu17	6.6(2)	3.566	0.84, 0.96
C146 and Cu16	9.7(2)	3.602	1.24, 0.85
C128 and Cu6	21.8(2)	3.795	1.81, 0.66

Table 3-10. π-stacking information for **13**. The least squares planes of the rings containing C101, Cu3, Cu9, C110, Cu7, Cu14, C137, Cu17, C146, Cu16, C128 and Cu6 rings are defined by the atoms, (C98, C99, C100, C101,C102, C103), (Cu3, O11, C27, C28, C29, O12), (Cu9, O9, C22, C23, C24, O10), (C107, C108, C109, C110, C111, C112), (Cu7, O7, C17, C18, C19, O8), (Cu14, O5, C12, C13, C14, O6), (C134 , C135, C136, C137, C138, C139), (Cu17, O1, O2, C2, C3, C4, O2), (C143, C144, C145, C146, C147, C148), (Cu16, O13, C32, C33, C34, O14), (C125, C126, C127, C128, C129, C130) and (Cu6, O15, C37, C38, C39, O16) respectively. The equations for the planes are given in Appendix 2

3.3.6 Ligand : Ligand interactions

The analysis of the structures presented in section 3.3 indicate that secondary bonding between groups outside the central copper alkynyl core has a significant effect on the 'shape' of the cluster and particularly the distribution of the alkynyl substituents and Cu-hfac rings about the core. In **11**, the introduction of a phenyl group to the 1,3-diketonyl ligand increased the potential for forming intramolecular secondary interactions between chelate rings and in **13** incorporating a phenyl group on the alkynyl ligand increased the number of secondary intramolecular interactions between chelate rings and alkynyl ligands. As a result structures are observed which consist of a central copper core surrounded by a network of interacting Cu-hfac and phenyl rings where ligands are orientated to achieve a degree of 'π-stacking' type overlap.

3.4 Nature of the central core in Cu_{16} to Cu_{20} clusters

Despite the differences in ligand distribution observed in the Cu_{16} to Cu_{20} series, there remain some striking similarities between the structures of the central cores. In all cases the core of copper atoms is bridged exclusively by the same number of σ-bonding terminal alkynyl ligands, with eight coppers and alkynyls in **10-12**, and twelve in **13**. The striking observation that the cores of the cluster always contain one or two Cu_4alkynyl$_4$ units and how the large cores are related to building blocks with general formula, $[Cu_4(C{\equiv}CR)_4(Cu\text{-}hfac)_x]$ defined in chapter 2 will be considered in the following section.

3.4.1 $[Cu_4(C{\equiv}CR)_4(Cu\text{-}hfac)_x]$ fragments in Cu_{16} – Cu_{20} clusters

When cluster aggregation is limited by the 'bulk' of the alkynyl ligands, clusters with ten and twelve copper atoms are obtained with the formula, $[Cu_4(C{\equiv}CR)_4(Cu\text{-}hfac)_x]$. In chapter 2 it was suggested that the higher nuclearity clusters with sixteen to twenty six copper atoms may arise from the assembly of these $[Cu_4(C{\equiv}CR)_4(Cu\text{-}hfac)_x]$ building block (Figure 3-20). In this section, structures of the Cu_{16} to Cu_{26} series of clusters and in particular their cores are analysed to identify structural features which are derived from these 'building blocks' (Figure 3-20).

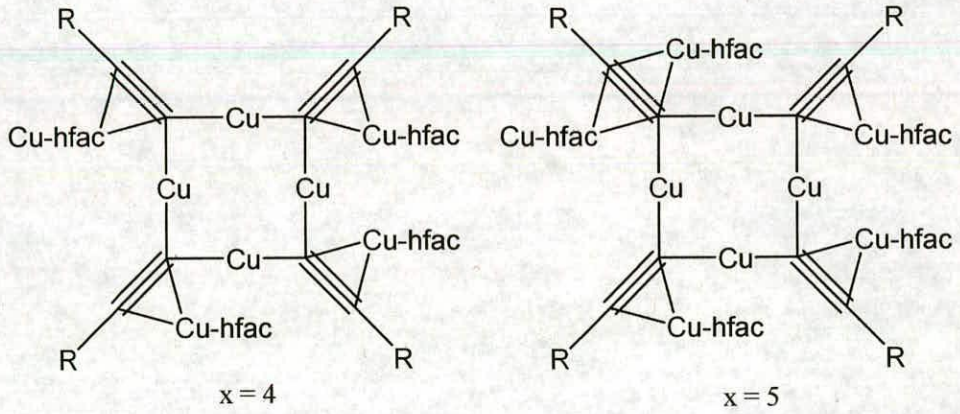

Figure 3-20. The proposed 'building blocks' with general formula $[Cu_4(C{\equiv}CR)_4(Cu\text{-}hfac)_x]$ in Cu_{16}-Cu_{20} clusters

The study showed that **10**, **11** and **12** are all composed of two 'half molecule' fragments with formula, $[Cu_4(C{\equiv}CR)_4(Cu\text{-}hfac)_x]$ (Table 3-11).

Cluster	'Half molecule' formula
10	$[Cu_4(C{\equiv}CBu^t)_4(Cu\text{-}hfac)_4]$
11	$[Cu_4(C{\equiv}CBu^n)_4(Cu\text{-}hfac)_5]$
12	$[Cu_4(C{\equiv}CBu^t)(C{\equiv}CPr)_3(Cu\text{-}hfac)_5]$

Table 3-11. 'Half molecule' building blocks in **10**, **11** and **12** which are related by crystallographic symmetry in each case.

The 'half molecules' closely resemble the structure of the Cu_{10} and Cu_{12} molecules and the clusters have been numbered to illustrate this. The numbering scheme is based on the generic Cu_{10} and Cu_{12} scheme used in chapter 2 and is shown in Figure 3-21.

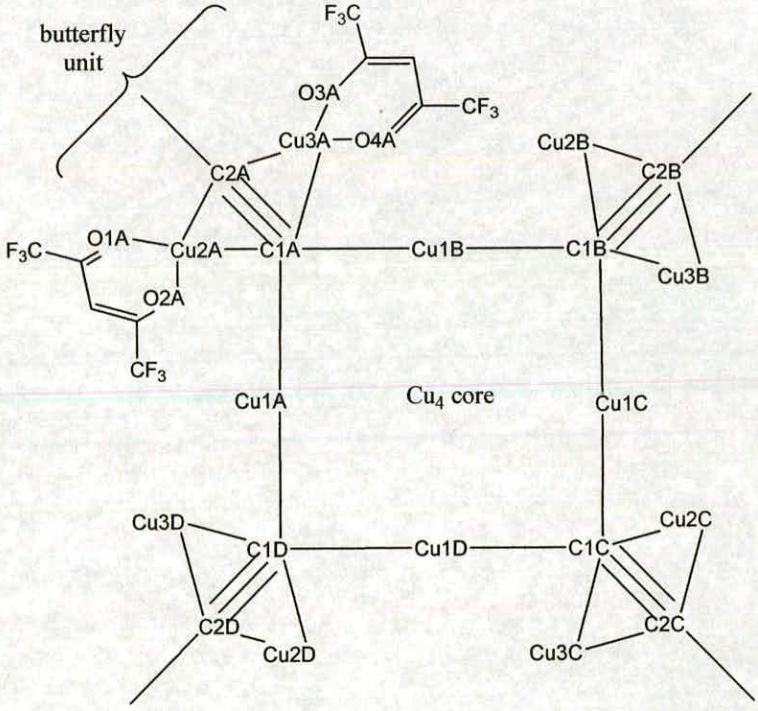

Figure 3-21. Numbering scheme for 'half molecules' in the structures of **10**, **11**, **12** and **13**. A key is enclosed in Appendix 1 relating the original numbering of each cluster to the scheme shown above.

The smallest of the clusters discussed in this chapter, **10,** can be used to illustrate how the 'building blocks' were identified. This relatively simple cluster has a complex network of Cu...Cu contacts making the identification of any structural features difficult. When only the central core of eight copper atoms is considered and only Cu...Cu contacts that fall below the sum of the Van der Waals radii of copper (2.8 Å) are included in structural diagrams the structure becomes easier to analyse (Figure 3-22).

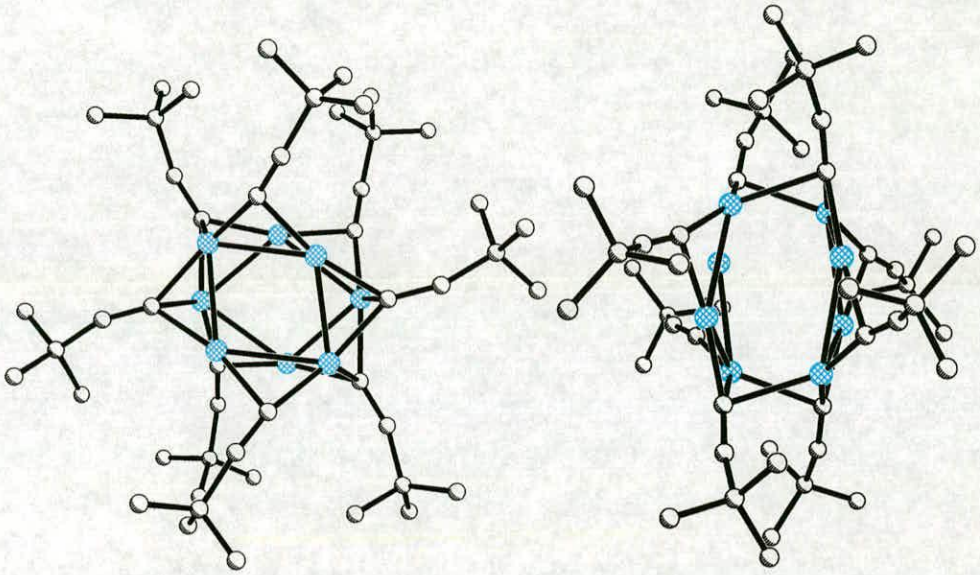

Figure 3-22. Views of **10** displaying only the alkynyl-bridged core, $Cu_8(C{\equiv}CBu^t)_8$ and Cu...Cu contacts shorter than the sum of the van der Waals radii of copper.

The fragment shown in Figure 3-22 can be further simplified by removing one half of the molecule that is generated by a two-fold axis of symmetry leaving a 'half molecule' (Figure 3-23).

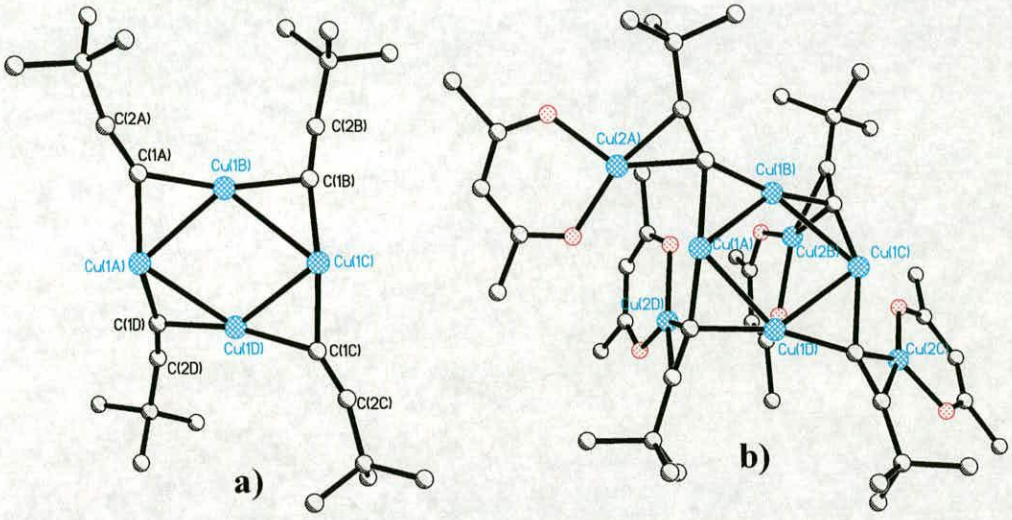

Figure 3-23. 'Half molecules' of **10** with, a) coordinating Cu-hfac groups removed and b) the full 'half molecule'.

The 'half molecule' fragment in **10** (Figure 3-23a) has identical connectivity to the $[Cu_4(alkynyl)_4]$ cores found in the low nuclearity series (chapter 2). Due to the similarity between 'half molecules' and low nuclearity clusters, for the purposes of comparing structures, the molecules have been renumbered so that 'half molecules' have a numbering scheme that corresponds to the generic Cu_{12} numbering scheme. A key to this numbering scheme for **10**, **11**, **12** and **13** is included in Appendix 1.

The 'half molecule' in **10** consists of four copper atoms (Cu1A, Cu1B, Cu1C and Cu1D) with four η^2-bridging alkynyl ligands (C1A≡C2A, C1B≡C2B, C1C≡C2C and C1D≡C2D). The Cu…Cu contacts along the edges of the Cu_4 'square' fall in the range 2.5159(6)-2.6428(6) Å with diagonal contacts Cu1B…Cu1D = 3.180(1) and Cu1A…Cu1C = 3.983(1) Å (Table 3-12). The Cu_4 core is relatively non-planar as the coppers are displaced from the Cu1, Cu4, Cu1B and Cu4B least square plane by 0.2027(3), -0.2027(3), -0.2027(3) and 0.2027(3) Å respectively (Table 3-12).

The full 'half molecule' structure of **10** [Figure 3-23(b)] contains four Cu-hfac capping groups each forming 'half-butterfly' units similar to those observed in the structures of

4a, **4b** and **5**, and hence corresponds to the 'building blocks' shown in Figure 3-20 with x=4.

	10	11	12	13	
				1	2
Cu_4 contacts (Å)					
Cu1A...Cu1B	2.5159(6)	2.577(2)	2.8130(16)	2.6223(10)	2.7051(10)
Cu1B...Cu1C	2.6428(6)	2.490(2)	2.4920(14)	2.5195(10)	2.9096(11)
Cu1C...Cu1D	2.5159(6)	2.493(2)	2.5199(15)	2.5018(10)	2.6235(10)
Cu1D...Cu1A	2.6428(6)	2.539(2)	2.6643(15)	2.8773(10)	2.7555(11)
Cu1A...C1C	3.983(1)	3.459(2)	3.622(2)	3.762(1)	4.040(1)
Cu1B...Cu1D	3.180(1)	3.191(2)	3.266(2)	3.163(1)	3.670(1)
Deviations from Cu_4 least squares plane (Å)					
Cu1A	0.2027(3)	0.503(4)	0.425(4)	0.416(4)	-0.1665(3)
Cu1B	-0.2027(3)	-0.355(5)	-0.524(5)	-0.494(4)	0.1567((3)
Cu1C	0.2027(3)	0.419(6)	0.524(6)	0.507(4)	-0.1630(3)
Cu1D	-0.2027(3)	-0.549(5)	-0.490(5)	-0.429(4)	0.1727(3)
Half molecule C-Cu bonds (Å)					
Cu1A-C1A	2.014(3)	1.93(2)	1.927(8)	1.915(5)	2.021(5)
Cu1B-C1A	1.949(4)	2.08(1)	2.190(8)	2.083(5)	1.875(6)
Cu1B-C1B	1.948(3)	2.00(2)	2.008(8)	2.066(6)	1.878(6)
Cu1C-C1B	1.933(3)	1.88(2)	1.902(9)	1.882(5)	2.078(5)
Cu1C-C1C	2.014(3)	1.89(2)	1.910(8)	1.877(5)	2.078(5)
Cu1D-C1C	1.949(4)	2.00(1)	2.010(8)	2.046(6)	1.935(5)
Cu1D-C1D	1.948(3)	2.09(1)	2.126(8)	2.085(5)	2.350(6)
Cu1A-C1D	1.933(3)	1.91(2)	1.907(8)	2.041(5)	1.894(5)

Table 3-12. Selected dimensions in the 'half molecules' in **10**, **11**, **12** and **13**. In **10**, **11** and **13** these are related by symmetry so only one fragment is included as the other half is identical. Equations for the planes are given in Appendix 2

The 'half molecules' in **10** are connected by four alkynyl-Cu bonds (Cu1A-C1A', Cu1C-C1C', Cu1A'-C1A and Cu1C-C1C = 2.270(4) Å) (Table 3-13) with two alkynyl ligands from each unit bonding to two copper atoms on the other fragment (Figure 3-24).

The ligands that connect the 'half molecules' (C1A≡C2A, C1C≡C2C, C1A'≡C2A' and C1C'≡C2C) act as μ_3-$(\eta_\sigma{}^1)^3(\eta_\pi{}^2)$ bridging units (Figure 24). They coordinate one Cu-hfac chelate ring forming a 'half butterfly'. They also bridge two copper atoms on the same 'half molecule' with distances falling in the range 1.949(4)-2.014(3) Å and

coordinate a third copper atom on the opposite 'half molecule' connecting the two fragments, generating the full molecule. These 'connecting' interactions are longer (2.270(4) Å) than the bridging bonds within the 'half molecule'.

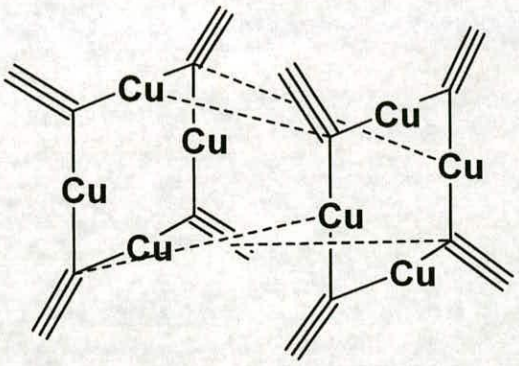

Figure 3-24. μ_3-$(\eta_\sigma{}^1)^3(\eta_\pi{}^2)$ and are μ_3-$(\eta_\sigma{}^1)^2(\eta_\pi{}^2)$ bridging alkynyl ligands in **10**

The other alkynyl groups (C17, C17A, C17B and C17C) are μ_3-$(\eta_\sigma{}^1)^2(\eta_\pi{}^2)$ bridging units and only form bonds to copper atoms in the same 'half molecule'.

C-Cu bonds linking 'half molecules' (Å)			
10			
Cu1A…C1A'	2.270(4)	Cu1A'…C1A	2.270(4)
Cu1C…C1C'	2.270(4)	Cu1C…C1C'	2.270(4)
11			
Cu1B…C1A'	2.192(13)	C1D…Cu1D'	2.086(11)
Cu1B'…C1A	2.191(13)	C1D'…Cu1D	2.086(11)
12			
Cu1B…C1D'	2.106(9)	Cu1B'…C1D	2.106(9)
Cu1D'…C1A	2.124(8)	Cu1D…C1A'	2.124(8)

Table 3-13. The Cu…C bonds linking 'half molecules' in **10**, **11**, **12**.

3.4.2 'Half molecules' in 11, 12

Pairs of 'half molecules' have been identified in **11** and **12** and have the formula $[Cu_4(C{\equiv}CBu^n)_4(Cu\text{-}hfac)_5]$ and $[Cu_4(C{\equiv}CBu^t)_2(C{\equiv}CPr)_2(Cu\text{-}hfac)_5]$, respectively. A key to the numbering scheme for both molecules is included in Appendix 1. As with **10**, they were identified by viewing the cluster with peripheral Cu-hfac chelate rings removed and considering only short Cu…Cu contacts (<2.8 Å) (Figure 3-25 and 3-26).

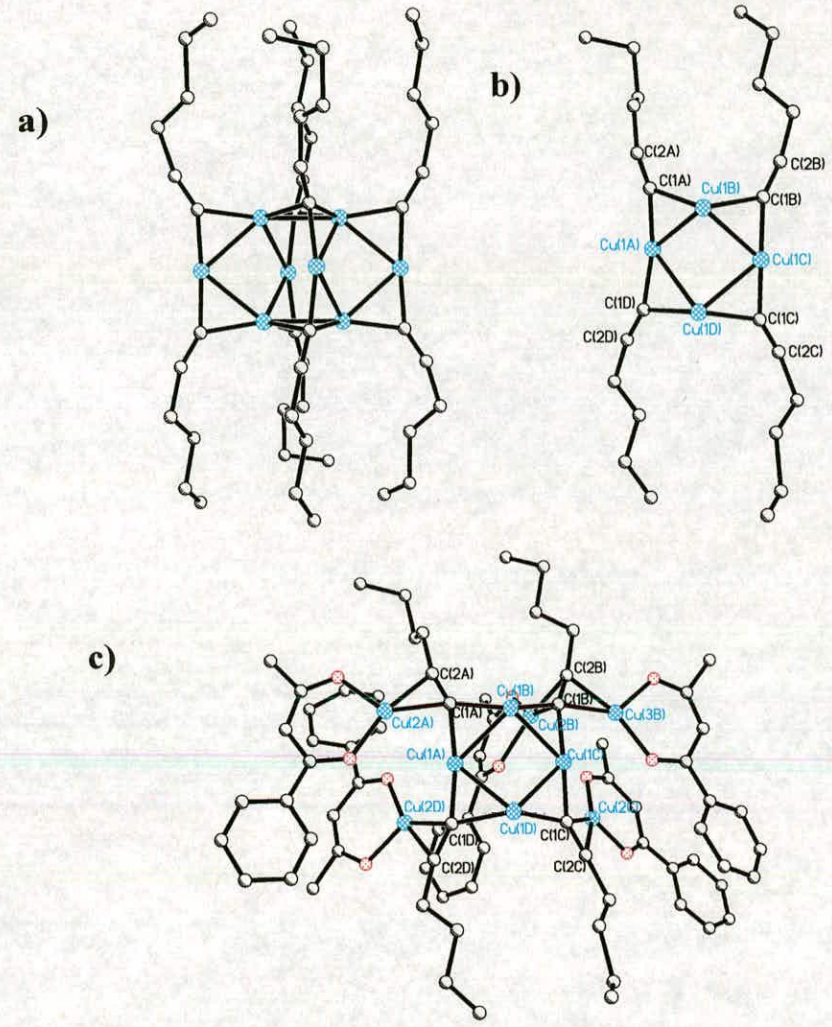

Figure 3-25. Views of **11** with, a) Cu-hfac chelate rings and Cu…Cu contacts greater than 2.8 Å removed, b) 'half molecule' of **11** with Cu-hfac rings removed and c) full 'half molecule' of **11** including Cu-hfac rings.

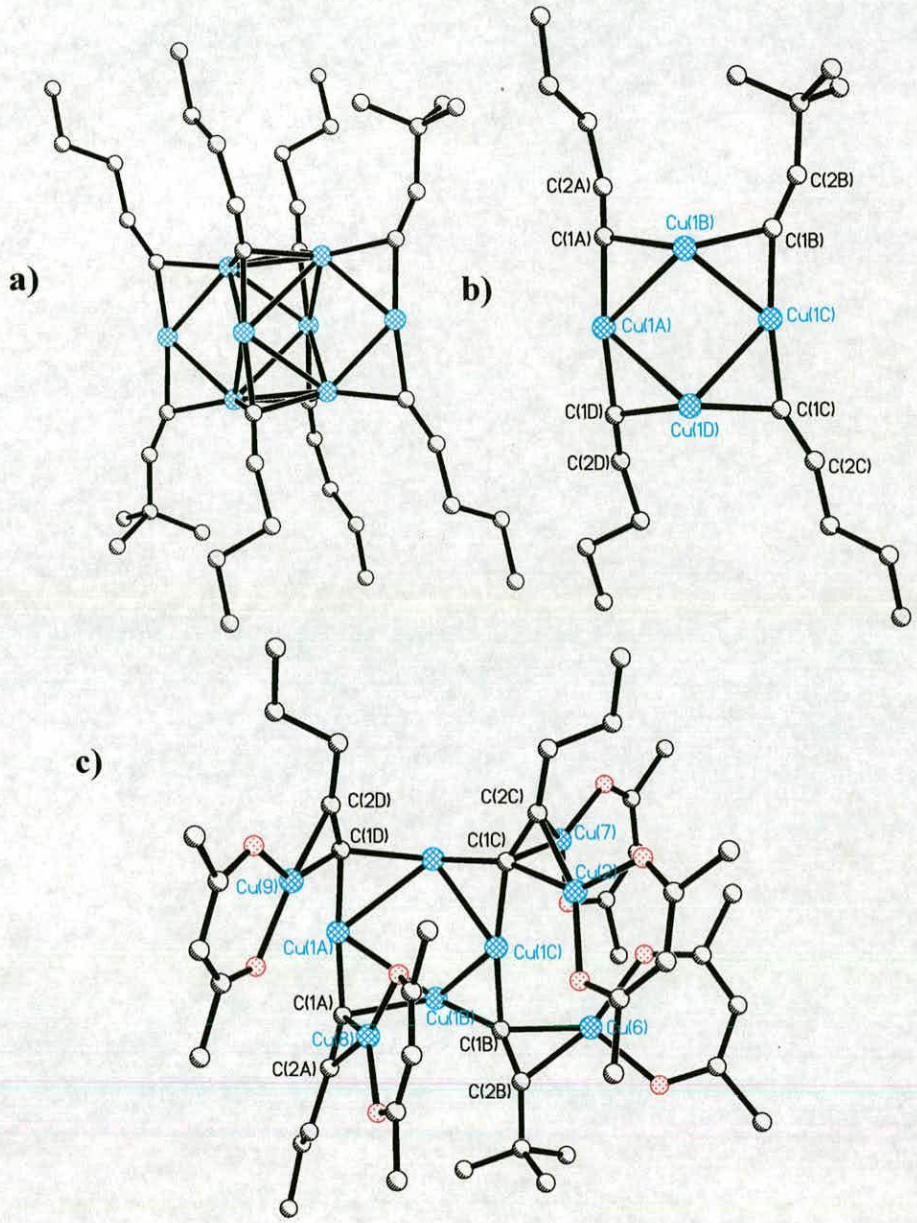

Figure 3-26. Views of **12** with, a) Cu-hfac chelate rings and Cu…Cu contacts greater than 2.8 Å removed, b) 'half molecule' of **12** with Cu-hfac rings removed and c) full 'half molecule' of **12** including Cu-hfac rings

11 and **12** have similar arrangements of 'half molecule' units to **10**. The 'edge' contact distances of the Cu_4 'squares' fall in range 2.490(2)-2.539(2) Å and 2.4920(14)-

2.8130(16) Å and the maximum displacement of copper atoms from the least squares mean plane of the central copper cores range between ±0.549(5) Å and ±0.524(5) Å for **11** and **12** respectively (Table 3-12). The 'half molecules' are connected by four alkynyl C…Cu interactions both structures that fall in the range 2.086(11) – 2.191(13) Å and 2.086(11) – 2.192(13) Å for **11** and **12** (Table 3-13).

The main difference between the 'half molecules' in **11** and **12** and those in **10** are that they both contain one additional Cu-hfac unit. Thus one alkynyl has a 'full butterfly' motif. The 'half-molecule' units are thus represented by the arrangement in Figure 3-21 with five Cu-hfac units i.e. x = 5.

3.4.3 'Cu_4' building blocks in 13

This compound differs from those described above and in chapter 2 in having a molecular formula with three $Cu_4(alkynyl)_4$ units. The arrangement of 'half molecules' in **13** is more complicated than in **10**, **11** and **12**. When Cu-hfac units are removed and only Cu…Cu contacts (2.2018(10)-4.040 Å) in the central Cu_{12} core are displayed as shown in Figure 3-27(a), two structural fragments can be identified that contain the $[Cu_4(C{\equiv}CR)_4(Cu\text{-}hfac)_x]$ motif [Figure 3-27 (a) and (b)]. They are not related by symmetry and have been denoted half molecule '1' and '2' (Figure 3-28). Cu…Cu contacts within the central Cu_4 core are slightly longer than in previous examples with distances in the ranges 2.5018(10)-2.8773(10) Å and 2.6235(10)-2.9096(11) Å and the four central copper atoms deviate from their least squares plane in the range, 0.5070 – (-0.4292) Å and 0.1727-(-0.1665) Å for 'half molecule' 1 and 2 respectively. The C…Cu distances are typical for η^2- bridging alkynyls[8] (Table 3-12) with the exception of the Cu1A…C1D…Cu1D bridging unit which is relatively unsymmetrical.

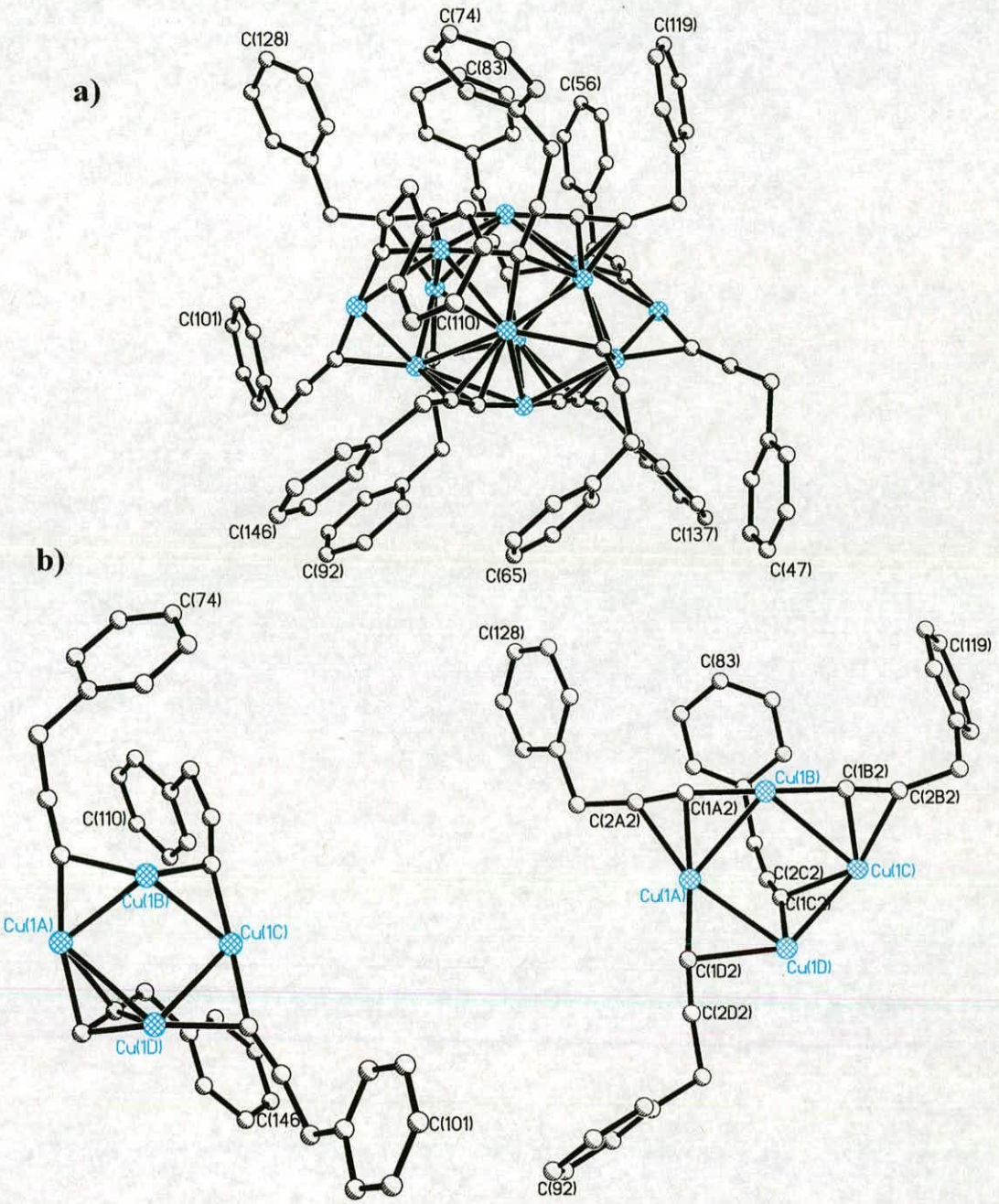

Figure 3-27. Continued…

c)

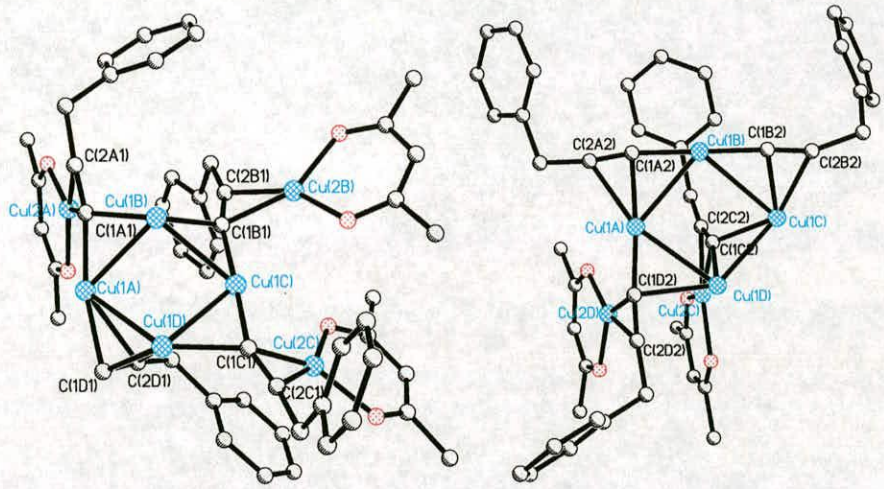

Figure 3-27. a) Views of **13** with a) Cu-hfac chelate rings removed and only relatively short Cu…Cu contact, b) two $Cu_4(alkynyl)_4$ motifs of **13** with Cu-hfac rings removed and c) the two full $Cu_4(alkynyl)_4$ motifs of **13** including Cu-hfac rings

Whilst these two $[Cu_4(C{\equiv}CR)_4(Cu\text{-}hfac)_x]$ building blocks (where x = 2 or 3, Figure 3-27 and 3-28) are formally similar to those in **10** – **12** there are significant differences. The relative planarity of the Cu_4C_4 'square' is lost with the alkynyl ligands, C1D1≡C2D1 and C1C2≡C2C2 (Figure 3-27) lying above the Cu_4 plane resulting in the loss of the 'square' appearance of the motif. This is due the phenyl substituent aligning to allow 'π-stacking' overlap with Cu-hfac chelate rings. Some of the Cu…Cu contacts within the building blocks are longer than similar distances in the Cu_4 cores in **10-12** (Table 3-12). In addition the alkynyl group, C1D1≡C2D1, bridges the copper atoms, Cu1A and Cu1D, *via* a μ_2-η^2 bridging motif compared to a conventional μ_2-η^1 motif.

It is possible to identify a third $[Cu_4(C{\equiv}CR)_4]$ motif in **13** with formula, $[Cu_4(C{\equiv}CBu^t)_4(Cu\text{-}hfac)_3]$ (Figure 3-29). It does not resemble the conventional 'Cu_4C_4' square, but has a structure apparently distorted by the requirement of the phenyl substituents to form π-interactions.

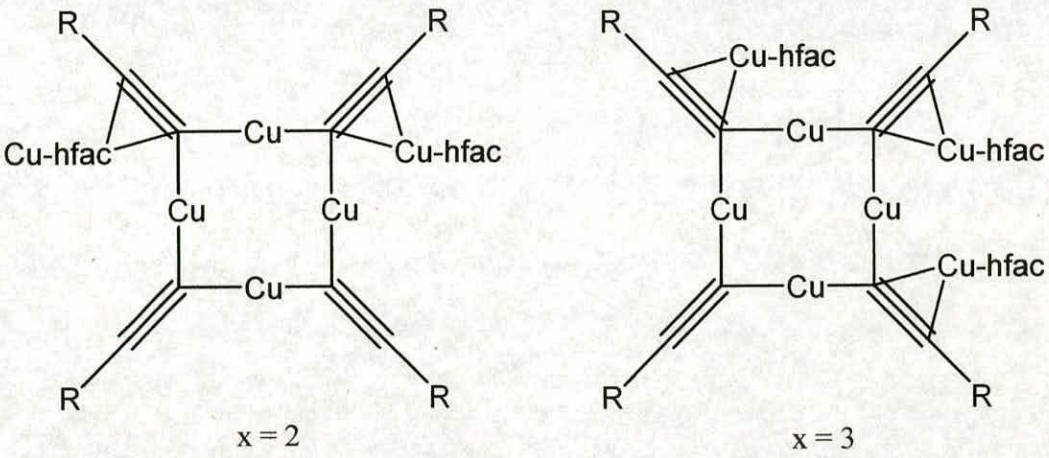

Figure 3-28. The proposed 'building blocks' with general formula $[Cu_4(C{\equiv}CR)_4(Cu\text{-}hfac)_x]$ (**13**)

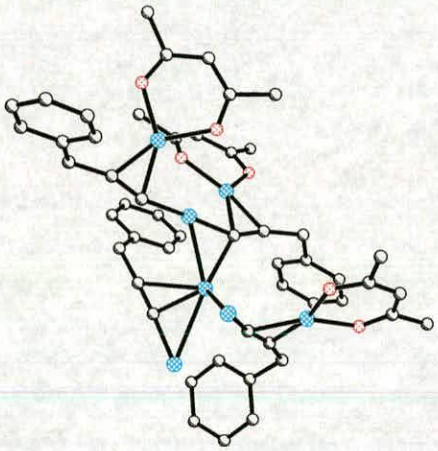

Figure 3-29. Non-conventional $[Cu_4(C{\equiv}CBu^t)_4(Cu\text{-}hfac)_3]$ fragment in **13.**

3.5 How do Cu_{16} to Cu_{20} clusters assemble?

It was shown in chapter 2 that 'bulky' alkynyl ligands limit cluster aggregation and the formation of clusters with formula $[Cu_{10}(C{\equiv}CR)_4(Cu\text{-}hfac)_6]$ and $[Cu_{12}(C{\equiv}CR)_4(Cu\text{-}hfac)_8]$ is observed. The RC-Cu-CR bridging modes in related $[Cu_4(aryl)_4]$ molecules have been studied in detail and shown to be stable which explains why low nuclearity $[Cu_{x+y}(hfac)_x(alkynyl)_y]$ clusters adopt a similar conformation. It was proposed that the

structure of the low nuclearity systems represented a 'building block' that, if appropriate ligands were present, could aggregated further to form higher nuclearity systems. In this chapter, four clusters (**10**, **11**, **12** and **13**) have been described that contain two 'half molecules' with formula, $[Cu_4(C{\equiv}CR)_4(Cu\text{-}hfac)_x]$, which closely resemble the 'building block' proposed in chapter 2. **13** contains an additional $[Cu_4(C{\equiv}CR)_4(Cu\text{-}hfac)_x]$ unit although the propensity of the phenyl group on the alkynyl ligands to form additional π-stacking interactions appears to distort this fragment from a conventional arrangement. The identification of these building blocks allows the aggregation mechanism proposed in chapter 2 (Scheme 2-2) to be extended to explain the formation of clusters containing between sixteen and twenty copper atoms (Scheme 3-2).

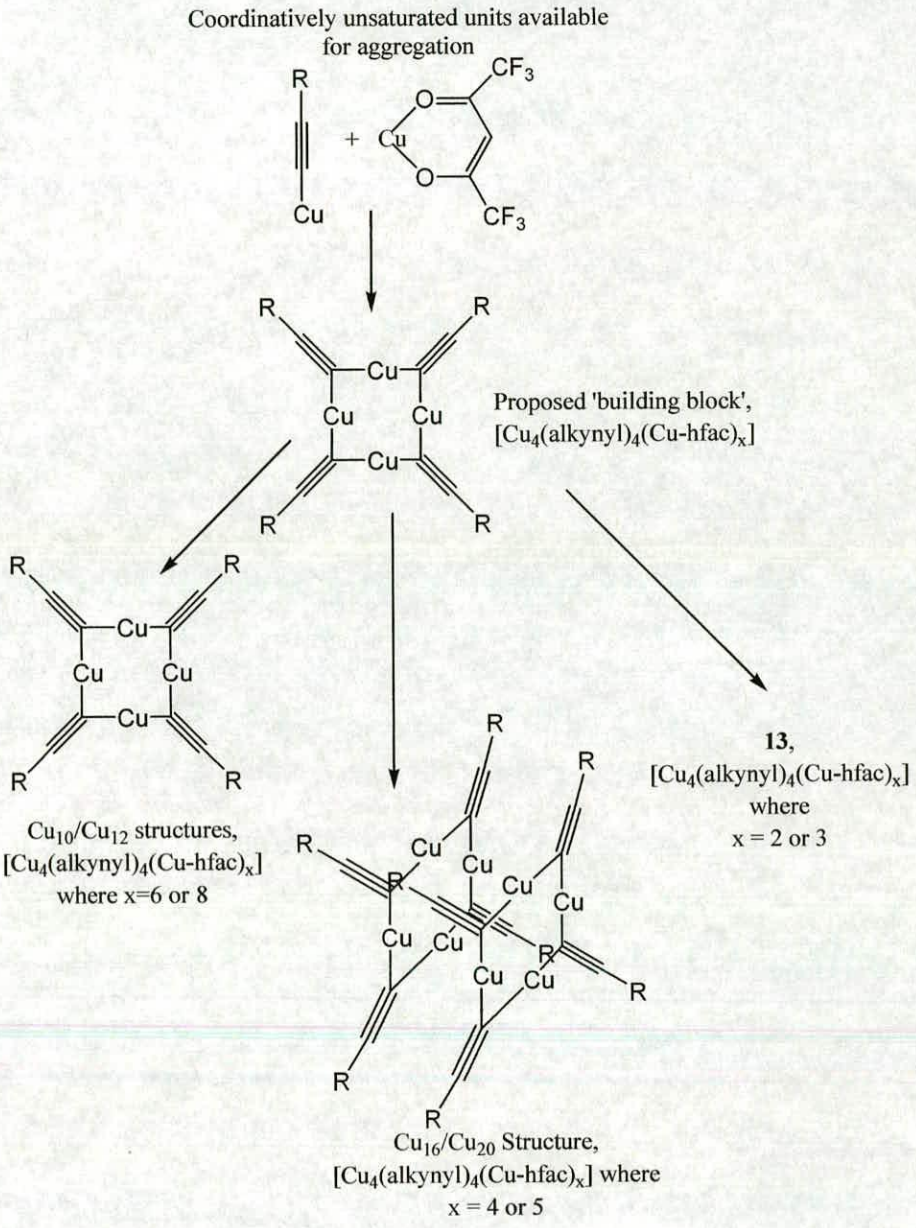

Scheme 3-2. Proposed aggregation of $Cu_4C{\equiv}CR_4$ units in Cu_{16} /Cu_{20} molecules

In the proposed aggregation mechanism (Scheme 3-2), coordinatively unsaturated Cu-hfac and Cu-alkynyl units assemble to form a 'building block' with formula,

$[Cu_4(C{\equiv}CR)_4(Cu\text{-}hfac)_x]$. If the bulk of the alkynyl ligands allows, they can either form a dimer which leads to the isolation of clusters with a $Cu_8(C{\equiv}CR)_8$ core or trimerise to produce cluster containing $Cu_{12}(C{\equiv}CR)_{12}$ cores. The aggregation of $Cu_4(alkynyl)_4$ building blocks is consistent with the observation that the number of alkynyl ligands in all the clusters isolated so far is divisible by four and that as the clusters increase in size, the hfac:alkynyl ratio becomes smaller.

In the case of the $HC{\equiv}CBu^t$ ligand, products from both pathways have been observed, **2** and **10**. **10** was synthesized from a reaction where cluster formation took place in the presence of a large excess of 3,3-dimethyl-1-butyne whereas during the synthesis of **2**, the alkynyl ligand was less abundant. This suggests that when there is sufficient 3,3-dimethyl-1-butyne present, 'dimerisation' of $[Cu_4(C{\equiv}CBu^t)_4]$ units is favoured resulting in the formations of a Cu_{16} cluster.

In the following chapter the role of the $[Cu_4(C{\equiv}CR)_4(Cu\text{-}hfac)_x]$ entity as a 'building block' in the aggregation of high nuclearity clusters, Cu_{24}-Cu_{26}, will be explored. This will be done by identifying the fragments of the clusters that have a $Cu_4(alkynyl)_4$ core.

3.6 Experimental

Materials and reagents

All reagents were obtained from Aldrich Chemicals and used without further purification. *n*-Hexane and diethyl ether was distilled from sodium/benzophenone/tetraglyme (trace) under N_2. N_2 gas was dried with 4Å molecular sieves and deoxygenated with BTS catalyst.[9] All preparations of copper(I) complexes were carried out under anaerobic and anhydrous conditions using standard Schlenk techniques. 3,3-Dimethyl-1-butyne, 3-phenyl-1-propyne and 1,1,1,5,5,5-hexafluoropentan-2,4-dione (hfacH) were degassed by freeze/vac/thaw cycles.

$[Cu_{16}(hfac)_8(C{\equiv}CBu^t)_8]$ (10)

Cu_2O (1.64 g, 11.5 mmol) and anhydrous $MgSO_4$ (*ca.* 2 g) were added to a solution of 3,3-dimethyl-1-butyne (5 g, 0.061 mol) in hexane (10 mL). Dropwise addition of hfacH (2.5 mL, 18 mmol) was accompanied by an exothermic reaction. After stirring for 18 hr at room temperature the mixture was cannula-filtered and the solid residue washed with hexane (3 × 10 mL). The combined lime green filtrate and washings were evacuated *in vacuo* and the resulting orange/yellow oil was heated *in vacuo* at 65°C for 2 hr and then dissolved in refluxing hexane (20 mL) and set aside at 4°C. After 48 hr dark red crystals suitable for x-ray diffraction studies had separated. The supernatent liquid was removed and the crystals were washed with hexane and dried *in vacuo*. Yield: 0.446 g (12 %). Found: C, 33.39; H, 2.71. Calc. for $C_{94}H_{94}O_{16}Cu_{16}F_{48}$: C, 33.12; H, 2.78%. δ_H (CD_2Cl_2, 250 MHz): 1.41 (s, 72 H, C*H*$_3$) and 6.03 (s, 8 H, C*H*). δ_F (CD_2Cl_2, 250 MHz): -76.73 (s, 48 F, C*F*$_3$). IR spectra (KBr disc): 2937s, 2874m, 2405w, 1860m, 1638s, 1555s and 1466s cm^{-1}.

$[Cu_{18}(phenyl\text{-}tfac)_{10}(C{\equiv}CBu^n)_8]$ (11)

To a suspension of Cu_2O (0.43g, 3.0 mmol), 1-hexyne (1.32g, 16.1 mmol) and anhydrous $MgSO_4$ (*ca.* 2g) in hexane (5 mLl) was added a solution of 4,4,4-trifluoro-1-phenyl-1,3-butanedione (1g, 4.6 mmol). The mixture was stirred for one hour and cannula filtered. The solid residue was washed with hexane (3 × 10 mL) and the washings and filtrate combined to give a pale yellow solution. From this solution the volatile components were removed *in vacuo* leaving a solid red residue. Soluble material was extracted into hexane (10 mL) and separated from intractable yellow solid (presumably polymeric) by cannula filtration. This solution was stored at 4 °C for 48 hours after which time orange crystals suitable for X-ray diffraction had separated. The crystals were collected by filtration, washed with hexane and dried *in vacuo*. Yield = 0.51 g (39 %). Found: C, 45.07; H, 3.37. Calc. for $C_{148}H_{132}O_{20}Cu_{18}F_{30}$: C, 44.96; H, 2.65%. IR spectra (KBr disc): 297s, 2924m, 2854w, 1606s, 1574s, 1538s, 1456m, 1320s, 1293s, 1191s and 1140s cm^{-1}.

$[Cu_{18}(hfac)_{10}(C{\equiv}CPr^{n})_4(C{\equiv}CBu^{t})_4]$ (12)

To a suspension of Cu_2O (1.64 g, 11.5 mmol) and $MgSO_4$ (*ca.* 2 g) in 1-pentyne (1.63 g, 24 mmol) / 3,3-dimethyl-1-butyne (2 g, 24 mmol) was added hfacH (2.5 ml, 18 mmol). This was stirred for 2 hours then cannula filtered. The solid residue was washed with hexane (2 × 10 ml) and the washings and filtrate combined giving a lime green solution. The volatiles were allowed to evaporate slowly by blowing N_2 (g) through the schlenk and out through a needle in the septum. After five days a brown solid material remained. This was dissolved in a refluxing hexane (7 mL), sealed and stored at 4 °C for 18 hours. After this time yellow crystals separated suitable for X-ray diffraction studies. These were collected by filtration, washed with hexane (3 × 5 ml) and dried *in vacuo*. Yield: 0.89 g (14 %). Found: C, 29.59; H, 2.30. Calc. for $Cu_{18}C_{94}H_{74}O_{20}F_{60}$: C, 29.65; H, 1.96%. δ_H (MeOD, 250 MHz): 0.94 (s, 12 H, C*H*$_3$), 1.41 (s, 36 H, C*H*$_3$), 1.68 (s, 8 H, C*H*$_2$), 2.57 (s, 8 H, C*H*$_2$) and 5.94 (s, 10 H, C*H*). IR spectra (KBr disc): 3447w, 3140w, 2975s, 2881m, 2403w, 1918s, 1644s, 1559s, 1530s, 1462s and 1210s cm^{-1}.

$[Cu_{20}(hfac)_8(C{\equiv}CCH_2Ph)_{16}]$ (13)

Cu_2O (1.64 g, 11.5 mmol) and anhydrous $MgSO_4$ (*ca.* 2 g) were added to a cooled (0°C) solution of hfacH (2.5 ml, 18 mmol) and 3-phenyl-1-propynyl (5 g, 43 mmol) in hexane (10 ml). After stirring for 48 hrs at room temperature the mixture was treated in the manner described above. Orange crystals suitable for X-ray structure determination separated from the hexane solution after 24hr. Yield: 1.09 g (14 %). Found: C, 41.34; H, 2.07. Calc. for $Cu_{20}C_{148}H_{96}O_{16}F_{48}$: C, 41.25; H, 2.15%. δ_H (CD_2Cl_2, 250 MHz): 3.36-3.78 (m, 24 H, C*H*$_2$), 5.95 (s, 8 H, C*H*) and 7.12-7.16 (m, 60 H, Ar*H*). δ_F (CD_2Cl_2, 250 MHz): -76.67 (s, 48 F, C*F*$_3$). IR spectra (KBr disc): 3064m, 3029m, 2360w, 1945w, 1637s, 1553s and 1467s cm^{-1}.

Ligand synthesis

4,4,4-trifluoro-1-phenyl-1,3-butanedione (14)

To a suspension of potassium tert-butoxide (12 g, 107 mmol) and acetophenone (10.71 g, 89 mmol) in benzene (250 ml), cooled to 10 °C, was added ethyl trifluoroacetate (12.8 ml, 107 mmol) dropwise. The suspension was stirred overnight then contacted with HCl solution (100 ml, 1M). The organic layer was collected, washed with water (2 × 200 ml) and dried over $MgSO_4$. The solvent was removed *in vacuo* leaving a yellow solid which was recrystallised from ethanol followed by methanol leaving a white solid. Yield: 17.43 g (91 %). Found: C, 55.01; H, 3.19. Calc. for $C_{10}H_7O_2F_3$: C, 55.56; H, 3.26%. δ_H (CD_2Cl_2, 250 MHz): 6.63 (s, 1 H, C*H*), 7.53-7.60 (m, 2 H, Ar*H*), 7.66-7.69 (m, 2 H, Ar*H*) and 7.98-8.02 (m, 2 H, Ar*H*). MS: (+FAB) m/z (% intensity) 215 (100 %).

References

1 T. C. Higgs, P. J. Bailey, S. Parsons, and P. A. Tasker, *Angew. Chem. Int. Ed.* , 2002, **41**, 3038.

2 T. C. Higgs, S. Parsons, P. J. Bailey, A. C. Jones, F. McLachlan, A. Parkin, A. Dawson, and P. A. Tasker, *Organometallics.*, 2002, **21**, 5692.

3 T. C. Higgs, S. Parsons, A. C. Jones, P. J. Bailey, and P. A. Tasker, *Dalton Trans.* , 2002, 3427.

4 J. C. Slater, *J. Chem. Phys.* , 1964, **41**, 3199.

5 J. A. Dean, 'Lange's Handbook of Chemistry', 1985.

6 G. M. Sheldrick, '*SHELXTL-97* Program for the Refinement of Crystal Structures.' 1997.

7 C. A. Hunter and J. K. M. Sanders, *J. Am. Chem. Soc.* , 1990, **112**, 5525.

8 R. Nast, *Coord. Chem. Rev.*, 1982, **47**, 89.

9 A. J. Gordon and R. A. Ford, *The Chemists Companion: A handbook of practical data, techniques and references, Wiley-Interscience.*

Chapter four

Cu_{24} and Cu_{26} Clusters

4.1 Introduction

This chapter extends the studies aimed at defining the scope and limitations of the Cu(I)-alkynyl cluster forming reaction[1] using a 'bulky' 1,3-diketone ligand, 6,6,6-trifluoro-2,2-dimethyl-3,5-hexanedione (^{t}Bu-tfacH), and a less 'bulky' ligand, 1,1,1-trifluoro-2,4-pentanedione (tfacH), (Figure 4-1) in place of hfacH.

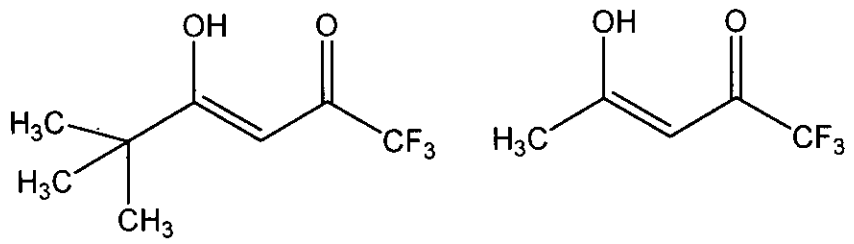

Figure 4-1. Structure of ^{t}Bu-tfac and tfacH

The synthesis and characterization of $[Cu_{24}(^t\text{Bu-tfac})_{12}(C{\equiv}CPr^n)_{12}]$ **(14)** and $[Cu_{26}(tfac)_{12}(C{\equiv}CBu^n)_{14}]$ **(15)** are reported and structures analysed to identify $[Cu_4(alkynyl)_4(Cu\text{-}hfac)_x]$ 'building blocks' described in chapters 2 and 3.

4.2 Cluster synthesis

Both clusters were synthesized using variations of the standard reaction first reported by Higgs *et al.*[1]

4.2.1 $[Cu_{24}(^t\text{Bu-tfac})_{12}(C{\equiv}CPr^n)_{12}]$ (14)

$[Cu_{24}(^t\text{Bu-tfac})_{12}(C{\equiv}CPr^n)_{12}]$ **(14)** was the major product of the reaction where 6,6,6-trifluoro-2,2-dimethyl-3,5-hexanedione (^{t}Bu-tfacH) was used in place of hfacH. The isolation of this cluster was of interest because it was the first example of a $[Cu_{x+y}(hfac)_x(C{\equiv}CR)_y]$ system containing twenty-four copper atoms. In addition the bulky ^{t}Bu- substituents causes a significant variation from previously observed structures. Crystals of **14** separated from a saturated hexane solution in the triclinic

space group *P*-1. The structure has no crystallographically imposed symmetry and is shown in Figure 4-10.

4.2.2 $[Cu_{26}(tfac)_{12}(C{\equiv}CPr^n)_{14}]$ (15)

$[Cu_{26}(tfac)_{12}(C{\equiv}CBu^n)_{14}]$ (**15**) was synthesized *via* the standard cluster forming reaction using the 1,3-diketone ligand, 1,1,1-trifluoro-2,4-pentanedione (tfacH). Crystalline material of **15** separated from a saturated hexane solution and crystallized in the monoclinic space group $P2_1/c$.

4.3 Structural Features

The two clusters, **14** and **15**, contain ligands related to hfacH where one $-CF_3$ group is substituted with $-Bu^t$ or $-CH_3$ groups. The following section discusses the effect of changing the properties of the 1,3-diketone ligand on the structure of the resulting cluster by comparing the novel systems, **14** and **15** with a 'conventional' structure, $[Cu_{26}(hfac)_{12}(C{\equiv}CBu^n)_{14}]$ (**16**).

4.3.1 Structure of $[Cu_{26}(hfac)_{12}(C{\equiv}CBu^n)_{14}]$ (16)

A number of clusters, with general formula $[Cu_{x+y}(hfac)_x(C{\equiv}CR)_y]$, where x+y = 26, have been reported previously.[1-3] They were obtained by varying the length of the *n*-alkyl chain of the alkyne used in the synthesis. 1-Pentyne, 1-hexyne, 1-heptyne and 1-octyne[1-3] give complexes with very similar structure. $[Cu_{26}(hfac)_{12}(C{\equiv}CBu^n)_{14}]$ (**16**) (Figure 4-2) is representative of the structural features that are observed throughout this series of Cu_{26} clusters. It crystallised in the rhombohedral *R*3*c* space group with the asymmetric unit containing 1/6 of the cluster. The whole molecule is generated by one C_3 and three C_2 axes of rotation.

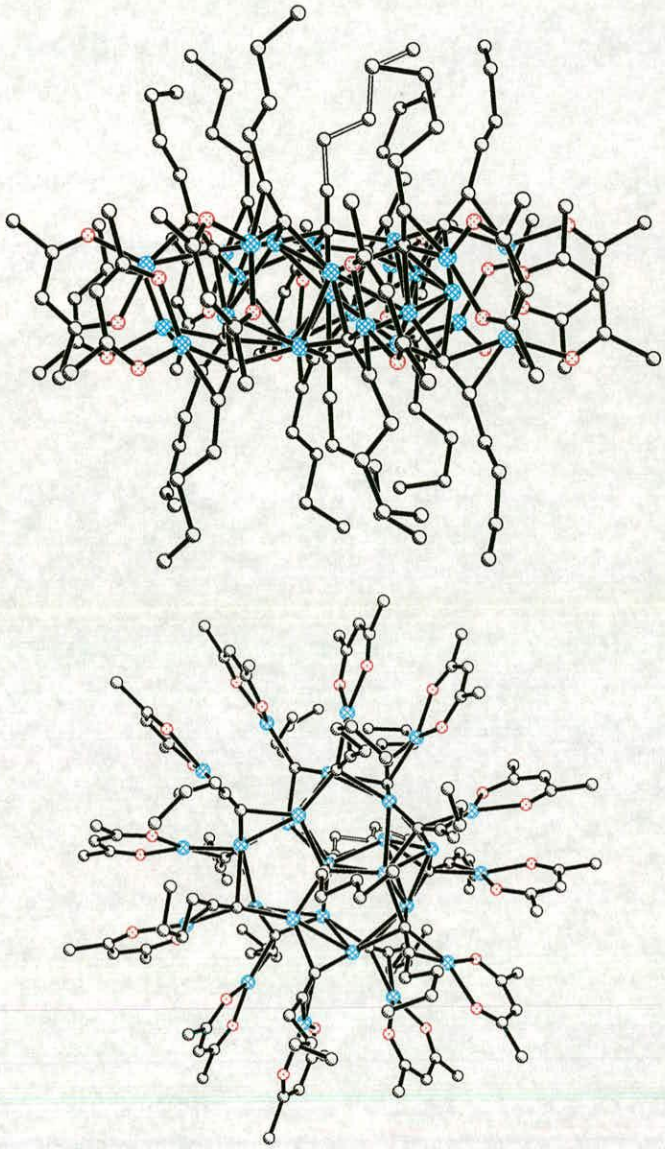

Figure 4-2. Two plots of $[Cu_{26}(hfac)_{12}(C{\equiv}CBu^n)_{14}]$ (**16**). Hydrogen and fluorine atoms have been removed for clarity.

Although larger than the clusters described so far in this thesis, **16** has some striking similarities to the Cu_{18} clusters described in chapter 3, $[Cu_{18}(hfac)_{10}(C{\equiv}CPr^n)_8]$ (**8**) and $[Cu_{18}(hfac)_{10}(C{\equiv}CBu^n)_8]$ (**9**). These Cu_{18} and Cu_{26} systems have an uneven distribution of hfac and alkynyl ligands around a central core of copper atoms. In **16** this disc-

shaped core consists of fourteen copper atoms linked exclusively by alkynyl ligands acting as (μ_2-η^1:μ-η^2) and (μ_3-η^1:μ-η^2) bridging units. The alkyl chains lie approximately parallel to each other in close proximity and point above and below the 'circular' face of the disc in a seven-up, seven-down arrangement.

As in the structures of **8** and **9**, the copper atoms not involved in the core are present in Cu-hfac chelate rings which form π-interactions with alkynyl ligands. Each of the twelve alkynyl units on the edge of the disc is associated with one Cu-hfac chelate ring resulting in a girdle of 'half butterfly' units surrounding the copper core (Figure 4-3).

In **8** and **9** the disposition of Cu-hfac chelate rings was shown to be due to chelate rings aligning in order to maximize cofacial overlap and attractive Cu…O intramolecular dipole-dipole interactions. This is also seen in **16** (Figure 4-3).

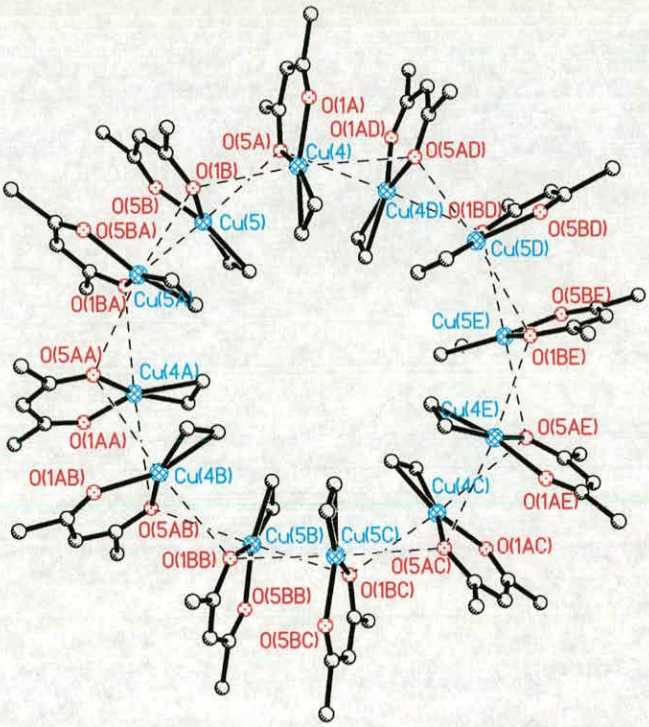

Figure 4-3. Distribution of Cu-hfac chelate rings in **16** showing Cu…O inter-ring contacts shorter than the sum of the Van der Waals radii (3.4 Å)[4]

The Cu-hfac units on the periphery of the cluster form six pairs of chelate rings aligned to maximize cofacial overlap and short Cu...O contacts. They are staggered to reduce

steric repulsion between $-CF_3$ groups (Figure 4-4). The least squares mean planes of the overlapping rings, defined by the six atoms in each chelate ring, are orientated at angles between 12.6 and 15.6° and Cu…O inter-ring distances fall in the range 3.105-3.342 Å (Table 4-1). Similar overlap of chelate rings has been observed in molecules described in chapters 2 and 3.

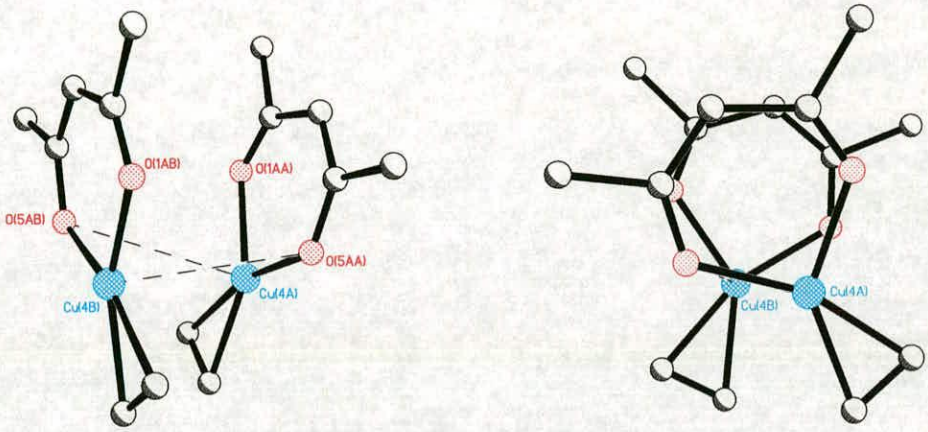

Figure 4-4. Approximate cofacial stacking of Cu-hfac rings in **16**

There are also short Cu…O interactions between adjacent non 'π-stacking' Cu-hfac rings (Figure 4-5) that fall in the range 3.100-3.103 Å. As a result the girdle of Cu-hfac rings that encircle the core of the cluster can be described as a network of six pairs of 'π-stacking' units connected by short inter-ring Cu…O interactions (Table 4-1).

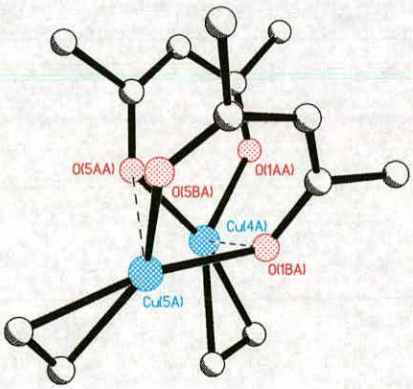

Figure 4-5. Short Cu…O contacts between adjacent non cofacially-overlapping Cu-hfac chelate rings in **16**

Intramolecular Cu…O contacts /Å			
'cofacial-stacking' Cu-hfac rings			
Cu4…O5A'	3.342	Cu5…O1B'	3.105
Cu4'…O5A	3.342	Cu5'…O1B	3.105
Non-stacking Cu-hfac rings			
Cu4…O1B	3.103	Cu5…O5A	3.100
Inclination between rings			
Rings	**Inclination /°**	**Rings**	**Inclination /°**
Cu4 – C4A and Cu4D-C4AD	15.6	Cu5-C4B and Cu5A-C4BA	12.6

Table 4-1. Cu…O contacts between Cu-hfac rings in the asymmetric unit of **16**. Atom numbers relate to the numbering scheme in Figure 4-3. The additional contacts in this cluster are generated by one C_3 and three C_2 axes of rotation. Planes are defined as (Cu4, O1A, O5A, C2A, C3A, C4A), (Cu4D, O1AD, O5AD, C2AD, C3AD, C4AD), (Cu5, O1B, O5B, C2B, C3B, C4B), (Cu5A, O1BA, O5BA, C2BA, C3BA, C4BA) respectively. Equations for the planes are given in appendix 2.

4.3.2 Structure of $[Cu_{26}(tfac)_{12}(C{\equiv}CPr^n)_{14}]$ (15)

The Cu_{26} cluster, **15** (Figure 4-6), which contains the tfac ligand has a similar structure to the analogous hfac Cu_{26} system, **16**.

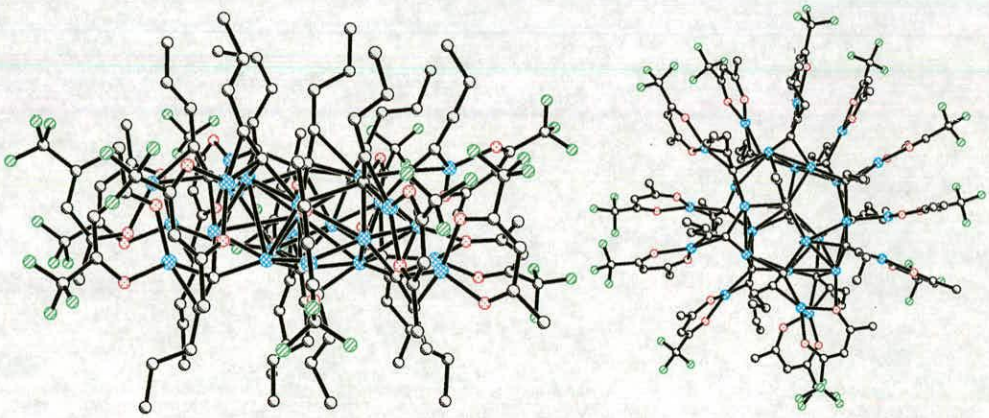

Figure 4-6. Perpendicular views of $[Cu_{26}(tfac)_{12}(C{\equiv}CBu^n)_{14}]$ (**15**)

As with all the structures in the high nuclearity series, **15** has a central disc-shaped core of copper atoms bridged exclusively by alkynyl ligands. The seven-up, seven-down arrangement of the alkynyl groups on the 'circular' face is very similar to that in **16**. Twelve Cu-tfac chelate rings are associated with the twelve alkynyl ligands on the rim of this disc, giving twelve 'half butterfly' units encircling the central core. As in **16** the 'half butterfly' units radiate from the core and are associated with neighbouring units through a network of short Cu…O interactions (Figure 4-7).

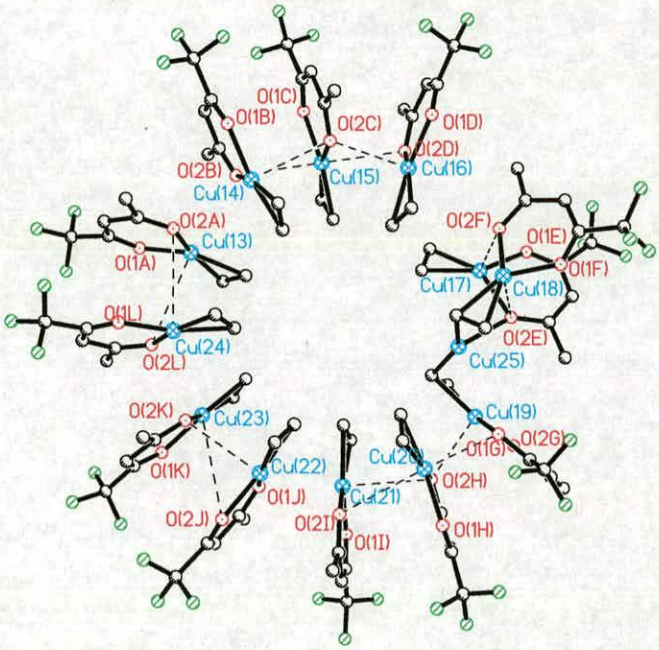

Figure 4-7. Distribution of Cu-tfac chelate rings in **15** showing short Cu…O inter-ring contacts

There are some deviations from the 'conventional' distribution of 'half butterflies. Four Cu-tfac units form two pairs of cofacial overlapping rings and six units form two triplets of overlapping rings (Figure 4-8) as opposed to six pairs of interacting rings in **16**. These interacting chelate rings are aligned approximately parallel to each other with Cu…O contacts falling in the range, 3.062(9)-3.838(8) Å (Table 4-2), with staggering of the $-CF_3$ groups (Figure 4-8) to minimise steric repulsion.

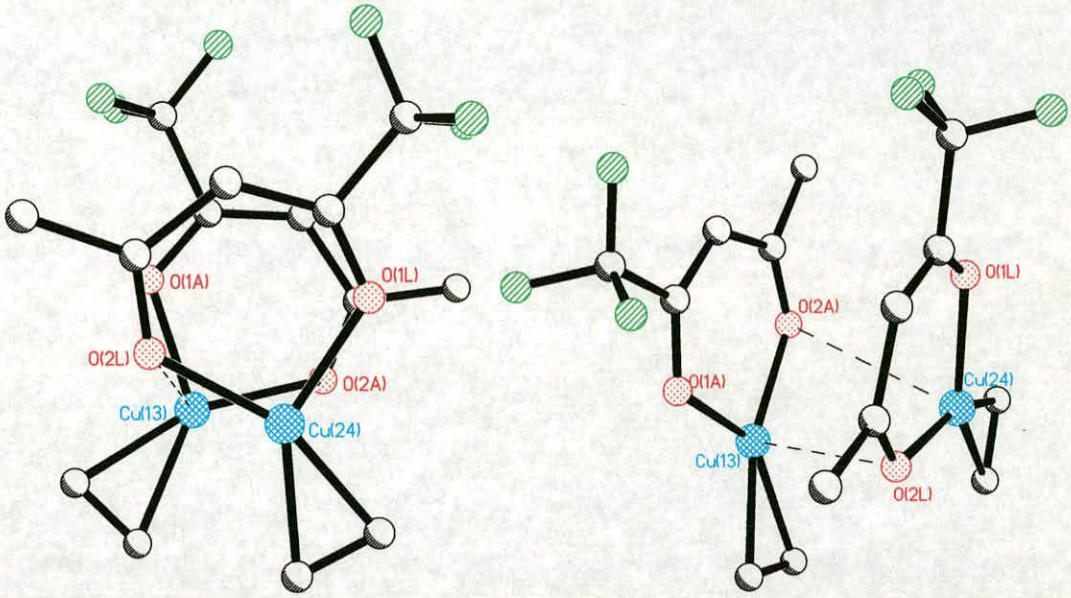

Figure 4-8. Example of 'π-stacking' type overlap in the pairs of chelate rings observed in **15**

The two Cu-tfac units containing Cu17 and Cu18 form a pair of rings that interact in a manner not previously observed in the series (Figure 4-9). The rings form a cofacial overlap type interaction but are also aligned to allow short contacts between an oxygen atom from the Cu-tfac unit containing Cu17 and a copper atom from the central core (Cu25) (Table 4-2). This additional interaction distorts the pair of chelate rings out of the plane defined by the other Cu-tfac units (Figure 4-7). The short contact observed in this pair of interacting chelate rings may not be possible with 'half butterflies' containing hfac ligand as the bulkier $-CF_3$ group would be too large to allow the units to lie sufficiently close to the central core.

Intramolecular Cu…O contacts (Å)			
'cofacial-stacking' Cu-tfac rings			
Cu14…O2C	3.062(9)	Cu20…O2I	3.105(8)
Cu15…O2B	3.074(9)	Cu21…O2H	2.968(8)
Cu22…O2K	3.091(8)	Cu24…O2A	3.248(9)
Cu23…O1J	3.161(9)	Cu13…O2L	3.285(9)
Cu17…O2F	2.569(8)		
Cu18…O2E	2.838(8)		
'non-stacking' Cu-tfac rings			
Cu15…O2D	2.823(8)	Cu19…O2H	2.585(8)
Cu16…O2C	2.708(8)	Cu20…O1G	2.706(8)
Cu…O contacts between tfac oxygen atom and central core copper (Å)			
O2E…Cu25	2.144(8)		
Inclination between rings			
Rings	**Inclination /°**	**Rings**	**Inclination /°**
Cu14-C13 and Cu15-C19	13.3(5)	Cu22-C34 and Cu23-C29	16.3(5)
Cu20-C44 and Cu21-C39	16.4(4)	Cu24-C4 and Cu13-C9	12.4(5)
Cu17-C54 and Cu18-C59	32.0(4)		

Table 4-2. Cu…O contacts between Cu-tfac rings in **15**. Atom numbers relate to the numbering scheme in Figure 4-7. The rings are defined as (Cu14, O1B, O2B, C11, C12, C13), (Cu15, O1C, O2C, C17, C18, C19), (Cu20, O1H, O2H, C42, C43, C44), (Cu21, O1I, O2I, C37, C38, C39), (Cu17, O1E, O2E, C52, C53, C54), (Cu18, O1F, O2F, C57, C58, C59), (Cu22, O1J, O2J, C32, C33, C34), (Cu23, O1K, O2K, C27, C28, C29), (Cu24, O1L, O2L, C2, C3, C4) and (Cu13, O1A, O2A, C7, C8, C9). Equations for the planes are given in appendix 2.

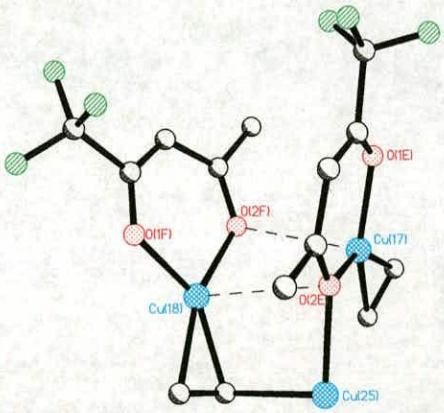

Figure 4-9. Interactions between Cu-tfac rings and central copper core seen in **15**

4.3.3 Structure of $[Cu_{24}(^{t}Bu\text{-}tfac)_{12}(C{\equiv}CPr^{n})_{12}]$ (14)

The structure of **14** (Figure 4-10) contains some of the common features associated with $[Cu_{x+y}(hfac)_x(C{\equiv}CR)_y]$ type cluster but deviates to a greater extent from the 'conventional' structure defined by **16**.

As in **15** and **16**, there is a central core of alkynyl bridged copper atoms in **14** but this consists of twelve copper atoms *c.f.* fourteen in **15** and **16**. All the twelve alkynyl groups are π-bonded to the copper atoms of a Cu-^{t}Bu-tfac ring.

The deviation from the 'conventional' structure shown by **15** and **16** can be attributed to the bulky –Bu^{t} substituent on the 1,3-diketonyl ligands which prevent the Cu-^{t}Bu-tfac rings from aligning cofacially about the copper core. Instead, the Cu-^{t}Bu-tfac rings are dispersed to minimize unfavourable steric interactions between ^{t}Bu- groups but allow the formation of overlapping 'π-stacking type' interactions (Figure 4-11). This results in a more even distribution of alkynyl chains and ^{t}Bu-tfac ligands over the surface of the cluster.

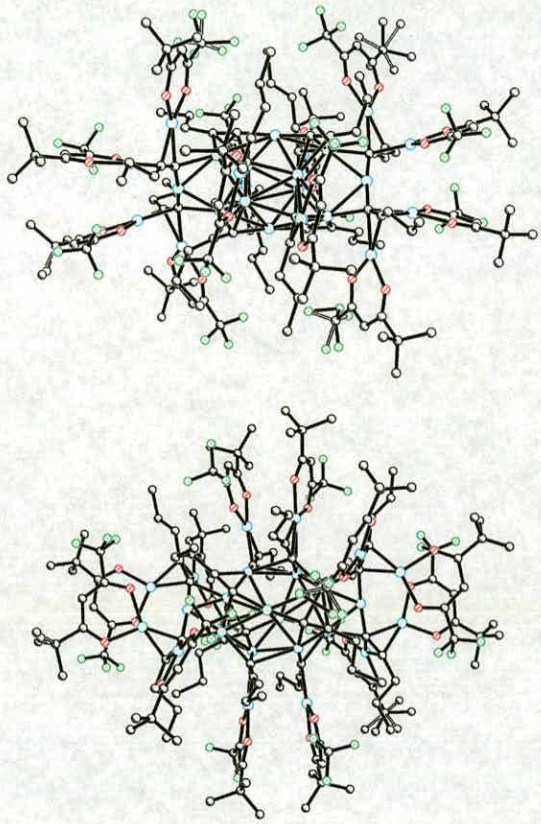

Figure 4-10. Plots of $[Cu_{24}(^{t}Bu\text{-tfac})_{12}(C{\equiv}CPr^{n})_{12}]$ (**14**)

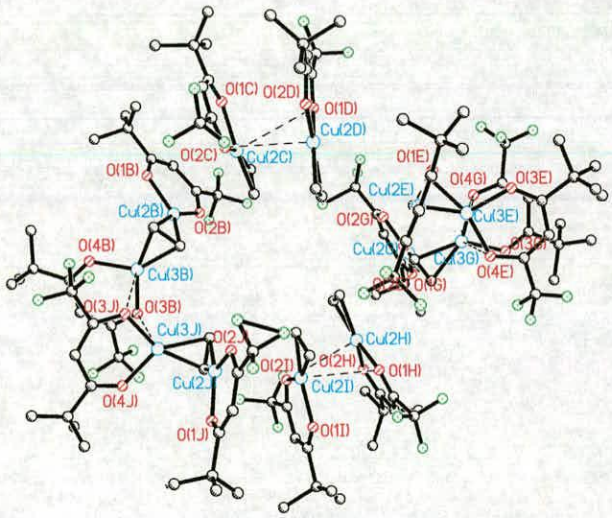

Figure 4-11. Distribution of Cu-^{t}Bu-tfac chelate rings in **14** showing short Cu…O inter-ring contacts

Despite the unusual distribution of Cu-^{t}Bu-tfac rings over the surface of the cluster in **14**, there remains a network of short Cu…O contacts and some cofacial type interactions although the network is not as extended as in previous examples (Figure 4-11). There are two 'full butterfly' and two 'half butterfly' units. Each 'full butterfly' forms one cofacial type interaction with another butterfly (Figure 4-12) (Table 4-3). Angles and distances between the planes of the interacting rings correspond to previous examples of similar interactions. The pairs of interacting butterflies lie on opposite sides of the central core (Figure 4-11).

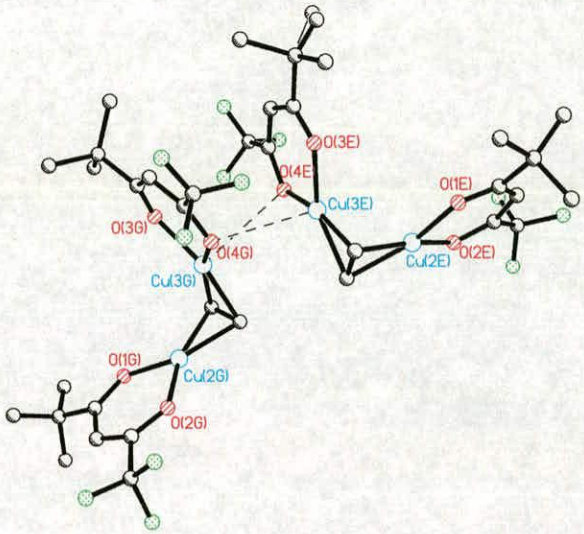

Figure 4-12. π-stacking interaction between butterfly units in **14**

The remaining four 'half butterfly' units form two pairs of cofacially stacking rings and these have Cu…O contacts and angles between planes that correspond to previous examples of this type of interaction (Table 4-3)

In the 'conventional' structure, interacting Cu-hfac units are associated with neighbouring units by additional Cu…O contacts resulting in a network of associated rings that encircle the central core. In **14**, the pairs of 'full butterflies' and 'half butterflies' units do not form additional interactions due to the steric bulk of the ^{t}Bu-group preventing more than two chelate rings lying in close proximity.

Intramolecular Cu...O contacts /Å			
Cu...O contacts between 'butterfly' units			
Cu3G...O4E	3.154(9)	Cu3J...O3B	3.135(9)
Cu3E...O4G	3.096(9)	Cu3B...O3J	3.094(8)
Cu...O contacts between 'half butterfly' units			
Cu2C...O1D	3.332(9)	Cu2H...O2I	3.231(8)
Cu2D...O2C	3.315(9)	Cu2I...O1H	3.156(8)
Inclination between rings			
Rings	**Inclination /°**	**Rings**	**Inclination /°**
Cu3G-C12 and Cu3E-C20	23.8(4)	Cu3J-C60 and Cu3B-C68	29.7(4)
Cu2C-C92 and Cu2D-C76	17.2(5)	Cu2H-C36 and Cu2I-C44	21.6(4)

Table 4-3. Cu...O contacts between Cu-Bu^t-tfac rings in **14**. Atom numbers relate to the numbering scheme in Figure 4-11. The rings are defined as (Cu3G, O3G, O4G, C10, C11, C12), (Cu3E, O3E, O4E, C18, C19, C20), (Cu3J, O3J, O4J, C58, C59, C60), (Cu3B, O3B, O4B, C66, C67, C68), (Cu2C, O1C, O2C, C90, C91, C92), (Cu2D, O1D, O2D, C74, C75, C76), (Cu2H, O1H, O2H, C34, C35, C36) and (Cu2I, O1I, O2I, C42, C43, C44) respectively. Equations for the planes are given in appendix 2.

4.3.4 Effects of variation of substituents on the hfac units

The effects of replacing CF_3 by CH_3 or $(CH_3)_3C$ appear to be mainly steric rather than electronic. The smaller tfac ligand gives Cu_{26} clusters with structures very similar to those of hfac complexes. The only major difference in **15** is the presence of an unusually short O...Cu contact between a copper in the central core and an oxygen atom from a peripheral Cu-tfac ring. It is unlikely that a similar interaction could occur between a hfac ligand and a central copper due to the greater bulk of the CF_3 group *c.f.* the CH_3 group. Other than this **15** and **16** are closely related which suggests that *reducing* the steric bulk of the diketone ligand has little effect on the nature of the cluster obtained.

The much larger ^{t}Bu-tfac prevents the formation of a network of parallel chelate rings associated by short Cu...O contacts. Instead pairs of cofacial Cu-^{t}Bu-tfac rings are

distributed around the copper core of the cluster and the uneven arrangement of alkynyl ligands and Cu-diketonyl chelate rings is lost. The bulk of ^{t}Bu-tfac is a factor that leads to the formation of a Cu_{24} compound as opposed to a Cu_{26}.

4.4 Nature of the central core in Cu_{24} to Cu_{26} clusters

In the clusters described in chapter 2 and 3, fragments with formula, $[Cu_4(C{\equiv}CR)_4(Cu\text{-}hfac)_x]$ have been identified which are defined as having Cu...Cu contacts along the edges of the Cu_4 square that are less than the sum of the van der Waals radii of copper (2.8 Å). In the following section similar building blocks in the high nuclearity series will be described and their significance in terms of the nature of these clusters considered.

4.4.1 $[Cu_4(C{\equiv}CR)_4(Cu\text{-}hfac)_x]$ fragments in (15)

In chapter 3 $[Cu_4(C{\equiv}CR)_4(Cu\text{-}hfac)_x]$ fragments in the Cu_{16} to Cu_{20} clusters were identified by defining Cu...Cu contacts of <2.8 Å in the copper cores. The same strategy has been applied to **15** and the central core can be seen in Figure 4-13.

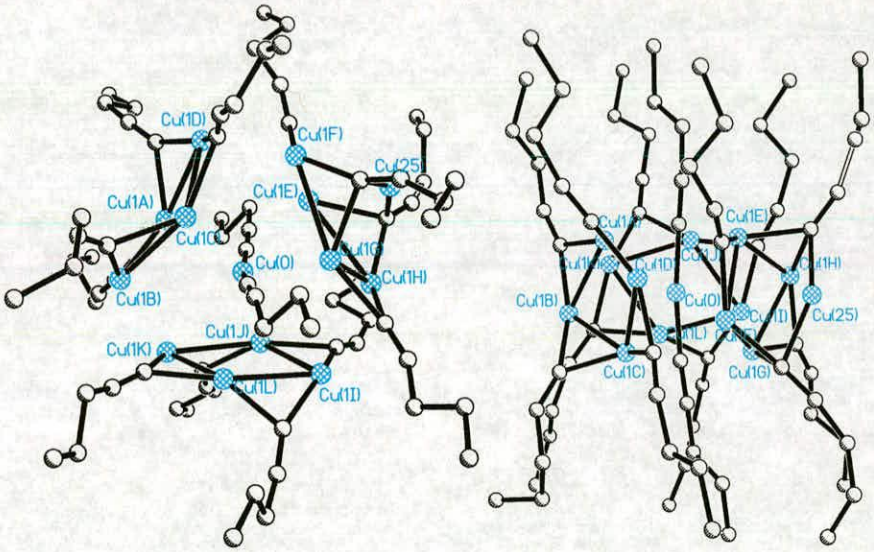

Figure 4-13. Two views of **15** with Cu-tfac chelate rings and Cu...Cu contacts greater than 2.8 Å removed. The structure has three $[Cu_4(C{\equiv}CR)_4]$ units, Fragment A, B and C

and a key is given in Appendix 1 that relates the numbering scheme shown to the original numbering scheme

By defining the central core in **15** with only Cu…Cu contacts <2.8 Å it is possible to identify motifs, with formula $[Cu_4(C{\equiv}CR)_4]$, that closely resemble the building blocks in the Cu_{18} systems. **15** differs from the lower nuclearity molecules, however, as there are three $[Cu_4(C{\equiv}CR)_4]$ units as opposed to two and there is a central RC≡C-Cu-C≡CR unit (Figure 4-13) around which the $[Cu_4(C{\equiv}CR)_4]$ fragments assemble.

Cu_4 contact distances /Å			
Fragment A			
Cu1A...Cu1B	2.504(2)	Cu1C...Cu1D	2.532(2)
Cu1B...Cu1C	2.552(2)	Cu1D...C1A	2.528(2)
Cu1A...Cu1C	3.080(2)	Cu1D...Cu1B	3.927(2)
Fragment B			
Cu1F...Cu1G	2.6623(10)	Cu1H...Cu1E	2.6656(19)
Cu1G...Cu1H	2.4944(18)	Cu1E...Cu1F	2.8561(18)
Cu1F...Cu1H	4.012(2)	Cu1G...Cu1E	3.205(2)
Fragment C			
Cu1J...Cu1I	2.553(2)	Cu1L...Cu1K	2.488(2)
Cu1I...Cu1L	2.493(3)	Cu1K...Cu1J	2.483(2)
Cu1J...Cu1L	2.871(2)	Cu1K...Cu1I	4.102(2)
Bridging alkynyl C-Cu bonds /Å			
Fragment A			
C1A-Cu1A	2.009(11)	C1C-Cu1C	2.048(10)
C1A-Cu1B	1.936(11)	C1C-Cu1D	1.958(10)
C1B-Cu1B	1.908(11)	C1D- Cu1D	1.902(11)
C1B-Cu1C	2.005(12)	C1D-Cu1A	1.972(11)
Fragment B			
C1E-Cu1F	2.050(10)	C1G-Cu1H	2.011(11)
C1E-Cu1E	2.032(10)	C1G-Cu1G	2.053(11)
C1H-Cu1E	2.075(10)	C1F- Cu1G	2.092(10)
C1H-Cu1H	1.955(10)	C1F-Cu1F	1.987(10)
Fragment C			
C1I-Cu1J	1.969(11)	C1K-Cu1L	1.947(11)
C1I-Cu1I	1.933(10)	C1K-Cu1K	1.939(10)
C1L-Cu1I	1.958(11)	C1J- Cu1K	1.923(11)
C1L-CuL	1.921(12)	C1J-Cu1J	1.953(11)
Alkynyl C...Cu bonds between $[Cu_4(C{\equiv}CR)_4(Cu\text{-}hfac)_x]$ fragments			
C1C-Cu1F	2.140(10)	C1K-Cu1B	2.318(10)
C1E-Cu1D	2.392(11)	C1G-Cu1I	2.267(11)
C1A-Cu1K	2.256(11)	C1I-Cu1H	2.153(10)
Deviations from the Cu_4 least squares mean plane /Å			
Cu1A	**Cu1B**	**Cu1C**	**Cu1D**
0.2088(8)	-0.2060(8)	0.2029(8)	-0.2057(8)
Cu1E	**Cu1F**	**Cu1G**	**Cu1H**
-0.2088(8)	0.2109(8)	-0.2196(8)	0.2175(8)
Cu1I	**Cu1J**	**Cu1K**	**Cu1L**
-0.0291	0.0289(8)	-0.0298(9)	0.0299(9)

Table 4-4. Cu...Cu, C-Cu distances and deviations from the Cu_4 cores /Å in the three $[Cu_4(C{\equiv}CR)_4(Cu\text{-}tfac)_x]$ fragments in **15**. Equations for the planes are given in Appendix 2.

The three $[Cu_4(C{\equiv}CR)_4(Cu\text{-}hfac)_x]$ units in **15** adopt a 'trimer' type arrangement with fragments inter-connected through alkynyl C...Cu interactions falling in the range, 2.140(10)-2.392(10) Å (Table 4-4). The 'trimers' are arranged around the central C2M≡C1M-Cu0-C1N≡C2N unit in the arrangement shown in Figure 4-14.

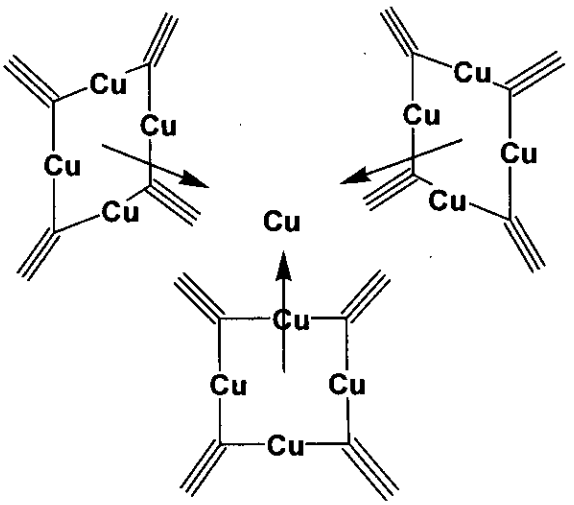

Figure 4-14. Schematic of the 'trimer' of $[Cu_4(alkynyl)_4]$ fragments arranged around the central atom, Cu0

The two central alkynyl groups, C2M≡C1M and C1N≡C2N, are linked to all three $[Cu_4(alkynyl)_4]$ fragments through alkynyl C...Cu interactions falling in the range, 2.082(11)-2.587(11) Å (Table 4-5). The central atom, Cu0, as well as being coordinated in an almost linear bonding mode by the central alkynyls, forms close contacts with the copper atoms in each of the $[Cu_4(alkynyl)_4]$ fragments with distances falling in the range 2.615(2)-2.722(2) Å (Table 4-5). There is a 14th copper atom, Cu25 (Figure 4-13), which resides on the periphery of the core and is not involved in a $[Cu_4(C{\equiv}CR)_4]$ unit. This 14th copper atom has been observed in the related Cu_{26} systems previously published[1-3] and is required to balance the overall charge of the molecule. In fact the position of the 14th copper in a Cu_{26} system is the distinguishing feature in a series of clusters that are structurally closely related. This observation has previously been discussed by Higgs *et al.*[1]

Central alkynyl C-Cu bonds /Å			
C1M-Cu1	2.179(11)	C1N-Cu4	2.264(11)
C1M-Cu2	2.082(11)	C1N-Cu5	2.110(11)
C1M-Cu3	2.587(11)	C1N-Cu6	2.382(10)
Central Cu0...Cu contacts /Å			
Cu0...Cu1	2.630(2)	Cu0...Cu5	2.705(2)
Cu0...Cu4	2.645(2)	Cu0...Cu3	2.722(2)
Cu0...Cu2	2.688(2)	Cu0...Cu6	2.615(2)

Table 4-5. Contact distances between the central C2M≡C1M-Cu0-C1N unit and the Cu_4 fragments.

The individual $[Cu_4(C{\equiv}CR)_4]$ units are shown in Figure 4-15 and selected bond lengths are given in Table 4-4. These closely resemble the $[Cu_4(C{\equiv}CR)_4]$ units identified in the clusters in chapter 2 and 3. The Cu...Cu contacts along the edges of the Cu_4 units fall in the range, 2.483(2)-2.6656(19) Å and diagonal Cu...Cu contacts fall in the range, 2.871-4.101 Å.

The Cu...Cu contacts in fragments A and C are approximately equal and adopt a rhombic arrangement with contacts between opposite copper atoms, Cu1A...Cu1C = 3.080 Å, Cu1B...Cu1D = 3.927 Å and Cu1E...Cu1G = 3.205 Å, Cu1F...Cu1H = 4.012 Å respectively. This rhombic distribution of copper atoms closely resembles the central cores observed in the Cu_{12} clusters reported in chapter 2.

Fragment B adopts a distorted rhombic arrangement with an uneven distribution of Cu...Cu contacts ranging between 2.4944(18)-2.8561(18) Å and opposite Cu...Cu contacts, Cu1E...Cu1G = 3.205 Å and Cu1F...Cu1H = 4.012 Å.

The Cu_4 cores in **15** are related to those in the 'half-molecule' fragments found in the Cu_{16} to Cu_{20} series, with the four copper atoms relatively non-planar compared with the Cu_4 cores observed in **2-5** in chapter 2 (Table 4-4).

Fragment A

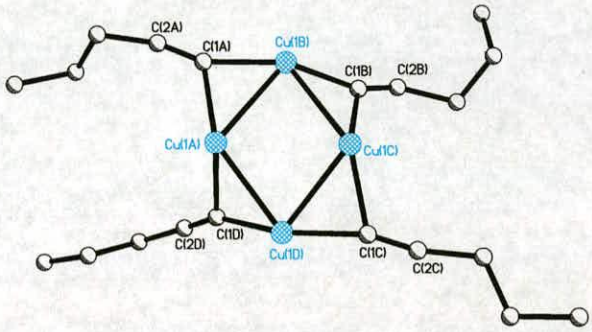

Fragment B

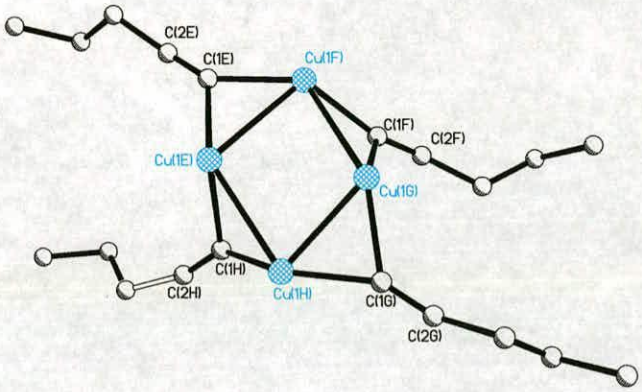

Fragment C

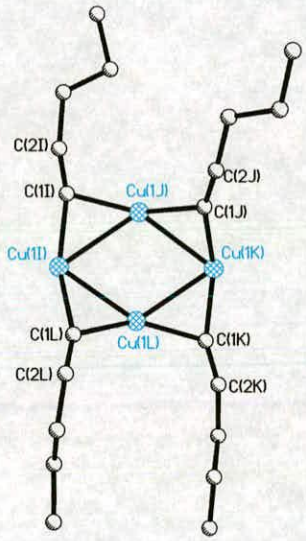

Figure 4-15. The three $[Cu_4(C{\equiv}CR)_4]$ fragments in **15**. The structure has been renumbered according to the generic numbering scheme used in chapters 2 and 3. A key is given in Appendix 1

The full $[Cu_4(C{\equiv}CR)_4(Cu\text{-}tfac)_4]$ fragments consist of one Cu-tfac chelate ring coordinated to each alkynyl ligand through a Cu-alkynyl π-bond. A plot of Fragment A

is shown in Figure 4-16. In the Cu_{10} and Cu_{12} systems the peripheral Cu-diketonyl chelate rings are displaced on either side of the Cu_4 plane in order to form inter-ring interactions. The Cu-tfac rings in the fragments in **15** also distort to allow inter-ring interactions but they lie on the same side of the Cu_4 plane, on the periphery of the cluster. The chelate ring associated with C1B≡C2B forms a cofacial interaction with the chelate ring bonded to C1D≡C2D. The non-cofacially interacting chelate rings are aligned to form short Cu…O contacts with the π-stacking rings (Figure 4-16). A similar arrangement is observed in Fragments B and C.

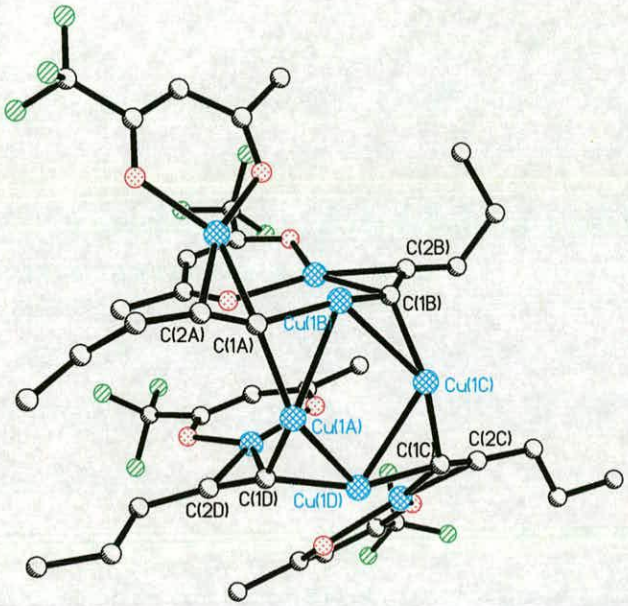

Figure 4-16. One full $[Cu_4(C{\equiv}CR)_4(Cu\text{-}tfac)_4]$ unit in **15** (Fragment A in Figure 4-14)

4.4.2 $[Cu_4(C{\equiv}CR)_4(Cu\text{-}^t Bu\text{-}tfac)_x]$ fragments in (14)

The central core of **14** is very different from that of **15** due to the bulky ^{t}Bu-tfac ligand and the $[Cu_4(C{\equiv}CR)_4(Cu\text{-}^t Bu\text{-}tfac)_x]$ 'building blocks' are less well defined. Two fragments with formula, $[Cu_4(C{\equiv}CPr^n)_4(Cu\text{-}^t Bu\text{-}tfac)_2]$ fragments and one smaller fragment with formula, $[Cu_3(C{\equiv}CPr^n)_3(Cu\text{-}^t Bu\text{-}tfac)_4]$ (Figure 4-18) have been identified.

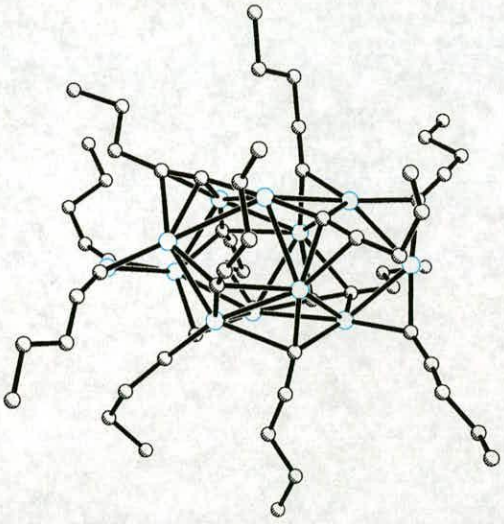

Figure 4-17. View of $[Cu_{24}(^{t}Bu\text{-}tfac)_{12}(C{\equiv}CPr^{n})_{12}]$ (**14**) with Cu-^{t}Bu-tfac chelate rings and Cu…Cu contacts greater than 2.8 Å removed

Fragments D and E (Figure 4-18) in **14** differ from the conventional $[Cu_4(C{\equiv}CR)_4]$ building blocks observed in chapters 2 and 3 despite having similar connectivities. The square Cu_4C_4 structure is not observed as one alkynyl ligand from each fragment is displaced from the plane of the Cu_4 core to allow a cofacial interaction between associated Cu-^{t}Bu-tfac fragments (Figure 4-19). Cu…Cu contacts along the edges of the Cu_4 unit are generally longer than the equivalent contacts in **15**, falling in the range 2.563(2)-2.934(2) Å (Table 4-6) and bridging alkynyl C-Cu bonds fall in the range, 1.845(13)-2.131(12) Å, which is typical of the μ_2-bridging modes observed throughout the series. Fragment F (Figure 4-18) contains three copper atoms, Cu1I, Cu1J and Cu1K, bridged by two alkynyl ligands with C-Cu distances in the range, 1.877(10)-2.074(11) Å.

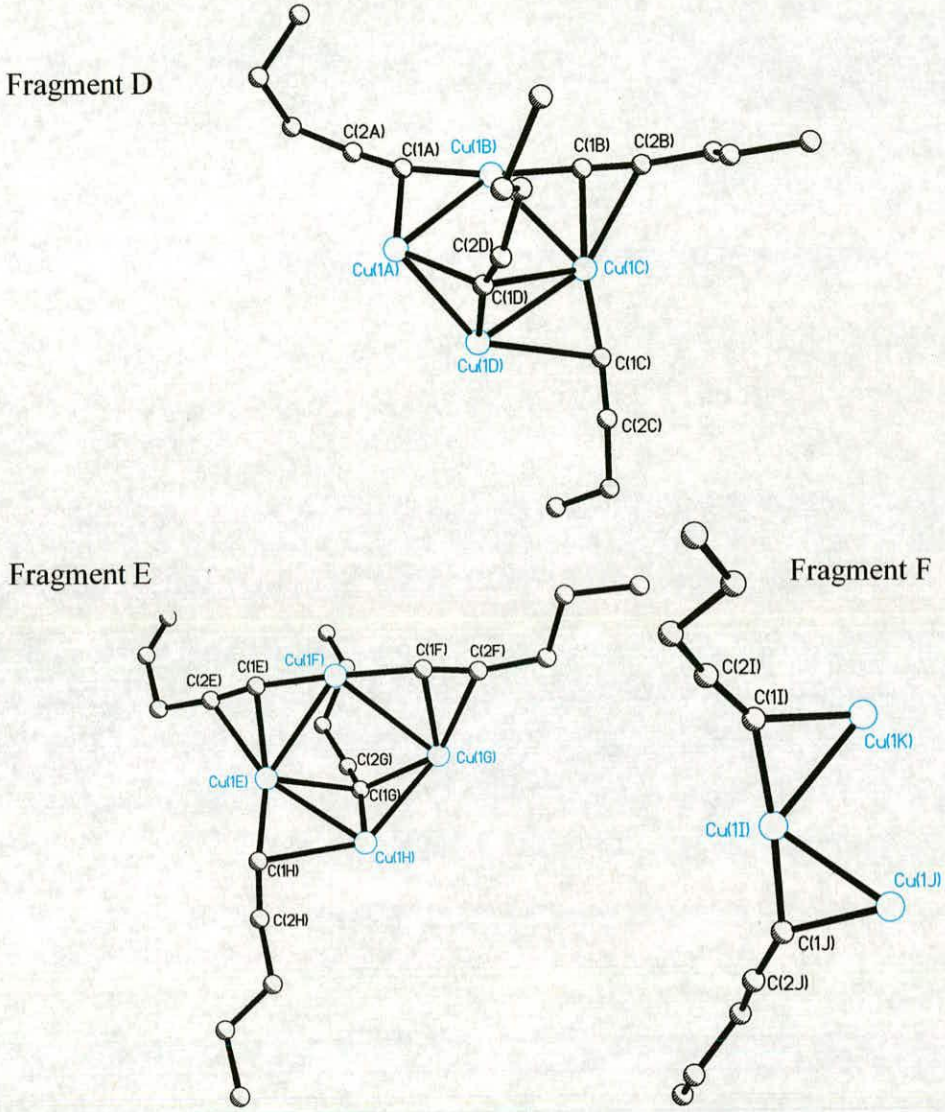

Figure 4-18. Two $[Cu_4(C{\equiv}CR)_4(Cu\text{-}^tBu\text{-}tfac)_x]$ fragments and the $[Cu_3(C{\equiv}CPr^n)_3(Cu\text{-}^tBu\text{-}tfac)_x]$ 'half fragment' in **14** with Cu-^{t}Bu-tfac rings removed

A simplified diagram of the structure of the core of **14** is shown in Figure 4-20. The bulk of the ^{t}Bu-tfac ligands appears to prevent three $[Cu_4(C{\equiv}CR)_4]$ units coming together to form a 'trimer' arrangement of the type observed in **15**. Instead two $[Cu_4(C{\equiv}CR)_4]$ units, fragments D and E, are connected, through alkynyl C-Cu bonds (Table 4-6), to an

incomplete $[Cu_4(C{\equiv}CR)_4]$ unit, fragment F, and an additional terminal fragment, C≡C-Cu-C≡C.

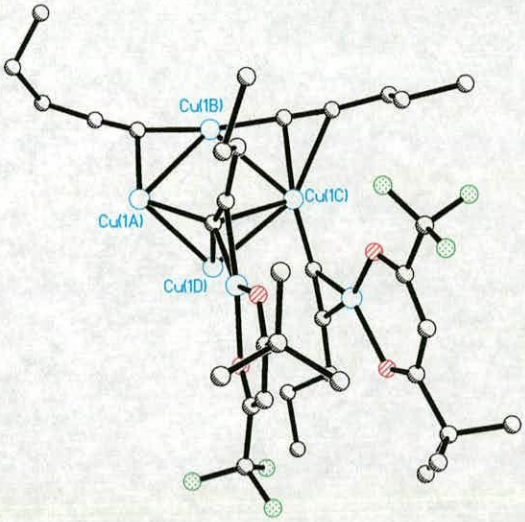

Figure 4-19. Fragment D including Cu-^{t}Bu-tfac rings

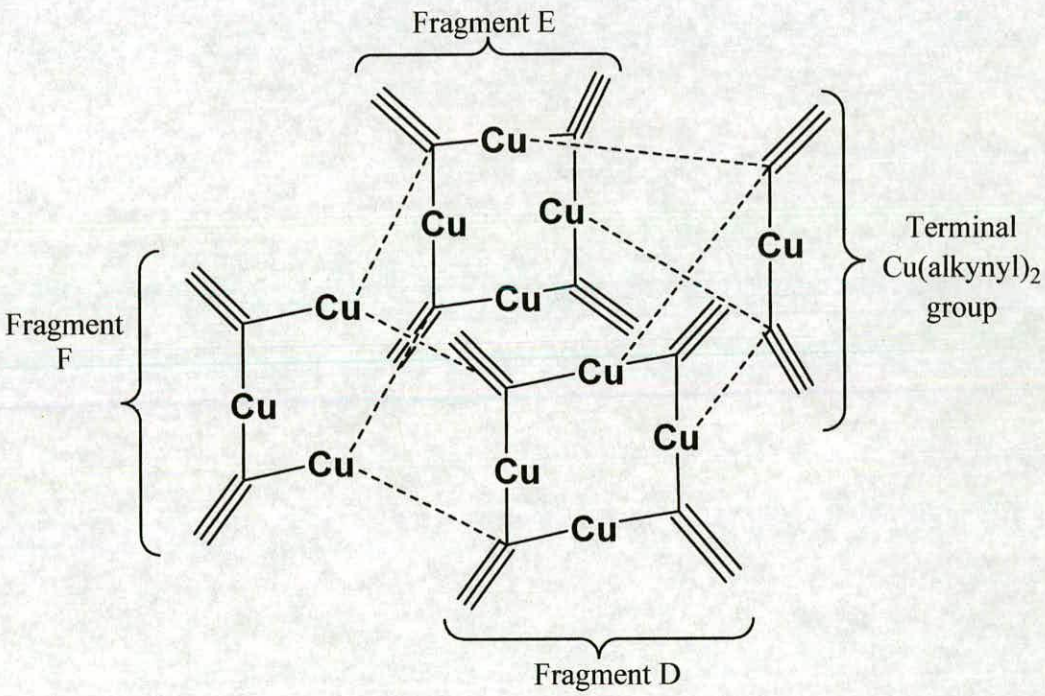

Figure 4-20. Diagram showing the arrangement of $[Cu_4(C{\equiv}CR)_4(Cu\text{-}^tBu\text{-}tfac)_x]$ units in **14**

Cu_4 contact distances (Å)			
Fragment D			
Cu1D...Cu1C	2.632(2)	Cu1B...Cu1A	2.574(2)
Cu1C...Cu1B	2.716(2)	Cu1A...Cu1D	2.563(2)
Cu1C...Cu1A	3.853(2)	Cu1D...Cu1B	3.412(2)
Fragment E			
Cu1H...Cu1E	2.620(2)	Cu1F...Cu1G	2.934(2)
Cu1E...Cu1F	2.737(2)	Cu1G...Cu1H	2.583(2)
Cu1E...Cu1G	3.864(2)	Cu1H...Cu1F	3.671(2)
Fragment F			
Cu1I...Cu1K	2.512(2)	Cu1K...Cu1J	3.396(2)
Cu1I...Cu1J	2.485(2)		
Cu1F...Cu1G	2.499(2)	Cu1F...Cu1E	2.027(11)
Bridging alkynyl C-Cu bonds (Å)			
Fragment D			
C1C-Cu1D	2.587(11)	C1A-Cu1B	1.899(12)
C1C-Cu1C	1.908(11)	C1A-Cu1A	2.093(11)
C1B-Cu1C	2.015(11)	C1D-Cu1A	2.093(12)
C1B-Cu1B	1.862(11)	C1D-Cu1D	1.899(12)
C1D-Cu1C	2.518(11)		
Fragment E			
C1I-Cu1H	2.400(10)	C1F-Cu1F	1.874(11)
C1I-Cu1E	1.898(10)	C1F-Cu1G	2.112(11)
C1E-Cu1E	2.040(12)	C1G-Cu1G	2.131(12)
C1E-Cu1F	1.845(13)	C1G-Cu1H	1.916(11)
C1G-Cu1E	2.442(12)		
Fragment F			
C1I-Cu1K	2.019(11)	C1J-Cu1I	1.918(10)
C1I-Cu1I	1.887(10)	C1J-Cu1J	2.057(10)
C1G-Cu1G	2.074(11)	C1E-Cu1F	1.928(12)
C1G-Cu1F	1.916(12)	C1E-Cu1E	2.027(11)
C-Cu bonds between $[Cu_4(C{\equiv}CR)_4(Cu\text{-}hfac)_2]$ fragments (Å)			
Cu1K-C1C	2.088(11)	Cu1J-C1H	2.120(11)
Cu1K-C1L	2.098(11)	Cu1J-C1B	2.133(12)
Cu1H-C1A	2.034(12)	C1F-Cu1D	1.978(12)
Deviations from the Cu_4 least squares mean plane (Å)			
Cu1A	**Cu1B**	**Cu1C**	**Cu1D**
0.2584(9)	-0.2431(8)	0.2395(8)	-0.2548(8)
Cu1E	**Cu1F**	**Cu1G**	**Cu1H**
-0.2670(8)	0.2342(7)	-0.2526(8)	0.2854(9)

Table 4-6. Cu...Cu contact and C-Cu bond distances and deviations from the Cu_4 core in **14**. Equations for the planes are given in Appendix 2.

4.4.3 Summary

The ligands, tfacH and ^{t}Bu-tfacH, used to synthesise **14** and **15** represent the two extremes in the types of diketone ligands successfully used to obtain $[Cu_{x+y}(hfac)_x(C{\equiv}CR)_y]$ compounds, tfacH being the least bulky and ^{t}Bu-tfacH the most bulky. The Cu_{26} cluster isolated using the less bulky ligand, **15**, closely resembles that obtained using hfac, **16**. The small differences in the conformation of the periphery of the cluster **15** can be attributed to reduced ligand bulk.

There are major differences between the cluster obtained using the bulky ^{t}Bu-tfacH ligand, **14** and the 'conventional' system, **16**. These can be attributed to the effect of steric bulk on the periphery of the cluster and may account for its lower nuclearity, Cu_{24}. In the following sections, the effects of the steric and electronic properties of both alkyne and diketonate ligands will be reviewed along with their significance in defining the nature of the clusters they form, making comparisons between all the systems characterised in chapters2-4.

4.5 Factors affecting cluster formation

One of the aims of this thesis was to investigate the scope and limitations of the cluster forming reaction. This was done by systematically varying the components of the reaction and studying the structures of the resulting compounds.

4.5.1 Effect of ligand steric properties on the nature of clusters

Throughout the series of $[Cu_{x+y}(hfac)_x(C{\equiv}CR)_y]$ compounds, structural motifs with formula, $[Cu_4(C{\equiv}CR)_4(Cu\text{-}hfac)_x]$ have been identified. Cu_{10}-Cu_{12} compounds contain one, Cu_{16}-Cu_{18} compounds contain two and Cu_{20}-Cu_{26} contain three of these units. In a simplified representation, clusters can be described as 'monomers', 'dimers' or 'trimers' of $[Cu_4(C{\equiv}CR)_4]$ units depending on their nuclearity (Figure 4-21). This is consistent with the observation that the number of copper atoms and alkynyl ligands in the cores of all the compounds are multiples of four, with the exception of the Cu_{26} systems where the added complexity of the structure requires an additional two Cu-alkynyl units.

In the 'dimer' and 'trimer' molecules, $[Cu_4(C{\equiv}CR)_4(Cu\text{-}hfac)_x]$ units are connected within the core by alkynyl C-Cu bonds and on the rim of the cluster through networks of cofacially overlapping chelate rings aligned to maximise inter-ring Cu...O contacts. The steric properties of the alkynyl and diketonate ligands in a cluster influence the ability of $[Cu_4(C{\equiv}CR)_4(Cu\text{-}hfac)_x]$ units to form these interactions.

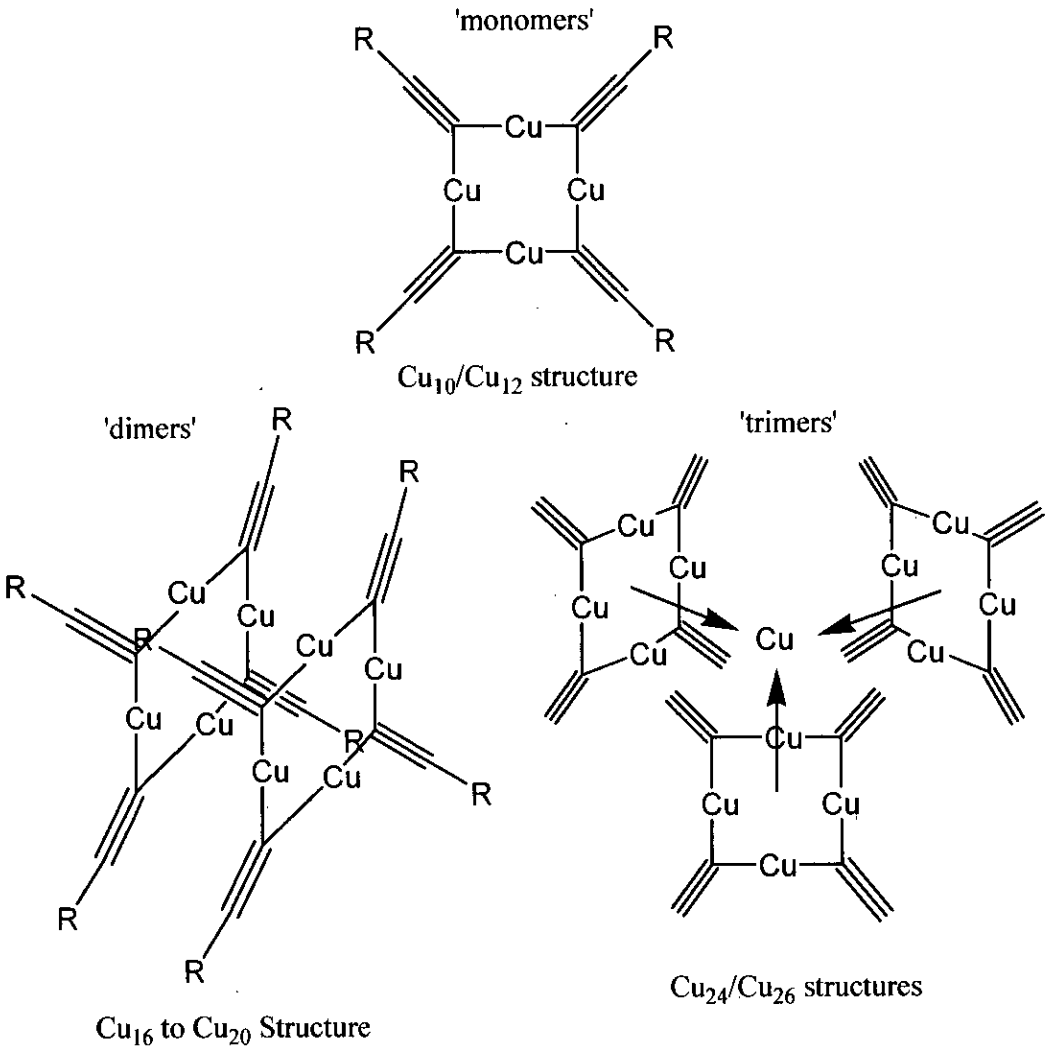

Figure 4-21 Simplified model of aggregations of $[Cu_{x+y}(hfac)_x(C{\equiv}CR)_y]$ units.

Where alkynyl ligands with little steric bulk are used, i.e. 1-pentyne or 1-hexyne, close packing of $[Cu_4(C{\equiv}CR)_4(Cu\text{-}hfac)_x]$ units is possible. In these cases, 'trimerisation' and 'dimerisation' occurs leading to the isolation of higher nuclearity systems, Cu_{16} – Cu_{26}. Where alkynyl ligands with greater steric bulk are used, i.e. (trimethylsilyl)acetylene, the close packing observed in the 'dimers' and 'trimers' becomes less favourable and formation of a 'monomer' is favoured, leading to Cu_{10}-Cu_{12} molecules. The connection between steric bulk and cluster nuclearity can be demonstrated by considering the two extremes of nuclearity observed in this thesis. The largest Cu_{26} cluster, **15**, was obtained using the least bulky alkynyl, 1-pentynyl, whereas the bulkiest alkynyl, $Me_3SiC{\equiv}C$, gave a Cu_{12} cluster as the sole product.

The diketonate ligands in the cluster do not directly influence the packing of $[Cu_4(C{\equiv}CR)_4]$ units in the core of the cluster. Consequently bulky diketonate ligands have less influence on the overall nuclearity of a cluster than bulky alkynyl ligands. This is demonstrated in **14** where a high nuclearity cluster was obtained using ^{t}Bu-tfac ligand with a core containing twelve copper atoms and alkynyl ligands. The bulk of the diketonate ligand does, however, affect the ability of the chelate rings on the rim of the cluster to align so as to maximise cofacial overlap and inter-ring Cu...O contacts. This leads to a different arrangement of the peripheral Cu-diketonate units. The requirement to reduce steric repulsions results in a distortion of $Cu_4alkynyl_4$ units and unconventional fragments are observed in **14**.

4.5.2 The effect of ligands with additional interacting functionality

As mentioned above, using bulky diketonate ligands, such as ^{t}Bu-tfacH, causes a distortion in the arrangement of Cu-diketonate chelate rings in the outer rim of the cluster compared to analogous compounds containing hfacH. Similar distortions are also observed when ligands that have the ability to form additional secondary interactions are incorporated. The structures containing the ligands $PhCH_2C{\equiv}CH$ and Ph-tfacH are comprised of cores containing $[Cu_4(alkynyl)_4]$ fragments but it is on the rim of the cluster where the main effects of the additional interactions are most striking. The cluster containing Ph-tfacH, **11**, has an extended network of Cu-Ph-tfac rings on the

rim of the cluster. In addition to the cofacial interactions between chelates observed in analogous Cu-hfac systems, there are 'π-stacking' type interactions between the ligand phenyl group and neighbouring units. There are similar 'π-stacking' interactions in the cluster containing $PhCH_2C{\equiv}C$, **13**, between phenyl groups and Cu-hfac rings. Although these interactions may not be as important as ligand steric interactions in determining the size of the cluster, they clearly influence interactions on the cluster periphery and result in compounds with interesting deviations from conventional systems.

4.5.3 Cuprophilicity in $[Cu_{x+y}(hfac)_x(C{\equiv}CR)_y]$ compounds

In chapter 2 the Cu_{10}-Cu_{12} series were compared to a family of compounds with formula, $[Cu_4(aryl)_4]$. Numerous studies on these systems have showed that the bond consists of sp^2 orbitals of the bridging aryl C^- atom overlapping the HOMO orbital of a Cu_2^{2+} fragment, a combination of the 4s orbitals with some contribution from $4p_y$ and $3d_{x^2-y^2}$ orbitals.[5] Cu-Cu bonding is therefore required to allow the formation of stable $[Cu_4aryl_4]$ species and it was proposed that similar bonding modes were present in the Cu_{10}-Cu_{12} clusters.

One of the remarkable features of the series of compounds described in this thesis is the similarity in $[Cu_4(alkynyl)_4]$ units. Where there are no additional steric influences causing distortion, the Cu...Cu contacts along the edges of the Cu_4 units are consistently less than the sum of the van der Waals radii of copper and are similar in length throughout the series. This may suggest that the bonding modes within the $[Cu_4(C{\equiv}CR)_4(Cu\text{-}hfac)_x]$ units are related to those in the $[Cu_4(aryl)_4]$ series and that the presence of cuprophilic interactions within the Cu-alkynyl cores of the $[Cu_{x+y}(hfac)_x(C{\equiv}CR)_y]$ may be an important factor in the stability of such intriguing molecules.

4.5.4 How the electronic properties of ligands affect cluster formation

Whilst the steric properties of the ligands used in cluster-forming reactions have been shown to be important in defining the structure of a cluster and its nuclearity, the electronic properties of the ligands determine whether successful cluster formation is

possible. The work so far described in this thesis deals with the structures of clusters successfully isolated from the 'standard' reaction described in Scheme 2-1. Syntheses using other alkynyl and diketone ligands (Figure 4-22) have also been attempted but proved unsuccessful. The failure of the ligands in Figure 4-22 to yield clusters provides some important information about the scope and limitations of the reaction and the electronic properties required for a ligand to be used successfully in cluster formation. Phenylacetylene [Figure 4-21 (a)] leads to instant polymerization under cluster-forming conditions. It has a relatively low pK_a compared to ligands that successfully form clusters (Table 4-7). It is possible that the formation of a [Cu(hfac)(alkyne)] monomer does not take place and deprotonation of the alkyne group followed by polymerization is favoured.

Alkynyl	pK_a
PhC≡CH[a]	18.5
HC≡CH[b]	25
^{t}BuC≡CH[c]	25.48
n-BuCC≡CH[d]	26.7

Table 4-7. Approximate pK_as for the reactions, *a*)[6] and *b*)[7] $RC{\equiv}CH + H_2O \rightarrow RC{\equiv}C^- + H_3O^+$, *c*)[8] $R^-Li^+ + RC{\equiv}CH \rightarrow RH + RC{\equiv}C^-Li^+$ and *d*)[9] $RC{\equiv}CH + DMSO \rightarrow RC{\equiv}C^- + DMSO{\cdot}{\cdot}{\cdot}H^+$ for selected alkyne ligands.

The remaining alkynyl ligands shown in Figure 4-22 contain, in addition to the alkyne functional group, coordinating atoms or functional groups containing oxygen or nitrogen atoms or alkene groups. When these ligands are used in the cluster-forming reaction, uncontrollable polymerization also takes place. This suggests that incorporation of any coordinating functionality into the alkyne ligand prevents the ordered assembly of $[Cu_4(C{\equiv}CR)_4(Cu\text{-}hfac)_x]$ 'building' blocks'.

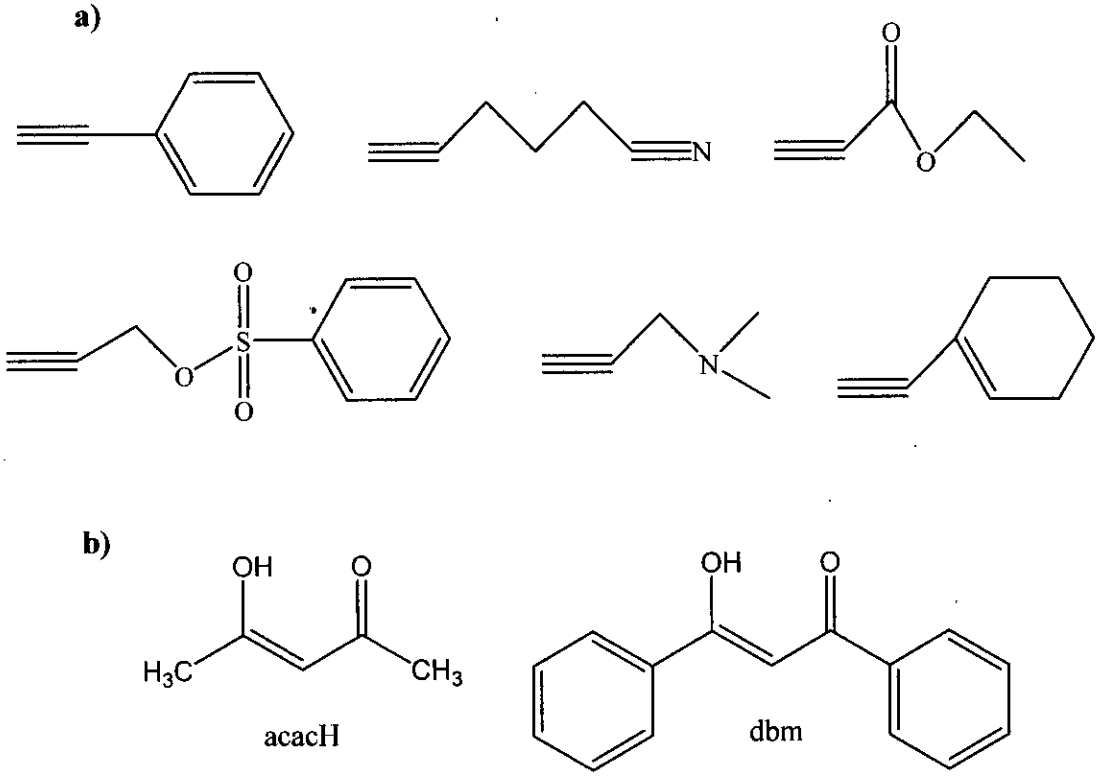

Figure 4-22. Some of the a) alkynes and b) diketones used in unsuccessful cluster forming reactions

Cluster forming reactions have also been attempted using the non-fluorinated 1,3-diketone ligands, acetyl acetonate (acacH) and 1,3-diphenyl-1,3-propanedione (dbm) (Figure 4-22). These are known to form complexes with Cu(I) and have been used to synthesise precursors for use in chemical vapour deposition applications.[10] Despite this neither has been successfully incorporated into a $[Cu_{x+y}(hfac)_x(C{\equiv}CR)_y]$ type cluster. Instead the [(1,3-diketonate)Cu(C≡CR)] complexes, (1,3-diketonyl = acac, dbm), obtained after the first step of the synthetic procedure, disproportionate under cluster aggregating conditions.

The family of complexes, [(β-diketonyl)CuL], (where L is a neutral ligand) are known to undergo disproportionation (Scheme 2)[11-14] and their stability with respect to disproportionation is dependent on ligand properties.

$$2[(\beta\text{-diketonyl})Cu(I)L] \rightarrow Cu(0) + Cu(II)(\beta\text{-diketonyl})_2 + 2L$$

Scheme 4-1. Disproportionation of [(β-diketonyl)CuL] complexes

Fluorinated β-diketonyl ligands form [(β-diketonyl)CuL] complexes that are more stable with respect to disproportionation than non-fluorinated ligands.[11-14] This may be due to the electron withdrawing effect of the $-CF_3$ group or conversely may be a result of the extra stability of $[Cu(II)(acac)_2]$ *c.f.* $[Cu(II)(hfac)_2]$. In order for successful cluster formation to take place, the [(β-diketonyl)Cu(I)L] complex must be stable with respect to disproportionation under reaction conditions. When non-fluorinated 1,3-diketone ligands are used, the [(β-diketonyl)Cu(I)L] complex is unstable and uncontrollable disproportionation occurs. The presence one or two $-CF_3$ substituents is sufficient to stabilize the complex to allow cluster formation to take place.

4.6 Conclusions

It is surprisingly easy to make a range of clusters with formula, $[Cu_{x+y}(hfac)_x(alkynyl)_y]$ using a straightforward synthetic procedure. The work described in the current and previous two chapters has given some important insights into the nature of this series and the scope and limitations of the cluster forming reaction. The conclusions that have been drawn as a result of this work are stated in this section.

Cluster synthesis is only successful using alkynes with relatively high pK_a and those containing no additional coordinating atoms or groups other than the alkynyl group.

Cluster synthesis is only successful using 1,3-diketone ligands that have at least one CF_3 substituent.

The clusters contain building blocks with formula, $[Cu_4(C{\equiv}CR)_4(Cu\text{-}hfac)_x]$. Compounds containing one such building block have nuclearity, Cu_{10}-Cu_{12}, compounds with two have nuclearity Cu_{16}-Cu_{18} and those with three have nuclearity Cu_{20}-Cu_{26}.

The $[Cu_4(C{\equiv}CR)_4(Cu\text{-}hfac)_x]$ building blocks are associated in the larger clusters through additional alkynyl C-Cu bonds in the core and through short inter-chelate Cu…O contacts on the rim of the cluster.

The steric bulk of the alkynyl ligand used in cluster synthesis affects the assembly of building blocks. High alkynyl bulk restricts aggregation and favours the formation of Cu_{10}-Cu_{12} clusters whereas low alkynyl bulk does not limit aggregation and Cu_{16}-Cu_{26} clusters are obtained.

Bulky diketonate ligands and ligands capable of forming additional π-stacking disrupt the network of interacting chelate rings on the periphery of the clusters, influencing the shapes of the clusters, and 'unconventional' structures are observed.

4.7 Experimental

Materials and reagents

All reagents were obtained from Aldrich Chemicals and used without further purification. *n*-Hexane was distilled from sodium/benzophenone/tetraglyme (trace) under N_2. N_2 gas was dried with 4Å molecular sieves and deoxygenated with BTS catalyst.[6] All preparations of copper(I) complexes were carried out under anaerobic and anhydrous conditions using standard Schlenk techniques. 1-Pentyne, 1,1,1-trifluoro-2, 4-pentanedione (tfacH) and 1,1,1,5,5,5-hexafluoropentan-2,4-dione (hfacH) were degassed by freeze/vac/thaw cycles.

$[Cu_{24}(^tBu\text{-}tfac)_{12}(C{\equiv}CPr^n)_{12}]$ (14)

Cu_2O (1.92 g, 13.4 mmol) and anhydrous $MgSO_4$ (*ca.* 2 g) were added to a solution of 1-pentyne (5 g, 0.061 mol) in hexane (10 ml). Dropwise addition of 6,6,6-trifluoro-2,2-dimethyl-3,5-hexanedione (^tBu-tfacH) (4.16 g, 21 mmol) was accompanied by an exothermic reaction. After stirring for 18 hr at room temperature the mixture was cannula-filtered and the solid residue washed with hexane (3 × 10 ml). The combined lime green filtrate and washings were evacuated *in vacuo* and the resulting orange/yellow oil was heated *in vacuo* at 65°C for 2 hr and then dissolved in refluxing hexane (20 ml) and set aside at 4°C. After 48 hr dark orange crystals suitable for x-ray diffraction studies had separated. The supernatent liquid was removed and the crystals were washed with hexane and dried *in vacuo*. Yield: 1.63 g (19 %). Found: C, 40.42; H, 4.62. Calc. for $C_{156}H_{216}O_{24}Cu_{24}F_{36}$: C, 40.00; H, 4.65%. IR spectra (KBr disc): 2963s, 1902s, 2840s, 1604s, 1538s and 1276s cm^{-1}.

$[Cu_{26}(tfac)_{12}(C{\equiv}CPr^n)_{14}]$ (15)

Cu_2O (1.92 g, 13.4 mmol) and anhydrous $MgSO_4$ (*ca.* 2 g) were added to a solution of 1-pentyne (5 g, 0.061 mol) in hexane (10 ml) followed by dropwise addition of 1,1,1-trifluoro-2, 4-pentanedione (tfacH) (2.5 ml, 21 mmol). After stirring for 24 hr at room temperature the mixture was cannula-filtered and the solid residue washed with hexane (3 × 10 ml). The combined lime green filtrate and washings were evacuated *in vacuo* leaving a white solid which turned red on heating *in vacuo* at 65°C for 2 hr. This was dissolved in refluxing hexane (20 ml) and set aside at 4°C. After 24 hr red crystals suitable for x-ray diffraction studies had separated. The supernatent liquid was removed and the crystals were washed with hexane and dried *in vacuo*. Yield: 0.72 g (32 %). Found: C, 35.85; H, 3.59. Calc. for $C_{130}H_{146}O_{24}Cu_{26}F_{36}$: C, 35.26; H, 3.32%. δ_H (CD_2Cl_2, 250 MHz): 0.98 (s, 42 H, C*H*$_3$), 1.71 (s, 36 H, C*H*$_3$), 2.03 (s, 28 H, C*H*$_2$), 2.58 (s, 28 H, C*H*$_2$) and 5.58 (s, 12 H, C*H*). IR spectra (KBr disc): 2955s, 1921s, 2853s, 1615s, 1543s, 1459, 1321s and 1290s cm^{-1}.

References

1 T. C. Higgs, P. J. Bailey, S. Parsons, and P. A. Tasker, *Angew. Chem. Int. Ed.* , 2002, **41**, 3038.

2 T. C. Higgs, S. Parsons, P. J. Bailey, A. C. Jones, F. McLachlan, A. Parkin, A. Dawson, and P. A. Tasker, *Organometallics.*, 2002, **21**, 5692.

3 T. C. Higgs, S. Parsons, A. C. Jones, P. J. Bailey, and P. A. Tasker, *Dalton Trans.* , 2002, 3427.

4 J. A. Dean, 'Lange's Handbook of Chemistry', 1985.

5 P. Belanzoni, M. Rosi, A. Sgamellotti, E. J. Baerends, and C. Floriani, *Chem. Phys. Lett.* , 1996, **257**, 41.

6 A. J. Gordon and R. A. Ford, *The Chemists Companion: A handbook of practical data, techniques and references, Wiley-Interscience.*

7 *Scifinder Scholar*, 2004.

8 A. Streitwieser, Jr. and D. M. E. Reuben, *J. Am. Chem. Soc.* , 1971, **93**, 1794.

9 J. Chrisment and J. J. Delpuech, *J. Chem. Res., Synop* . , 1978, 340.

10 H. K. Shin, K. M. Chi, M. J. Hampden-Smith, T. T. Kodas, J. D. Farr, and M. Paffett, *Chem. Mater.* , 1992, **4**, 788.

11 H. K. Shin, K. M. Chi, J. Farkas, M. J. Hampden-Smith, T. T. Kodas, and E. N. Duesler, *Inorg. Chem.*, 1992, **31**, 424.

12 A. Jain, K. M. Chi, T. T. Kodas, M. J. Hampden-Smith, J. D. Farr, and M. F. Paffett, *Chem. Mater.* , 1991, **3**, 995.

13 K. M. Chi, H. K. Shin, M. J. Hampden-smith, T. T. Kodas, and E. N. Duesler, *Inorg. Chem.*, 1991, **30**, 4293.

14 K.-M. Chi, H.-C. Hou, P.-T. u. Hung, S.-M. Peng, and G.-H. Lee, *Organometallics.*, 1995, **14**, 2641.

Chapter five

Photoluminescence studies

5.1 Introduction to photoluminescence spectroscopy

The absorption of a photon can often be attributed to a transition within a specific group or type of electrons. *d-d* transitions occur when electrons absorb energy by making transitions between non-degenerate d orbitals. These transitions are forbidden according to the Laporte selection rules and are very weak. Charge transfer transitions take place when radiation is absorbed as a result of the transfer of an electron from a ligand into a vacant metal *d* orbital (LMCT) or a metal *d*-electron is transferred to a vacant ligand orbital (MLCT). A $\pi^* \leftarrow \pi$ transition involves the excitation of an electron in a π-orbital of a delocalised system to an antibonding π^* orbital whereas a $\pi^* \leftarrow n$ transition involves the transfer of an electron from an orbital confined largely to one atom. Charge transfer and $\pi^* \leftarrow \pi$ transition are generally intense whereas $\pi^* \leftarrow n$ transitions, which are symmetry forbidden, are weak.

Once excited, a molecule discards its excitation energy through radiative or non-radiative processes. The non-radiative process is the most common and involves the transfer of excess energy into the vibration, rotation and translation of the surrounding molecules. This results in the conversion of excitation energy into thermal energy. A radiative decay process results in a molecule discarding excitation energy through the emission of a photon. This phenomenum is commonly known as photoluminescence and consists of two types radiation, fluorescence and phosphorescence.

Fluorescent radiation is emitted as a result of a transition without a change in multiplicity, i.e. a spin allowed transition, and ceases immediately after the exciting radiation is extinguished. Phosphorescence occurs because of a spin forbidden transition between states of different multiplicity following the process of inter-system crossing (Figure 5-1). As a result phosphorescence radiation has a longer lifetime ($>10^{-4}$s) than fluorescent radiation($<10^{-4}$s).

There are two types of photoluminescence spectra, excitation and emission spectra. An excitation spectrum is obtained by exciting a molecule over a range of wavelengths and measuring its emission at a certain wavelength (λ_{emm}). A molecule can only luminesce after it has absorbed radiation; therefore the excitation spectrum identifies the wavelengths of light at which the sample absorbs photons. As the

luminescence intensity is proportional to the extinction coefficient in dilute solutions, the bands in the excitation spectrum directly correspond to peaks in the absorption spectrum. An emission spectrum is obtained by maintaining a constant excitation wavelength where the sample is known to absorb (λ_{ex}), and measuring the spectral distribution of the emitted radiation.

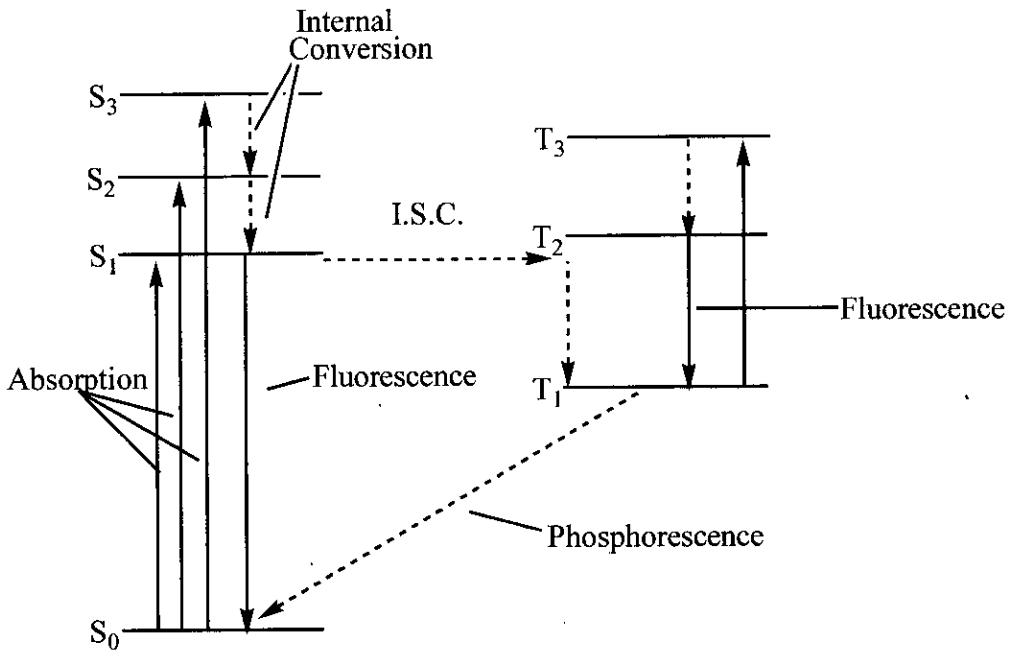

Figure 5-1. Energy level diagram to Illustrate Photoluminescent Emission

5.1.1 Photoluminescence properties of Cu-alkynyl complexes

The photoluminescence properties of Cu-alkynyl complexes were discussed in detail in chapter 1 and it was shown that these species have rich luminescent properties.[1-6] The transitions that give rise to photoluminescent emissions in Cu-alkynyl complexes were assigned tentatively and often involve a mixture of states. Despite this the emitting states are thought derive from an admixture of metal centred transitions (d → s), alkynyl to metal charge transfers ($RC{\equiv}C^- \rightarrow Cu$), and substantial intra-ligand transitions ($\pi \rightarrow \pi^*$).[1]

One of the aims of this project was to identify and study any interesting physical properties of $[Cu_{x+y}(hfac)_x(RC{\equiv}C)_y]$ type clusters. These systems have extensive, alkynyl-bridged copper cores with numerous short Cu…Cu distances that fall below

the sum of the van der Waals radii for copper (2.8 Å).[7] It seemed reasonable to suppose, therefore, that $[Cu_{x+y}(hfac)_x(RC{\equiv}C)_y]$ clusters could display luminescence properties similar in nature to previously reported systems due to transitions within this core. As a result a programme of research was initiated looking at the photoluminescence properties of $[Cu_{x+y}(hfac)_x(RC{\equiv}C)_y]$ clusters and the results are discussed in the following chapter.

5.2 Complex and cluster synthesis

The synthesis of the clusters, $[Cu_{16}(hfac)_8(C{\equiv}CBu^t)_8]$ (**10**) and $[Cu_{20}(hfac)_8(C{\equiv}CCH_2Ph)_{16}]$ (**13**), analysed in this chapter was described in chapter 3 and additional clusters, isolated and by Timothy Higgs, were synthesised using the conventional cluster forming reaction.[8]

5.2.1 Monomeric [Cu(hfac)L] complex synthesis

To allow comparisons between the photophysical properties of polynuclear clusters and related mononuclear complexes, a series of complexes were obtained, $[Cu(hfac)(HC{\equiv}CCH_2OMe]$ (**17**), $[Cu(hfac)(Me_3SiC{\equiv}CSiMe_3)]$ (**18**) and [Cu(hfac)(COD)] (**19**) (Figure 5-2).

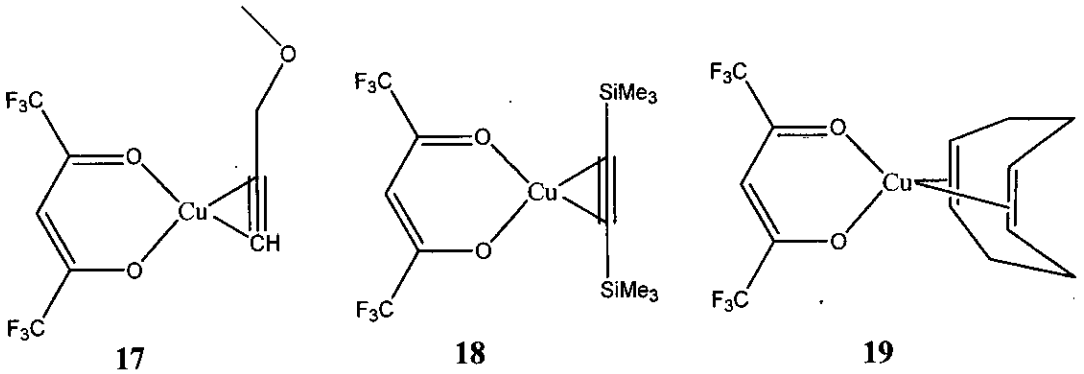

Figure 5-2. Structure of **17**, **18** and **19**.

18 was obtained from the Sigma-Aldrich chemical company and **19** was prepared using a reported method.[9] The preparation of **17** was carried out under conditions similar to those used in the first stage of cluster preparation, using anhydrous/degassed hexane as solvent. Yellow crystals suitable for X-ray structure

determination separated directly from the reaction solution after the filtration step and without being heated *in vacuo*. The X-ray structure showed that the complex (Figure 5-3) has a trigonal planar disposition of the hfac oxygen atoms and the alkyne bond, with deviations from the least squares plane defined by the donor atoms of 0.0329, 0.0072, -0.0073, -0.0173 and 0.0174 Å for Cu(1), O(1), O(2), C(6) and C(7) respectively. The symmetrical coordination of the alkyne atoms C(6) and C(7) and the large deviation of the C(6)-C(7)-C(8) angle, 163.1(3)°, from linearity is consistent with a strong metal to ligand π* bonding interaction.[10, 11] The terminal hydrogen atom attached to C(6) was identified from a difference Fourier map and refined satisfactorily (C(6)-H(6A) = 0.91(2) Å) confirming that a neutral form of the ligand is present.

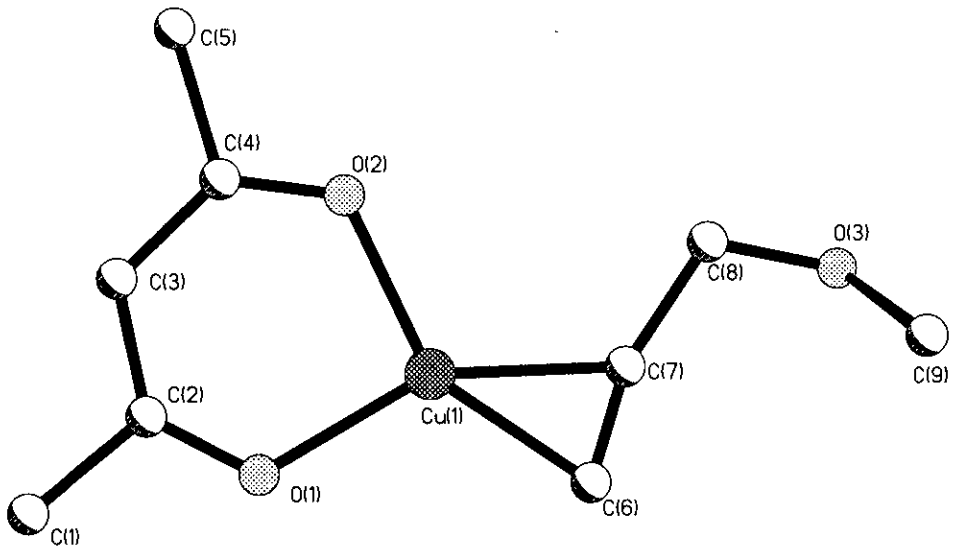

Figure 5-3. The structure of [Cu(hfac)(HC≡CCH$_2$OMe)] (**17**). Bondlengths from Cu(1) to O(1) and O(2) are 1.957(2) and 1.953(2) and to C(6) and C(7) are 1.944(3) and 1.961(3) Å respectively. Angles/° defined at the copper atom by pairs of donor atoms are: O(1)-O(2), 94.61(9); O(2)-C(7), 113.62(11); C(7)-C(6) 36.02(12); C(6)-O(1), 115.69(11); O(1)-C(7), 151.71(10); O(2)-C(6), 149.54(11).

5.3 Photoluminescence of [Cu$_{x+y}$(hfac)$_x$(RC≡C)$_y$] clusters

As part of the study into the photoluminescence properties of [Cu$_{x+y}$(hfac)$_x$(RC≡C)$_y$] clusters, room temperature luminesence and UV/Vis spectra of **10** (Figure 5-4) and **13** were obtained. The details are shown in Table 5-1. In conjunction with this

work, spectra of $[Cu_{18}(hfac)_{10}(C{\equiv}CC_4H_9^n)_8]$ (**9**) (Figure 5-5) and $[Cu_{26}(hfac)_{11}(C{\equiv}CC_3H_7^n)_{15}]$ (**20**) were also obtained by Dr Timothy Higgs and details of these spectra are given in Table 5-1.

10, 13, 9 and **20** have similar UV-vis spectra. All show a high energy (280-287 nm) band and a shoulder at 300-330 nm which can be assigned to internal ligand transitions ($\pi{\rightarrow}\pi^*$, $n{\rightarrow}\pi^*$). In addition, each cluster shows one weak absorption in the region 379 and 453 nm which can be tentatively assigned to M→L or L→M charge transfer within the highly delocalised Cu-alkynyl bridging networks.

All four clusters show very similar excitation and emission spectra. The shape and relative intensities of the peaks in the overlaid excitation and emission spectra of **10** and **9** (Figure 5-4 and 5-5) are representative of all four clusters. The excitation spectra (λ_{em}, 400 nm) of **10**, **13**, **9** and **20** display two bands at wavelengths 291-293 nm and 329-335 nm. These represent the excitations from which the luminescent emissions are derived and correspond to absorptions observed in the UV-vis spectra.

As with absorption and excitation spectra, the emission spectra in **10**, **13**, **9** and **20** are all remarkably similar with emissions occurring at approximately the same wavelengths in all cases. Emission spectra were obtained by exciting the clusters in solution in *n*-hexane with $\lambda_{excitation}$ = 280, 330 and 340 nm (Table 5-1). For excitation at λ_{ex} = 280 nm, an intense emission at *ca.* 344nm is observed and when λ_{ex} = 330 and 340 nm emission peaks at *ca.* 366 and 383 nm, respectively, are observed. This similarity is surprising as each species contains a different number of copper atoms and has a unique core structure. It is unlikely, therefore, that the luminescent properties of these clusters are due to MLCT, LMCT and intra-ligand charge transfer within the extensively bridged Cu-alkynyl networks.

The possibility that the bands in the luminescence spectra arise from Cu(hfac) components on the cluster periphery and not from transitions within the alkynyl bridged copper core was considered by investigating emission spectra for the mononuclear complexes, $[Cu(hfac)(HC{\equiv}CCH_2OMe]$ (**17**), $[Cu(hfac)(Me_3SiC{\equiv}CSiMe_3)]$ (**18**) and [Cu(hfac)(COD)] (**19**).

	UV-vis Absorption (ε_{max}/dm^3 mol^{-1} cm^{-1})	Excitation, λ_{em}, 400nm	Emission, λ_{ex}, 280nm	Emission, λ_{ex}, 330nm & 340nm
10	287 (104551)	292	344	366
	333sh (36285)	330 356*		382
	453sh. (2214)			
13	281 (188376)	292	344	366
	338sh. (43086)	334 357*		383
	423sh. (23046)			
9	291 (14551)	289	345	368
	330 (6251)	336 357*		383
20	281sh. (99420)	293	344 307*	367*
	305 (89480)	336 357* 379*		382
	437br.sh (8822).			
17	285 (259421)	294	343	366
	330 (95576	333 357*		380
	379 (27307			
18 silyl	245 (17529) 279.16 (16889)	293 357*	345	368
	327 (6813)	327		383
19 cod	290 (16042)	292	343	366
	328 (6318)	331 356*		383

(*denotes solvent Raman Bands)

Table 5-1. Wavelengths of intensity maxima in the UV-vis, excitation and emission spectra for **10**, **13**, **9**, **20**, **17**, **18** and **19** in *n*-hexane at RT

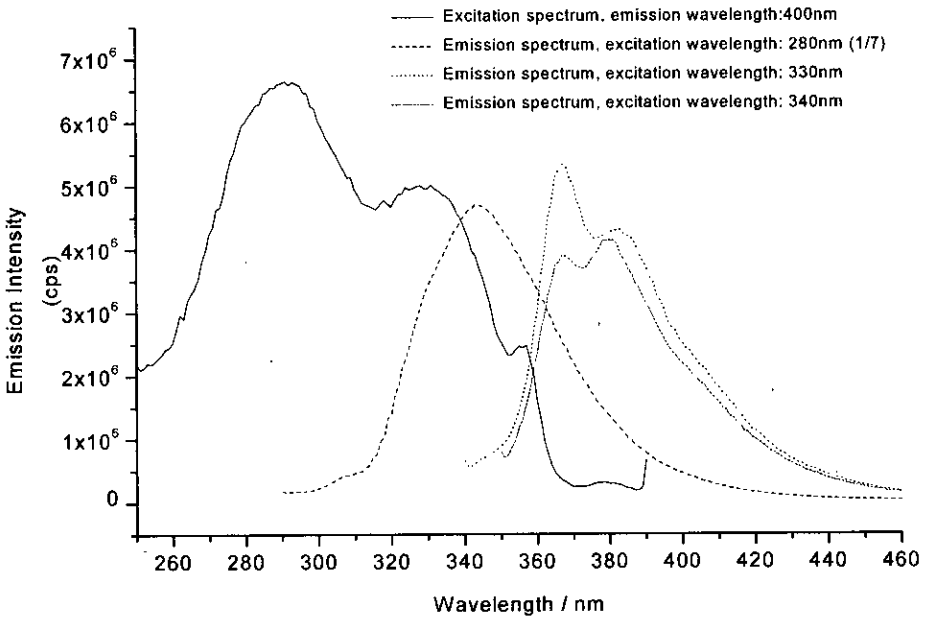

Figure 5-4. Excitation and emission spectra of $[Cu_{16}(hfac)_8(t\text{-butylalkynyl})_8]$ (**10**) in *n*-hexane at RT

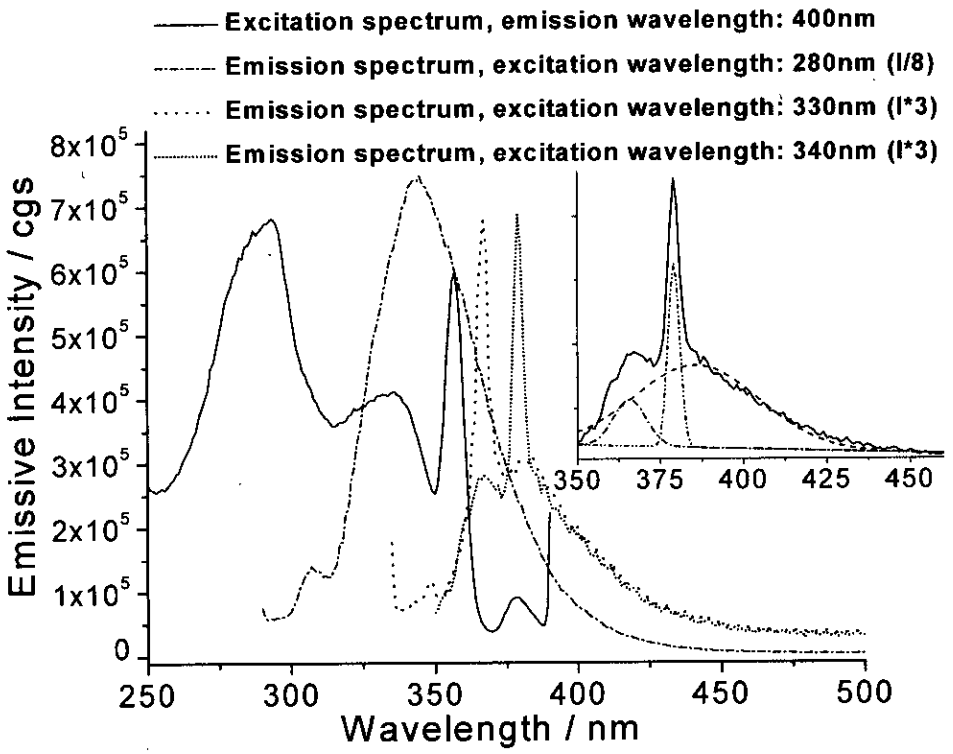

Figure 5-5. Excitation and emission spectra of $[Cu_{18}(hfac)_{10}(C{\equiv}CC_4H_9)_8]$ (**9**) in *n*-hexane at RT. **Inset:** Detail of emission spectrum at excitation wavelength of 340 nm and its Gaussian deconvolution fit with three peaks at 365.9, 379.2 (solvent raman band) and 385.9 nm respectively

5.4 Photoluminescence properties of [Cu(hfac)L] mononuclear complexes

To the best of our knowledge, there have only been two studies of discrete complexes containing a metal-hfac chelate ring published. Halverson *et al.* reported the luminescence spectrum of $[Eu(hfac)_3]$ and $[La(hfac)_3]$ in various solutions[12] and Gafney *et al.*, the spectrum of $[Fe(hfac)_3]$.[13]

In both studies, rich luminescence is observed and, in the case of $[Fe(hfac)_3]$, assigned to ligand $\pi^* \leftarrow \pi$ and ligand to metal charge transfers.

For comparison, Gafney *et al.*[13] also reported the emission spectrum of free hfacH in ethanol at 77K. It was shown to be a structured envelope in the range, 450 –525 nm due to phosphorescence (i.e. the result of a spin-forbidden transition).

5.4.1 Photoluminescence of 17, 18 and 19

The room temperature luminescence spectra of **17**, **18** and **19** were obtained. Excitation and emission spectra of **17** are shown in Figure 5-6 and are representative of the spectra obtained for all three molecules.

The excitation spectra for all three complexes show intense bands between 288-293 nm and 330-335 nm (Table 5-1) which correspond to peaks in the absorption spectra of each complex. The emission spectra of the three mononuclear complexes are also very similar (Table 5-1) and are typified by those shown for **17** in Figure 5-6. When the samples were excited at λ_{ex} = 280 nm, intense emission was observed between 343-344 nm (Table 5-1). When excited at λ_{ex} = 330 and 340 nm, emission peaks at *ca.* 366 and 382 nm were observed. Similar emission spectra were observed for $[Fe(hfac)_3]$, $[Eu(hfac)_3]$ and $[La(hfac)_3]$ by Gafney *et al*[13]. and Halverson *et al.*[12]

It is clear that the clusters and related mononuclear complexes display almost identical luminescence behaviour despite the considerable differences in their structures and sizes. As the Cu-hfac moiety is the only common feature within all of the species analysed it appears that the luminescence properties are derived from the delocalised electronic system in the chelate unit and any contribution made by the Cu-alkynyl network in solution is masked by the more intense bands of the Cu-hfac rings.

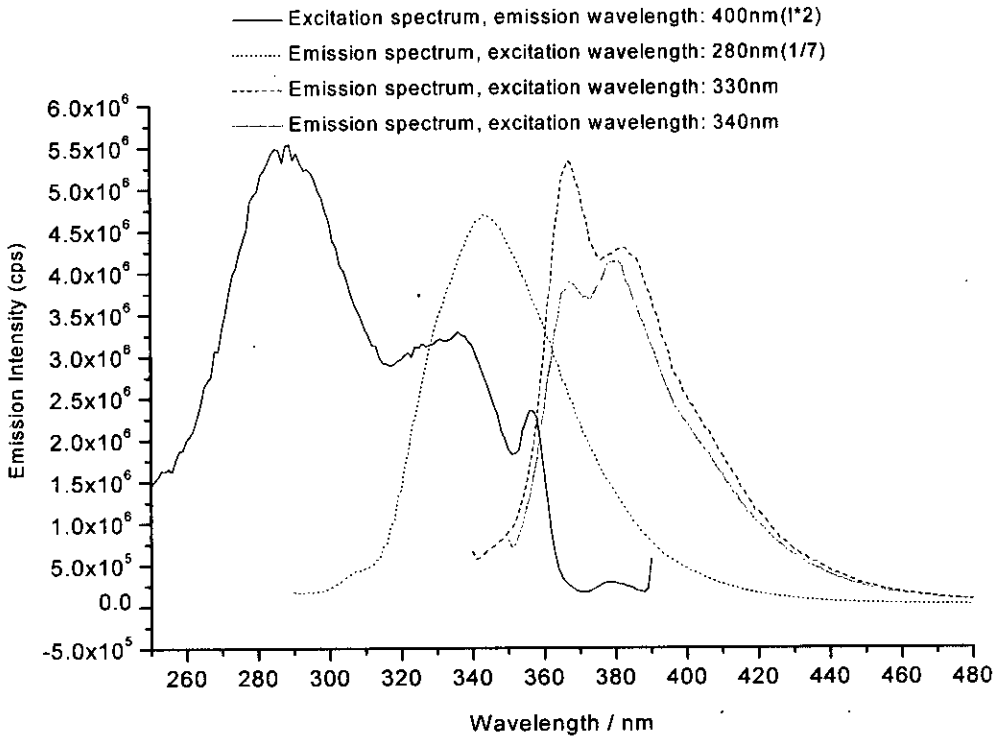

Figure 5-6. Excitation and emission solution spectra of **17** in *n*-hexane at RT

5.4.2 Lifetime studies and low temperature luminescence

The observation that $[Cu_{x+y}(hfac)_x(RC{\equiv}C)_y]$ clusters display almost identical room temperature luminescence spectra to those of mono-nuclear Cu-hfac complexes, **17**, **18** and **19**, is a clear indication that emission arises from transitions within the delocalised Cu-hfac rings and not, as was expected, from within the copper-alkynyl core. In order to extract more information about the nature of the emitting transitions, lifetime and low temperature studies were undertaken by Dr Timothy Higgs.[14] These studies were performed on $[Cu_{26}(hfac)_{12}(C{\equiv}CC_6H_{13})_{14}]$ (**21**),[14] a cluster whose room temperature spectra closely resemble those shown in Figure 5-4 and 5-5.

Upon excitation at 240-310 nm at 293 K, **21** displayed an intense emission with λ_{max} = 344 nm. The lifetime of this emission was determined to be 2 ns, indicating that it results from a spin-allowed transition and is fluorescent in nature. On excitation between 320-350 nm, an emission band with two maxima, λ_{max} = 344 and 382 nm become apparent with lifetimes determined to be 9 ns. These are also spin-allowed transitions.

The low temperature (77 K) n-hexane solvent glass spectra of **21** showed some intriguing features (Figure 5-7).

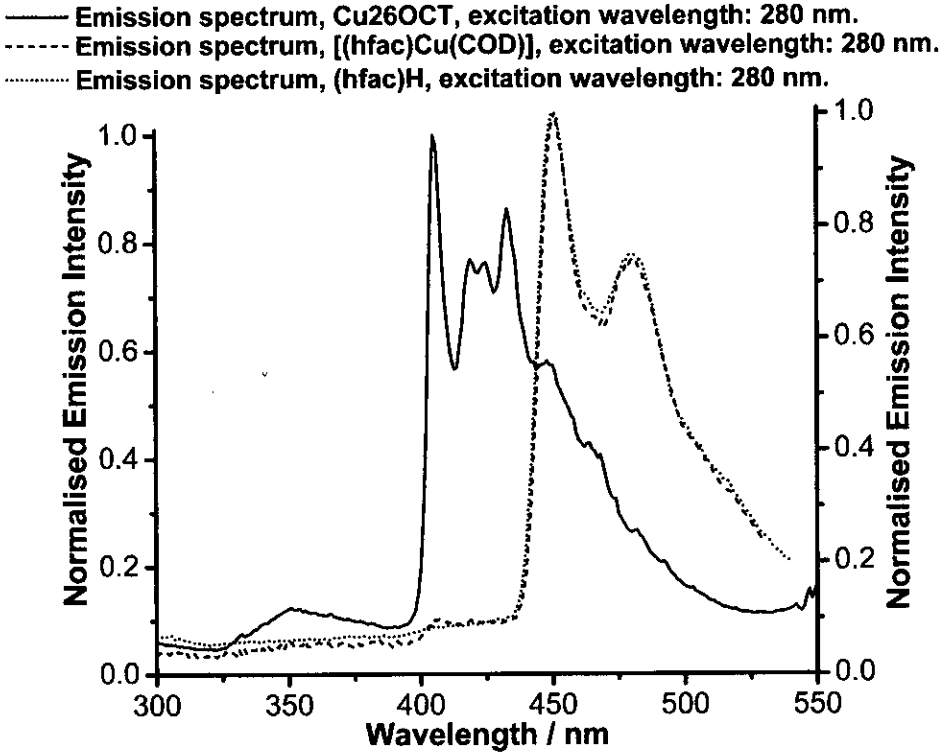

Figure 5-7. Emission spectra of hfacH and **19** in ethanol and **21** in *n*-hexane at 77 K, all at an excitation wavelength of 280 nm.

Excitation at 280 nm results in two emission bands. The shorter wavelength, relatively weak band at 350 nm corresponds to the room temperature band at 344 nm. A longer wavelength, more intense emission is observed between 406 and 448 nm with shoulders at 464 and 482 nm. Gaussian deconvolution of this complicated emission envelope has shown the presence of at least six underlying features with maxima at 406, 419, 425, 433, 448 and 482 nm. The absence of a corresponding emission at 293 K indicates that it is phosphorescence (i.e. a spin-forbidden emission), which, at room temperature is quenched by solvent collisions. The lifetime of this emission was estimated to be 170 ms, confirming a long lived spin-forbidden excited state.

To allow the assignment of these features, the spectra of free hfacH and **19** were investigated in ethanol solvent glass at 77 K (Figure 5-7) for comparison. Gafney *et al.*[13] reported the 77 K emission spectra of hfacH to consist of phosphorescence with

a structured envelope in the range, 450 –525 nm and this is confirmed in Figure 5-7. The similarity between the spectra of hfacH and **19** indicates that the emissive character of **19** is hfac$^-$ based. The emissive features displayed by **21** in the range, 450-525 nm, can also be attributed to hfac-based transitions.

It is clear that the intense emission bands observed in **21** at 77 K in the range, 406-433, are derived from transitions from a component within the structure other than the Cu-hfac chelate rings as neither hfacH or **19** displays emission in this region (Figure 5-7). It is likely, therefore, that the phosophorescent emission between 406 and 482 nm is derived from transitions from within the Cu-alkynyl core of **21**. There are numerous literature precedents to suggest that Cu-alkynyl transitions result in phosphorescent emission. In particular, low temperature luminescence of $[Ag_4Cu_2(\mu\text{-}Ph_2PNHPPh_2)_4(C{\equiv}CC_6H_5)_4](ClO_4)_2$ and related molecules reported by Zon-Wan Mao *et al.*[15] shows close resemblance to the results obtained in this work. They report the luminescence spectroscopy at 77 K of clusters with alkynyl-bridged cores containing between six and twelve metals. The spectra observed are similar in appearance to the spectra of **21** and have lifetimes in the micro-second range, indicating phosphorescent emission, however, the bands are red-shifted with respect to the bands observed in the spectra of **21**. This is most probably due to the greater σ-donating properties of the phenylacetylide ligands in $[Ag_4Cu_2(\mu\text{-}Ph_2PNHPPh_2)_4(C{\equiv}CC_6H_5)_4](ClO_4)_2]$ relative to the 1-octynyl ligands in **21**.

The emissive states of $[Ag_4Cu_2(\mu\text{-}Ph_2PNHPPh_2)_4(C{\equiv}CC_6H_5)_4](ClO_4)_2]$ and related systems were tentatively assigned to being derived from a LMCT ($C{\equiv}CC_6H_4R$-4$\rightarrow Ag_4Cu_2$ or Ag_6Cu_2) transition mixed with a metal cluster centred ($d\rightarrow s$) excited state modified by metal-metal interactions in view of the short Cu…Cu, Ag…Ag and Cu…Ag contacts observed. As **21** contains a central core of alkynyl-bridged copper atoms with short Cu…Cu contacts, it seems reasonable to suggest that similar transitions are responsible for the low temperature luminescence observed.

5.5 Conclusion and further work

The comparison of room temperature luminesence spectra of **10**, **13**, **9** and **20** with Cu-hfac mononuclear complexes, **17**, **18** and **19**, shows that emission spectra of $[Cu_{x+y}(hfac)_x(RC{\equiv}C)_y]$ type clusters are derived from transitions within the

delocalised Cu-hfac chelate rings on the cluster periphery. As a result there is no variation between clusters of differing size and nuclearity.

The luminescence spectra of **21** show a phosphorescent emissive feature, not evident at room temperature, which is not observed in the spectra of **17**, **18** and **19** or free hfacH. This feature resembles previous spectra of d^{10} metal-alkynyl networks and can be tentatively assigned to transitions within the copper alkynyl core.

Gaining a detailed understanding into the nature of the transitions that lead to the low temperature emission spectra of $[Cu_{x+y}(hfac)_x(RC{\equiv}C)_y]$ clusters could be an interesting area for further study. As part of this investigation it would be useful to study the low temperature spectra of a range of clusters with differing nuclearity and to ascertain how the size of the central alkynyl copper core affects the emissive properties of a cluster.

5.6 Experimental

UV-vis absorption spectra were obtained on an ATI UNICAM UV/vis spectrometer with 1 cm path length quartz cuvettes and fluorescence spectra on a Jobin-Yvon FluoroMax photon counting spectrometer. Fluorescence lifetimes were measured using a time-correlated single photon counting system (Edinburgh Instruments) with an instrument response function of 70 ps (fwhm); the excitation source was the third harmonic of a mode-locked Ti:sapphire laser (Coherent Mira).

n-Hexane was distilled over Na/benzophenone/tetraglyme under $N_2(g)$. Spectroscopic grade ethanol was obtained from Sigma-Aldrich chemical company.

5.6.1 Cluster synthesis

The synthesis of $[Cu_{16}(hfac)_8(C{\equiv}CBu^t)_8]$ (**10**) and $[Cu_{20}(hfac)_8(C{\equiv}CCH_2Ph)_{12}]$ (**13**) are described in chapter three and the synthesis of $[Cu_{18}(hfac)_{10}(C{\equiv}CC_4H_9{}^n)_8]$ (**9**), $[Cu_{26}(hfac)_{11}(C{\equiv}CC_3H_7{}^n)_{15}]$ (**20**) and $[Cu_{26}(hfac)_{12}(C_6H_{13})_{14}]$ (**21**) are reported by Dr Timothy Higgs.[8, 14, 16]

5.6.2 Complex synthesis

[Cu(hfac)($Me_3SiC{\equiv}CSiMe_3$)] (**18**) was obtained from the Sigma-Aldrich chemical supplier and [Cu(hfac)(COD)] (**19**) was obtained from Dr Timothy Higgs and had been prepared using a reported method.[9]

[Cu(hfac)($HC{\equiv}CCH_2OMe$)] (18)

Cu_2O (1.64 g, 11.5 mmol) and anhydrous $MgSO_4$ (*ca.* 2 g) were added under N_2 to methyl 2-propynyl ether (5 g, 71 mmol). hfacH (2.5 ml, 18 mmol) was added dropwise, followed by hexane (10 ml). After stirring for 4 hr the mixture was cannula filtered and yellow crystals separated over several days from the green/yellow filtrate. Yield: 1.09 g (14 %). Found: C, 31.63; H, 1.96. Calc for $CuC_9H_7O_3F_6$: C, 31.73 ; 2.07 H, %. IR spectra (KBr disc): 1672s, 1654s, 1314w, 1256s, 1208s, 1148s, 789m, 768w, 736w, 662s, 579m and 525w cm^{-1}.

References

1 V. W. W. Yam and K. K. W. Lo, *Chem. Soc. Rev.*, 1999, **28**, 323.

2 V. W. W. Yam, W. K. Lee, and T. F. Lai, *Organometallics.*, 1993, **12**, 2383.

3 V. W. W. Yam, W. K. M. Fung, and K. K. Cheung, *J. Clust. Sci.*, 1999, **10**, 37.

4 V. W. W. Yam, W. K. M. Fung, and M. T. Wong, *Organometallics.*, 1997, **16**, 1772.

5 V. W.-W. Yam, W. K.-M. Fumg, and K.-K. Cheung, *Angew. Chem. Int. Ed.* , 1996, **35**, 1100.

6 V. W. W. Yam, W. K. M. Fung, and K. K. Cheung, *Chem. Commun.*, 1997, 963.

7 J. C. Slater, *J. Chem. Phys.* , 1964, **41**, 3199.

8 T. C. Higgs, P. J. Bailey, S. Parsons, and P. A. Tasker, *Angew. Chem. Int. Ed.* , 2002, **41**, 3038.

9 K. M. Chi, H. K. Shin, M. J. Hampdensmith, E. N. Duesler, and T. T. Kodas, *Polyhedron*, 1991, **10**, 2293.

10 R. Nast, *Coord. Chem. Rev.*, 1982, **47**, 89.

11 J. Manna, K. D. John, and M. D. Hopkins, *Adv. Organomet. Chem.* , 1995, **38**, 79.

12 F. Halverson, J. S. Brinen, and J. R. Leto, *J. Chem. Phys.* , 1964, **40**, 2790.

13 H. D. Gafney, R. L. Lintvedt, and I. S. Jaworiwsky, *Inorg. Chem.*, 1970, **9**, 1728.

14 T. C. Higgs, S. Parsons, P. J. Bailey, A. C. Jones, F. McLachlan, A. Parkin, A. Dawson, and P. A. Tasker, *Organometallics.*, 2002, **21**, 5692.

15 Q.-H. Wei, G.-Q. Yin, L.-Y. Zhang, L.-X. Shi, Z.-W. Mao, and Z.-N. Chen, *Inorg. Chem.*, 2004, **43**, 3484.

16 T. C. Higgs, S. Parsons, A. C. Jones, P. J. Bailey, and P. A. Tasker, *Dalton Trans.* , 2002, 3427.

Chapter six

Strategies to assemble networks of Cu_5-clusters

6.1 Introduction

Assembling clusters in an organised and predictable array is a challenging target for synthetic chemists. In the following section attempts to create extended networks containing clusters with general formula, $[Cu_5(bta)_6(acac)_4]$ and related transition metal-benzotriazole complexes will be discussed.

6.1.1 Benzotriazole cluster chemistry

The benzotriazole ligand (Figure 6-1) was discovered in 1876 and found to be a weak acid of pKa 8.76.[1] Since the discovery in the 1950's that it is an effective inhibitor of copper corrosion there has been considerable interest in copper/benzotriazole chemistry.[2]

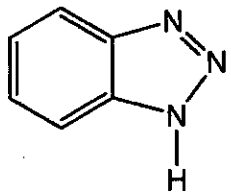

Figure 6-1. Structure of benzotriazole (btaH).

A number of techniques have been used to study the nature of the interaction between btaH and copper surfaces. These have included XPS depth profiling,[3] Extended X-ray Absorption Fine Structure Spectroscopy (EXAFS),[4] Auger Emission Spectroscopy [5] and Near Edge X-ray Absorption Fine Structure Spectroscopy (NEXAFS).[6] Despite the numerous surface studies the detail of the bonding is not known although several possible bonding modes have been proposed (Figure 6-2).[7-9]

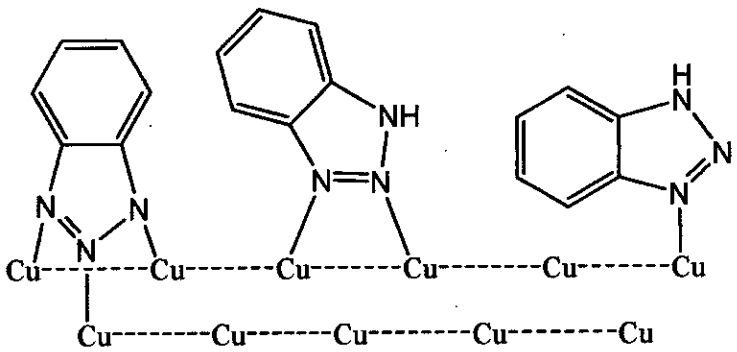

Figure 6-2. Tri-, bi-, and mono-nucleating bonding modes

In light of the difficulties faced in determining the nature of bta–copper interactions using surface analysis techniques there have been efforts to synthesise a model of the interaction using conventional coordination chemistry. The most significant discovery in this area made by Marshall *et al.*[10] in 1978 when they reported the synthesis of the first bta bridged pentametallic Cu(II) cluster, hexakis(benzotriazole) tetrakis(2,4-pentanedionato) pentacopper(II) ($[Cu_5(bta)_6(acac)_4]$). A structure where the copper atoms were bridged by bta^- ligands in a μ_3-tridentate 'arrowhead' mode was confirmed when the structure of $[Cu_5(bta)_6(acac)_4]$ was reported by Handley *et al.*[11] (Figure 6-3).

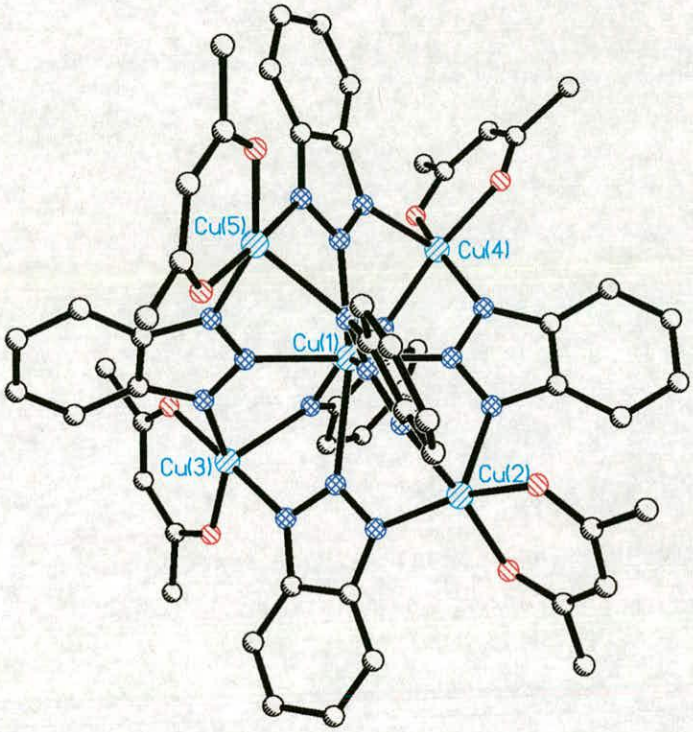

Figure 6-3. Structure of $[Cu_5(bta)_6(acac)_4]$.[11]

The location of the five copper atoms in this structure can be visualised using a cube (Figure 6-4). The four outer coppers are arranged in a distorted tetrahedron at four vertices with the remaining copper in the centre of the cube. The four peripheral copper atoms are five coordinate with three bta nitrogen atoms and two acac oxygen atoms in the coordination sphere. The central copper has a tetragonally distorted octahedral geometry consistent with a Jahn-Teller distortion observed in d^9 systems, bonding to the central nitrogen atom of each of the six bta^- groups.

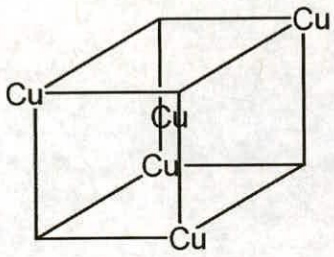

Figure 6-4. The arrangement of copper atoms in the crystal structure of $[Cu_5(bta)_6(acac)_4]$.

The six bta^- groups bridge all the pairs of outer copper atoms capping all the faces of the cube, with the plane of the triazole ring containing the Cu...Cu diagonals. The Jahn-Teller distortion observed for the central copper atoms in a series of 5 structures [12] suggests that two of the bta^- ligands are less strongly bonded to the cluster implying that these could be more readily displaced, providing a mechanism for assembling arrays of clusters using polytriazole ligands (see below). A number of related pentacopper clusters have been isolated with formula, $[Cu_5(bta)_6(L)_4]$ where acac is replaced with related bidentate oxygen donating ligands.[13, 14] Pentametallic zinc and nickel clusters have been obtained as well as a series of mixed metal systems.[13, 15, 16]

Recently the bta ligand has been used in the synthesis of clusters with metals in the +3 oxidation state such as Fe(III) and Mn(III).[17, 18] Low *et al.* reported the most significant discovery in this area with the publication of an iron (III) cluster containing fourteen metal atoms, $[Fe_{14}O_6(bta)_6(OMe)_{18}(Cl)_6]$ (Figure 6-5).[18] As well as having a remarkably complex structure the Fe_{14} cluster was shown to have spin as large as $S = 25$.[18, 19]

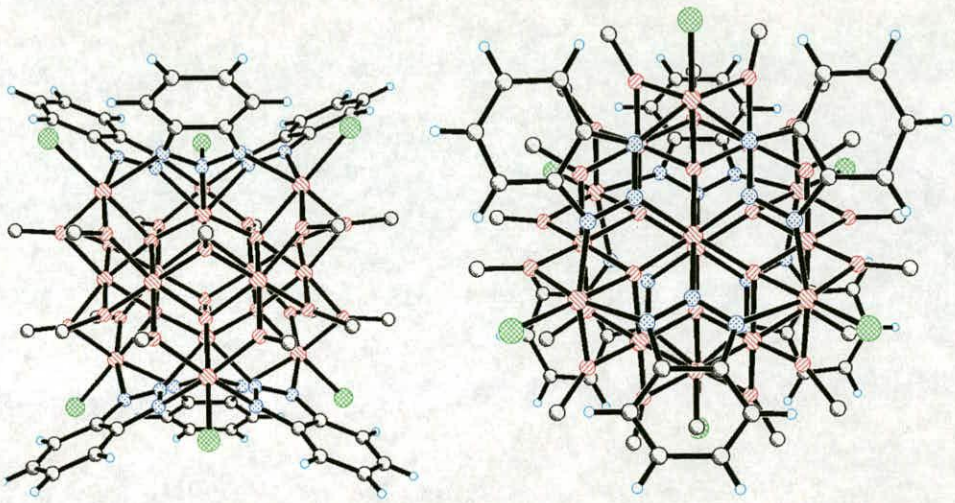

Figure 6-5. Two views of $[Fe_{14}O_6(bta)_6(OMe)_{18}(Cl)_6]$[18]

6.1.2 Linking and organising clusters

A variety of transition metal clusters have been shown to have unusual magnetic,[20, 21] liquid crystalline,[22] non-linear optical[23] and luminescence properties.[24] As a result, the field of cluster chemistry is attracting increasing attention for use in advanced material applications. These molecular devices present challenges and opportunities for synthetic chemists in developing rational methods of preparation so that their properties can be fully explored and tuned. One approach is to 'anchor' clusters to a well-defined surface. This could be done by modifying clusters with suitable-surface binding functionality or by modifying a surface with a layer containing functionality capable of cluster-coordination. This area has not yet been extensively explored although there have been promising reports of the successful anchoring of Mn_{12} molecular magnets to gold and silicon substrates using undecanoic acid.[25, 26]

Another approach to the organisation of individual metal clusters is to create extended arrays connected by suitable 'linker' molecules. This is a particularly challenging task as clusters tend to undergo fragmentation and aggregation and often have multiple and undistinguishable reactive sites on their exteriors which will lead to the generation of complex mixtures of products. Despite this there have been some examples of Pt_3 and Pt_6 clusters linked by σ-alkynyl spacers[27] that suggests this approach has great potential.

6.2 Strategies for connecting benzotriazole-based clusters

One approach considered in this preliminary investigation was to use 'crosslinking' ligands which contain one or more benzotriazole groups to link $[Cu_5(bta)_6(acac)_4]$ type clusters clusters together or attach them to surfaces. These Cu_5-clusters were selected for studies and if successful this approach could then be extended to more interesting Fe_{14}-type molecules.

6.2.1 Substitution of ligands on the $[Cu_5(bta)_6(acac)_4]$ units with bifunctional linkers

The bta ligands are distributed around the central copper atom of a $[Cu_5(bta)_6(acac)_4]$ cluster in a tetragonally distorted octahedron (section 6.1.1). If these bta ligands could be substituted by a bis-triazole linker, where the triazolate groups are linearly directed, it would be possible, in theory, to link clusters to form dimmers, oligomers, polymers or three dimensional networks (Figure 6-6).

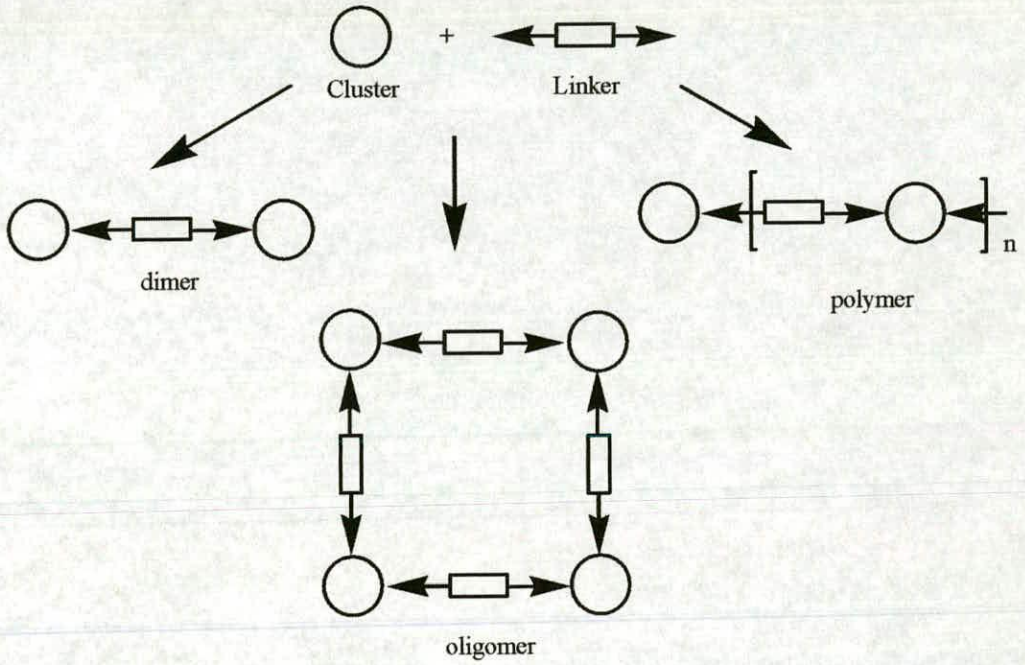

Figure 6-6. Formation of dimeric, oligomeric and polymeric Cu_5 assemblies using bis-triazole crosslinking ligands. Three dimensional networks could arise if more than two bta^- ligands in the clusters are replaced by bridging triazole ligands

For this strategy to be successful, $[Cu_5(bta)_6(acac)_4]$ units must be stable in solution but the bta ligands must be sufficiently labile for ligand exchange to be possible. It is likely that the higher molecular weight assemblies will be considerably less soluble than the starting materials so controlled precipitation of product will be necessary in order to isolate simple products rather than complex mixtures.

Alternatively, we could substitute acac ligands on the cluster using bifunctional crosslinkers containing two β-diketonate functional groups.

Control of the type and structure of polycluster assemblies depends crucially on the geometric disposition of the two triazole units or the two β-diketonyl groups in the linker and on the relative disposition of the bta ligands which are displaced from the starting $[Cu_5(bta)_6(acac)_4]$ building blocks. At the outset of this work we envisaged using linkers with a linear disposition of the triazole or the diketonyl groups, but ease of synthesis and obtaining linkers with good solubility led to other arrangements being considered.

Bifunctional ligands could also be used to attach $[Cu_5(bta)_6(acac)_4]$ clusters to a well defined surface. A ligand that incorporates a triazole group and a surface-binding group separated by a linker could, by bta-substitution, connect cluster units to a surface as shown in Figure 6-7.

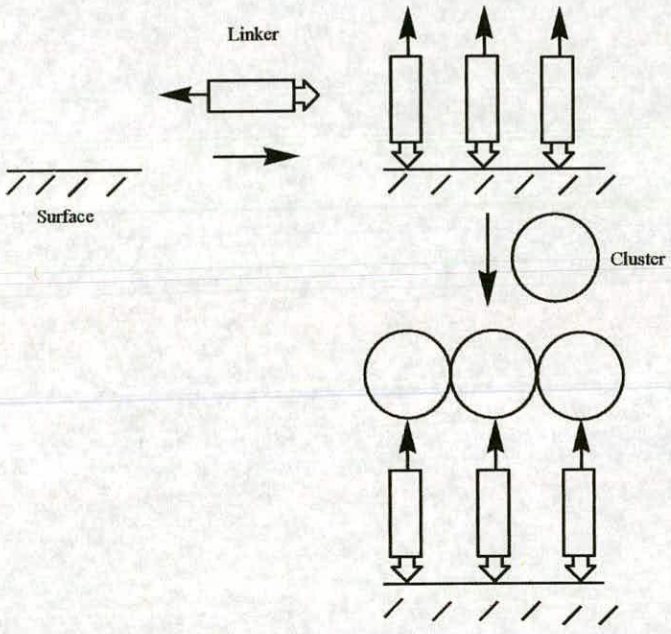

Figure 6-7. Diagram showing surface binding strategy

In practise the design, syntheses and testing of ligands to attach clusters to surfaces was not attempted in this thesis although it is a promising field for further study.

6.2.2 Reaction of peripheral functional groups on the acac or bta ligands in Cu_5 clusters

By synthesising $[Cu_5(L)_6(acac)_4]$ clusters where L is a bta ligand with an additional reactive functional group, a pre-formed cluster could react with an appropriate crosslinker to assemble Cu_5 clusters as shown in Figure 6-8.

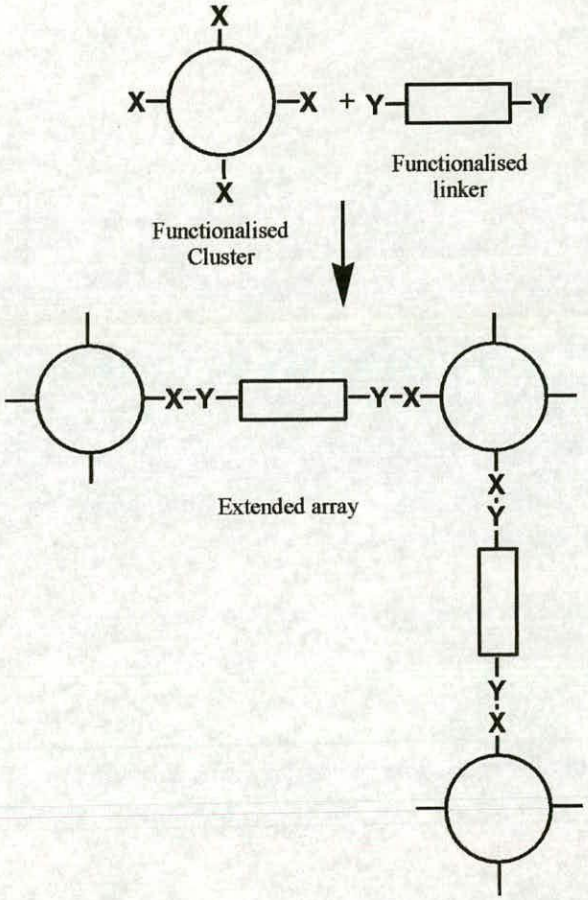

Figure 6-8. Proposed mechanism for linking clusters through the reaction of peripheral functional groups

Clusters could be covalently linked as a result of a condensation reaction between a functional group on the periphery of the cluster and a complementary group on

bifunctional linker molecules. Alternatively, if the bta functional group had ligating properties the link could be formed through co-ordination of a metal.

In order for this approach to be successful a $[Cu_5(L)_6(acac)_4]$ cluster must be synthesised that is sufficiently soluble for further reactions to take place and the ligand, L, must be have the required properties to allow crosslinking. To form a covalently linked system, L must contain a functional group that readily undergoes condensation with the chosen linker functional group. To form an array of clusters linked by L-M-L interactions, where M is a suitable metal ion, L must be able to form complexes with M.

6.2.3 Preparation of the cluster units in the presence of bifunctional crosslinking ligands

In this approach a mixture of monofunctional and bifunctional 'linker' ligands would be used in the cluster-forming reaction. $[Cu_5(bta)_6(acac)_4]$ type clusters assemble in solution following the reaction of $[Cu(acac)_2]$ with btaH. If a bifunctional ligand of the type described in section 6.1.1 (Figure 6-9) was added to this reaction in appropriate quantities, linking of clusters could be achieved. The degree of linking would be controlled by varying ratios of bta : bifunctional bta ligands.

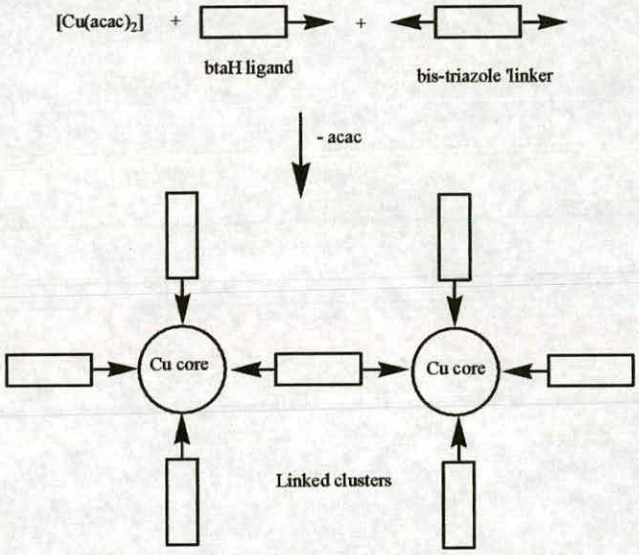

Figure 6-9. Reaction scheme for the assembly of networks of Cu_5 clusters directly from Cu(II) and capping and linking triazole or diketonyl ligands

For this approach to be successful a bifunctional ligand is required that has comparable solubility properties to the other starting materials in the cluster forming reaction.

6.3 Ligand exchange in $[Cu_5(bta)_6(acac)_4]$ clusters

In order to establish the feasibility of linking clusters by ligand exchange of bifunctional ligands it was necessary to investigate the propensity for ligand substitution in $[Cu_5(bta)_6(acac)_4]$ clusters. The extent to which ligand exchange is possible is considered in the following section.

6.3.1 Mass spectrometry of $[Cu_5(bta)_6(acac)_4]$ (22) and $[Cu_5(bta)_6(hfac)_4]$ (23)

The pentametallic $[Cu_5(bta)_6(acac)_4]$ (**22**) cluster and related systems are known to respond well to positive ion fast atom bombardment (FAB^+) mass spectrometry and well defined fragmentation patterns are observed (Figure 6-10).[14]

The first fragmentation involves the loss of a bta anion, followed by the stepwise loss of two $acac^-$, a bta^- and two more $acac^-$ ligands. The $[Cu_5(bta)_4]^+$ fragment then loses a [Cu(bta)] unit leaving a $[Cu_4(bta)_3]^+$ fragment.

In this thesis a novel pentanuclear cluster, $[Cu_5(bta)_6(hfac)_4]$ (**23**), was synthesised for comparison with $[Cu_5(bta)_6(acac)_4]$ and for use in ligand substitution experiments. The peaks observed in the FAB^+ mass spectrum of **23** are shown in Table 6-1. A similar fragmentation pattern to **22** is observed with the stepwise loss of ligand components clearly apparent from the spectra.

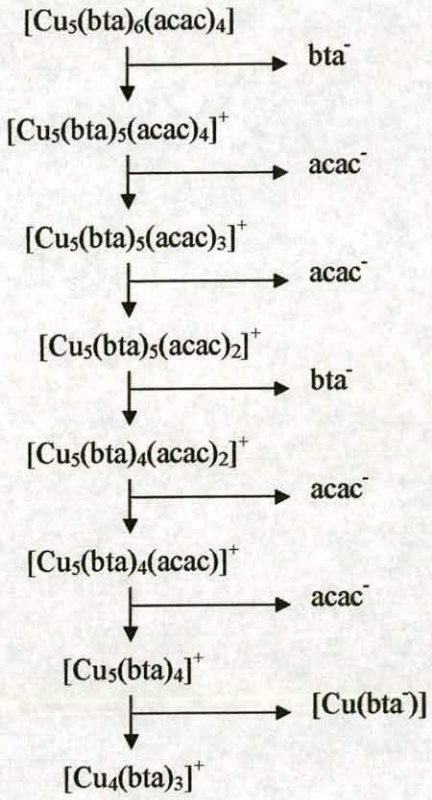

Figure 6-10. The fragmentation pattern of **22**

Fragment of $[Cu_5(bta)_6(hfac)_4]$	**Fragment peak (m/z)**
$[Cu_5(bta)_5(hfac)_4]$	1737
$[Cu_5(bta)_6(hfac)_3]$	1647
$[Cu_5(bta)_5(hfac)_3]$	1530
$[Cu_5(bta)_6(hfac)_2]$	1441
$[Cu_5(bta)_5(hfac)_2]$	1321
$[Cu_5(bta)_4(hfac)_2]$	1203
$[Cu_5(bta)_5(hfac)]$	1113
$[Cu_5(bta)_4(hfac)]$	995
$[Cu_5(bta)_5]$	906
$[Cu_5(bta)_4]$	789
$[Cu_4(bta)_3]$	608

Table 6-1. Peaks observed in the FAB^+ mass spectrum of **23**

6.3.2 Ligand substitution experiments

A convenient technique was developed to follow the exchange of triazole or diketonyl ligands in $[Cu_5(bta)_6(acac)_4]$-type clusters. To monitor triazole replacements the two parent clusters with formulae, $[Cu_5(bta)_6(acac)_4]$ **(22)** or $[Cu_5(bta)_6(hfac)_4]$ **(23)** were dissolved in an appropriate solvent containing a different triazole and were set aside at room temperature. The solvent was removed after 18 hr and the residue analysed by FAB^+ mass spectrometry to establish the relative numbers of the of the triazole ligands present in the clusters. 1H-1,2,3-triazole (traH) and 5,6–dinitro-1H-benzotriazole (dnbtaH) (Figure 6-10) were used initially as replacement ligands. Major peaks in the FAB mass spectra of the products are shown in Tables 6-2 and 6-3.

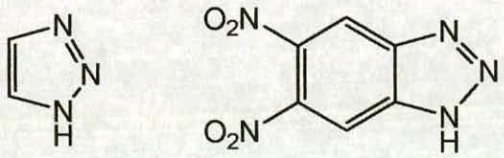

traH dnbtaH

Figure 6-11. Structure of traH and dnbtaH

Fragment of Product of $[Cu_5(bta)_6(hfac)_4]$/traH reaction	**Fragment peak (m/z)**	**Fragment of Product of $[Cu_5(bta)_6(hfac)_4]$/dnbtaH reaction**	**Fragment peak (m/z)**
$[Cu_5(tra)_3(bta)_2(hfac)_4]$	1587	$[Cu_5(dnbta)_2(bta)_3(hfac)_4]$	1917
$[Cu_5(tra)_5(hfac)_4]$	1485	$[Cu_5(dnbta)(bta)_4(hfac)_4]$	1827
$[Cu_5(tra)_3(bta)_2(hfac)_3]$	1380	$[Cu_5(bta)_5(hfac)_3]$	1737
$[Cu_5(tra)(bta)(hfac)_4]$	1328	$[Cu_5(bta)_4(hfac)_4]$	1620
$[Cu_5(bta)_3(hfac)_4]$	1289	$[Cu_5(dnbta)(bta)_4(hfac)_4]$	1411
$[Cu_5(tra)(bta)_2(hfac)_3]$	1239	$[Cu_5(dnbta)(bta)_3(hfac)_3]$	1293
$[Cu_5(bta)_2(hfac)_3]$	1173	$[Cu_5(dnbta)_2(bta)_4(hfac)_3]$	969
$[Cu_5(tra)(bta)(hfac)_3]$	1121	$[Cu_5(bta)_4(hfac)_3]$	879
$[Cu_5(bta)(hfac)_3]$	1053	$[Cu_4(bta)_3(hfac)_3]$	700
		$[Cu_4(bta)_3]$	608

Table 6-2. Peaks observed in FAB^+ mass spectrum of the products of the reactions of $[Cu_5(bta)_6(hfac)_4]$ with 1H-1,2,3-triazole (traH) and 5,6 –dinitro-1H-benzotriazole (dnbtaH) respectively

Fragment of Product of $[Cu_5(bta)_6(acac)_4]$/btaH reaction	**Fragment peak (m/z)**	**Fragment of Product of $[Cu_5(bta)_6(acac)_4]$/dnbtaH reaction**	**Fragment peak (m/z)**
$[Cu_3(L1)(bta)_2]$	496	$[Cu_5(dnbta)_4(bta)(acac)_4]$	1665
	460	$[Cu_5(dnbta)_3(bta)_2(acac)_4]$	1575
$[Cu_3(bta)_2]$	426	$[Cu_5(dnbta)_2(bta)_5(acac)_4]$	1483
	391	$[Cu_5(dnbta)_2(bta)_5(acac)_3]$	1384
	291	$[Cu_5(dnbta)_3(bta)]$	1059
	273	$[Cu_5(dnbta)_2(bta)_2]$	969
		$[Cu_5(dnbta)(bta)_3]$	879
		$[Cu_5(bta)_4]$	788
		$[Cu_4(dnbta)(bta)_2(acac)_3]$	698
		$[Cu_4(bta)_3]$	608

Table 6-3. Peaks observed in FAB^+ mass spectrum of the products of the reactions between $[Cu_5(bta)_6(acac)_4]$ with traH and dnbtaH respectively

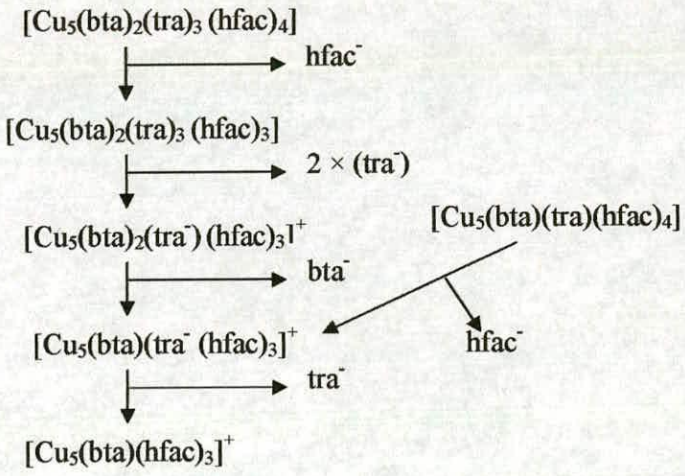

Figure 6-12. Fragmentation pattern of FAB^+ mass spectrum form $[Cu_5(bta)_6(hfac)_4]$/traH reaction

The fragmentation pattern shown in Figure 6-11, obtained from the reaction between **23** and traH, is representative of all the products obtained from the reactions of $[Cu_5(bta)_6(hfac)_4]$ **(23)** with other triazoles.

The presence of fragments of Cu_5 clusters in the FAB^+ mass spectra containing mixtures of bta/tra and bta/dnbta ligands (Tables 6-3 and 6-4) provides compelling evidence for triazole ligand exchange. The FAB^+ mass spectrometry technique does

not allow quantitative conclusions to be drawn as to the composition of the solid-state product as the intensities of peaks are not directly proportional to the concentration of individual compounds in the mixture. Consequently the relative concentrations of mono-, di- or tri- substituted products cannot be determined. Also no information on the relative positions of substitution, e.g. *cis* or *trans* about the central *pseudo*-octahedral Cu(II), can be gained. Nevertheless as the reactions leading to the products shown in Tables 6-2 and 6-3 were performed under similar conditions some useful comparisons can be made.

The spectrum for the products of the reaction between $[Cu_5(bta)_6(acac)_4]$ and traH had no high molecular weight peaks. Consequently it is not possible to establish patterns for substitution on the cluster. It is probable, in this case, that decomposition of the Cu_5 complex *in solution* occurs in the presence of the more basic triazole, traH, giving lower nuclearity Cu/tra$^-$ complexes.

The spectra obtained from the products of the reaction between $[Cu_5(bta)_6(hfac)_4]$ and dnbtaH (Table 6-2) suggests that two bta ligands are readily replaced by dnbta$^-$ ligands. This is consistent with the suggestion that the two 'axial' bta ligands are more labile than the 'equatorial' bta's in the tetragonally distorted cluster (see section 6.1.1) as a result of the Jahn-Teller effect. The possibility of exploiting this lability in selective substitution of a Cu_5 complex is an attractive prospect as it would lead to a controllable route to linearly disposed linker-Cu_5-linker-Cu_5 'chains'.

The reaction between $[Cu_5(bta)_6(acac)_4]$ and traH gave products (Table 6-2) showing a much higher level of triazole exchange than was observed with dnbta$^-$.

It is also interesting to note the differing extent of triazole substitution between $[Cu_5(bta)_6(hfac)_4]$ with dnbtaH *c.f.* traH. hfacH is an electron-withdrawing ligand therefore the copper atoms within the Cu_5 core are relatively electron deficient. The formation of clusters containing up to five tra$^-$ ligands may be favoured by the stabilising effect of the relatively basic tra$^-$ ligand increasing electron density in the Cu_5 core. Conversely the less basic dnbtaH ligand appears to replace a maximum of two bta ligands and as a result the number of dnbta$^-$ ligands which can be accommodated by the Cu_5 framework in the hfac cluster is limited.

When $[Cu_5(bta)_6(acac)_4]$ reacted with dnbtaH, a high level of substitution was observed compared with the corresponding reaction with $[Cu_5(bta)_6(hfac)_4]$. The

acac ligand is relatively electron donating *c.f.* hfac therefore it is possible that the copper atoms within the complex are relatively electron rich. It is reasonable to suggest that such a Cu_5 complex would be more stable when bridged by ligands with electron withdrawing properties which could explain why as many as four bta^-'s are replaced by $dnbta^-$'s on reaction with $[Cu_5(bta)_6(acac)_4]$. Also consistent with this explanation is the fact that the presence of the basic traH ligand resulted in decomposition of the Cu_5 cluster.

The results of this preliminary study into triazole exhange on Cu_5 clusters has highlighted a possible connection between the electronic properties of triazole and diketonate ligands in influencing the extent of ligand exchange reactions of these Cu_5 clusters. A more detailed investigation could be an interesting area for further study. As far as the strategy for linking Cu_5 clusters is concerned, the fact that triazole exchange occurs on a practical timescale is an encouraging result.

Fragment of product of $[Cu_5(bta)_6(L1)_4]$/L2	**Fragment peak (m/z)**
$[Cu_5(bta)_5(hfac)_4]$	1735
$[Cu_5(bta)_6(hfac)_3(acac)]$	1627
$[Cu_5(bta)_5(hfac)_3]$	1530
$[Cu_5(bta)_5(acac)_2]$	1519
$[Cu_5(bta)_6(hfac)_2]$	1439
$[Cu_5(bta)_4(hfac)_2]$	1205
$[Cu_5(bta)_4(hfac)(acac)]$	1095

Table 6-4. Peaks observed in the FAB^+ mass spectrum of the product of the reaction between $[Cu_5(bta)_6(hfac)_4]$ and acacH

The same technique was used to probe the exchange of diketonate ligands. The spectrum shown in Table 6-4 was obtained from the product of the reaction of $[Cu_5(bta)_6(hfac)_4]$ (**23**) and acacH. The presence of fragments containing both hfac and acac is evidence for β-diketonyl ligand exchange on a practiceable timescale. This opens up the possibility of linking Cu_5 clusters using bifunctional β-diketonyl ligands.

The results of the mass spectrometry studies are promising as they demonstrate the feasibility of performing ligand substitution to link clusters or attach them to surfaces. It has been shown that the bta units are labile in solution and that ligand

substitution is possible. If a suitable bifunctional bis-triazole linker could be designed it should be possible to replace mono-triazole ligands, creating a network of connected pentametallic clusters. Similarly bis-diketonate ligands could be used to replace mono- diketonate units such as $acac^-$ or $hfac^-$.

6.4 Ligand design and synthesis

A number of ligands were designed, based on the criteria for cross-linking described in section 6.1. In the following section a number of designs are considered and the synthesis of the selected ligands described.

6.4.1 Linear bis-triazole linker ligands

A suitable bifunctional benzotriazole ligand must have two triazole functional groups, linearly directed relative to each other, separated by a linker unit. Two ligands which meet this criteria, benzo[1,2-*d* : 4,5-*d'*]bistriazole (**24**) and di[1,2,3-benzotriazolo[5,6-b;5',6'-k]]-18-crown-6 (**25**) are shown in Figure 6-13.

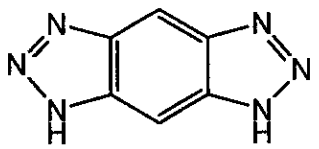

(**24**)

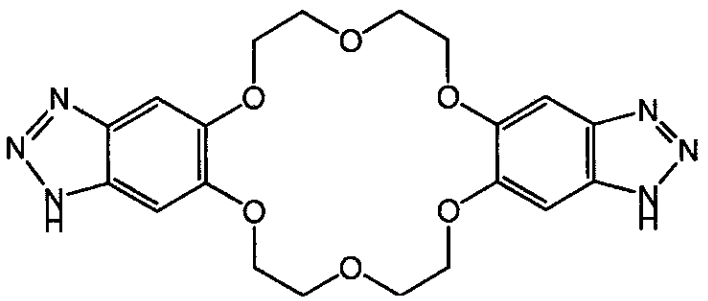

(**25**)

Figure 6-13. Structure of **24** and **25**

24 and **25** were obtained using procedures reported by Hart *et al.*[28] and Ivanov *et al.*[29] The reaction schemes are shown in Figure 6-14.

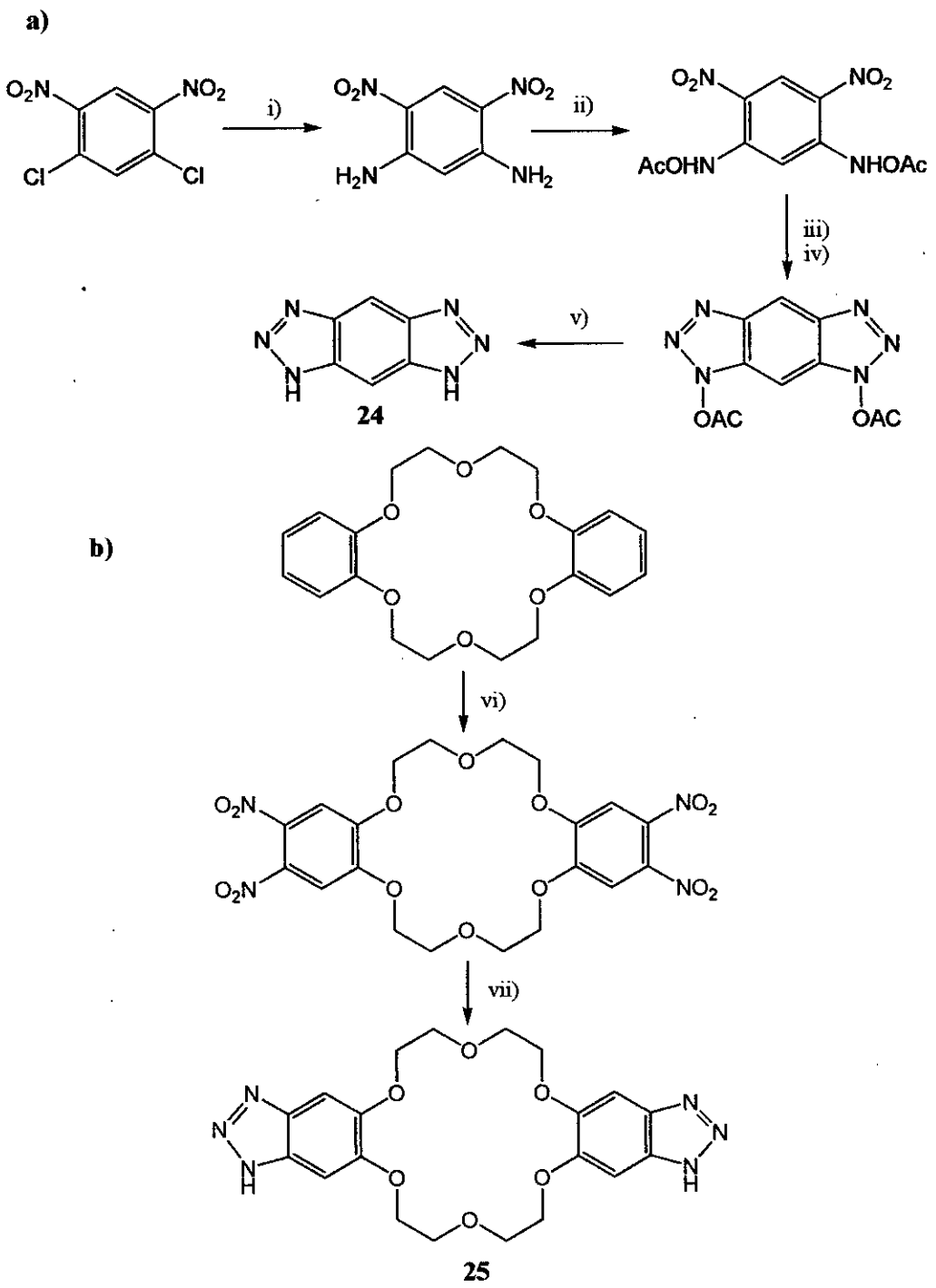

Figure 6-14. Reaction mechanism for a) **3**, and b) **4**. i) NH_3(g),/Ethylene glycol,/140°C, ii) Ac_2O/H_2SO_4/140°C, iii) H_2(g)/Pd/C (10%)/ethanol, iv) $NaNO_2$/HCl/0°C/ethanol and v) H_2SO_4/ethanol/H_2O. vi) HNO_3 (70 %)/H_2SO_4(conc)/CH_2Cl_2 and vii) $H_2NNH_2.H_2O$ (80 %)

25 was obtained as a very insoluble and involatile red powder. The insolubility in all common solvents prevented any effective purification and characterisation of the material and it cannot be confirmed that the material claimed to be **25** by Ivanov *et al.* is indeed the bis-triazole. In any case the insolubility will preclude its use in aggregation of clusters using the strategies outlined in section 6.2.

24 is also relatively intractable although solubility in dimethyl sulphoxide allowed characterisation by nmr and mass spectrometry. Elemental analysis showed good agreement with calculated values. The use of **24** in cluster linking experiments is discussed in section 6.4.

6.4.2 Non-linear bis-triazole linker ligands

As a result of the few reported molecules with a linear disposition of two triazole units and the synthetic challenges involved in synthesising novel ligands of this type a series of non-linear analogues was considered which could be prepared from readily available starting materials. A procedure was developed in which two 5-amino-benzotriazole molecules undergo schiff base condensations with one bis-aldehyde linker molecule.

This strategy was successfully employed using terephthaldicarboxaldehyde and isophthalaldehyde as bis-aldehyde linkers resulting in the isolation of 1,4–bis{[(E)-3*H*-benzotriazol-5-ylimino]-methyl}-benzene (**26**) and 1,3–bis{[(E)-3*H*-benzotriazol-5-ylimino]-methyl}-benzene (**27**) (Figure 6-15). Using phthalic dicarboxaldehyde as the bis-aldehyde linker resulted in an intramolecular cyclisation and using benzil as the linker resulted in no reaction.

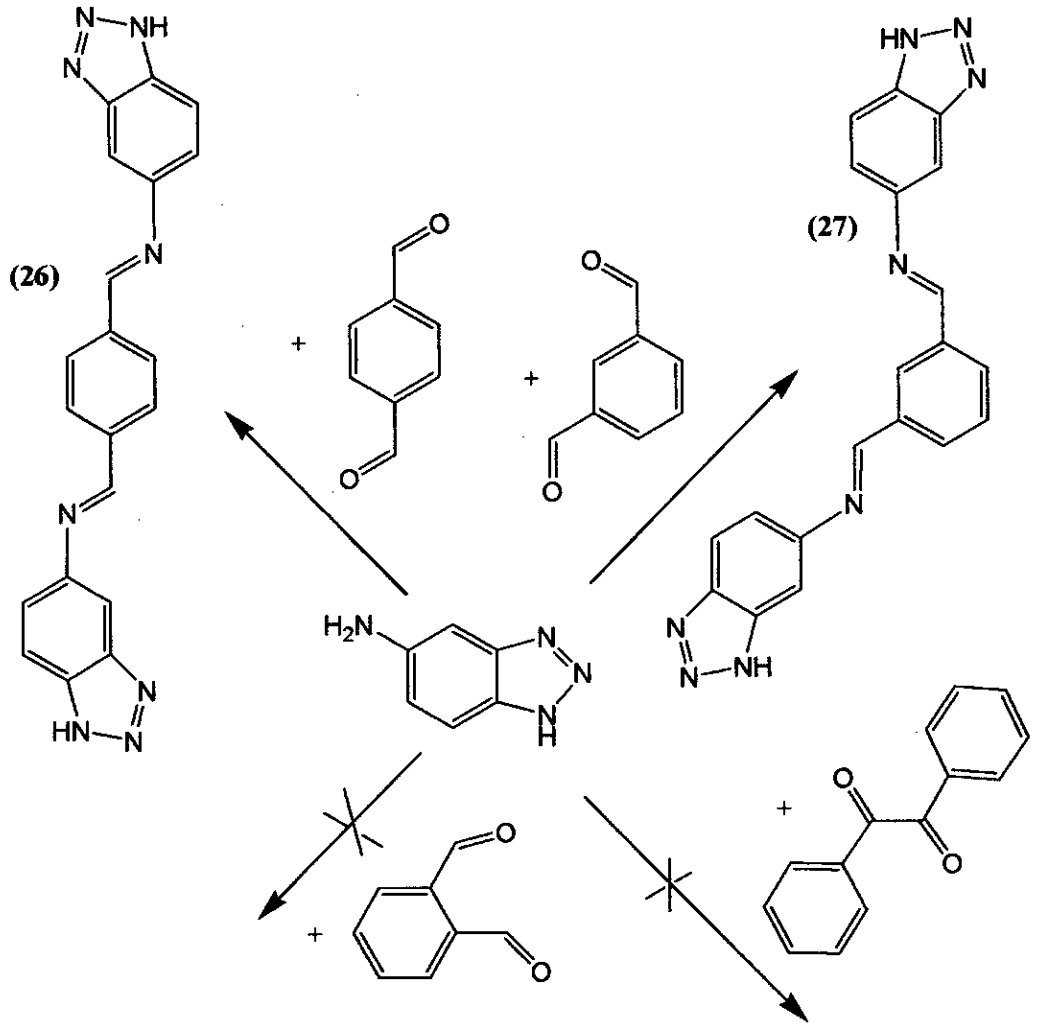

Figure 6-15. Attempted preparations of bis-triazole ligands from 5-aminobenzotriazole and a) terephthalaldehyde, b) isophthalaldehyde, c) phthalaldehyde and d) benzil

26 and **27** were obtained almost quantitatively. Both are relatively intractable although, as with **24**, solubility in dimethyl sulphoxide allows characterisation by nmr and mass spectrometry. Solid state IR spectra confirm the presence of a C-N group in both ligands by an absorption peak at 1629 cm^{-1} for **26** and 1612 cm^{-1} for **27**. Insolubility of these ligands prevented effective recrystallisation and consequently microanalyses show poor agreement with calculated values. These could be due to small quantities of partially reacted byproducts with similar solubility to **5** and **6** being present, and weak C=O stretches in the IR of both

compounds confirm this. As these can be present in only small quantities, **26** and **27** were used in cluster-linking experiments without further purification.

6.4.3 Triazole ligands with additional chelating properties

Using a Schiff base condensation of 5-amino benzotriazole with salicylaldehyde, 2-{[(E)-3*H*-benzotriazol-5-ylimino]-methyl}-phenol **(28)** was prepared that incorporates a benzotriazole group linked to a bidentate chelating group (Figure 6-16). The aim was to incorporate this ligand into a Cu_5 cluster and crosslink the clusters through the formation of chelate rings with the peripheral bidentate salicylaldimine groups of two or more clusters and additional metal ions using as described in section 6.2.2.

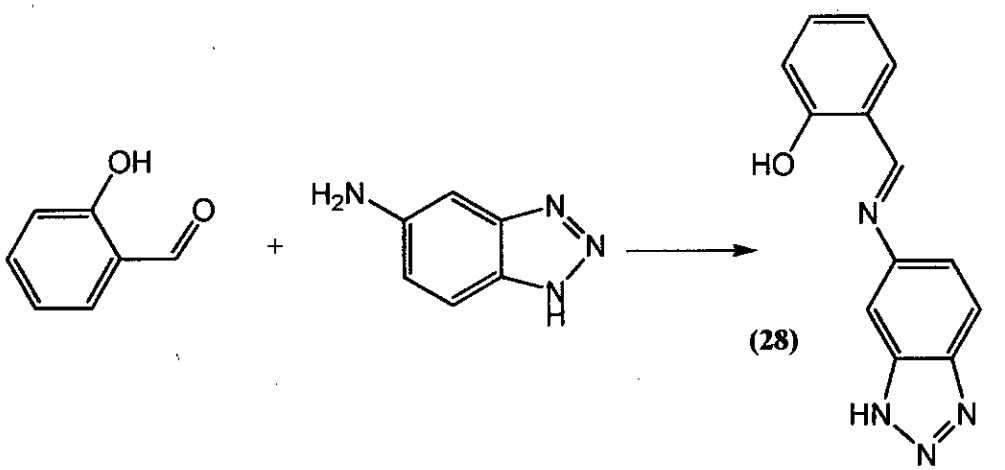

Figure 6-16. Synthesis of **28**

28 was isolated in high yields and was fully characterised by nmr, mass spectroscopy, infrared spectroscopy and elemental analysis. This type of ligand could also be readily prepared with large alkyl groups *para* to the phenol group as the precursor salicylaldehydes are readily available, being used to prepare kerosene soluble metal extractants.

6.4.4 Bis-diketonate linker ligands

The substitution experiments described in previous sections show evidence for exchange of β-diketonate ligands in solutions of $[Cu_5(bta)_6(acac)_4]$ type clusters. As

a result the possibility of linking clusters by substitution of hfac or acac units with linked acac based ligands has been considered.

Bis-β-diketone ligands have recently been used in studies aimed at constructing interesting metallo-supramolecular structures due to the number of allowable orientations of chelating groups.[30] Ligands (L) with the general structure shown in Figure 6-17 were reacted with $CuCl_2.(H_2O)_2$ to yield trinuclear copper complexes, $[Cu_3(L)_3]$. These complexes had three copper(II) ions occupying the corners of an equilateral triangle with the dianionic ligands comprising the sides.

The bis-β-diketone ligand with R = *n*-octyl (**29**) was chosen for use in Cu_5 cluster linking reactions. This ligand has well separated diketone groups and solubility in common organic solvents. It was proposed that substitution of acac on the Cu_5 clusters with the **29** could occur, resulting in interlinking of clusters.

A sample of **29** was obtained from the group of Len Lindoy at the University of Sydney. It was synthesised by a Claisen condensation between dimethyl terephthalate and octan-2-one in the presence of NaH in diethyl ether.[30] The details of attempted cluster linking experiments are given in Section 6.4.

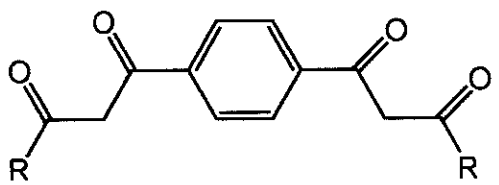

R = Me, Et, Pr, t-Bu, Ph

Figure 6-17. Structure of bis-β-diketone ligands

6.5 Attempted Cu_5-cluster linking reactions

A number of experiments were attempted using the ligands **24**, **26**, **27**, **28** and **29**. Details of outcome of these experiments are given in the following section along with a discussion of the conclusions drawn from these experiments.

6.5.1 Ligand substitution

Substitution reactions were attempted using **24**, **26**, **27**, **28** and **29** using a procedure similar to that described in Section 6.3. Clusters with formula, $[Cu_5(bta)_6(L)_4]$ (L = acac or hfac) were dissolved in an appropriate solvent and five equivalents of bifunctional ligand added. The reactions were stirred for 18 hours, the solvent was removed and the residue analysed by FAB^+ mass spectrometry,

The bis-triazole ligands, **24**, **26** and **27** have low solubility in common organic solvents. As a result homogeneous reactions between the cluster and the ligands could only be attempted in very polar solvents such as DMSO and DMF. FAB^+ mass spectrometry of the product from the reaction between **22** and **24** showed evidence for ligand substitution (Table 6-5). There was no evidence however for cluster linking as no species with more than five copper atoms were detected and attempts to obtain a pure product by recrystallisation were unsuccessful. It is likely that failure to successfully link clusters using **24** is due to the short separation of the triazole functional groups. This prevents two linked clusters residing in close proximity due to unfavourable steric interactions between peripheral Cu-acac chelate rings.

Fragment of product of $[Cu_5(bta)_6(acac)_4]$/ L1	**Fragment peak (m/z)**
$[Cu_5(bta)_3(L1)_2(acac)_4]$	1390
$[Cu_5(bta)_4(L1)(acac)_4]$	1345
$[Cu_5(bta)_5(acac)_4]$	1306
$[Cu_5(bta)_4(L1)_3(acac)_4]$	1286
$[Cu_5(bta)_4(L1)(acac)_3]$	1247
$[Cu_5(bta)_5(acac)_3]$	1206
$[Cu_5(L1)_4(acac)_2]$	1157
$[Cu_5(bta)(L1)_3(acac)_2]$	1115
$[Cu_5(bta)_2(L1)_2(acac)_2]$	1070
$[Cu_5(bta)_3(L1)(acac)_2]$	1030
$[Cu_5(bta)_4(acac)]$	989
$[Cu_5(bta)(L1)_3]$	912
$[Cu_5(bta)_2(L1)_2]$	871
$[Cu_5(bta)_3(L1)]$	830
$[Cu_5(bta)_4]$	789
$[Cu_4(bta)_3]$	608

Table 6-5. Peaks observed in the FAB^+ mass spectrum of the product of the reaction between $[Cu_5(bta)_6(acac)_4]$ and L1, (L1 = **24**).

No product was obtained from the reaction of **26** and cluster **22**. The FAB^+ mass spectrum of solids obtained after evaporation of the solvent showed the characteristic fragmentation pattern of **22** and no evidence of substitution of bta^- groups was observed.

The bifunctional acac ligand, **29** had good solubility in organic solvents so substitution reactions could be undertaken in relatively non-polar solvents. A number of ligand substitution reactions were attempted however FAB^+ mass spectroscopy showed the product of these reactions to be unreacted starting materials.

6.5.2 Cross linking of preformed clusters

The preparation of clusters with formula, $[Cu_5(L)_6(acac)_4]$ [L = 5-amino–benzotriazole (abtaH) benzotriazole-5-carboxylic acid (cbtaH)] was attempted by reacting $[Cu(acac)_2]$ with the appropriate benzotriazole. The intention was to synthesise pentametallic clusters with peripheral functional groups that would allow additional cross-linking between molecules as outlined in section 6.2.2.

The reaction involving benzotriazole-5-carboxylic acid was carried out in DMF due to poor ligand solubility in common organic solvents. Following removal of DMF *in vacuo* an intractable green material was obtained that could not be effectively purified.

When cluster formation was attempted using 5-aminobenzotriazole an oily green material was obtained. This contained a mixture of products that could not be separated and the FAB^+ mass spectra of the material provided no evidence to suggest that cluster formation had been successful. As a result, further crosslinking experiments were not undertaken.

6.5.3 Cluster formation reactions using bifunctional ligands

Cluster formation reactions were attempted by reacting $[Cu(acac)_2]$ with a mixture of bta and one of the bis-triazole ligands, **24**, **26** and **27**. The lack of solubility of these ligands meant that homogeneous reactions could only take place in very polar solvents such as DMSO and DMF. No identifiable product was obtained from any of these reactions.

In addition a number of cluster forming reactions were also attempted aimed at using **24**, **26** and **27** to bridge Fe_{14} type clusters. These experiments were undertaken at the University of Manchester in collaboration with Dr Eric McInnes of the University of Manchester and Dr Euan Brechin of the University of Edinburgh. The reaction used to synthesise Fe_{14} clusters at room temperature[17] was adapted to incorporate bis-triazole ligands as well as benzotriazole. The poor solubility of the bis-triazoles prevented reactivity so the reactions were carried out using a solvothermal technique. This involved heating the reactions in a sealed bomb to increases the reaction pressure, potentially altering the solubility properties of the reactants. It was hoped that by treating the relatively insoluble bifunctional bta units in this way, the solubility could be improved to allow the ligands to react. A summary of the reactions undertaken is shown in Figure 6-18.

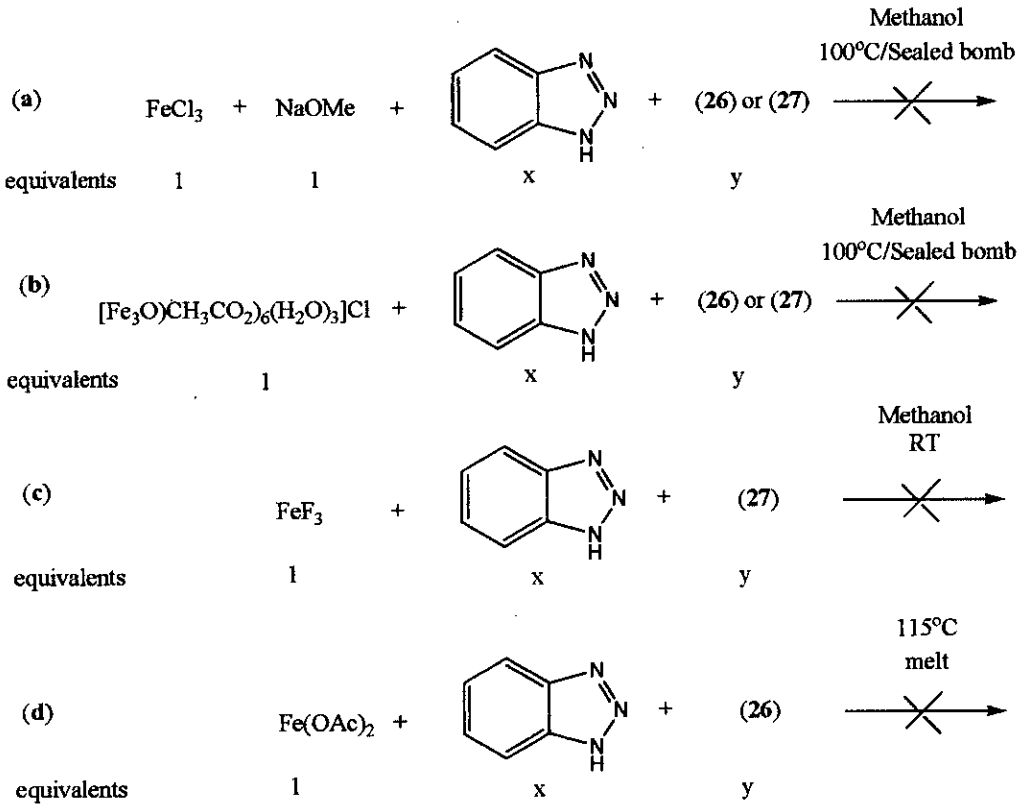

Figure 6-18. Summary of reactions attempted to link iron-based clusters using **26** and **27**. For **(a)** and **(b)**, x = 0.1-0.9 equivalents, y = 1-x equivalents. For **(c)**, x = 3 and y = 0.1 equivalents. For **(d)**, x = 2 and y = 0.1 equivalents

No identifiable products were isolated from the reactions shown in Figure 6-18. In some cases crystalline material separated although this was shown to be the standard Fe_{14} cluster. The solvothermal technique did not appear to improve ligand solubility to allow successful ligand substitution.

6.6 Conclusion

This chapter considers strategies to link $[Cu_5(bta)_6(acac)_4]$ type clusters using bifunctional ligands. Although the overall aim has not been achieved, some interesting discoveries have been made about ligand substitution in $[Cu_5(bta)_6(acac)_4]$ type clusters and novel types of bifunctional ligands have been synthesised. The observation that both bta and acac ligands can be replaced in solution with the parent Cu_5-structure remaining intact indicates that linking such clusters through bifunctional ligand substitution remains a promising approach. The challenge is to design and synthesise suitable linker ligands. They must have well separated functional groups that are capable of displacing either bta or acac ligands in the cluster and they must have sufficient solubility to allow substitution in common organic solvents. If these criteria are met it should be possible to assemble extended arrays of pentametallic clusters.

This is an important area for further study as it could allow the organisation of magnetically interesting building blocks to be assembled in ordered arrays in materials or on surfaces. A similar approach could also be taken to create extended arrays of $[Cu_{x+y}(hfac)_x(C{\equiv}CR)_y]$ clusters using bifunctional alkyne or diketone ligands. If highly delocalised alkynye linkers were successfully used to connect these molecules they could display potentially useful physical properties such as conductivity or non-linear optical properties.

6.7 Experimental

$[Cu_5(bta)_6(acac)_4]$ (22)

1 was prepared using the method described by Handley *et al.*[11] and was recrystallised from dichloromethane : cyclohexane. Yield: 0.8 g (34 %). Found: 46.91; H, 3.76; N, 17.73. Calc. for $C_{56}H_{52}O_8N_{18}Cu_5O_8$: C, 47.27; H, 3.66; N, 17.73%. IR spectra

(KBr disc): 1589s, 1516s, 1387s, 1270m, 1212m, 1022w, 995w, 927w, 789w and 745s cm^{-1}. UV/vis. (CH_2Cl_2) λ nm (ε/dm^3 $mol^{-1}cm^{-1}$) 275 (10.7×10^4), 301 (7.0×10^4), 659 (532). MS: (+FAB) m/z (% intensity) 1305 (35 %), 1204 (12), 1105 (11), 987 (15), 889 (10), 789 (100), 608 (95), 371 (48), 216 (78), 153 (58), 63 (32).

$[Cu_5(bta)_6(hfac)_4]$ (23)

To a solution of $Cu(hfac)_2$ (1 g, 2.1 mmol) in THF (50 ml) was added benzotriazole (0.5 g, 4.2 mmol). The reaction was stirred for two hours and the solvent removed *in vacuo* leaving a green oily residue. This was dissolved in a minimum volume of refluxing hexane : THF (1 : 2) and the solution was allowed to cool slowly. After 24 hours green crystalline material separated which were collected by filtration, washed with hexane (3 × 10 ml) and dried *in vacuo*. Yield: 0.4 g (29 %). Found: 36.02; H, 1.58; N, 13.51. Calc. for $C_{56}H_{34}O_8N_{18}F_{24}Cu_5$: C, 36.34; H, 1.85; N, 13.62%. IR spectra (KBr disc): 1545s, 1512s, 1390s, 1295s, m, 1212m, 1002w, 996w, 920w and 750s cm^{-1}. UV/vis. (CH_2Cl_2) λ nm (ε/dm^3 $mol^{-1}cm^{-1}$) 276 (9.7×10^4), 320 (370×10^4), 695 (445). MS: (+FAB) m/z (% intensity) 1737 (11 %), 1647 (7), 1530 (11), 1441 (5), 1321 (8), 1203 (10), 1113 (3), 995 (7), 906 (10), 789 (91), 608 (78), 371 (20).

Benzo[1,2-*d* : 4,5-*d'*]bistriazole (24)

4 was prepared *via* a five step synthesis originally reported by Hart *et al.*[28]

1,5-Diamino-2, 4-dinitrobenzene. Yield: 18.5 g (75 %). Found: 36.30; H, 3.02; N, 28.10. Calc. for $C_6H_6O_4N_4$: C, 36.37; H, 3.05; N, 28.28%. δ_H ($CDCl_3$, 250 MHz): 6.63 (s, 1 H, C*H*), 7.53-7.60 (m, 2 H, Ar*H*), 7.66-7.69 (m, 2 H, Ar*H*) and 7.98-8.02 (m, 2 H, Ar*H*). MS: (+EI) m/z (% intensity) 198 (100 %).

1,5-Bis[acetylamino]-2, 4-dinitrobenzene. Yield: 14.6 g (69 %). Found: 42.44; H, 3.50; N, 19.46. Calc. for $C_{10}H_{10}O_6N_4$: C, 42.56; H, 3.57; N, 19.85%. δ_H ($CDCl_3$, 250 MHz): 2.16 (s, 6 H, CH_3), 9.18 (s, 1 H, Ar*H*), 10.29 (s, 1 H, Ar*H*) and 10.60 (s, 2 H, -N*H*). MS: (+FAB) m/z (% intensity) 283 (84 %).

1,7-Diacetylbenzo[1,2-*d*:4,5-*d'*]bistriazole. Yield: 2.1 g (61 %). Found: 42.45; H, 3.60; N, 18.77. Calc. for $C_{10}H_{10}O_6N_4$: C, 42.54; H, 3.57; N, 19.86 %. δ_H ($CDCl_3$, 250 MHz): 2.99 (s, 6 H, CH_3), 9.81 (s, 1 H, Ar*H*) and 9.07 (s, 1 H, Ar*H*). MS: (+FAB) m/z (% intensity) 281 (54 %).

Benzo[1,2-*d*:4,5-*d*']bistriazole (3). Yield: 0.66 g (79 %). Found: 45.01; H, 2.62; N, 52.48. Calc. for $C_6H_4N_6$: C, 45.0; H, 2.62; N, 51.78 %. δ_H (DMSO, 250 MHz): 8.50 (s, 2 H, Ar*H*), 15.53 (s, 2 H, N*H*). MS: (+FAB) m/z (% intensity) 159 (100 %).

Di[1,2,3-benzotriazolo[5,6-b;5',6'-k]]-18-crown-6 (25)

3 was prepared using the method described by Ivanov *et al.*.[29] A red solid precipitated from a DMSO solution. The lack of solubility prevented detailed analysis. Yield: 0.65 g (91 %). Found: 43.58; H, 5.50; N, 12.53. Calc. for $C_{20}H_{22}O_6N_6.(C_2H_6S_2O_3)$: C, 45.20; H, 4.83; N, 14.38%.

1,4–bis{[(E)-3*H*-benzotriazol-5-ylimino]-methyl}-benzene (26)

To a solution of terephthaldicarboxaldehyde (100 mg, 0.75 mmol) in methanol (25 ml) was added 5-aminobenzotriazole (200 mg, 1.5 mmol). After five minutes pale yellow solid separated which was collected by filtration, washed with methanol and dried *in vacuo*. Yield: 0.24 g (88 %). Found: 58.84; H, 4.11; N, 28.78. Calc. for $C_{20}H_{14}N_8$: C, 56.56; H, 3.85; N, 30.58 %. IR spectra (KBr disc): 3043s, 2813s, 2361s, 1692w, 1630s, 1503m, 1221m, 1130w and 810m cm^{-1}. δ_H (DMSO, 250 MHz): 7.45-7.52 (d, 2 H, Ar*H*), 7.72 (s, 2 H, Ar*H*), 7.92-7.96 (d, 2 H, Ar*H*), 8.10 (s, 4 H, Ar*H*) and 8.84 (s, 2 H, N=C*H*). MS: (+FAB) m/z (% intensity) 367 (36.4 %), 232 (61.2).

1,3–bis{[(E)-3*H*-benzotriazol-5-ylimino]-methyl}-benzene (27)

6 was prepared using the same preparative procedure used for **5**. Yield: 0.25 g (92 %). Found: 56.29; H, 4.26; N, 28.26. Calc. for $C_{20}H_{14}N_8$: C, 65.56; H, 3.85; N, 30.58 %. IR spectra (KBr disc): 3068s, 2873s, 2361s, 1694w, 1612s, 1503m, 1393m, 1194s, 877m and 813s cm^{-1}. δ_H (DMSO, 250 MHz): 7.69-7.74 (d, 2 H, Ar*H*), 8.02 (s, 2 H, Ar*H*), 8.21-8.25 (d, 2 H, Ar*H*), 8.32-8.41 (m, 3 H, Ar*H*), 8.86 (s, 1 H, Ar*H*) and 9.12 (s, 2 H, N=C*H*). MS: (+FAB) m/z (% intensity) 367 (50.1 %).

2-{[(E)-3*H*-benzotriazol-5-ylimino]-methyl}-phenol (28)

To a solution of 5-aminobenzotriazole (120 mg, 0.9 mmol) in methanol (15 ml) was added salicylaldehyde (100 mg, 0.8 mmol) dissolved in methanol (1 ml). The reaction mixture was stirred for 1.5 hours then the solvent removed *in vacuo*. The residual oily yellow material was recrystallised from refluxing toluene (20 ml) and followed by acetonitrile (20 ml). The resultant yellow solid was collected by filtration and dried *in vacuo*. Yield: 0.18 g (95 %). Found: 59.62; H, 4.41; N, 23.17. Calc. for $C_{13}H_{10}N_4O$: C, 64.28; H, 4.23; N, 23.52 %. IR spectra (KBr disc): 3046s, 2976s, 1610s, 11573s, 1388m, 1282s, 1198s, 1146s, 995m, 813m and 761s cm^{-1}. δ_H (MeOH, 250 MHz): 7.18-7.23 (m, 2 H, Ar*H*), 7.72 – 7.78 (m, 3 H, Ar*H*), 7.97 (s, 1 H, Ar*H*), 8.15-8.19 (d, 1 H, Ar*H*) and 9.12 (s, 1 H, N=C*H*). MS: (+FAB) m/z (% intensity) 239 (100 %).

Ligand substitution experiments

The generic procedure used to analyse ligand substitution in pentametallic clusters was to dissolve a cluster with formula, $[Cu_5(bta)_6(\beta\text{-diketonyl})_4]$ (β-diketonyl = acac or hfac) (50 mg) in THF (50 ml) and add 5 equivalents of a competitive benzotriazole ligand, L1 or L2 (L1 = 1H-1,2,3-triazole, L2 = 5,6 –dinitro-1H-benzotriazole). The reaction was stirred for 18 hours, the solvent removed *in vacuo* and the residue analysed by FAB^+ mass spectrometry.

The same procedure was used to analyse the reaction between $[Cu_5(bta)_6(acac)_4]$ and Benzo[1,2-*d*:4,5-*d'*]bistriazole (**24**) using DMSO as the solvent in place of THF.

Substitution of $[Cu_5(bta)_6(hfac)_4]$ by acacH was studied using the same procedure whereby $[Cu_5(bta)_6(hfac)_4]$ (50 mg) was dissolved in THF (50 ml), acacH (50 mg) added and the reaction stirred for 18 hours. The solvent was removed and the residue analysed using FAB^{+-} mass spectrometry.

$[Cu_5(bta)_6(hfac)_4]$/L1

MS: (+FAB) m/z (% intensity) 1587 (36 %), 1537 (100) 1485 (68), 1380 (72), 1332 (98), 1289 (71), 1239 (62), 1173 (59), 1121 (61) and 1053 (87).

MS: (+FAB) m/z (% intensity) 739 (7 %), 689 (10), 639 (12), 560 (5), 537 (19), 508 (9), 458 (7) and 120 (100).

$[Cu_5(bta)_6(hfac)_4]$/L2

MS: (+FAB) m/z (% intensity) 1917 (29 %), 1827 (100), 1737 (80), 1620 (43), 1530 (34), 1411 (20), 1293 (31) and 1205 (39).

MS: (+FAB) m/z (% intensity) 1205 (8 %), 969 (19), 879 (47), 789 (50), 725 (20), 700 (28) and 608 (54).

$[Cu_5(bta)_6(acac)_4]$/L1

MS: (+FAB) m/z (% intensity) 496 (12 %), 460 (24), 426 (11), 391 (51), 373 (9), 291 (80) and 273 (60).

$[Cu_5(bta)_6(acac)_4]$/L2

MS: (+FAB) m/z (% intensity) 1665 (47 %), 1575 (100), 1483 (57), 1384 (30) and 1059 (83).

MS: (+FAB) m/z (% intensity) 1059 (5 %), 969 (15), 879 (10), 788 (8), 698 (14) and 608 (10) and 43 (100).

$[Cu_5(bta)_6(acac)_4]$/(3)

MS: (+FAB) m/z (% intensity) 1390 (100 %), 1345 (97), 1306 (50), 1286 (31), 1247 (32), 1206 (14), 1157 (17), 1115 (33), 1070 (48) and 1030 (78).

MS: (+FAB) m/z (% intensity) 1115 (3 %), 1070 (5), 1030 (7), 989 (7), 912 (10), 871 (35), 830 (60), 789 (58) and 608 (100).

$[Cu_5(bta)_6(hfac)_4]$/acacH

MS: (+FAB) m/z (% intensity) 1735 (25 %), 1627 (54), 1519 (46), 1439 (47), 1389 (83), 1205 (54), 1153 (100), 1115 (33) and 1095 (48).

References

1 D. S. Moore and S. D. Robinson, *Adv. Inorg. Chem.* , 1988, **32**, 171.
2 I. Dugdale and J. B. Cotton, *Corros. Sci.* , 1963, **3**, 69.
3 R. F. Roberts, *J. Electron. Spectrosc. Relat. Phenom.* , 1974, **4**, 273.
4 S. Pizzini, K. J. Roberts, I. S. Dring, R. J. Oldman, and D. C. Cupertino, *J. Mater. Chem.* , 1993, **3**, 811.
5 Z. Xu, S. Lau, and P. W. Bohn, *Surf. Sci.* , 1993, **296**, 57.
6 J. F. Walsh, H. S. Dhariwal, A. Gutierrez-Sosa, P. Finetti, C. A. Muryn, N. B. Brookes, R. J. Oldman, and G. Thornton, *Surf. Sci.* , 1998, **415**, 423.
7 J. B. Cotton and I. R. Scholes, *Br. Corros. J.* , 1967, **2**, 1.
8 G. W. Poling, *Corros. Sci.* , 1970, **10**, 359.
9 B. S. Fang, C. G. Olson, and D. W. Lynch, *Surf. Sci.* , 1986, **176**, 476.
10 J. H. Marshall, *Inorg. Chem.*, 1978, **17**, 3711.
11 J. Handley, D. Collison, C. D. Garner, M. Helliwell, R. Docherty, J. R. Lawson, and P. A. Tasker, *Angew. Chem.* , 1993, **105**, 1085.
12 R. Smith, 'Masters Project: Studies of benzotriazole bridged Cu5 complexes', University of Edinburgh, Edinburgh, 2000.
13 M. Murrie, 'Polynuclear Transition Metal Complexes of Benzotriazole', University of Manchester, Manchester, 1997.
14 M. Murrie, D. Collison, C. D. Garner, M. Helliwell, P. A. Tasker, and S. S. Turner, *Polyhedron*, 1998, **17**, 3031.
15 E. G. Balakbassis, E. Diamantopoulou, S. P. Perlepes, C. P. Raptopoulou, V. Tangoulis, A. Terzis, and T. F. Zafiropoulos, *Chem. Commun.* , 1995, 1347.
16 J. S. Burns, 'The structural, spectroscopic and magnetic properties of pentanuclear 3d transition metal complexes of benzotriazole', University of Manchester, Manchester, 2001.
17 L. F. Jones, 'Rigid vs flexible ligands: ligand flexibility in M(II) paramagnetic cluster formation.' University of Manchester, Manchester, 2003.
18 D. M. Low, L. F. Jones, A. Bell, E. K. Brechin, T. Mallah, E. Riviere, S. J. Teat, and E. J. L. McInnes, *Angew. Chem. Int. Ed.* , 2003, **42**, 3781.
19 G. Rajaraman, J. Cano, E. K. Brechin, and E. J. L. McInnes, *Chem. Commun.*, 2004, 1476.
20 E. K. Brechin, A. Graham, P. E. Y. Milne, M. Murrie, S. Parsons, and R. E. P. Winpenny, *Special Publication - Royal Society of Chemistry*, 2000, **252**, 260.
21 R. E. P. Winpenny, *Comprehensive Coordination Chemistry II*, 2004, **7**, 125.
22 D. W. Bruce, 'Inorganic Materials', ed. D. W. Bruce and D. O'Hare, Wiley, 1996.
23 N. J. Long, *Angew. Chem.-Int. Edit. Engl.*, 1995, **34**, 21.
24 V. W.-W. Yam, *Acc. Chem. Res.*, 2002, **35**, 555.
25 G. G. Condorelli, A. Motta, I. Fragala, F. Giannazzo, V. Raineri, A. Caneschi, and D. Gatteschi, *Angew. Chem. Int. Ed.* , 2004, **43**, 4081.
26 A. Cornia, C. Fabretti Antonio, M. Pacchioni, L. Zobbi, D. Bonacchi, A. Caneschi, D. Gatteschi, R. Biagi, U. Del Pennino, V. De Renzi, L. Gurevich, and S. J. Van der Zant Herre, *Angew. Chem. Int. Ed.* , 2003, **42**, 1645.

[27] A. Albinati, P. Leoni, L. Marchetti, and S. Rizzato, *Angew. Chem. Int. Ed.* , 2003, **42**, 5990.

[28] H. Hart and D. Ok, *J. Org. Chem.* , 1986, **51**, 979.

[29] E. I. Ivanov, A. A. Polishchuk, and P. B. Terent'ev, *Khimiya Geterotsiklicheskikh Soedinenii*, 1988, 256.

[30] J. K. Clegg, L. F. Lindoy, B. Moubaraki, K. S. Murray, and J. C. McMurtrie, *Dalton Trans.* , 2004, 2417.

Appendix 1

Generic atom number	Actual atom number				
	2	**3**	**4a**	**4b**	**5**
Cu1A	Cu1A	Cu1A	Cu1A	Cu1A	Cu1A
Cu1B	Cu1B	Cu1B	Cu1B	Cu1B	Cu1B
Cu1C	Cu1C	Cu1C	Cu1C	Cu1C	Cu1C
Cu1D	Cu1D	Cu1D	Cu1D	Cu1D	Cu1D
Cu2A	Cu2A	Cu2A	Cu2A	Cu2A	Cu2A
Cu3A	Cu3A	Cu3A	Cu3A	Cu3A	Cu3A
Cu2B	Cu2B	Cu2B	Cu2B	Cu2B	Cu2B
Cu3B	Cu3B	Cu3B	-	-	-
Cu2C	Cu2C	Cu2C	Cu2C	Cu2C	Cu2C
Cu3C	Cu3C	Cu3C	-	-	-
Cu2D	Cu2D	Cu2D	Cu2D	Cu2D	Cu2D
Cu3D	Cu3D	Cu3D	Cu3D	Cu3D	Cu3D
C1A	C1A	C1A	C1A	C1A	C1A
C2A	C2A	C2A	C2A	C2A	C2A
O1A	O1A	O1A	O1A	O1A	O1A
O2A	O2A	O2A	O2A	O2A	O2A
O3A	O3A	O3A	O3A	O3A	O3A
O4A	O4A	O4A	O4A	O4A	O4A
C1B	C1B	C1B	C1B	C1B	C1B
C2B	C2B	C2B	C2B	C2B	C2B
O1B	O1B	O1B	O1B	O1B	O1B
O2B	O2B	O2B	O2B	O2B	O2B
O3B	O3B	O3B	-	-	-
O4B	O4B	O4B	-	-	-
C1C	C1C	C1BA	C1C	C1C	C1BA
C2C	C2C	C2BA	C2C	C2C	C2BA
O1C	O1C	O1BA	O3C	O3C	O1BA
O2C	O2C	O2BA	O4C	O4C	O2BA
O3C	O3C	O3BA	-	-	-
O4C	O4C	O4BA	-	-	-
C1D	C1D	C1AA	C1D	C1D	C1AA
C2D	C2D	C2AA	C2D	C2D	C2AA
O1D	O1D	O1AA	O1D	O1D	O1DA
O2D	O2D	O2AA	O2D	O2D	O2DA
O3D	O3D	O3AA	O3D	O3D	O3DA
O4D	O4D	O4AA	O4D	O4D	O4DA

Table 1. Key to the generic numbering scheme used in chapter 2

Generic atom number	Actual atom number	Generic atom number	Actual atom number
Cu1A	Cu1	**Cu1A'**	Cu1A
Cu1B	Cu4	**Cu1B'**	Cu4A
Cu1C	Cu1B	**Cu1C'**	Cu1C
Cu1D	Cu1D	**Cu1D'**	Cu4C
Cu2A	Cu2	**Cu2A'**	Cu2A
Cu3A	-	**Cu3A'**	-
Cu2B	Cu3B	**Cu2B'**	Cu3C
Cu3B	-	**Cu3B'**	-
Cu2C	Cu2B	**Cu2C'**	Cu2C
Cu3C	-	**Cu3C'**	-
Cu2D	Cu3	**Cu2D'**	Cu3A
Cu3D	-	**Cu3D'**	-
C1A	C11	**C1A'**	C11A
C2A	C12	**C2A'**	C12A
C1B	C17B	**C1B'**	C17C
C2B	C18B	**C2B'**	C18C
C1C	C11B	**C1C'**	C11C
C2C	C12B	**C2C'**	C12C
C1D	C17	**C1D'**	C17A
C2D	C18	**C2D'**	C18A

Table 2. Key to numbering scheme used for **10**.

Generic atom number	Actual atom number	Generic atom number	Actual atom number
Cu1A(1)	Cu1A	**Cu1A(2)**	Cu1E
Cu1B(1)	Cu1H	**Cu1B(2)**	Cu1B
Cu1C(1)	Cu1G	**Cu1C(2)**	Cu1C
Cu1D(1)	Cu1F	**Cu1D(2)**	Cu1D
Cu2A(1)	C2A	**Cu2A(2)**	Cu2E
Cu3A(1)	-	**Cu3A(2)**	-
Cu2B(1)	Cu3A	**Cu2B(2)**	Cu2B
Cu3B(1)	Cu2G	**Cu3B(2)**	-
Cu2C(1)	Cu2H	**Cu2C(2)**	Cu2C
Cu3C(1)	-	**Cu3C(2)**	Cu3C
Cu2D(1)	Cu2D	**Cu2D(2)**	Cu2F
Cu3D(1)	-	**Cu3D(2)**	-
C1A(1)	C1A	**C1A(2)**	C1DA
C2A(1)	C2A	**C2A(2)**	C2DA
C1B(1)	C1CA	**C1B(2)**	C1B
C2B(1)	C2CA	**C2B(2)**	C2B
C1C(1)	C1BA	**C1C(2)**	C1C
C2C(1)	C2BA	**C2C(2)**	C2C
C1D(1)	C1D	**C1D(2)**	C1AA
C2D(1)	C1D	**C2D(2)**	C2AA

Table 3. Key to numbering scheme used for **11**.

Generic atom number	Actual atom number	Generic atom number	Actual atom number
Cu1A	Cu3	**Cu1A'**	Cu3A
Cu1B	Cu1	**Cu1B'**	Cu1A
Cu1C	Cu5	**Cu1C'**	Cu5A
Cu1D	Cu4A	**Cu1D'**	Cu4
Cu2A	Cu8	**Cu2A'**	Cu8A
Cu3A	-	**Cu3A'**	-
Cu2B	Cu6	**Cu2B'**	Cu6A
Cu3B	-	**Cu3B'**	-
Cu2C	Cu2	**Cu2C'**	Cu2A
Cu3C	Cu7	**Cu3C'**	Cu7A
Cu2D	Cu9	**Cu2D'**	Cu9A
Cu3D	-	**Cu3D'**	-
C1A	C36	**C1A'**	C36A
C2A	C37	**C2A'**	C37A
C1B	C41	**C1B'**	C41A
C2B	C42	**C2B'**	C42A
C1C	C26	**C1C'**	C26A
C2C	C27	**C2C'**	C27A
C1D	C31	**C1D'**	C31A
C2D	C32	**C2D'**	C32A

Table 4. Key to numbering scheme used for **12**.

Generic atom number	Actual atom number	Generic atom number	Actual atom number
Cu1A(1)	Cu8	**Cu1A(2)**	Cu11
Cu1B(1)	Cu1	**Cu1B(2)**	Cu18
Cu1C(1)	Cu13	**Cu1C(2)**	Cu10
Cu1D(1)	Cu5	**Cu1D(2)**	Cu2
Cu2A(1)	Cu7	**Cu2A(2)**	-
Cu3A(1)	-	**Cu3A(2)**	-
Cu2B(1)	Cu6	**Cu2B(2)**	-
Cu3B(1)	-	**Cu3B(2)**	-
Cu2C(1)	Cu16	**Cu2C(2)**	Cu9
Cu3C(1)	-	**Cu3C(2)**	-
Cu2D(1)	-	**Cu2D(2)**	Cu3
Cu3D(1)	-	**Cu3D(2)**	-
C1A(1)	C68	**C1A(2)**	C122
C2A(1)	C69	**C2A(2)**	C123
C1B(1)	C104	**C1B(2)**	C113
C2B(1)	C105	**C2B(2)**	C114
C1C(1)	C95	**C1C(2)**	C78
C2C(1)	C96	**C2C(2)**	C78
C1D(1)	C140	**C1D(2)**	C86
C2D(1)	C141	**C2D(2)**	C87

Table 5. Key to numbering scheme used for **13**.

Appendix 1

Generic atom number	Actual atom number	Generic atom number	Actual atom number	Generic atom number	Actual atom number
Cu1A	Cu1E	**Cu1E**	Cu1I	**Cu1I**	Cu1A
Cu1B	Cu4B	**Cu1F**	Cu4A	**Cu1J**	Cu1J
Cu1C	Cu1C	**Cu1G**	Cu1G	**Cu1K**	Cu1B
Cu1D	Cu1D	**Cu1H**	Cu1H	**Cu2I**	Cu2B
Cu2A	-	**Cu2E**	-	**Cu3I**	Cu3B
Cu3A	-	**Cu3E**	-	**Cu2J**	Cu2J
Cu2B	-	**Cu2F**	-	**Cu3J**	Cu3J
Cu3B	-	**Cu3F**	-	**C1I**	C1B
Cu2C	Cu2C	**Cu2G**	Cu2H	**C2I**	C2B
Cu3C	-	**Cu3G**	-	**C1J**	C1J
Cu2D	Cu2D	**Cu2H**	Cu1I	**C2J**	C2J
Cu3D	-	**Cu3H**	-		
C1A	C1M	**C1E**	C1L		
C2A	C2M	**C2E**	C2L		
C1B	C1N	**C1F**	C1K		
C2B	C2N	**C2F**	C2K		
C1C	C1C	**C1G**	C1H		
C2C	C2C	**C2G**	C2H		
C1D	C1D	**C1H**	C1I		
C2D	C2D	**C2H**	C2I		

Table 6. Key to numbering scheme used for **14**.

Appendix 1

Generic atom number	Actual atom number	Generic atom number	Actual atom number	Generic atom number	Actual atom number
Cu1A	Cu4	**Cu1E**	Cu5	**Cu1I**	Cu11
Cu1B	Cu7	**Cu1F**	Cu9	**Cu1J**	Cu6
Cu1C	Cu1	**Cu1G**	Cu2	**Cu1K**	Cu12
Cu1D	Cu8	**Cu1H**	Cu10	**Cu1L**	Cu3
Cu2A	Cu13	**Cu2E**	Cu17	**Cu2I**	Cu21
Cu3A	-	**Cu3E**	-	**Cu3I**	-
Cu2B	Cu14	**Cu2F**	Cu18	**Cu2J**	Cu23
Cu3B	-	**Cu3F**	-	**Cu3J**	-
Cu2C	Cu16	**Cu2G**	Cu20	**Cu2K**	Cu24
Cu3C	-	**Cu3G**	-	**Cu3K**	-
Cu2D	Cu15	**Cu2H**	Cu19	**Cu2L**	Cu22
Cu3D	-	**Cu3H**	-	**Cu3HL**	-
C1A	C1A	**C1E**	C1E	**C1I**	C1I
C2A	C2A	**C2E**	C2E	**C2I**	C2I
C1B	C1B	**C1F**	C1F	**C1J**	C1K
C2B	C2B	**C2F**	C2F	**C2J**	C2K
C1C	C1D	**C1G**	C1H	**C1K**	C1L
C2C	C2D	**C2G**	C2H	**C2K**	C2L
C1D	C1C	**C1H**	C1G	**C1L**	C1J
C2D	C2C	**C2H**	C1G	**C2L**	C1J

Table 7. Key to numbering scheme used for **15**.

Appendix 2

Equations for the planes in Table 2-2 and 2-6

Equations for planes defined by the atoms Cu1A, Cu1B, Cu1C and Cu1D are **1**, 6.59(1)x + -11.88(1)y + 15.18(1)z = -13.71(1); **2**, 6.719(5)x + -12.03(1)y + 17.34(1)z = 16.094(5); **3**, 14.926(4)x + 0.000(0)y + 5.29(2)z = 11.43(2); **4a**, 6.135(4)x + -6.168(4)y + 18.452(4)z = 7.680(6); **4b**, 8.969(3)x + -8.973(3)y + 13.584(7)z = 0.952(2); **5**, 1.31(1) x + 0.000(0) y - 21.83(6) z = 5.45(2).

Equations for the planes in Table 3-4.

Equations are 3.78(2)x + -5.37(2)y + 20.17(1)z = 0.29(1), 5.37(2)x + -3.78(2)y + 20.17(1)z = 5.21(2), -3.78(2)x + 5.37(2)y + 20.17(1)z = 7.25(2) and -5.37(2)x + -3.78(2)y + 20.17(1)z = 7.41(1) for the rings (Cu3, O1, O2, C2, C3, C4), (Cu3B, O1B, O2B, C2B, C3B C4B), (Cu3A, O1A, O2A, C2A, C3A, C4A) and (Cu3C, O1C, O2C, C2C, C3C, C4C) respectively.

Equations for the planes in Table 3-6.

Equations are 16.410(34)x + 9.915(98)y + 1.39(19)z = 24.02(16), 16.25(3)x + 9.91(9)y + 0.39(19)z = 19.92(17), 8.73(6)x - 10.86(6)y - 0.18(12)z = 4.49(13), -6.62(9)x + 12.61(17)y - 0.73(11)z = -4.50(6), 16.95(18)x + 5.48(13)y + 6.52(9)z = 23.48(16) and 16.78(31)x + 4.98(13)y + 8.49(6)z = 21.10(18) for the rings, (C44, C45, C46, C47 C48, C49), C54, (C55, C56, C57, C58, C59), (Cu2D, O1D, O2D, C11, C12, C13), (C34A, C35A, C36A, C37A, C38A, C39A), (Cu2G, O1CA, O2CA, C41A, C42A, C43A) and (C24A, C25A, C26A, C27A, C28A, C29A) respectively.

Equations for the planes in Table 3-8.

Equations are 16.16(3)x - 12.30(7)y - 3.64(8)z = -0.10(6), 14.51(3)x - 0.99(8)y - 16.57(5)z = -8.74(4), 16.16(3)x - 12.30(7)y - 3.64(8)z = -2.64(8), 14.51(3)x - 0.99(8)y - 16.57(5)z = -7.83(4) for the rings, (Cu6, O7, O8, C17, C18, C19), (Cu2, O5, O6, C12, C13, C14), (Cu6A, O7A, O8A, C17A, C18A, C19A) and (Cu2A, O5A, O6A, C12A, C13A, C14A) respectively.

Equations for the planes in Table 3-10

Equations are -5.20(8)x + 21.50(3)y + 9.40(8)z = 15.18(9), -2.50(4)x + 21.47(2)y + 9.38(5)z = 11.63(5), -6.22(4)x + 21.53(1)y + 8.96(5)z = 8.108(7), 6.18(6)x + 21.28(3)y + -9.94(7)z = 13.11(3), 1.45(4)x + 22.696(7)y + -3.66(5)z = 9.65(2), 5.19(4)x + 22.433(8)y + -3.84(5)z = 7.99(2), -10.38(8)x + 13.67(9)y + 21.98(2)z = 7.99(5), -11.79(5)x + 11.51(5)y + 23.64(2)z = 4.61(5), 10.39(7)x + -10.97(5)y + 14.89(9)z = 3.80(5), 12.68(3)x + -7.67(2)y + 14.56(8)z = 3.20(4), 4.14(4)x + 18.79(2)y + 11.75(5)z = 12.94(3) and 10.13(8)x + 13.08(9)y + 13.54(8)z = 13.83(9) for the rings, (C98, C99, C100, C101,C102, C103), (Cu3, O11, C27, C28, C29, O12), (Cu9, O9, C22, C23, C24, O10), (C107, C108, C109, C110, C111, C112), (Cu7, O7, C17, C18, C19, O8), (Cu14, O5, C12, C13, C14, O6), (C134 , C135, C136, C137, C138, C139), (Cu17, O1, O2, C2, C3, C4, O2), (C143, C144, C145, C146, C147, C148), (Cu16, O13, C32, C33, C34, O14), (C125, C126, C127, C128, C129, C130) and (Cu6, O15, C37, C38, C39, O16) respectively.

Equations for the planes in Table 3-12

Equations for the Cu_4 planes are **10**, 11.811(1)x + 11.811(1)y + 0.000z = 16.45(2); **11**, 14.889x + 1.016y + 12.875z = 22.9411; **12**, 18.14(1)x + -5.15(2)y + 3.38(1)z = 2.713(1); **13(1)**,19.287(7)x + 10.942(6)y + 4.214(9)z = 11.999(3) ; **13(2)**, 22.223(5)x + 1.856(5)y + 4.192(6) z = 6.017(2).

Equations for the planes in Table 4-1

Cu4-C4A, Cu4D-C4AD, Cu5-C4B and Cu5A-C4BA rings contain the atoms (Cu4, O1A, O5A, C2A, C3A, C4A), (Cu4D, O1AD, O5AD, C2AD, C3AD, C4AD), (Cu5, O1B, O5B, C2B, C3B, C4B), (Cu5A, O1BA, O5BA, C2BA, C3BA, C4BA) respectively and least squares planes have the equations, -19.258x + 16.262y + -12.626z = -16.3961, -16.262x + 19.258y + -12.626z = -8.8565, 19.612x + -2.423y + 9.030z = 25.3092 and 17.189x + 2.423y + 9.030z = 29.5514 respectively.

Equations for the planes in Table 4-2

Cu14-C13, Cu15-C19, Cu20-C44, Cu21-C39, Cu17-C54, Cu18-C59, Cu22-C34, Cu23-C29, Cu24-C4 and Cu13-C9 rings contain the atoms, (Cu14, O1B, O2B, C11, C12, C13), (Cu15, O1C, O2C, C17, C18, C19), (Cu20, O1H, O2H, C42, C43, C44), (Cu21, O1I, O2I, C37, C38, C39), (Cu17, O1E, O2E, C52, C53, C54), (Cu18, O1F, O2F, C57, C58, C59), (Cu22, O1J, O2J, C32, C33, C34), (Cu23, O1K, O2K, C27, C28, C29), (Cu24, O1L, O2L, C2, C3, C4) and (Cu13, O1A, O2A, C7, C8, C9) and the equations for the least squares planes of these rings are -8.39(6)x + 8.37(8)y + 36.08(9)z = 26.0(1), -7.24(8)x + 12.38(6)y + 31.35(9)z = 25.4(1), -1.87(8)x + 11.17(6)y + 34.38(8)z = 32.17(6), 0.14(8)x + 15.28(5)y + 26.6(1)z = 26.44(8), 13.08(6)x + -7.64(8)y + 23.24(6)z = 28.41(8), -13.03(6)x + 14.85(8)y + -6.12(8)z = -11.48(6), 4.8(6)x + 19.57(8)y + 1.52(8)z = 10.26(8), 6.15(8) + 18.88(6)y + -10.11(6)z = -0.46(8), -10.44(6)x + -11.91(8)y + 29.3(1)z = 14.64(8) and -11.18(6)x + -8.19(8)y + 33.89(9)z = 20.7(1) respectively.

Equations for the planes in Table 4-3

Cu3G-C12, Cu3E-C20, Cu3J-C60, Cu3B-C68, Cu2C-C92, Cu2D-C76, Cu2H-C36 and Cu2I-C44 rings contain the atoms, (Cu3G, O3G, O4G, C10, C11, C12), (Cu3E, O3E, O4E, C18, C19, C20), (Cu3J, O3J, O4J, C58, C59, C60), (Cu3B, O3B, O4B, C66, C67, C68), (Cu2C, O1C, O2C, C90, C91, C92), (Cu2D, O1D, O2D, C74, C75, C76), (Cu2H, O1H, O2H, C34, C35, C36) and (Cu2I, O1I, O2I, C42, C43, C44) respectively and the least squares mean plane of the rings have the equations, 10.840(47)x + 14.552(38)y + -1.14(11)z = 11.388(42), 15.326(33)x + 8.832(63)y + -0.56(12)z = 13.616(56), 9.568(50)x + 15.760(39)y + -0.31(11)z = 11.044(65), 15.260(37)x + 8.777(61)y + -0.94(12)z = 13.894(66), -8.568(64)x + 15.606(46)y + 4.36(11)z = -2.095(87), -9.698(64)x + 14.490(52)y + -4.86(11)z = -3.984(89), 13.189(43)x + -10.328(59)y + -5.422(95)z = 5.293(49) and 15.136(36)x + -8.348(63)y + 6.113(94)z = 11.434(45) respectively.

Equations for the planes in Table 4-4

Equations for the planes are 3.864(15)x + 16.667(7)y + -23.04(2)z = -15.88(2), -1.660(13)x + 17.819(6)y + 19.464(18)z = 21.654(18) and -5.138(18)x + 0.931(12)y + 41.180(9)z = 29.655(17) for the planes defined by the atoms Cu1A-Cu1D, Cu1E-Cu1H and Cu1I-Cu1L respectively.

Equations for the planes in Table 4-6

The equations are 10.29(1)x + 12.291(9)y + 24.96(1)z = 18.915(5) and 12.403(8)x + 11.189(9)y + 23.54(1)z = 16.84(3) for the planes defined by the atoms Cu1A-Cu1D and Cu1E-Cu1H respectively.

Appendix 3

Crystallographic Tables

	2	3	4
Empirical formula	$C_{64}H_{44}Cu_{12}F_{48}O_{16}$	$C_{60}H_{44}Cu_{12}F_{48}O_{16}Si_4$	$C_{115}H_{102}Cu_{20}F_{72}O_{16}$
Formula weight	2743.47	2807.79	4539.76
Temperature	150(2) K	150(2) K	150(2) K
Wavelength	0.71073 Å	0.71073 Å	0.71073 Å
Crystal system	Monoclinic	Orthorhombic	Triclinic
Space group	$P2_1/n$ (alt. No. 14)	$C222_1$	$P1$ (No. 1)
Unit cell dimensions	a=12.7505(13) Å α = 90°	a = 15.3619(8) Å α= 90°	a = 13.8102(7) Å α= 98.0770(10)°
	b=30.793(3) Å β = 90.432(16)°	b = 28.2000(13) Å β= 90°	b = 14.0182(8) Å β= 101.3170(10)°
	c=23.094(2) Å γ = 90°	c = 22.3712(11) Å γ= 90°	c = 23.3814(13) Å γ= 114.3360(10)°
Volume	9067.0(2) Å^3	9691.3(8) Å^3	3918.0(4) Å^3
Z	4	4	1
Density (calculated)	2.010 Mg/m^3	1.924 Mg/m^3	1.924 Mg/m^3
Absorption coefficient	2.908 mm^{-1}	2.770 mm^{-1}	2.796 mm^{-1}
F(000)	5344	5472	2228
Crystal size	0.07 × 0.14 × 0.46 mm^3	0.19 × 0.25 × 0.35 mm^3	0.49 × 0.40 × 0.32 mm^3
Theta range for data collection	1.32 to 22.57°	3.52 to 23.00°	1.65 to 25.00°
Reflections collected	36456	20997	28761
Independent reflections	11935 [R(int) = 0.0747]	6732 [R(int) = 0.0496]	25181 [R(int) = 0.0139]
Abs. Correction	SADABS	SADABS	SADABS
T_{max}, T_{min}	1, 0.657	1, 0.744	1, 0.898
H-atom placement	Geometric	Geometric	Geometric
Data/restraints/parameters	11935 / 0 / 1261	6732 / 0 / 526	25181/ 241 / 2097
R_1 [|F|>4σ(|F|)]	0.0512	0.0722	0.0449
wR_2 [All Data]	0.1334	0.1905	0.1189
Largest peak, e.Å^{-3}	0.721	1.437	1.107
Largest Hole, e.Å^{-3}	-0.750	-0.628	-0.543

Table 8. Crystallographic data for **2**, **3** and **4**.

	5	**7**
Empirical formula	$C_{59}H_{52}Cu_{10}F_{36}O_{13}$	$C_{16}H_{12}Cu_2F_{12}O_4$
Formula weight	2288.41	623.34
Temperature	150(2) K	150(2) K
Wavelength	0.71073 Å	0.71073 Å
Crystal system	Monoclinic	Monoclinic
Space group	*C*2/*c*	$P2_1/n$ (alt. No. 14)
Unit cell dimensions	a = 26.649(6) Å α= 90°	a = 12.353(8) Å α= 90°
	b = 15.601(3) Å β= 115.242(3)°	b = 18.764(12) Å β= 97.513(5)°
	c = 23.619(5) Å γ= 90°	c = 20.208(13) Å γ= 90°
Volume	8882(3) Å^3	4644(5) Å^3
Z	4	8
Density (calculated)	1.711 Mg/m^3	1.783 Mg/m^3
Absorption coefficient	2.467 mm^{-1}	1.947 mm^{-1}
F(000)	4496	2448
Crystal size	0.28 × 0.49 × 0.45 mm^3	0.35 × 0.27 × 0.17 mm^3
Theta range for data collection	1.55 to 24.71°	3.74 to 22.00°
Reflections collected	21806	19179
Independent reflections	7542 [R(int) = 0.0294]	5513 [R(int) = 0.0864]
Abs. Correction	SADABS	SADABS
T_{max}, T_{min}	0.862, 0.705	1, 0.805
H-atom placement	Geometric	Geometric
Data/restraints/parameters	7542/ 0 / 536	5513/ 27 / 622
R_1 [$\|F\|>4\sigma(\|F\|)$]	0.0496	0.0914
wR_2 [All Data]	0.1327	0.2303
Largest peak, e.Å^{-3}	0.451	1.318
Largest Hole, e.Å^{-3}	-0.077	-0.813

Table 9. Crystallographic data for **5** and **7**.

	10	**11**
Empirical formula	$C_{88}H_{80}Cu_{16}F_{48}O_{16}$	$C_{148}H_{132}Cu_{18}F_{30}O_{20}$
Formula weight	3322.16	3944.26
Temperature	150(2)	150(2)
Wavelength	0.71073 Å	0.71073 Å
Crystal system	Tetragonal	Monoclinic
Space group	P-4*n*2	*P*-1
Unit cell dimensions	*a*=16.7029(10) Å α = 90°	*a*=17.0572(19) Å α = 71.640(2)°
	b=16.7029*(10)* Å β = 90°	*b*=18.479(2) Å β = 78.009(2)°
	c=21.9360(19) Å γ = 90°	*c*=27.893(3) Å Å γ = 67.225(2)°
Volume	6119.9(7) Å^3	7656.8(15)
Z	2	2
Density (calculated)	1.803 Mg/m^3	1.711 Mg/m^3
Absorption coefficient	2.841 mm^{-1}	2.539
F(000)	3264	3944
Crystal size	0.45 × 0.45 × 0.45 mm^3 (orange block)	0.20 × 0.28 × 0.37 mm^3
Theta range for data collection	1.53 to 26.39°	4.32 to 56.91 °
Reflections collected	33913	37760
Independent reflections	6274 [R(int) = 0.0389]	16277 [R(int) = 0.0795]
Abs. Correction	SADABS	SADABS
T_{max}, T_{min}	0.928, 0.575	1, 0.737
H-atom placement	Geometric	Geometric
Data/restraints/parameters	6274 / 60 / 419	16277 / 142 / 1889
R_1 [$\|F\|>4\sigma(\|F\|)$]	0.0360	0.0727
wR_2 [All Data]	0.0718	0.1850
Largest peak, e.Å^{-3}	0.477	0.948
Largest Hole, e.Å^{-3}	-0.375	-0.503

Table 10. Crystallographic data for **10** and **11**.

	12	**13**
Empirical formula	$C_{92}H_{70}Cu_{18}F_{60}O_{20}$	$C_{148}H_{92}Cu_{20}F_{48}O_{16}$
Formula weight	3779.2	4309.02
Temperature	150(2) K	150(2) K
Wavelength	0.71073 Å	0.71073 Å
Crystal system	Orthorhombic	Monoclinic
Space group	*Pbca*	$P2_1/c$
Unit cell dimensions	a = 18.680(3) Å α= 90°	a = 27.149(4) Å α= 90°
	b = 25.498(4) Å β= 90°	b = 22.902(4) Å β= 115.969(2)°
	c = 26.374(4) Å γ= 90°	c = 27.428(4) Å γ= 90°
Volume	12562(3) Å^3	15332(4) Å^3
Z	4	4
Density (calculated)	1.998 Mg/m^3	1.867 Mg/m^3
Absorption coefficient	3.123 mm^{-1}	2.827 mm^{-1}
F(000)	7376	8480
Crystal size	0.80 × 0.40 × 0.40 mm^3	0.80 × 0.40 × 0.40 mm^3
Theta range for data collection	1.60 to 24.99°	1.21 to 25.13°
Reflections collected	10271	76769
Independent reflections	10271 [R(int) = 0.0447]	27227 [R(int) = 0.0437]
Abs. Correction	SADABS	SADABS
T_{max}, T_{min}	1,0.812	0.693, 0.476
H-atom placement	Geometric	Geometric
Data/restraints/parameters	10271 / 3202 / 940	27227 / 3708 / 2163
R_1 [$\|F\|>4\sigma(\|F\|)$]	0.0724	0.0412
wR_2 [All Data]	0.2256	0.1124
Largest peak, e.Å^{-3}	3.19	0.953
Largest Hole, e.Å^{-3}	-1.11	-0.527

Table 11. Crystallographic data for **12** and **13**.

	14	**15**	**17**
Empirical formula	$C_{156}H_{204}Cu_{24}O_{24}F_{36}$	$C_{130}H_{146}Cu_{26}O_{24}F_{36}$	$C_9H_7CuF_6O_3$
Formula weight	4670.73	4428.51	340.69
Temperature	150(2)	150(2)	260(2) K
Wavelength	0.71073 Å	0.71073 Å	0.71073 Å
Crystal system	Triclinic	Monoclinic	Monoclinic
Space group	*P*-1	$P2_1/c$	$P2_1/n$
Unit cell dimensions	a= 17.875(2) Å α = 76.823(2)°	a= 20.787(4) Å α = 90.00°	a = 16.276(9) Å α= 90°
	b= 19.060(2) Å β = 74.189(2)°	b= 20.195(4) Å β = 99.782(2) °	b = 4.635(3) Å β= 99.627(9)°
	c= 30.863(3) Å γ = 84.200(2)°	c= 41.354(8) Å γ = 90.00 °	c = 16.522(9) Å γ= 90°
Volume	9842.2(18) $Å^3$	17108(6) $Å^3$	1228.9(11) $Å^3$
Z	2	4	4
Density (calculated)	1.620 Mg/m^3	1.719 Mg/m^3	1.841 Mg/m^3
Absorption coefficient	2.621 mm^{-1}	3.248 mm^{-1}	1.853 mm^{-1}
F(000)	4854	8784	672
Crystal size	0.65 × 0.30 × 0.40 mm^3 (orange block)	0.65 × 0.30 × 0.40 mm^3 (orange block)	0.83 × 0.22 × 0.19 mm^3
Theta range for data collection	3.52 to 20.00°	3.85 to 21.00 °	1.92 to 28.65°
Reflections collected	27991	47726	6898
Independent reflections	17880 [R(int) = 0.0410]	18127 [R(int) = 0.0646]	2872 [R(int) = 0.0301]
Abs. Correction	SADABS	SADABS	SADABS
T_{max}, T_{min}	1, 0.802	1, 0.656	0.928, 0.328
H-atom placement	Geometric	Geometric	Geometric
Data/restraints/parameters	17880 / 582 / 2141	18127 / 2461/ 1923	2872/ 25 / 204
R_1 [|F|>4σ(|F|)]	0.0785	0.0650	0.04670
wR_2 [All Data]	0.1654	0.2052	0.1059
Largest peak, $e.Å^{-3}$	0.879	0.995	0.875
Largest Hole, $e.Å^{-3}$	-0.694	-0.813	-0.394

Table 9. Crystallographic data for **14**, **15** and **17**.